UNIVERSITY OF Southampton

School of Civil Engineering and the Environment

Turbine wheel - a hydropower converter for head differences between 2.5 and 5 m

Ph.D Thesis

Helmizar

Supervisors:

Dr.Gerald Müller

February 2016

CONTENTS

List of Figures

List of Tables

List of alphabetical symbols

Symbol	Description	Unit
C_d	The empirical losses coefficient	
D_{bo}	Diameter of the bolt	[m]
D_{out}	Outer Diameter of The Water Wheel	[m]
D_{in}	Hub Diameter of The Water Wheel	[m]
D_{nr}	Diameter of the nut on the rim	[m]
D_{rbr}	Diameter of the rod bolt rim	[m]
F	Force that contribute to power output	[kg m/s^2]
F_A	force that acts at area A	[kg m/s^2]
F_B	force that acts at area B	[kg m/s^2]
F_C	force that acts at area C	[kg m/s^2]
F_b	Body force	[kg m/s^2]
F_{blade}	Blade reaction force	[kg m/s^2]
F_{dse}	downstream force that acts on the control volume	[kg m/s^2]
$F_{friciton}$	Friction force	[kg m/s^2]
F_{hub}	Hub reaction force	[kg m/s^2]
F_m	force	[kg m/s^2]
F_p	Prototype force	[kg m/s^2]
F_{pe}	Upstream force that acts on the control volume	[kg m/s^2]
F_r	Hub Reaction force	[kg m/s^2]
F_{rb}	Hub Reaction force in the case of blade width and channel width is not the same	[kg m/s^2]
F_{rotor}	Reaction force from rotor that acts on the control volume	[kg m/s^2]
F_s	Surface force	[kg m/s^2]
F_{side}	Side reaction force	[kg m/s^2]
F_t	Force that acting on the blade	[kg m/s^2]
F_{tr}	Turbulence force losses	[kg m/s^2]
F_{us}	Upstream force	[kg m/s^2]
F_1	Total force in upstream	[kg m/s^2]
F_2	Total force in downstream	[kg m/s^2]
F_{3dacc}	3D acceleration forces	[kg m/s^2]
F_τ	Tangential force at the upper chord	[kg m/s^2]
H	Head difference	[m]
Hub_{cm}	Hub Current Machine	[m]
K	turbulent constant	
L	Length of the vertical bar	[m]
N	weight of the motor	[kg]
P	Power	[W]
P_{out}	Measured Power output	[W]
$P_{loss\ acc\ in}$	Power loss due to inlet acceleration	[W]
$P_{exit\ loss}$	Power loss due to exit flow acceleration	[W]

P_m	Model power	[W]
$P_{max\ sharp}$	Max power output based on the water flow rate passes through sharp crested weir	[W]
P_{mi}	Max power output based on the water flow rate passes through water wheel blade	[W]
P_p	Prototype power	[W]
P_r	Dimensionless power	
P_{in}	Power input	[W]
P_{inmax}	Power input max	[W]
$\overline{P}$	Balancing Forces	[kg m/s^2]
P_{fm}	Final force measured	[kg m/s^2]
P_{im}	Pretension force	[kg m/s^2]
P_{ten}	some portion of pretension force at the vertical bar contributes to the tension force on the upper and lower chord	[kg m/s^2]
PZ_{vent}	Power loss due to elevation losses	[W]
P_1	Tension Force at chord	[kg m/s^2]
Q	Water Flow rate	[m^3/s]
Q_{bh}	Water flow rate which replace by bolt hub	[m^3/s]
Q_{bl}	Water flow rate which replace by blade	[m^3/s]
Q_c	Water flow rate which replace by cell	[m^3/s]
Q_{ho}	Water flow rate which replace by hook of the blade	[m^3/s]
Q_{lea}	Leakage water flow rate	[m^3/s]
Q_m	Model flow rate	[m^3/s]
Q_{max}	Max design water flow rate	[m^3/s]
Q_{nr}	Water flow rate which replace by nut rim	[m^3/s]
Q_p	Prototype flow rate	[m^3/s]
Q_r	Flow rate dimensionless	
Q_{rbr}	Water flow rate which replace by rod bolt rim	[m^3/s]
Q_{sharp}	Measured water flow rate/water flow rate passes sharp crested weir	[m^3/s]
Q_{th}	Theoretical water flow rate/ water flow rate passes wheel blade	[m^3/s]
Q_w	Flow rate water passes through the wheel	[m^3/s]
Q_1	The leakage that is coming from the gap between the hub and the wall	[m^3/s]
Q_2	The leakage which is coming from the gap between the blade and the wall	[m^3/s]
Q_3	The leakage which is coming from the gap between the channel bed and the blade	[m^3/s]
R	Pulley radius	[m]
R_{mean}	The mean radius	[m]
Rs	Resistance	[Ohm]
S_1	Upstream distance passes by fluid	[m]
T	Torque	[Nm]
T_A	Torque due to the force A (F_A)	[Nm]
T_B	Torque due to the force B (F_B)	[Nm]

T_C	Torque due to the force C (F_C)	[Nm]
T_b	Torque at the vertical bar	[Nm]
T_w	Torque at the pulley B	[Nm]
T_{acc}	Opposing torque	[Nm]
V	Volume of the water	[m^3]
W	Weight of the vertical bar	[kg]
X	Horizontal distance from Centre of gravity motor and holder to hinge centre	[m]
Y	Distance between centre weight of the motor to the centre of the hinge	[m]
Z	Horizontal distance between centre of the hinge to the centre weight of the vertical bar	[m]
Z_{vent}	The increasing of the height of the water from where it should drop	[m]
a	Acceleration	[m/s^2]
b	Blade width	[m]
c	Clearance between base plat to the lowest positiion of the wheel	[m]
d_1	Upstream water level	[m]
d_2	Downstream water level	[m]
f	Rotational Speed	[rps]
f_r	Dynamic similarity	
g	Gravity Constant	[m/s^2]
g_s	Gap between channel wall and water wheel	[m]
g_b	Gap between channel bed and the blade	[m]
h_{bo}	High of the bolt	[m]
h_{nr}	High of nut rim	[m]
h_{rbr}	High of rod bolt rim	[m]
l	Blade length	[m]
l_r	Geometric similarity	
l_h	Hook length	[m]
l_p	Length of prototype	[m]
l_m	Length of model	[m]
m_w	Moment on the DC motor	[Nm]
n	No of blade	
p_a	Pressure at point **a**	[kg /m s^2]
p_{av}	Average pressure	[kg /m s^2]
p_b	Pressure at point **b**	[kg /m s^2]
p_c	Pressure at point **c**	[kg /m s^2]
r	Radius of the wheel	[m]
r_i	inner radius of the wheel	[m]
r_o	Outer radius of the wheel	[m]
t	Blade thickness	[m]
t_1	Water Depth	[m]
v	Velocity of the cell	[m/s]

v_b	Blade tangential velocity	[m/s]
v_1	Upstream water velocity	[m/s]
v_{max}	Free fall velocity of the water	[m/s]
v_m	Velocity of the model	[m/s]
v_p	Velocity of the prototype	[m/s]
v_{tan}	Tangential velocity	[m/s]
v_r	Kinematic similarity	
w	Width of the flume	[m]
w_{ch}	Channel width	[m]
w_h	Hook width	[m]
w_t	Double Blade width	[m]
w_{wh}	Wide of the wheel	[m]
w_1	Upstream channel width	[m]
w_2	Downstream channel width	[m]

List of Greek symbols

Symbol	**Description**	**Unit**
Δh	Head drop	[m]
Δt	Time changing	[s]
Δv	Velocity changing	[m/s]
ΔZ	Weir Height	[m]
η	Efficiency	
η_{wl}	Efficiency excluding leakage	
ρ	Density	[kg/m^3]
ρ_w	Density of the water	[kg/m^3]
ω	Angular speed	[rad/s]

ACADEMIC THESIS: DECLARATION OF AUTHORSHIP

I, Helmizar declare that this thesis and the work presented in it are my own and has been generated by me as the result of my own original research *Turbine wheel – a hydropower converter for head differences between 2.5 and 5 m*.

I confirm that:

1. This work was done wholly or mainly while in candidature for a research degree at this University;
2. Where any part of this thesis has previously been submitted for a degree or any other qualification at this University or any other institution, this has been clearly stated;
3. Where I have consulted the published work of others, this is always clearly attributed;
4. Where I have quoted from the work of others, the source is always given. With the exception of such quotations, this thesis is entirely my own work;
5. I have acknowledged all main sources of help;
6. Where the thesis is based on work done by myself jointly with others, I have made clear exactly what was done by others and what I have contributed myself;
7. Part of this work was presented in Hydroenergia Conference in Istanbul-Turkey at May 21st to May 23rd 2014

Signed: ……

Date: ……

ACKNOWLEDGMENTS

A great many people have very kindly aided me over the four years of work represented by this thesis.

First my thanks go to my supervisors: Dr. Gerald Müller for his supervising in this project in the first place and, Dr. Costa Manes and Dr. Gustavo A. M. de Almeida for their critical advice in writing up of the thesis.

I also want to thank everyone who helped me a lot during the research at various times, including Dr. Toru Tsuzaki, Karl Scammell, and Earl Peters for their great enthusiasm for all things, including discussion, model preparation, facility, and also the extraordinarily generous hospitality during my time in the lab. Thanks are also extended to Dr. Nick Linton for all the discussions and critical thinking that was very valuable during the process of writing this thesis

Mention must also be made of the extraordinarily generous hospitality given to the me by all PPI Soton (Persatuan Pelajar Indonesia Southampton) members, and also some PhD colleagues such as Fikri alami, Dwi Cahyo Utomo, Didiek Sri Wiyono, Niken Syafitri, Gunawan Budi Prasetyo, Mailizar Ali and the others who I can not mention one by one, for their warmth and nice friendship.

Thanks also go to Dikti RI (Direktorat Pendidikan Tinggi Republik Indonesia) for the opportunity that they have given me, and the scholarship support so that I have had the opportunity to study my PhD in the University of Southampton UK.

Finally I wish to thank to my wife Elvy listiany, my son Hazhel Muhammad Nur Fadlan for their understanding while I leave them at home. Also to my parent, parent in law, brothers, sisters and also brothers and sisters in law for their full support during my PhD.

ABSTRACT

Large scale hydropower energy recovery is now an established technology. However the recovery of hydropower energy from small scale resources has yet to be exploited. The potential of this small scale energy resource in Indonesia is 450 MW. This source of energy is currently unexploited due to non-existence of an economically viable technology to extract the energy from these low power sites.

The turbine wheel is one type of water wheel which was proposed in 1848 as an alternative machine for small scale hydropower. The application for this machine was for use in water courses where the head differences ranges of 2.5-5m. This research is conducted in order to observe the performance and the characteristics the turbine wheel. The research was undertaken by testing a turbine wheel in a recirculating flume.

The experiments undertaken shows that the efficiency of this machine approaches 70%. The water flow volume of this machine is in the range of 1.85 m^3/s to 5.23m^3/s per m width. In addition, the maximum power output is between 28.74 kW and 162.56kW per m width. A theory is proposed which calculates theoretical power output for the machine correlates well with the experimental results. Furthermore, the power losses can be identified as turbulent losses only, with the turbulence coefficient *Cd* of 3.8.

CHAPTER 1

INTRODUCTION

1.1 Background

Hydropower is currently the most common form of renewable energy and plays an important part in global power generation. Worldwide hydropower production is 3229 TWh/yr. However, the gross theoretical capacity[1] for hydropower is estimated to be more than 15720 TWh/yr (World Energy Council 2013). There is a gap between the existing hydropower produced and the potential that could be exploited.

In Indonesia the hydropower potential is around 75 GW, although the current installed capacity is approximately 5 GW (Ferial 2014). The smallest hydropower generating capacity is Agam hydro power station located in west Sumatra with a generating capacity of 10MW (3x3.5 MW). Whereas the largest capacity is cirata hydro in Bali with a generating capacity of 1 GW (8x126MW). Overal 30 hydro power station operated and produced power. Meanwhile the target for the Indonesian government to utilize hydropower energy in 2025 is around 14 GW (Maria 2011).

In 2014 the percentage of Indonesians who do not have access to electricity is around 17.63% (Ketenagalistrikan 2014). One frequent cause for this problem is the large number of dispersed rural locations with challenging geographical conditions (Usman Muhammad 2012). An additional cause is the uneven distribution of population which has led to an ineffective electrical distribution infrastructure (Eberhard et al. 2011).

Small scale Hydro-Power plants are a solution to solve this problem. What is small scale hydropower plant? There is no internationally agreed definition of ‘small’ hydro plant; the

[1] Gross theoretical capacity means the capacity of hydropower generation possible if all natural water flows contained as many 100% efficient turbines as possible (International Hydropower Association 2013).

upper limit varies between 2.5 and 25 MW. A maximum of 10 MW is the most widely accepted value worldwide. In the industrial world, the term 'mini' hydro typically refers to schemes below 2 MW, micro-hydro ranging from 10kW-500 kW and pico-hydro below 10 kW (Paish 2002b). In addition, according to ESHA (the European Small Hydropower Association), small hydropower is the hydropower below 10 MW (TN SHP 2005). Small scale hydropower schemes could be a solution for rural areas that have natural resources such as lakes, irrigation canals, rivers or waterfalls. Small scale hydro is in most cases 'run-of-river'; in other words any dam or barrage is quite small, usually just a weir, and generally little or no water is stored (Paish 2002b).

The installed cost of a large hydropower station is in the range of 1050-7650 USD/kW, whereas for a small hydropower station, it is in the range of 1300-8000 USD/kW (International Renewable Energy Agency (IRENA) 2012). The largest proportion of installation costs for a large hydropower plant is typically taken up by civil works for the construction of the dam, tunnels, canal and construction of powerhouse, etc. The site-specific factors that influence the civil construction costs consist of hydrological characteristics, site accessibility, land topography, geological conditions, the construction and design of the hydropower plant and how far from the existing infrastructure and the existing grid. The cost of the civil works for hydropower plant also depends on commodity prices and labour costs within the country. The cost of civil works in developing countries is sometimes lower than in developed countries. Yet, this is not always the case since poorer infrastructure or remote sites will generate significant additional costs. Small hydropower plants are more likely to be run-of- river facilities, therefore the civil works cost for small hydropower is smaller than large scale. The costs of electro-mechanical equipment dominates the total costs for small scale hydropower plant, due to the high specific costs of such small-scale equipment. The electro-mechanical equipment used in hydropower plants is a mature technology. Therefore this electro-mechanical equipment such as grid network instalation, a frequency response reserve, power factor correction device is available comercially. Small hydropower, where a suitable site exists, is often a very cost-effective electrical energy generation option. Small hydropower can be a cost-competitive alternative for rural electrification especially for remote communities and isolated local grid, which are most prevalent in developing

countries. The drawback of small hydropower generating capacity, is that due to natural seasonal flow variations within the river system, continuous generating ability may not be possible. Therefore other generation sources may be required to ensure continuous supply during dry periods. In addition, sometimes, the variability of the load could make unstable frequency and voltage output of the small hydropower plant. Thus, they require a frequency response reserve to ensure the stability of both small hydropower plant frequency and voltage outputs in spite of varying users load. A fast-start generator could be installed as a frequency response reserve. The addition of the fast start generator will add an installation cost to a small hydro power plant. Power factor correction device are sometimes is added to the load bus or switched with the induction machines to provide a source of reactive power at the terminals of a motor or generator. This is needed to make sure that the current in the grid is enough to produce a certain power output as required. The addition of this power factor correction device will again add additional installation cost of to the small hydropower plant. In this thesis hereafter the small scale hydropower that will be discussed is in the range of micro-hydro .

In Indonesia, the amount of installed micro/mini hydro power is around ≈98.47 MW (Ketenagalistrikan 2013), whereas the potential is 450 MW (Kementrian Energi Sumber daya Mineral 2015).

There are several kinds of micro hydro power converter have been developed at this time. The development of low head hydro power converter can be divided into three groups. This ranges from water wheel technology, established technology such as modern turbine technology (cross flow turbine for example), through to novel technology such as Archimedes Screw. Most of the operation of the modern turbines technology and novel hydro power converters are sufficiently understood and supported by scientific theory. However, the novel and turbine technology for low head hydropower does not satisfactorily meet the economic and ecological requirements required by investors and authorities. To satisfy these requirements, low head hydropower technology has to be developed for head differences from 2.5 to 5m. Low-head hydropower refers to sites with a head (i.e., water surface elevation difference) of less than five meters (European Communities 2009)(Campbell 2010).

1.2 Aim and Objectives

The project aims at the development of a cost-effective and ecologically compatible solutions for a small hydropower machine which is capable of operating at head differences between 2.5 and 5 m. This machine is designed to match head differences between 2.5-5m as stated by by walter zuppinger (Delabar 1855). In addition for head differences of less than 2.5m the zuppinger undershot water wheel is more suitable. Whereas for the head differences greater than 5m, the overshot water wheel and modern turbines would be more appropriate. In this case the machine that will be investigated and developed is the Zuppingerrad water wheel which is also called as turbine wheel. The following objectives should be met in order to achieve aforementioned goals:

- Investigate the existing low head hydropower technologies and their limitations.
- Test the performance of several turbine wheels by improving the methodology of power measurement.
- Each turbine wheel is progressively modified and then the effect on the performance of the machine were investigated
- Identify the characteristics of the water wheel from the experimental results.
- Propose theory of turbine wheel.

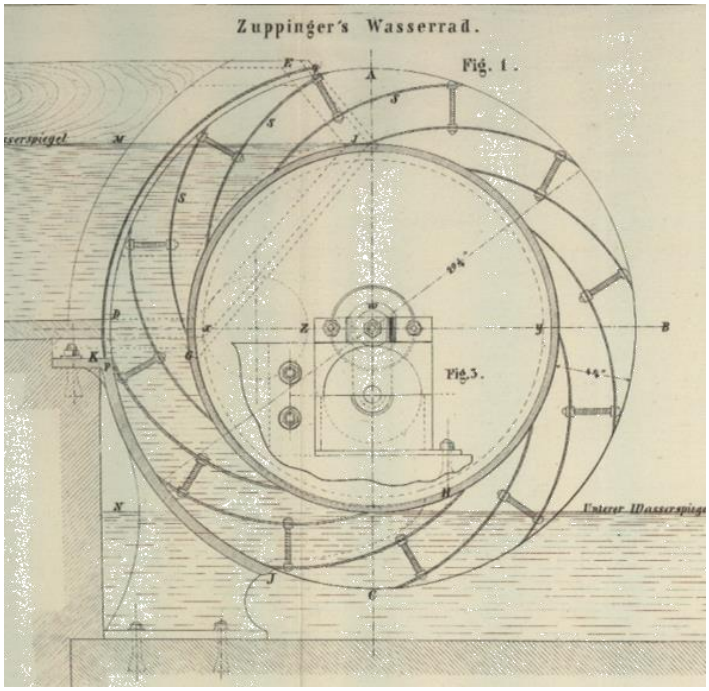

Figure 1.1:The turbine wheel from 1848 (Delabar 1855)

CHAPTER 2

LITERATURE REVIEW

2.1 Hydropower energy as a new renewable energy sources

In part 2.1 an introduction to hydropower, including the definition, the potential, and also the criteria that are needed to build water wheel will be explained. The justifications for developing low head hydropower and low flow rate are defined. In addition, some factors that are relevant to hydropower technology are discussed, including environmental issues and operational costs. In part 2.2 the current hydropower technology that exists for exploiting very low head hydropower will be reviewed.

2.1.1 Introduction to Hydropower

Hydro-power is power derived from the potential and kinetic energy of flowing water, which may be harnessed for widespread of uses. Since ancient times, hydro-power has been used for irrigation and the operation of various mechanical devices, such as watermills, sawmills, textile mills, dock cranes, domestic lifts, power houses and paint making. Since the early 20th century, the term has been used almost exclusively in conjunction with the modern development of hydro-electric power, which allowed use of distant energy sources. A typical hydropower installation is depicted in Fig 2.1. Kinetic energy of flowing water (when it moves from higher potential to lower potential) rotates the blades/propellers of turbine, which rotates the axle. The source of water in the most of cases is natural, ranging from streams flowing down mountains to rivers and canals flowing along plains. A hydropower resource can be evaluated by the availability of the power. The extracted Power P is a function of the hydraulic head H, rate of fluid flow Q, density of water ρ, the converter efficiency η, and the local acceleration due to gravity g. The power is formulated as equation 2.1:

$$P = \eta \rho_w Q g H \qquad 2.1$$

where

- P is power [W]
- η is the dimensionless efficiency of the turbine
- ρ_w is the density of water [kg/m^3]
- Q is the flow [m^3/s]
- g is the acceleration due to gravity [9.8 m/s^2]
- H is the height difference between inlet and outlet [m]

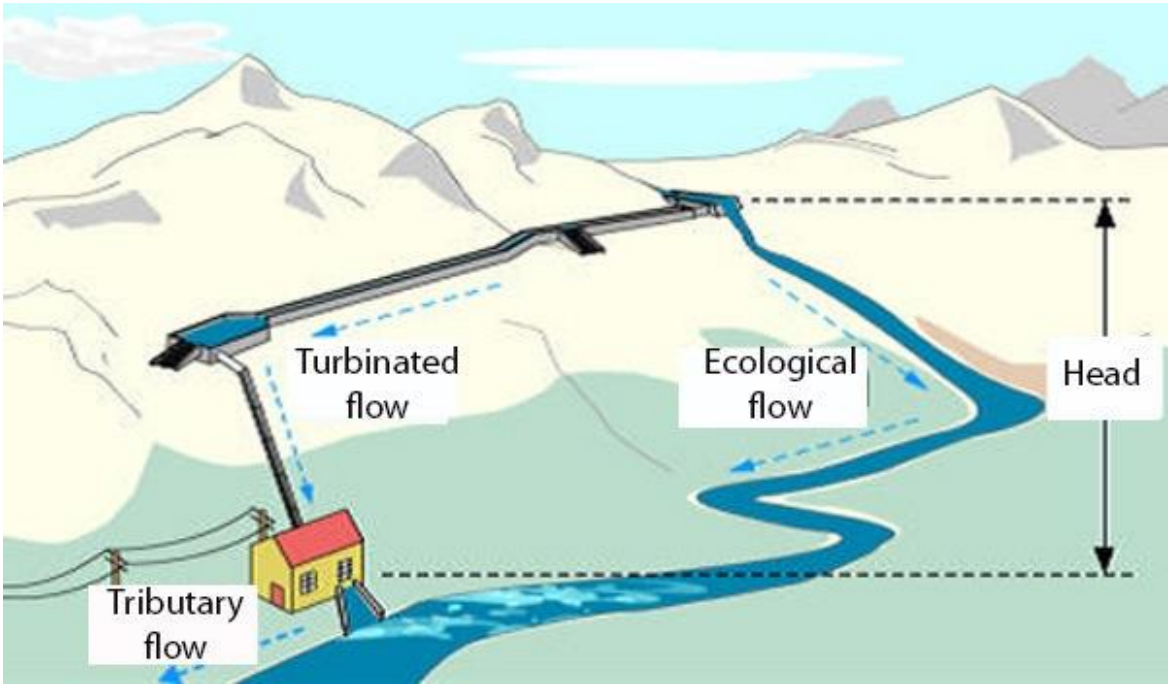

Figure 2.1:A Typical hydro power instalation (Gesthidro Recursos Hidroenergeticos 2013)

2.1.2 Potency of Hydropower

The potential energy of water in the world is very large, the gross theoretical capacity is approximately 15 720.23 TWh/yr (World Energy Council 2013) which could potentially be used. At presents, only 16.2% of the electricity generated is supplied by hydro power, whereas most of the electricity generated is currently produced by using the burning of fossil fuels such as coal and natural gas (International Energy Agency 2014), as shown in Fig 2.2.

Coal, gas, and oil are the fossil fuels responsible for most of the world's electricity and energy demands. Coal, which is readily available in most of the developing and developed world, has been used as a major source of fuel even in ancient human civilizations. However there are also some significant disadvantages of coal fired plants including Greenhouse Gas (GHG) Emissions, mining destruction, generation of millions of tons of waste, and emission of harmful substances. Like other fossil fuels, natural gas still does create carbon dioxide, carbon monoxide and other carbon compounds which are greenhouse gases that cause global warming and climate change. In addition, leaks of natural gas are tremendously dangerous. Such leaks may cause explosions or fire. When inhaled, the gas is highly toxic. The main danger is that it is odorless and leaks cannot be detected unless some odorant has been added to the gas. In the case of an underground leak, we are helpless as odorant becomes weaker and the gas leak goes undetected. Nuclear power is once again considered a prominent alternative. This is because it is now being touted as a more environmentally beneficial solution since it emits far fewer greenhouse gases during electricity generation than coal or other traditional power plants. Nevertheless, there are some disadvantages of nuclear energy that can be elaborated. Radioactive waste : The waste produced by nuclear reactors needs to be disposed off at a safe place since they are extremely hazardous and can leak radiations if not stored properly. Accidents in nuclear technology could cause massive disaster as seen by events in Chernobyl and more recently at Fukushima and the risk associated with them are relatively high. People who work at nuclear power plants and live near those areas are at a higher risk of being exposed to harmfull levels of nuclear radiation, if an accident occurs. Another practical disadvantage of using nuclear energy is that it needs a lot of investment to set up a nuclear power station. It is not always possible by the developing countries to afford such a costly source of alternative energy.

Hydropower is another source of energy. Hydropower does not pollute like power plant that burns fossil fuels such as coal or natural gas. It is a renewable resource and therefore does not cause significant depletion of water sources.

Compared to the aforementioned power generation system, hydroelectricity is much safer. There is no risk of radiation or fuel waste as occurs with nuclear power plant. Furthermore, Hydropower is fueled by water, so it' is a clean fuel source, meaning it will not pollute the air unlike power plants that burn fossil fuels, such as coal or natural gas. In addition, hydroelectric power is a domestic source of energy, allowing each state to produce their own energy without being reliant on international fuel sources. In addition, water is an energy resource which has yet to be fully exploited technically. According to the latest data that been published only about 3756 TWh/yr hydropower has been utilized (International Energy Agency 2014). Meanwhile this amount of energy is actually only about 24% of the total potential energy of the water in the world. Therefore there is still potential to increase the usage of this resource.

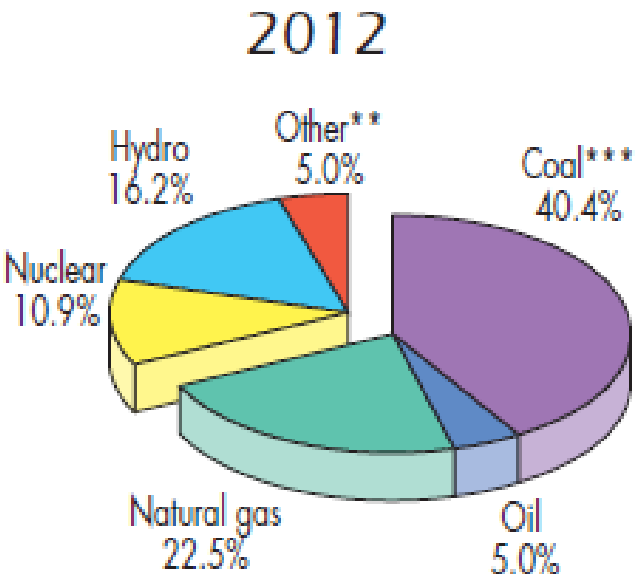

Figure 2.2:World primary energy supply in 2012 (International Energy Agency 2014)

If we look at the hydroelectric generation among several countries in the world, China is the country that utilises the most water energy, as shown in Fig 2.3. The main reason is to supply energy for industrial processes, considering the economic growth of this

country over recent years, and rankings 2nd for economic growth in the world (Hakim 2013). China needs a huge amount of cheap and clean energy to support their industry. Hydropower production cost is relatively cheaper than oil.

Geographically the spread of the potential energy of water in the world is shown in Fig 2.5. This figure shows that the Asian continent has a large enough potential energy, it is about 47 percent of the potential energy of water in the world (Pradhan 2013). However, annual hydropower production only reached 35 percent of the energy use of water in the world as shown in Fig 2.4. This suggests that in the world especially in Asian continent, water energy utilization still have opportunity to be enhanced.

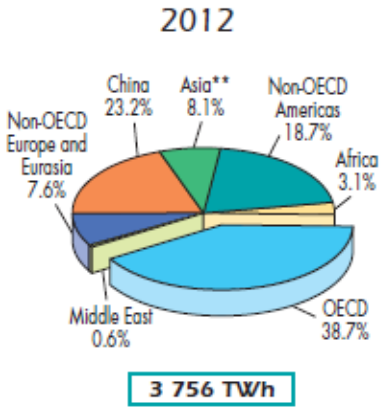

Figure 2.3:Pie chart of water energy usage for electricity among several countries (International Energy Agency 2014)

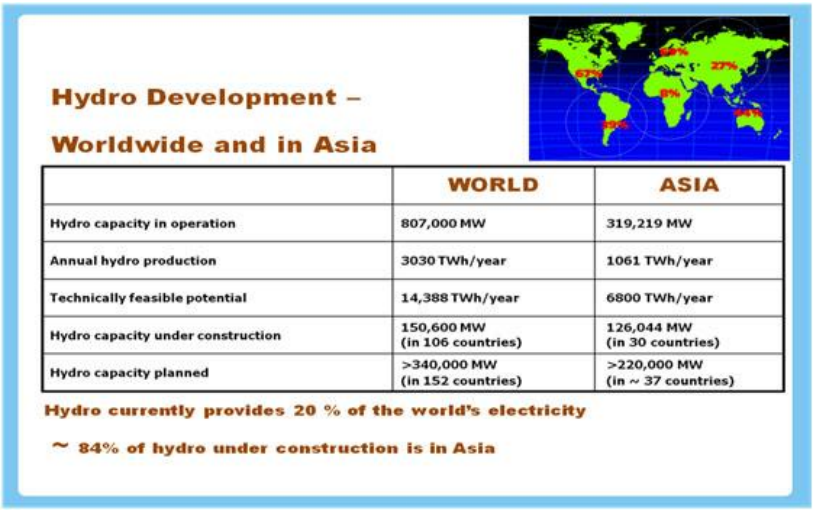

Figure 2.4:world hydraulics energy usage (Pradhan 2013)

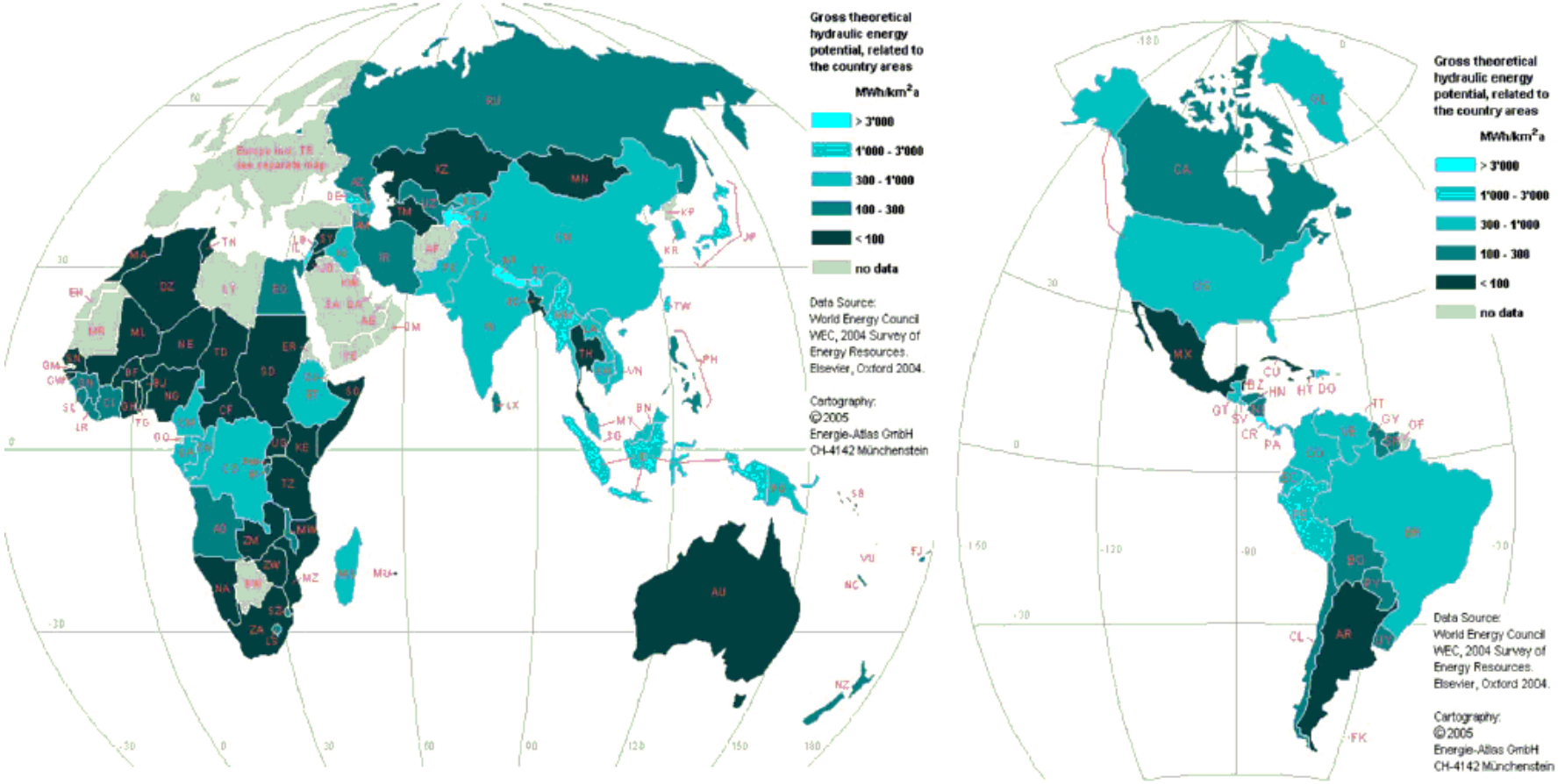

Figure 2.5:World hydraulics energy distribution(Institute Global Energy Network 2013)

2.1.3 The need for small scale hydro power technology

Referring to the explanation above, water flow has been used as a source of energy across the world. However, large hydropower account for a significant proportion of this energy generated from hydropower devices. The capacity of the generated power from large hydropower is more than 10 MW per-plant, whereas less than 10 MW is considered as small hydropower. As has been explained previously, hydropower generation incomparison to alternative forms of electricity generation offers some advantages, however there remain significant environmental and social consequences of large scale hydropower generation plant. These are as follows:

- ***Damaging ecosystem and alleviation of land***.

Construction of the dam and the creation of reservoir disrupt river ecosystem habitats and breeding cycles of fish species. Large areas of land are flooded as huge reservoirs are created, representing a loss of land which could be used for other purposes such as settlement, farming, or as a natural ecosystem.

- ***Displacement of population***.

The large amount of flooding in creating a reservoir necessitates the displacement of any people who work or live near the site of the hydropower plant. An estimated 40-80 million people were displaced around the world due to dam construction in 2008, causing loss of homes as well as loss of livelihood (International River 2008).

- ***Failure risks***.

If dams are poorly constructed or are situated in earthquake susceptible areas, they can fail causing the release of an enormous quantity of stored water, this may result in catastrophic damage to downstream settlements and infrastructure.

With the aforementioned drawbacks, it is worthwhile considering the developing of small scale hydropower technology. At the present time only a small percentage of

hydropower resources have been built for small scale hydropower plant. The statistical data that was taken from Indonesia shows that the ratio of active small hydropower site against the technical viable recoverable resources is 17.22% (Kementrian Pekerjaan umum badan penelitian dan pengembangan sosial ekonomi dan lingkungan 2011). This low percentage maybe due to the unavailablity of cheap and simple technology that could be used to utilize small scale hydropower resources. Below are detailed some justification to support the idea of building small scale hydro power plants.

- An enormous resource potentially exists if the output of all scattered small scale hydropower resources were combined.

There are a significant amounts of small scale energy sources of water which are scattered throughout the world, which if the energy was recovered from these sources then it would represent a significant amount of recoverable energy. However the existing technology for small scale hydropower is considerable complex and therefore it is unsuitable for unskill villagers who do not have requisite technical knowledge to maintain and operate highly specialized generating equipment. This is the reason, why small scale water energy sources are not fully utilized as maximum potency it has, even though the accumulation of the potential power is promising, i.e. about 500 MW (Kementrian Pekerjaan umum badan penelitian dan pengembangan sosial ekonomi dan lingkungan 2011). People in remote areas prefer to have a simple, cheap, system that can be maintained using local resources. In order to exploit this low head hydropower sources, low cost, simple and local manufacturable low head hydropower devices, i.e. water wheel need to be developed.

- Environmentally and fish friendly

Water wheel technology is one form of energy generation machine that utilises low head water resources which produce small power therefore this technology is quite favourable for small scale hydropower plant. This technology is also fish friendly due to the low rotational speed and large bucket/cell size, compared with the large scale hydropower technology, most of which are turbine based technology. Large scale hydropower technology has an adverse impact on the environment. It needs a store of water upstream (i.e.reservoir) before it is

released into the turbine. The development of this reservoir creates several problems for the environment, whereas low head hydropower technology, does not required large scale reservoir, therefore it will not create large disturbances to the river flow characteristics (Campbell 2010).

The established low head technologies can be seen in Fig 2.6, which is taken from (Senior 2009) who cited it from (Giesecke & Monsonyi 1998). This graph includes traditional waterwheels, where the head differences is less than 10m and the flow rate is less than $5m^3/s$. Indicated on the graph, is the area of demand which must be targeted if the power output and economics of very low head hydropower are to be improved. This constitutes head differences under 5m with flow rates greater than $5m^3/s$ per unit. From this figure we can see that water wheel is one of choices to fulfill the need of the low head hydropower technology.

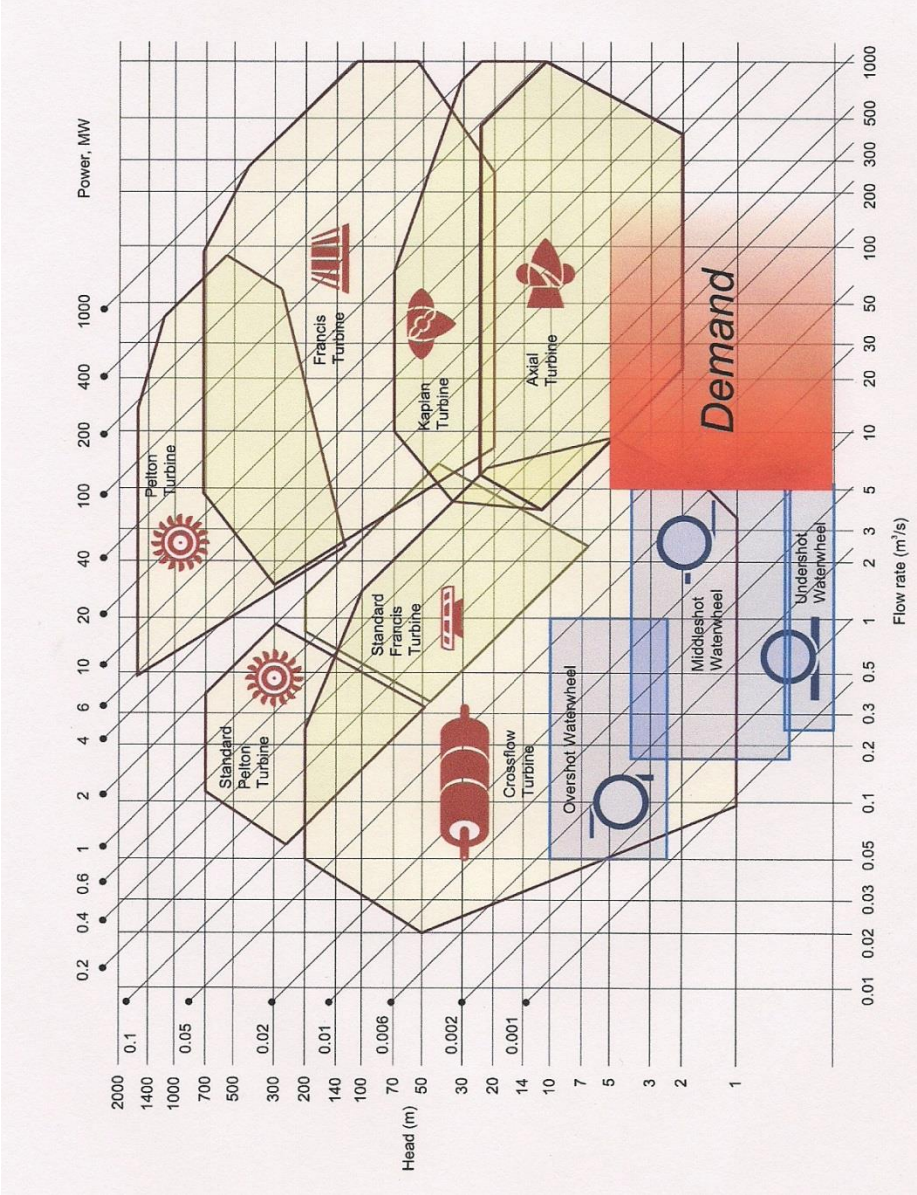

Figure 2.6:Established hydropower machines and demand for new technology, taken from (Senior 2009) ***where cite it from*** (Giesecke & Monsonyi 1998)

2.2 Existing Small Scale Hydropower Technology

In Part 2.2, all of the relevant low head technologies which are already in existence will be discussed. This is classified in three groups of technologies, which are water wheel technology, turbine technology and novel technology. The review will go through technical

aspects, which consists of power, the heads, flow rates and efficiencies of the machines. Moreover the principle of operation of each machine will be discussed. These describe the fundamental principles behind how each machine exploits the hydraulic power of the water, converting it to mechanical power. This chapter concludes and leads to the need of low head hydropower technology.

2.2.1 Water Wheel Technology

The knowledge on how to gain energy from flowing water has been understood for 2000 years, by several scientists, engineers and mathematical experts, such as Da Vinci, Smeaton and Bernoulli as documented by (Smith 1976). Investigations of water wheels started before there was a significant understanding of hydraulics or energy theory. This is reflected from the fact that Antoine Parent (1666 –1716) a French mathematician proposed his jets theory which limited the hydraulic efficiency of all waterwheels to just 14.8%. This claim by Antoine Parent was proven mathematically incorrect and not applicable to all types of waterwheel by John Smeaton in 1756. John Smeaton explained fundamental differences and benefits of overshot versus undershot water wheels. He published experimental data which concluded that undershot were no more than 22% efficiency whereas overshot were 63% efficiency (Denny 2004) who quote from (WaterWheels 98AD) and (Smeaton 1759). As time progress theories and manufacturing methods of accepted waterwheel designs neared perfection. In the 19th century efficient hydraulic turbine were developed which superseded water wheel technology at that time and waterwheel development effectively ended (Denny 2004).

Water wheels are classified by the way in which water is applied to the wheel, relative to the wheel's axle. These are the undershot, overshot and middleshot (or breast-shot) waterwheels.

1. Undershot water wheel

An undershot wheel (also called a *stream wheel*) is a vertically mounted water wheel that is rotated by water striking paddles or blades at the bottom of the wheel. This water

wheel type can be used for very small head differences, ranging from 0.5-2.5 m, and flow rates in the range of 0.5-0.95 m^3/s per m width (Müller & Kauppert 2004). This type of wheel was originally used as an impulse wheel, which employs kinetic energy. The name *undershot* comes from water striking the blade at the bottom of the wheel. Traditional undershot waterwheels consist of a series of flat blades fixed to the rim of a wheel. The blades were typically mounted so they faced straight out along the radius of the wheel. When water from the mill stock flowed past the wheel, it hit the blades, and some of its momentum was transferred to the wheel. However, much of it was also reflected off the blade and lost as heat. This process was not efficient; much of the original velocity in the water remained in it, meaning that potential energy was not being captured. Typical undershot wheels were around 30% efficient (Reynolds 2002). This water wheel is depicted in Fig 2.7.

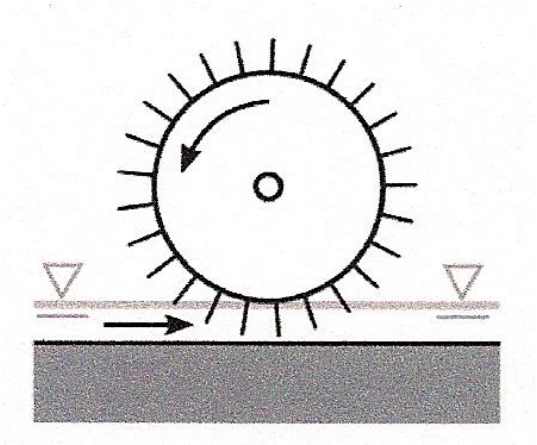

Figure 2.7:Undershot water wheel (Senior 2009)

The design of the traditional undershot water wheel was improved by Jean-Victor Poncelet who replaced the straight blades on ordinary wheels with curved or cylindrical blades. His design used curved blades positioned so the water met the blade flat to its edge instead of the side. This eliminated the "bounce" that robbed power from typical design of the time. He estimated that practical wheels would reach efficiency between 70 -85% (Schobert 2002). The picture of the Poncelet water wheel is presented in Fig 2.8

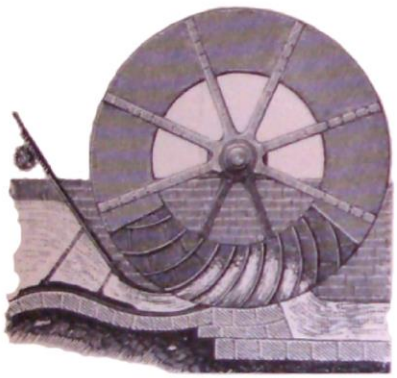

Figure 2.8:Poncelet water wheel (Brockhaus 1903)

Walter Zuppinger a Swiss hydraulic engineer designed another type of undershot water wheel, which was believed to be the most efficient water wheel. He proposed a new design the Zuppinger undershot waterwheel. This had curved tips on the blades which would exit the water more vertically and therefore more cleanly. These machines had efficiencies up to 77% (Müller & Kauppert 2004). The working principle of Zuppinger water wheel is shown in Fig 2.9

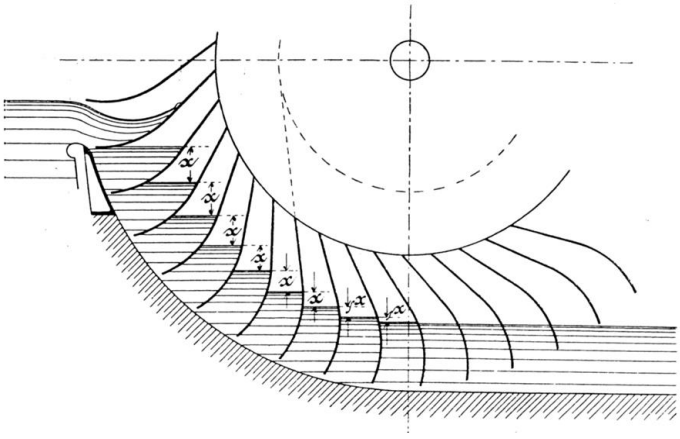

Figure 2.9:Working principle of Zuppinger water wheel (Müller 1899)

A further development of undershot Zuppinger is known as very low head Zuppinger water wheel. The specific flow volumes range from 1.0 to 1.2 m^3/s per m width with power ratings from 5.3 to 12.8 kW/m width. This water wheel designed for very low head, about 0.7-1.5 m

which has efficiencies up to 75%. (Bozhinova et al. 2012). The very low head Zuppinger water wheel is shown in Fig 2.10.

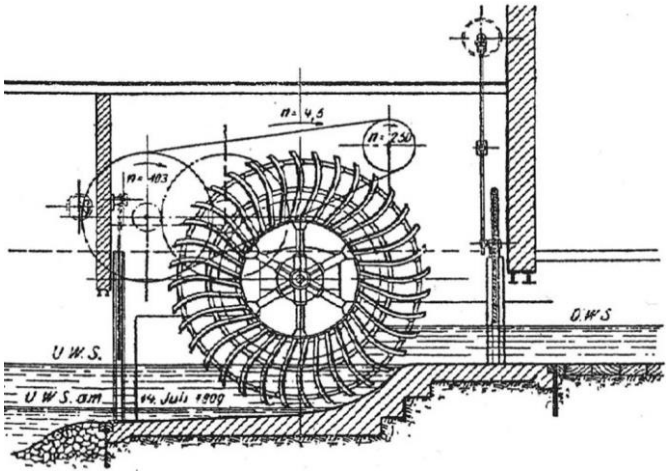

Figure 2.10: The very low head Zuppinger water wheel(Müller 1899)

2. Breastshot water wheel

Breastshot is another type of water wheel where the water enters the wheel approximately at the level of the central axis. This wheel type was used for head differences of 1.5-4 m, and flow rates of 0.35-0.65 m^3/s per m blade width (Müller & Kauppert 2004). This type of water wheel reached efficiencies of up to 80-85%, compared to typical undershot wheels which have efficiency of approximately 30% (Reynolds 2002). A typical breastshot water wheel installation would consist of a weir in the main river, which generates a head difference, an intake structure, the mill race, the water wheel itself, and finally the tail race which leads the water extracted from the river back to its source (Müller & Wolter 2004). A typical type of breastshot is shown in Fig 2.11

Alphonse Sagebien a French hydraulic engineer in 1848 also proposed another type of breastshot water wheel. The Sagebien wheel had the water enter through a channel, the water could enter the wheel effectively horizontal as the blade was angled downwards to achieve smooth inlet flow. The inside of the wheel was open, so the water could flow up into the

channel without the air pressure building up and impeding the flow. The water flowed back out again after a short time, the wheel turning perhaps 30 to 45 degrees, into the lower tailrace. The Sagebien water wheel is shown in Fig 2.12. This Sagebien waterwheel, is appropriate for small water flow rate, this allow the water wheel to rotate at a slow speed. This machine is noted has the efficiency in the range of 80-90%, with the diameter of 11 m and 6 m wide with the power output 125 Hp (93.2 kW) and 4.6 m^3/s (Le Moulin XII 2015).

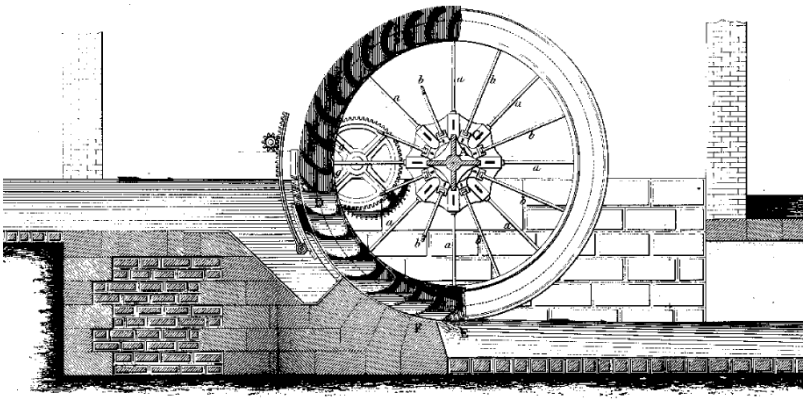

Figure 2.11:A typical Breashot water wheel (Fairbairn 1849)

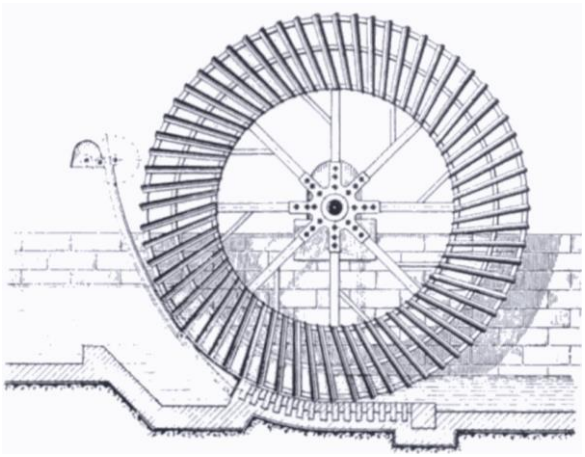

Figure 2.12:Sagebien water wheel (Reynolds 2002)

Figure 2.13:A typical Sagebien water wheel (meauxfiles 2015)

3. Overshot water wheel

A vertically mounted water wheel that is rotated by falling water striking paddles, blades or buckets near the top of the wheel is said to be overshot. This water wheel was employed for head differences of 2.5-10 m, and flow rates of 0.1-0.2 m^3/s per m blade width. A typical overshot wheel has the water channelled to the top of the wheel. The water collects in the uppermost buckets just off centre, making it heavier than the other "empty" side. The weight turns the wheel, and the water flows out into the tail-water when the wheel rotates enough to invert the buckets. Fig 2.14 is an example of overshot water wheel with a sluice gate.

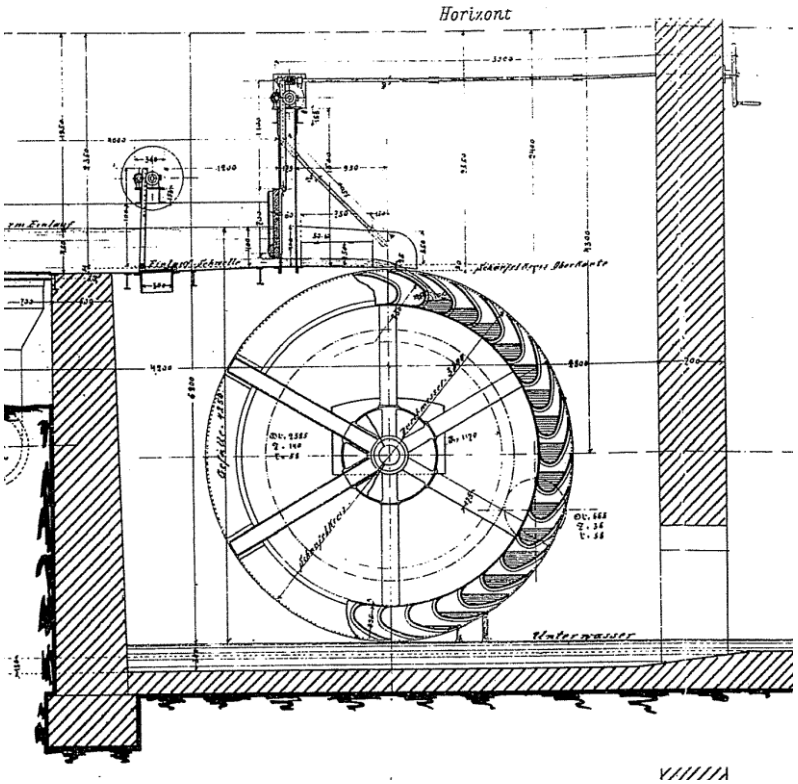

Figure 2.14:A typical overshot water wheel (Müller 1899)

The water can enter each cell at its natural angle of fall, by forming the cells in certain curvature. Fig 2.15 shows the efficiency of overshot water wheels from three reported test as a function of the ratio of actual flow rate Q and design flow rate Q_{max}. The graph shows a consistent result, whereas the efficiency is constant at certain flow rate, mostly above 80%. Even for small flow rate (let say Q/Q_{max}=0.2) the efficiencies remains at a constant value.

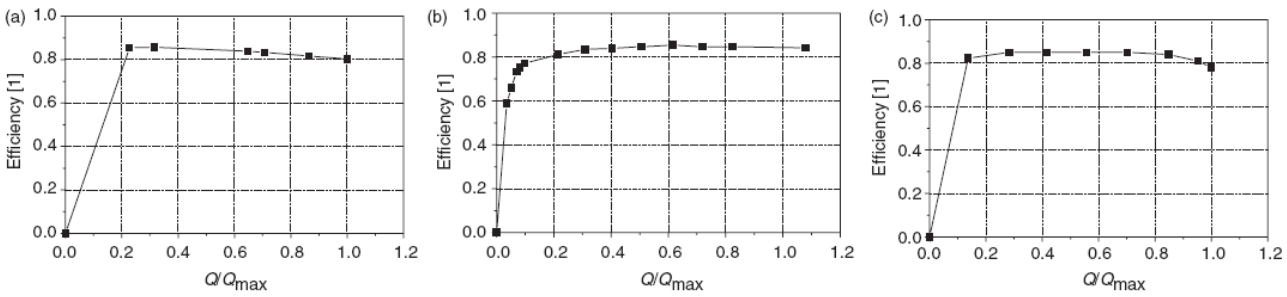

Figure 2.15:Measured efficiency curves for overshot water wheels(Müller & Kauppert 2004) ***(a) Efficiency of a 3.054m wheel quoting from***(Weidner 1913b)(Weidner 1913a)***; (b) efficiency of a 3.60m wheel quoting from*** (Staus 1928)***; (c) efficiency curve for a 3.60m wheel at 9.0 rpm quoting from*** (Meerwarth 1935)

4. Zuppingerrad water wheel/turbine wheel

Walter Zuppinger is known as the Swiss engineer who improved the undershot water wheel design, with efficiency values as high as 77%. In 1848 he patented another turbine-like water wheel to operate with head differences between 2 and 5 m. This wheel was designed to bridge the gap between low-head water wheels, and overshot water wheels (H = 2 to 5 m, Q = 1 to 10 m^3/s) (Delabar 1855). With this flow rate and head, this type of water wheel could achieve efficiencies as good as the overshot water wheel. This machine is called a zuppinger water wheel, zuppingerrad water wheel or a turbine wheel. Hereinafter in this thesis, this machine is called a turbine wheel. The turbine wheel that was designed for this range of head is presented in Fig 2.16. A turbine wheel model test with an outer diameter 755.65 mm, hub diameter was 539.75 mm and two side blades with a width of 120.65 mm has been reported by (Delabar 1855). This turbine wheel worked well, with efficiency in between 75-80% .

This machine consists of a central hub which also acts as a weir and of curved blades somewhat similar to those of an overshot. The outflow occurs within the downstream water level. From a current point of view, this wheel with its simple construction (without any components below the water level) and the possibility to process large volumes of water over an appreciable head difference, could be employed for head difference of 2-5 m. A theory is mentioned in the literature, but was apparently never published. No measurements, or indeed, actual constructions of such a wheel are reported. There is very little available published

literature which elaborates or discusses this turbine wheel. To the author's knowledge, all previously discussed wheels with the exception of the turbine wheel have been built and tested at full scale.

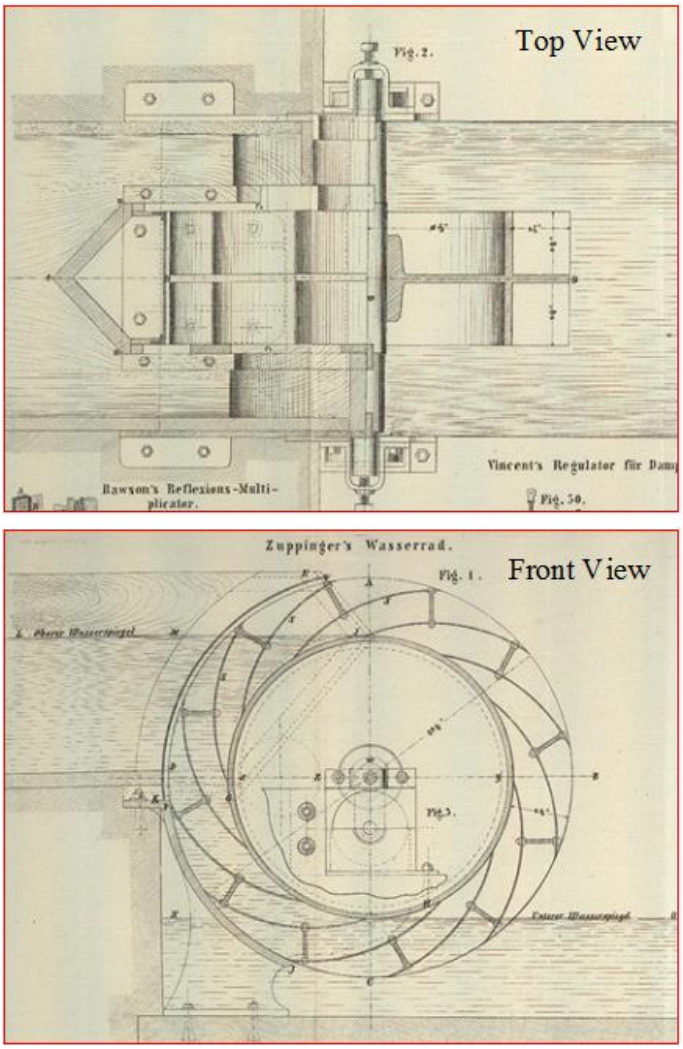

Figure 2.16:The top view and front view of Zupingerrad water wheel from 1848 (Delabar 1855)

2.2.2 Turbine Technology

A French engineer Benoît Fourneyron built the first commercial water turbine in 1827. He designed a turbine in order to fulfil the need for more power, as at that time the

industrial revolution encouraged engineers to build new machine to generate huge power. In subsequent years, scientists and engineers undertook research to develop turbines that were more efficient and capable of generating higher power output. The advantages of turbines have led to the more wide spread use of turbine instead of water wheel as power generator machine. Current technology allows sophisticated turbine design, such as the Three Gorges Dam in Hubei (China) where each main water turbine can generate a power output of 700 MW. Turbine design is relatively compact, efficient and having the capability to process large flow rates and generate large power outputs. Most of the turbines are operated for large power generation with either large flow rate or high head differences. However there are two type of turbine technology which can be employed in a small scale hydropower source i.e. Cross flow turbine and Kaplan turbine.

1. Cross flow turbine

A Cross flow turbine is basically grouped as an impulse turbine, as it is converting potential energy via a high pressure supply pipe, to kinetic energy and then the flow of water hits the blade. Similar to the principle of water wheels, the water is admitted at the turbine's edge. The guide vane imparts a rectangular cross-section to the water jet. This flow through the blade ring of the cylindrical rotor, first from the outside inward, then after passing through the inside of the rotor and out again. This flow arrangement also has the advantage that in practice leaves, grass, which when the water enters is pressed between the rotor will then be flushed out again by the emerging water – assisted by centrifugal force– after half a revolution of the rotor. The cross-flow turbine is a low-speed machine that is well suited for locations with a low head but high flow. One of the companies which manufacture this type of turbine is Ossberger. This machine can be either in Crossflow Inflow horizontal or Crossflow Inflow vertical. The company claims that this turbine can be employed with head H ranges between 2.5-200m and flow rate Q 0.04-13m^3/s, with power output 15-3000 kW. The water flows on this machine is sketched at Fig 2.17.

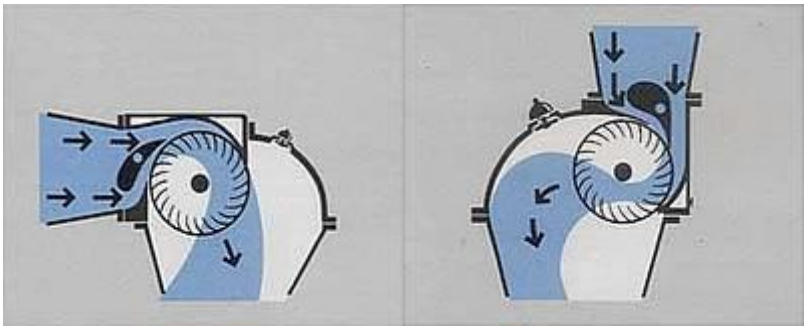

Figure 2.17:Water flow at Crossflow Inflow horizontal and Crossflow Inflow vertical (Water 21 2011)

Since for small scale hydropower, the water supply can be quite variable, the Ossberger is built as a multi-cell turbine, so this machine can always reach its optimum efficiency. The efficiency of this machine could reach 86% as demonstrated in Fig 2.18. Fig 2.18 shows an Osberger machine which consist of three series arrangement of blade in order to optimize the efficiency of the machine, the amount of water that will be expanded to the machine can be varied, depending upon the availability of the water. At a low flow rate for example 30% of the designed flow rate, in order to achieve 85% efficiency, one series of blade is used. Whereas when the availability of the water reaches the maximum designed flow rate, then all the blades can be operated to achieve 85% efficiency.

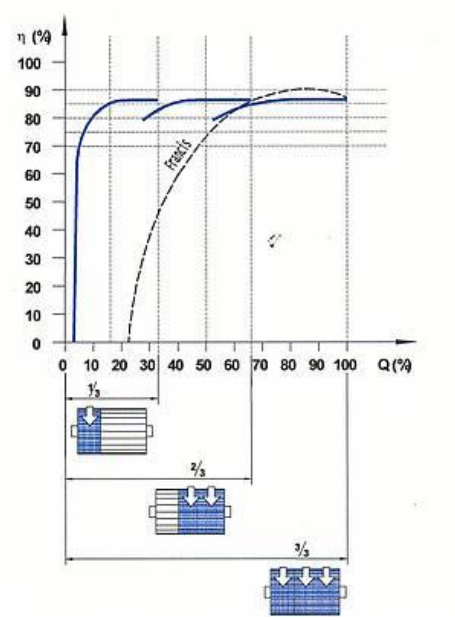

Figure 2.18:Efficiency characteristic of an Ossberger turbine developed from the 3 efficiency curves of ossberger machine, compared with the Francis turbine.(Water 21 2011)

The efficiency curve above clearly illustrates the advantages of the Ossberger turbine in the partial load range. A comparison against a Francis turbine shows that the Francis turbine offers high peak efficiency, however it only works well in narrow range of water flow rate.

2. Kaplan turbine

This turbine is developed by Austrian engineer Victor Kaplan in 1915. The Kaplan Turbine is of the reaction type where the runner is fully submerged and operates under pressure differences between two blade surfaces. At the inlet the water is entering the runner through spiral casing which directs it by using guide vanes, passing through the runner and finally exiting the turbine after passing its energy to the generator. The water flows in parallel down the turbine shaft and impinges on the fully admitted runner blades, where the flow is reduced further. The units are designed specifically in order to prevent cavitation by using draft tube. A draft tube at the end of the turbine increases the pressure of the exiting fluid at the expense of its velocity. This means that the turbine can reduce pressure to a higher extent without fear of back flow from the tail race. Moreover, it also converts the wasteful kinetic

energy at the exit of the runner into useful pressure energy. Water flow is regulated by adjustable guide vanes. An example of a Kaplan turbine with couple generator is shown in Fig 2.19.

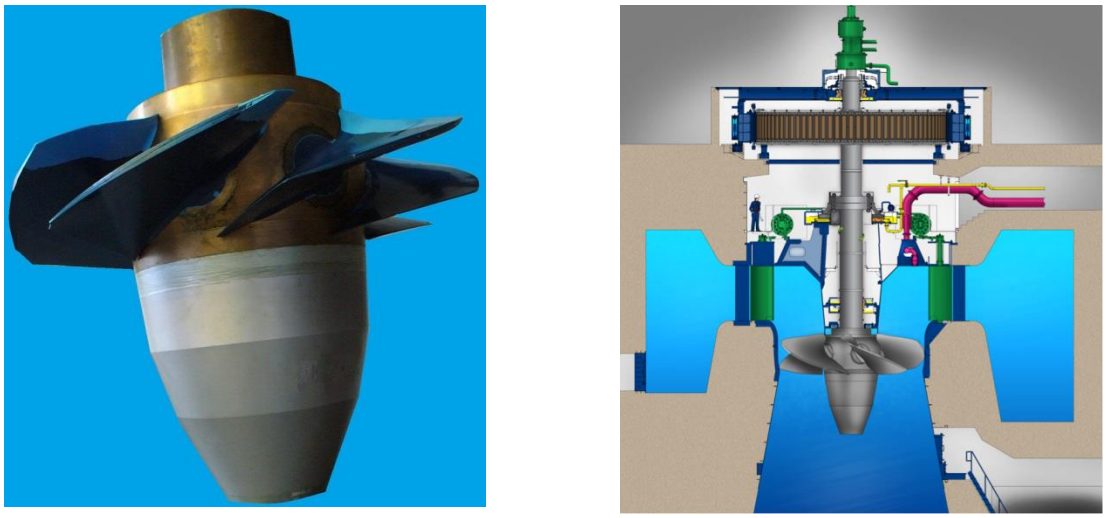

a **b**

Figure 2.19: (a) an example of Kaplan turbine ((Hydropower Generation 2016) (b) A typical vertical-Kaplan turbine with generator (Misoury river 2016)

To achieve optimum efficiency at varying flows, the runner blades and or wicket gate are adjustable. Ossberger is one of the manufacturer of this turbine, claim that this turbine can be employed at low head (1.5-15 m) and wide range of flow rate (Ossberger 2014). Performance of Kaplan Turbine mostly depend on the flow rate, however for double adjustable blade and gates, the performance of the Kaplan turbine is almost constant about 90% as shown at Fig 2.21.

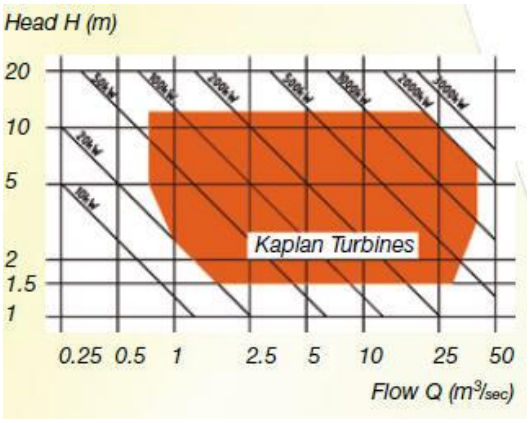

Figure 2.20:Kaplan turbine selection chart(Ossberger 2014)

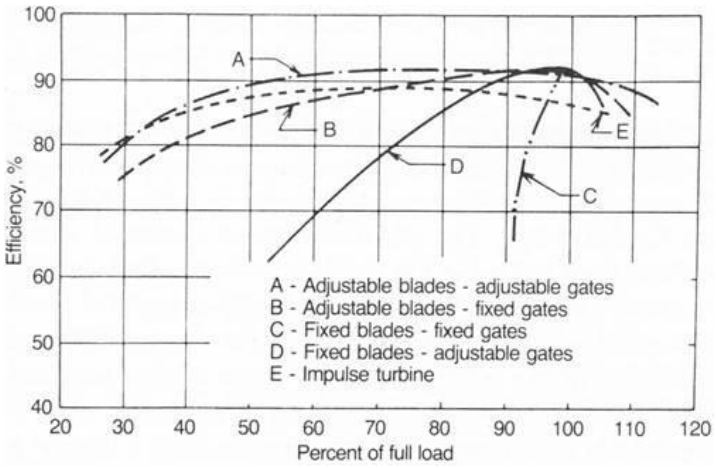

Figure 2.21:The efficiency of the Kaplan Turbine (Lars Fjærvold 2012)

There are several variations of the Kaplan turbine, these variations are described below:

- **Bulb Turbine**

The bulb turbine is designed into a water delivery tube. A case which looks like a bulb is installed in the centre of the water pipe. This case encapsulates the generator, wicket gate and runner. The water from the reservoir flows through the bulb head and then enters into the turbine along the passage between the outer wall of the bulb body and the powerhouse

concrete. The guide vane spindles are normally inclined to 60^0 in relation to the turbine shaft and thus results in a conical wicked gates that cascade which is different to the other types of turbines. The runner of a bulb turbine may have different numbers of blades depending on the head and water flow. The bulb turbines have higher full-load efficiency and higher flow capacity as compared to others Kaplan turbines. It has relatively lower construction costs. The bulb turbines can be utilized to generate electrical power from fast flowing rivers. Bulb turbines are the best choice for exploitation of tidal power and hydraulic power with extremely low heads with extremely large flow rates. It has high specific speed and high efficiency, and needs less excavation in civil works. This machine can be exploited in the range of 2 to 18m in water head, with power output of 50KW to 30MW (Chongqing Hydropower Equipment Co. 2016). Fig 2.22 shows a typical bulb turbine instalation.

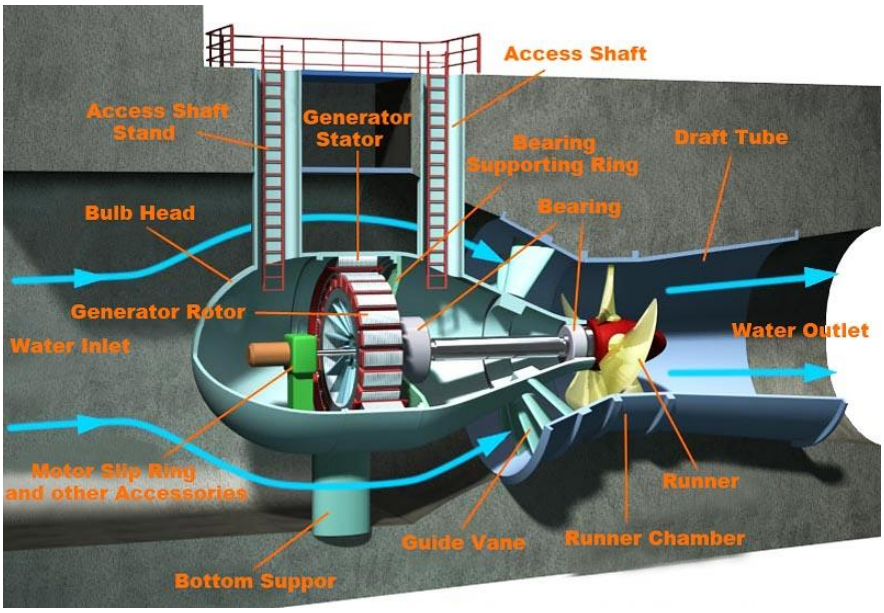

Figure 2.22:Bulb turbine instalation (Eternoo Machinery 2016)

- **Pit Turbine**

Pit turbines are similar to bulb turbines in that all the mechanical components which are located upstream of the runner. Bulb units are only available in larger diameters, and the

existence of the bulb needs a bigger installation area, whereas a pit type unit is more preferable in the case of smaller installation area. This type is a bulb turbines with a gear box which can increase the rotational speed of the machine. This allows for a smaller generator and bulb. The fitting of a gearwheel between the turbine and the generator provides the possibility of selecting a generator with a higher speed. The pit configuration has the advantage of easy access to all the equipment components, in particular the coupling of turbine and speed increaser/gear box, and the generator. A pit installation has an open-topped bulb, permitting far easier access to the generator. This facilitates inspection, maintenance and repair. Pit turbines are frequently favored for economic solutions in small hydro applications in the head range of 1.5 to 10 m unit capacity below 15MW. A typical installation is shown in Fig 2.23.

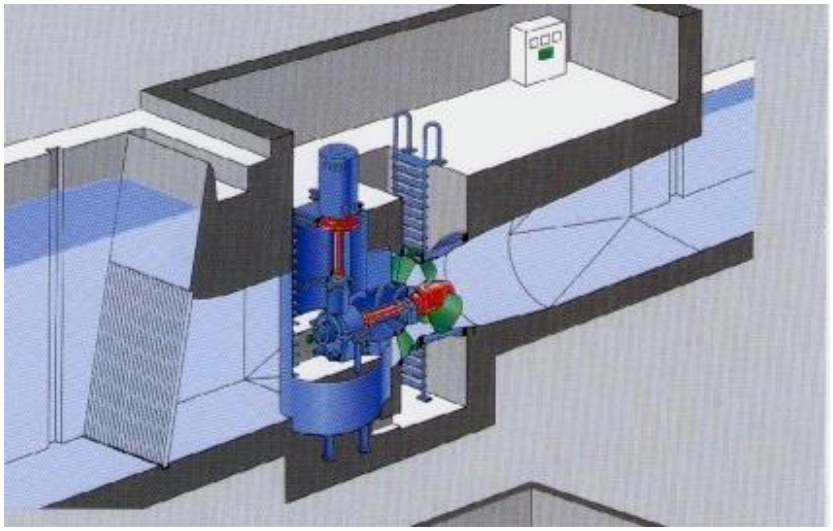

Figure 2.23: Horizontal axis pit Kaplan turbine with right-angle gear driven generator (J. L. Gordon 2003)

- **S type Kaplan Turbine**

In order to eliminate the need for bulb housing, the generator of the S type kaplan turbine is placed outside of the water channel. This is accomplished with a bend in the water channel and a shaft connecting the runner and generator. The generator is situated outside of the tube. The turbine shaft passes out of the tube at the point where the tube changes direction. The propeller usually has three to six blades, and the water flow is regulated by wicket gates just upstream of the propeller. This turbine is characterized by high efficiency in a broad band of flow rates. S-type tubular turbine is applicable in the range of 3.5 to 25m in water head, and power output of 50KW to 15MW, with 0.4 to 5m in runner diameter. In order to optimize the efficiency of this machine, the guide vane and the blade angle is adjustable, which is called the double regulation Kaplan. This turbine is suitable for certain run-of-river generating stations where the flow varies considerably. Fig 2.24 shows a typical S type Kaplan turbine.

a b

Figure 2.24: (a) An instalation of the S type Kaplan Turbine (Chongqing Hydropower Equipment Co. 2016) (b)cross section of an S-turbine and generator(voith hydro 2016)

- **Compact Axial Turbine (CAT)**

This turbine is a double regulated vertical axial turbine. The distributor consists of a conical guide vane and runner in which the blade angle can be adjusted. The water passage passes the intake elbow where the stay vanes and the conical guide vanes (distributor) are located. The deflector conical guide vanes are adjustable to enable the efficient operation by directing water to the runner blades. The runner consist of four to six blades, which can also be regulated. Below the runner, there is a relatively short conical diffuser with an elbow and a square-sectioned draft tube. This machine is a compact machine and appropriate for net heads ranging from several meters up to more than 30 m and discharges from 6 up to 85 m^3/s. The turbine output power range spans from 0,5 MW up to 20 MW. Fig 2.25b shows typical cross section through powerhouse and water passage with inlet conduit, the CAT turbine, draft tube and an independently placed generator.

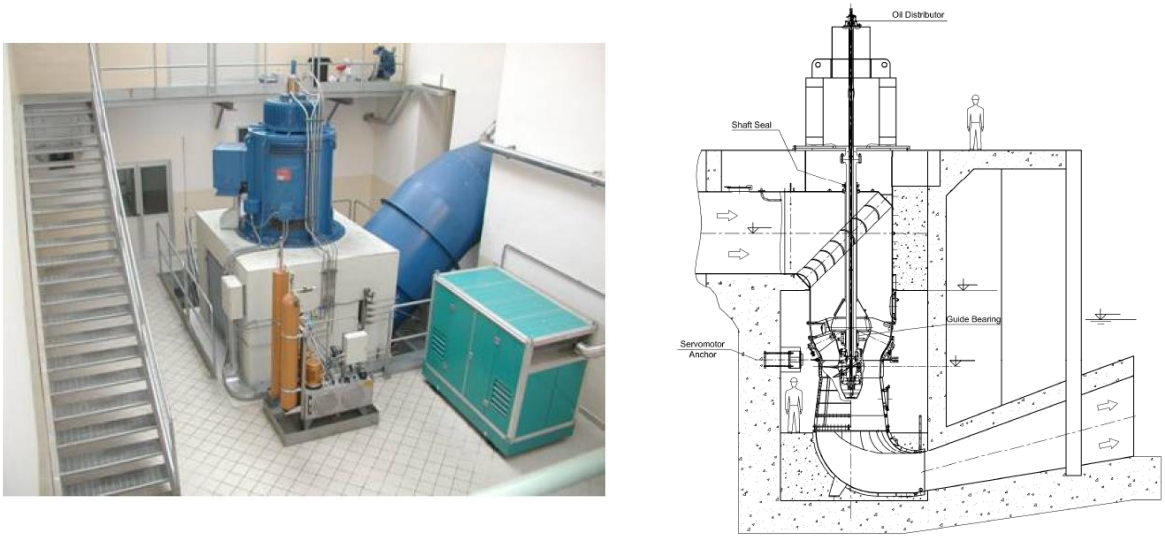

a b

Figure 2.25: (a) A typical Compact axial turbine (Andritz vatech hydro 2008) (b) cross section view of the compact axial turbine (J. Gale, E. Höfler 2010)

- **Siphon-Turbine**

The word siphon refers to a tube which is formed like an inverted 'U' shape. This shape causes a liquid to flow upward, reach the surface of a reservoir, with no pump application, but powered by the fall of the liquid as it flows down the tube under the pull of gravity. The water then discharges at a level lower than the surface of the upstream reservoir where the water came from.

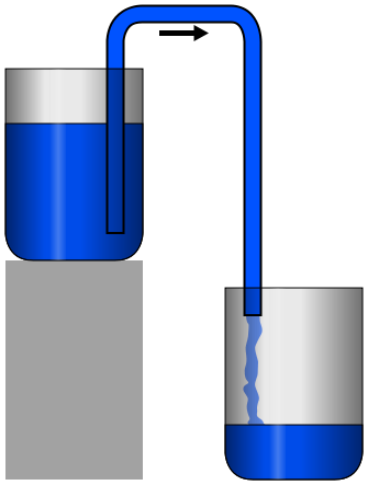

Figure 2.26: Siphon principle

The siphon turbine consist of a propeller just like other variants of the kaplan turbine. The interesting feature is the water flow which turns the turbine occurs by utilizing this siphon concept. The turbine works starting with a vacum pump that evacuates the required quantity of air from the upper space in the spiral casing. The water is then directed to the runner after passing the turbine stay-vanes. The blades of the Kaplan runners are adjustable to make optimal exploitation of available flow. As water flows to the runner, the turbine begins to turn, and the generator is rotating. The water then flows to the draft tube which exits downstream.

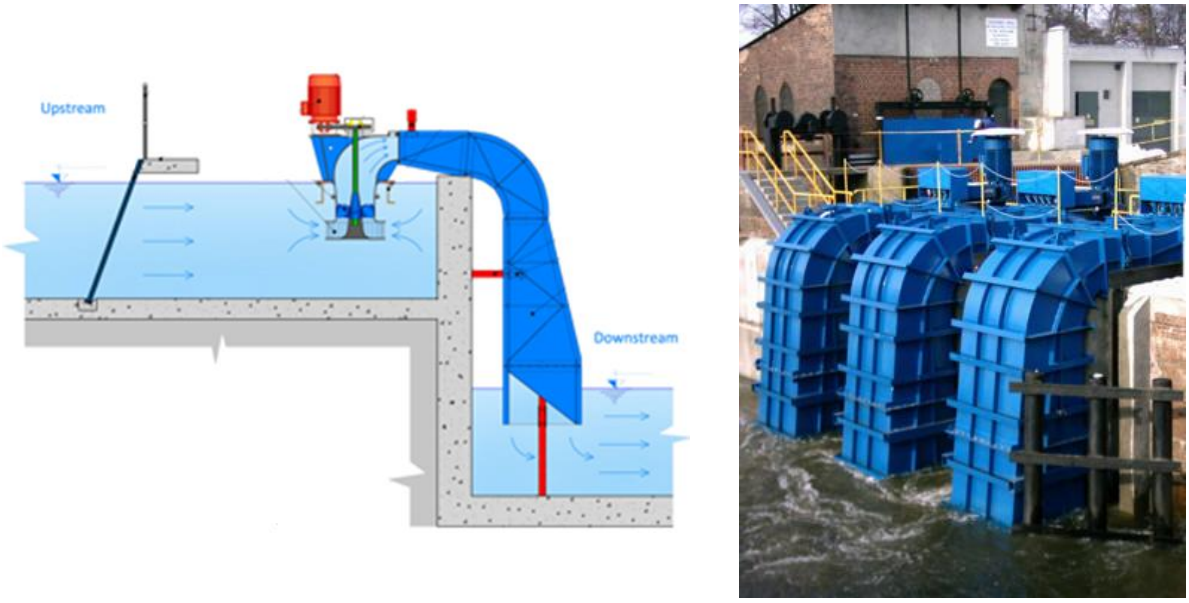

a ***b***

Figure 2.27: (a) A siphon turbine concept (Mavel 2016) (b) a typical sample of siphon turbine(Pioneer systems 2016)

Turbine plants with a siphon can directly utilize irrigation canals and rivers with a very low/ ultra-low head (h <3 m) with the power output in the range of 5-100 kW (Widhiatmaka 2010).

- **Dive-Turbine**

The DIVE turbine is a turbine for low head drop (2 to 25 m), with an installed capacity of 50 to 1300 kW per turbine. The compact unit, consisting of turbine and generator, runs completely submerged under water with a unique sealing system that needs no maintenance and is not subject to wear and tear. It is operated with variable speeds and noise free. The direct connection of the high efficiency permanent magnet generator and the turbine runner - without mechanical transmission - offers several advantages, which considerably reduces the expense of building the power plant as a whole and minimises the operating risk and costs during operation. The DIVE turbine is also capable of integrating into an ecological power plant with little trouble, which enables the requirements with regard to fish protection and ecological concern to be fulfilled. Fig 2.27a shows a schematic of the dive turbine, whereas fig 2.27b shows a typical instalation of dive turbine.

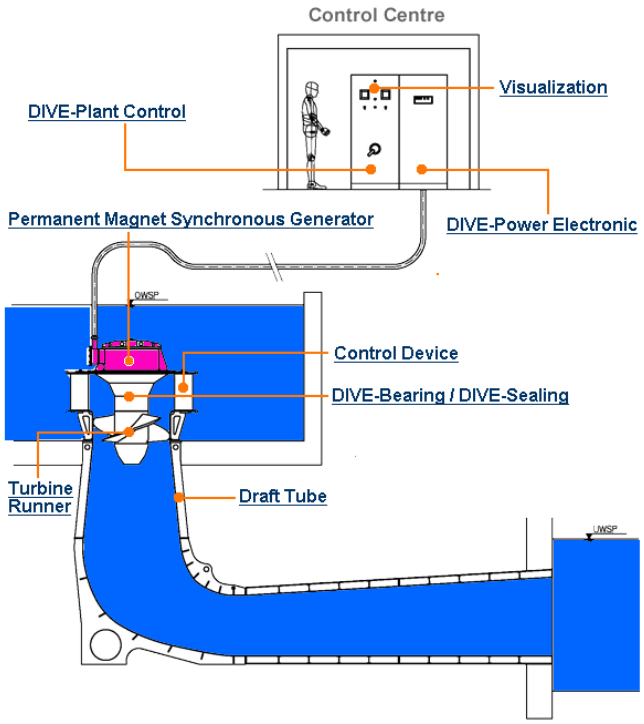

a ***b***

Figure 2.28: (a) A schematic of dive turbine (Dive turbinen 2016a) ***(b) a typical sample of dive turbine*** (Dive turbinen 2016b)

3. Francis turbine

Francis turbines are the most common water turbine technology in use today. This machine was invented by James B. Francis in Lowell, Massachusetts. In the modern Francis turbine, the water enters the runner of the turbine in the radial direction at outlet and leaves in the axial direction at the inlet of the runner. When water enters the runner, it creates pressure differential between the two sides of the blade, and this pressure differential generates a lift force which rotates the runner. In addition, when water leaves the runner axially, it hits the blade surface which generates an impulse force which also rotates the runner. Thus the Francis turbine is called mixed flow turbine, since water enter the runner radially and produce power through a reaction force and leaves the runner axially and produces power through an

impulse force. The runner is sitting inside a scroll casing. The runner vane is used to control the flow rate of the water and to synchronize power output with power demand. The draft tube position is on the exit side of the turbine. The design criteria for the draft tube is critical, because low pressure in the outlet side can generate cavitation, which is a serious problem. The drawing of typical Francis turbine as shown at Fig 2.29.

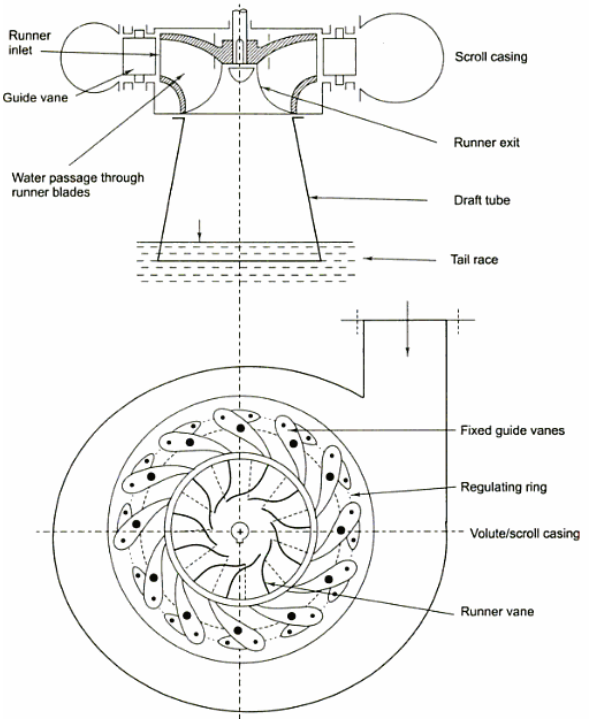

Figure 2.29:a typical Francis turbine (Gupta 2006)

This machine generally produces power in the range of 100 KW to 1 GW, with head difference from 10 to 650 m. Though for open flume Francis turbine installations the water head may be lower, between 1 and 10 m, as shown in Fig 2.32. An open flume Francis turbine is a hydropower machine in which the required head is lower than 10 m. Most low head mill sites started with water wheels and changed to water turbines as more power and higher shaft speeds were required to drive modern machinery and generators. These turbines were installed with vertical power shafts to get equipment above flood levels in open flumes beneath the mill (see Fig 2.30). In cases where only the weir remains, simple open flumes can be built from poured concrete or vertical corrugated steel tubes.

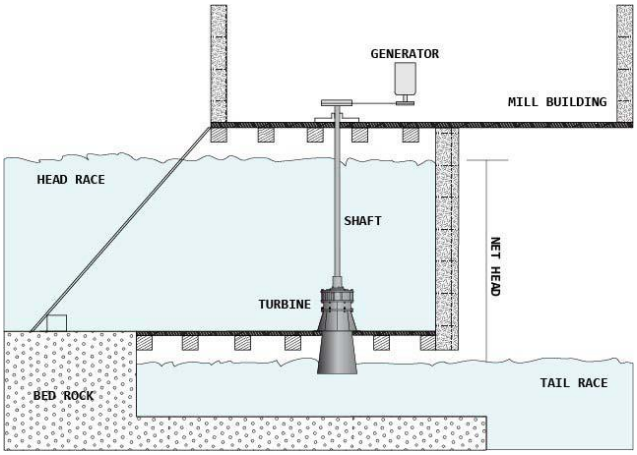

Figure 2.30: Open flume Francis turbine (Nautilus LLC 2012)

The max efficiency of Francis turbine can reach 90% as shown in Fig 2.31. Francis turbines are almost always mounted with the shaft vertical to keep water away from the attached generator and to facilitate installation and maintenance access to it and the turbine.

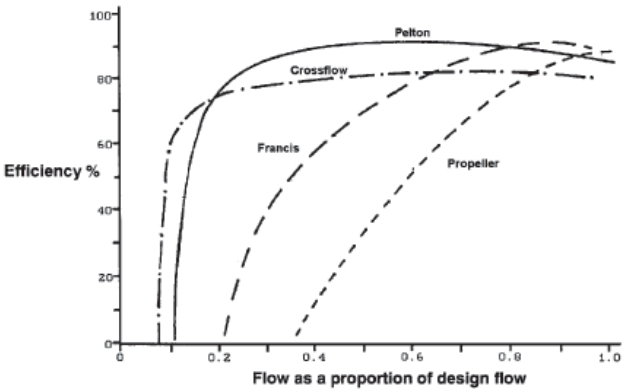

Figure 2.31:Part-flow efficiencies of several turbine (Paish 2002a)

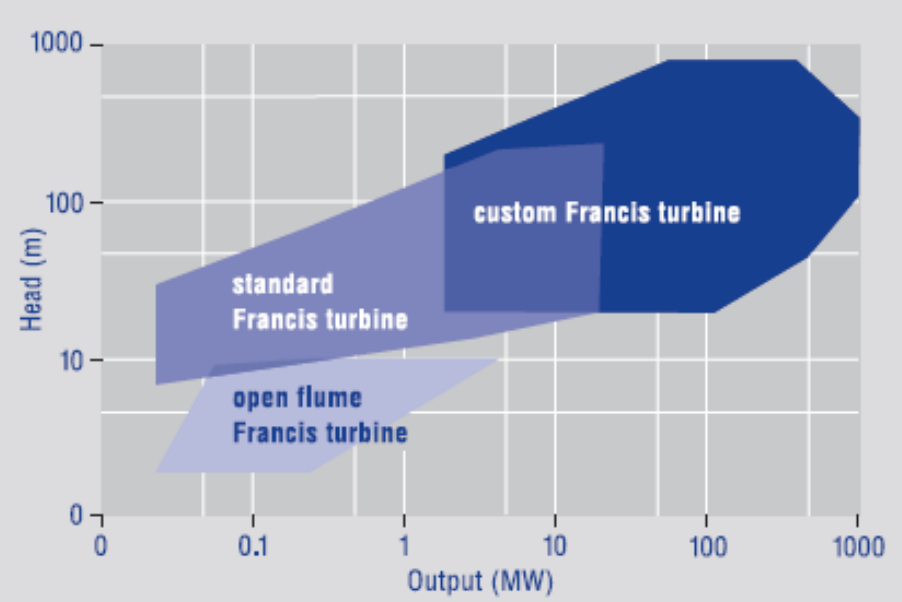

Figure 2.32:Application Range of Francis Turbine(Hydro 2009)

4. Pump as turbine

A pump-as-turbine (PAT) is running a pump in reverse as a turbine which is used as power machine instead of pumping water. The turbine runner is actually the impeler of a centrifugal pump running backward and the generator is simply the pump's induction motor. There are several advantages of using this machine as power generator, such as

- Pump and motor can be purchased for use as a turbine as a single unit where the pump and generator are a direct arrangement.
  The advantages of using this direct drive arrangement make for very low friction losses in the drive. It also makes it easier to install.
- the investment costs of PATs may be less than 50% of those against a comparable turbine (especially for small units below 50 kW)
- As the connection between turbine/pump and generator is direct, make less maintenance is required.

- Spare parts such as seals and bearing are readily available since major pump manufacturers offer after- sales services almost throughout the world
- Easy installation as it uses standard pipe fittings.

A pump is designed for one particular operation in which run with a constant speed, head and flow. Hence the pump does not require a regulating device (guide vane). As a turbine, variation of head and flow conditions could occur. This could be a problem with running the pump as a turbine, as PAT does not have adjustable guide vanes for adapting to fluctuations in the water supply. To overcome this water supply fluctuation, it is normal to employ a number of differently sized units to distribute the total volume of water available. However this solution will increase cost as more unit needed. The advantages of PAT over conventional turbines may be significant for micro hydro up to 500 kW, however for larger outputs, standard pumps are not suitable. as the cost advantage of PAT is reduced. Fig 2.33 shows a typical instalation of pump as turbine (PAT).

Figure 2.33:A typical instalation of PAT (Orchard 2009)

2.2.3 Novel Technology For Low Head Water

1. Archimedes Screw

The Archimedes screw is also called the Archimedean screw or screw pump, In brief, an Archimedean screw consists of a cylinder containing several continuous helical walls that, when the entire cylinder is rotated on its longitudinal axis, scoop up water at the open lower end and dump it out the upper end (Dalley & Oleson 2003). Some scientist stated that this machine was used during the reign of the Assyrian king Sennacherib (704–681B.C.) and that the design was put to use in spectacular fashion to water his palace garden at Nineveh (was an ancient Assyrian city) (Dalley 1993). However, another scientist said that this machine was invented by Archimedes (287–212 B.C.) (Drachmann 1958) (Oleson 1984) (Wikander 2000). Who invented this machine still under debate see (Dalley & Oleson 2003), however most people agree to name this machine as an Archimedes Screw. In recent years, the Archimedes Screw has been used working in reverse as a hydropower machine. If water is poured into the top of an Archimedes' screw, the water is lowered within cells which form between the blades and the trough, then it will force the screw to rotate. The rotating shaft which the screw attached then drives an electric generator. Such an installation has the same benefits as using the screw for pumping: the ability to handle very dirty water and widely varying rates of flow at high efficiency. The installation of the Archimedes Screw as power generator is shown in Fig 2.34

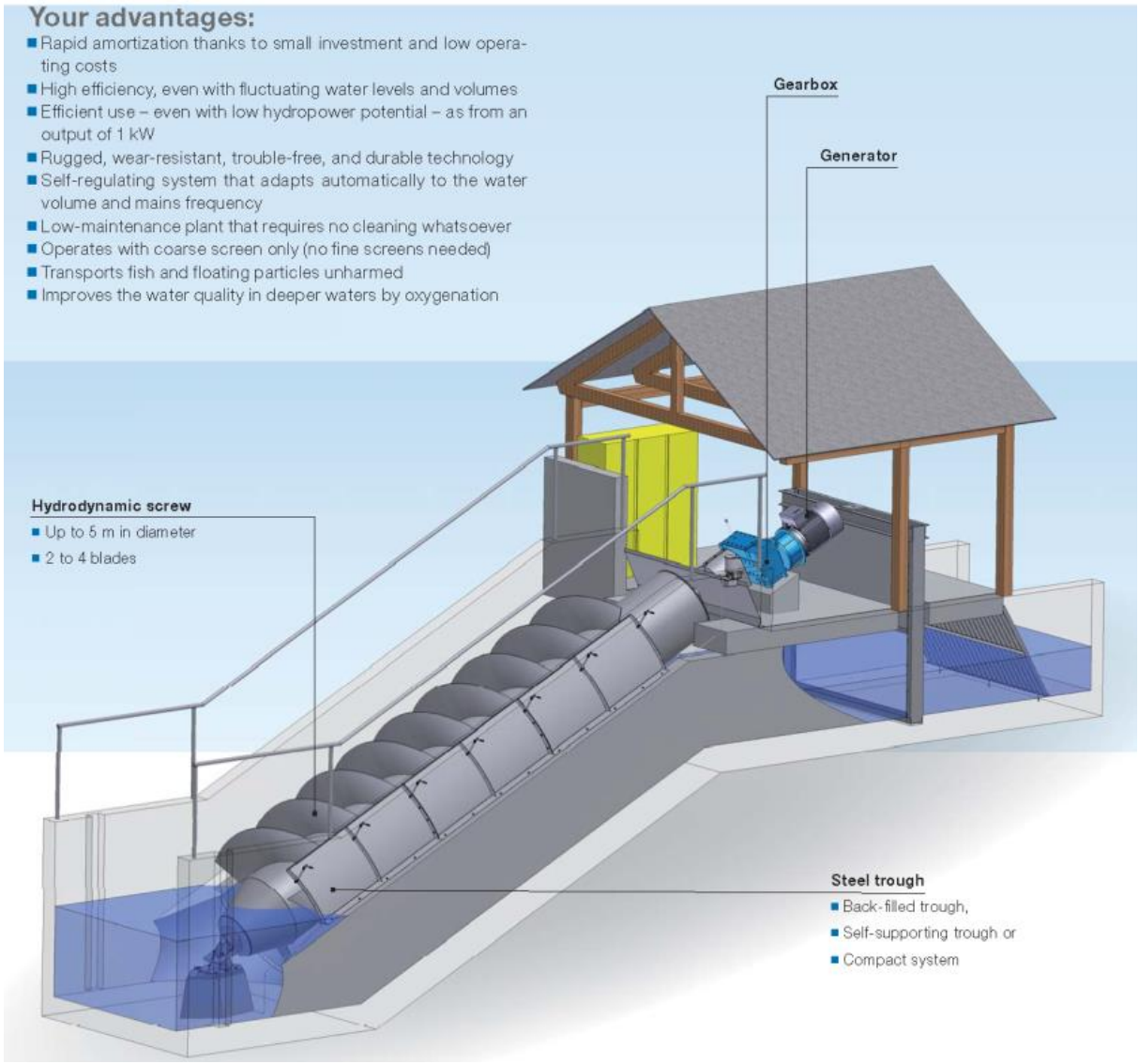

Figure 2.34: Archimides power screw (Atro 2013)

(Müller & Senior 2009) proposed theory to assess the performance of the Archimides screw, and it was found that the performance is a function of geometry and leakage. This theory was match with the experimental results from (Brada 1999), which found the maximum efficiency of the Archimides screw to be about 80%. However, (Lyons & David 2013) found that the efficiency was about 70%. Varying water heads and varying water flow rates upstream and downstream of the screw only have a marginal effect on the efficiency and do not affect their functioning and operation. With hydrodynamic screws, even small hydrodynamic potentials at powers from 1 kW (up to 500 kW) can be exploited economically. Fig 2.35 shows the map

of head, power and water flow rate that is suitable for the Archimedes screw. The principle of this machine is claimed as the static pressure difference between upstream and downstream of the water.

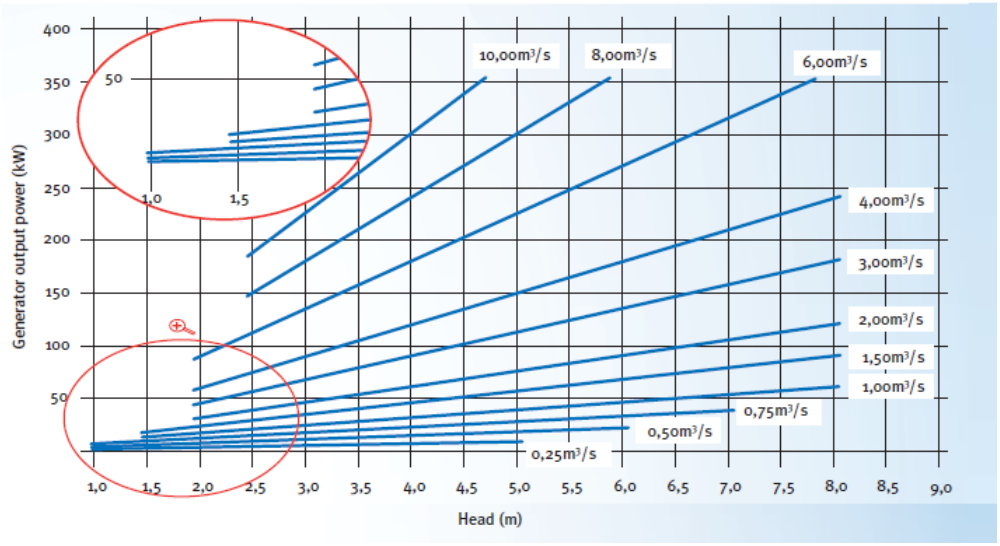

Figure 2.35:Archimedes Screw operating range (Atro 2013)

2. The Rotary Hydraulic Pressure Machine (RHPM)

The working principle of this machine is based on the static pressure difference between upstream and downstream. The rotational movement of the blade is caused by the static pressure upstream is greater than static pressure downstream. Theoretical analysis of this machine has been developed by (Senior et al. 2008) accompanied with experimental work, to analyse the performance of this machine. According to (Senior et al. 2008), this machine can be applied to hydropower sources with head up to 5 m. The experimental work that was done by Senior, was shown that the efficiency of this machine can reach 80%. A case study was conducted comparing the RHPM to a traditional Zuppinger waterwheel installation and found that the larger flow capacity and relative simplicity of the machine could result in a 40% to 50% lower specific cost (Senior et al. 2008). The test model that was used by (Senior et al. 2008) is shown in Fig 2.36

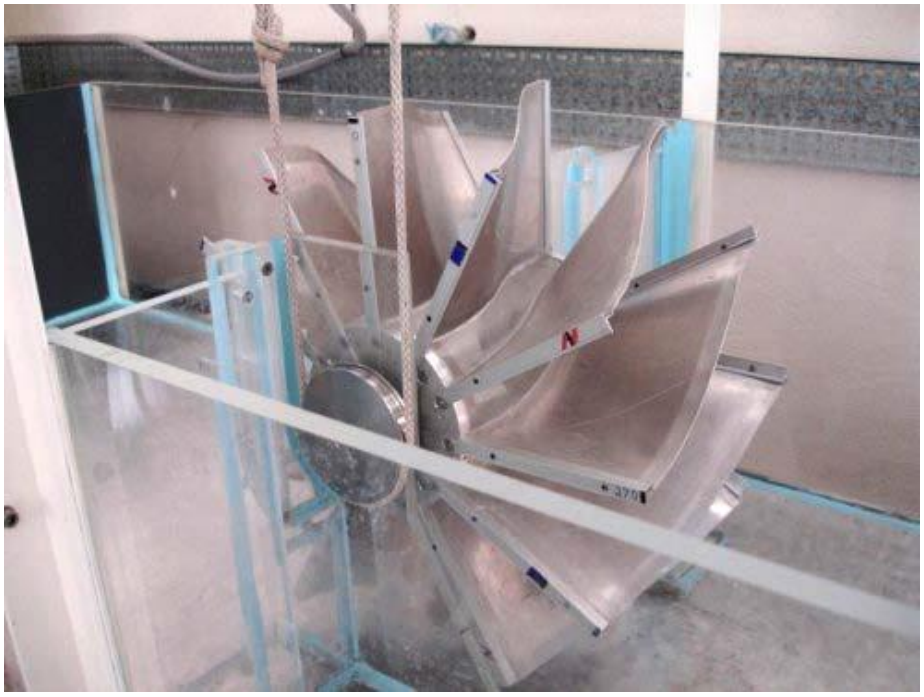

Figure 2.36:Rotary Hydraulic Pressure Machine(Senior et al. 2008)

3. Very low head turbine (VLH-Turbine)

This machine was developed through an internationally cooperated project which combines the joint effort of French and Canadian partners (Leclerc 2007) (Fraser et al. 2007) a general manager at MJ2 Technology in France. This was tested for the first time in 2007. This machine is claimed to achieve efficiencies of up to 90%. The VLH turbine is an axial turbine with 8 blades. The picture of the VLH-turbine is shown in Fig 2.37.

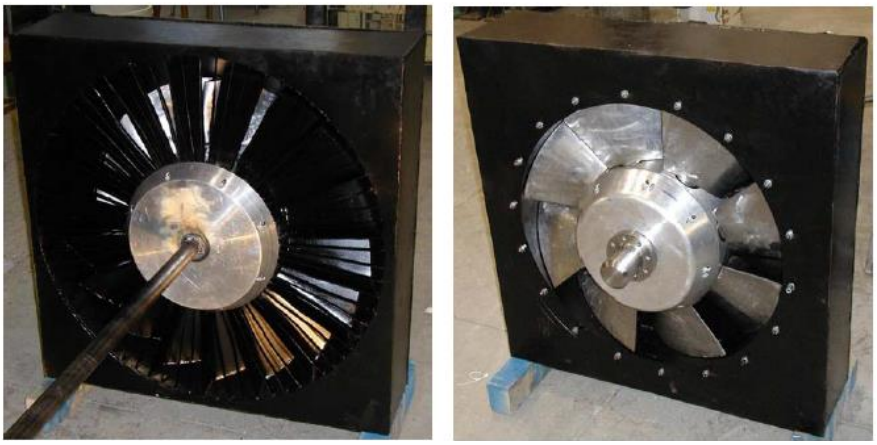

Figure 2.37:Very low head turbine (Fraser et al. 2007)

This technology is claimed to be working on a head range of 1.4 - 3 m with water flow rate Q = 10-30 m^3/s. This machine is designed to fullfill the need of a unit that requires very little civil works, is easy to install and offers a high degree of reliability at a reasonable cost per installed kW. Therefore this machine concept takes a completely different approach from the traditional turbine design, in which using large runners to practically eliminate the expensive civil structures of other machines. It includes the use of advanced technological characteristics such as Directly driven Permanent Magnet Variable speed Generator. MJ2 Technology as manufacturer has standardized this product with five ranges of runner diameter size (available) and the generator output range is between 100 to 500 KW. This machine is claimed to be safe for fish passing through it, the results of the study showed that 95% of fish passing through the machine survive. This machine is easily maintained and designed with a hinge at one end, so that when maintenance is required it can be done simply by lifting up one end. The installation of this turbine is depicted in Fig 2:38

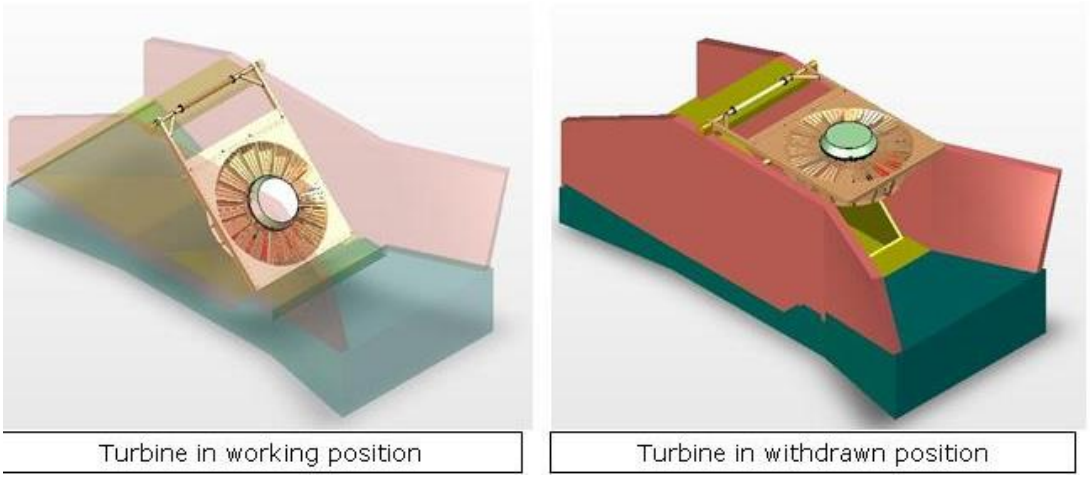

Figure 2.38:very low head turbine (Coastal Hydropower Corp. 2011)

4. Gravitation water vortex power plant

The principle of this type of technology is the dynamic force of the vortex generated by the blade design. An analogy of the principle of operation is that of an upside-down snail - through a large, straight inlet the water enters tangentially into a round basin, forming a powerful vortex, which finds its outlet at the center bottom of the shallow basin. This machine originally was design in order to aerate the water of small stream by Zotlöterer. When he thought of this idea, his plan was not only to give air to the water, but also take from it some of the kinetic energy that is always inherent in the stream. This technology can be applied for head 0.7 m (Lepisto 2007). Prototype of this model has been made in 2006, with a 1.2 m head, water flow rate $1m^3/s$, and the output power 6.2 kW(Zotlöterer 2005), and maximum efficiency 80%. Gravitation water vortex power machine is shown in Fig 2.39.

Figure 2.39:Gravitation water vortex power machine (Zotlöterer 2005)

2.3 Discussion

All hydropower plants that were mentioned above are machines that can be used for small-scale power generation. Most of the group of turbine based machines have been manufactured by several companies and are available commercially. On the other hand, the group of water wheel technology is an interesting choice. It is simple and easy to manufacture by using simple technology and unskilled people can manufacture it therefore it could be utilized in developing countries. Table 2.1 is summary of several small hydropower machines. Some data which could not be found is left as blank in the table.

Several research results have been reported to improve the performance of the water wheel, such as (Müller 1899), who modify the shape of the blade undershot water wheel. Overshot water wheel is an interesting choice to generate hydropower, since it exploits potential energy of the water, water, giving high efficiencies (of up to 85%). However this machine needs a high head difference in comparison with other type of water wheel which work well at head difference 2.5-10 m and flow rate of 0.1-0.2 m^3/s (Müller & Kauppert 2004). The breastshot water wheel is another choice that can be developed. Research has been undertaken on this type of machine (Senior 2009). He grouped this machine as type 2 hydrostatic pressure converter (type 2 HPC), and named this machine as Rotary hydrostatic

pressure machine (RHPM). The technology that is needed to manufacture this machine is simple.

Table 2.1: Summary of Several Small Hydropower Machine

No	Machine	Generated Power	Head (m)	Efficiency	Flow rate m^3/s	Speed (rpm)	Instalation Cost£/kWh	Working principle
1	Overshot water wheel		2.5-10	85%	0.1-0.2	6-12	3000	Weight of water in bucket
2	Undershot Water wheel/old zuppinger		0.5-2.5	75%	0.5-0.95		1000-6000	Impulse machine
3	Breastshot water wheel	16 kW/m	1.5-2.5	80-85%	0.5-2.5			Hydrostatic pressure
4	Cross flow turbine	15-3000 kW	2.5-200	80%	0.04-13		1170	Impulse turbine
5	Kaplan Turbine	20-2000 kW	1.5-15	90%	0.75-30	90	731-1294	Reaction turbine
6	Bulb turbine	50kW-30MW	2- 18	96%	6-25	138		Reaction turbine
7	Pit Turbine	<15MW	1.5-10		20-100			Reaction turbine
8	S type Kaplan Turbine	50kWto 5MW	3.5 -25	90%	3-65	200		Reaction turbine
9	Compact Axial Turbine (CAT)	0,5MW-20MW	Up to 30 m		6 - 85			Reaction turbine
10	Siphon-Turbine	5-100 kW	h <3 m	65%	550-750			Reaction turbine
11	Dive turbine	50-1300 kW	2-25 m	95-98%	0.6 – 40			Reaction turbine
12	Pump as turbine/reverse centrifugal pump	<500 kW	h<22m	72%	22			Reaction turbine
13	Francis turbine	100-500 kW	3-10	75-85%	0.4-20		1600	Reaction turbine and impulse turbine
14	Archimedes Screw	1-500 kW	1-9	70-80%	0.25-10		1393-2991	Hydrostatic pressure
15	Rotary Hydraulic Pressure Machine	1.4-43.7 kW	Under 2.5	80%	0.5-3.6		2197.51-612.13	Hydrostatic pressure
16	Very Low Head Turbine	100-500 kW	1.4-3	86-90%	10-30		1315.32	
17	Gravitation Water Vortex	6.2 kW	0.7-1.2	73-80%	1.3	21	5944.43	
18	Zuppingerrad/turbine wheel	25-300 kW	2-5	75-80%	1-10			

Rotary hydrostatic pressure machine (RHPM) is a machine that derived from the S*taudruckmaschine* then analysed by James Senior (Senior 2009). This Rotary hydrostatic pressure machine (RHPM) is projected to be employed in the head differences of below 2.5 m and flow rate of 0.5-3.6 m^3/s (Senior 2009) . The research on this RHPM also has been undertaken by (Linton 2014). He defined the machine as the hydrostatic pressure machine (HPM), which basically can be grouped as a breastshot water wheel. He researched the mechanism of power production at a particular blade. He also developed the theory on the

mechanism of losses from the machine. The RHPM is machine claimed to achieve efficiency at 80%, where the losses come from leakage, inertial reaction force, reducing head because of the acceleration from upstream to downstream and turbulence. The leakage problem is reduced by James Senior by installing a shoe under the wheel and also improving side filling. Whereas the inertial reaction is difficult to solve, since it is the nature of the force. Reducing the head always occurs as the water accelerates from the upstream side to the downstream side of the wheel. Another source of the losses is turbulence. This loss is difficult to deal with due to air entrapment within the cell. In this case air does not have enough time to release from the cell as water fills it. A further issue is that in the upstream, the blade also experiences water slamming which occurs when the blade hits the water body. In the downstream some water also become entraped in the blade and also becomes a source of losses. James Senior and Nick Linton tried to deal with this problem by modifying the blade on their machine (Senior machine Fig 2.36, Linton machine Fig 2.40). The Linton wheel consist of a helical blade shape inclined at 15° to the rotor shaft axis, whereas The Senior wheel has a hand shaped twisted blade[2].

Figure 2.40: The machine developed by Nick Linton (Linton 2014)

Water slamming on the upstream and uplifting water on the downstream obviously contribute to the turbulent losses. As can be seen from Fig 2.41 where water splash as water entering the machine. The turbine wheel might offer a potential improvement in order to reduce these

[2] A hand shaped twisted blade means the blade is formed manually by hand as the picture of the blade can be seen from fig 2.36.

losses because the blade is shaped as shown in Fig 2.16. In addition, the machine could be filled in from the side instead of from the front with the existence of an upper shroud which potentially could reduce the water slamming effect, even though the effect of this upper shroud needs to be confirmed.

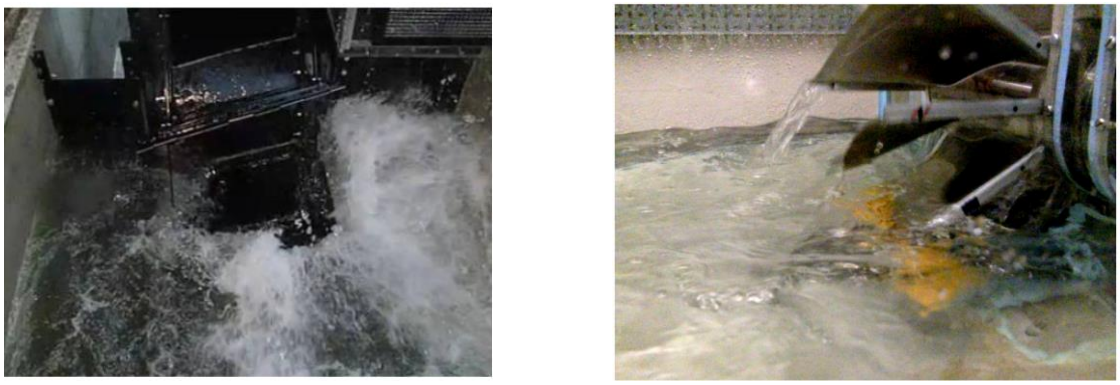

Figure 2.41:the situation on the upstream of the nick linton machine (left) and james senior machine (right)

The blade shape of the turbine wheel is also expected to contribute in reducing the losses, either from upstream (water slamming) or from downstream (uplifting losses). Furthermore there is no published information regarding this turbine wheel. A reference given in an encyclopaedia 1903 (Brockhaus 1903), give a brief description that says the upstream channel is wider than the wheel. It has open sides, as access for water to enter and air to ventilate from the sides. It will be interesting to investigate this turbine wheel in detail.

2.4 Research on hydrostatic pressure converter/machine/ (HPC/M)

Research on Hydrostatic machine has been undertaken at the University of Southampton since 2006, initiated by James Senior and followed by Nick Linton under Dr Gerald Muller. With both of these researches the characteristics of the HPC/M has been explored. James Senior has developed the basic theory of the HPC from his experimental work on the hydrostatic pressure converter, whereas Nick Linton developed it further by adding losses mechanism theory to strengthen the previous theory.

2.4.1 Research on hydrostatic pressure converter (HPC)

James senior (Senior 2009) built and tested a hydrostatic pressure converter (HPC), which he categorized this machine in two groups which are:

2.4.1.1 Type one HPC

This type of machine has a working surface which extends from the channel beds up to the upstream water surface. A simple example of this machine is the undershot water wheel, which operates in non-impulse condition. The representation of this machine is shown in Fig 2.42. The depth differences between upstream and downstream creates pressure difference which drives the wheel to rotate. Force diagram for type one HPC which blade has width *w* is shown in Fig 2.43

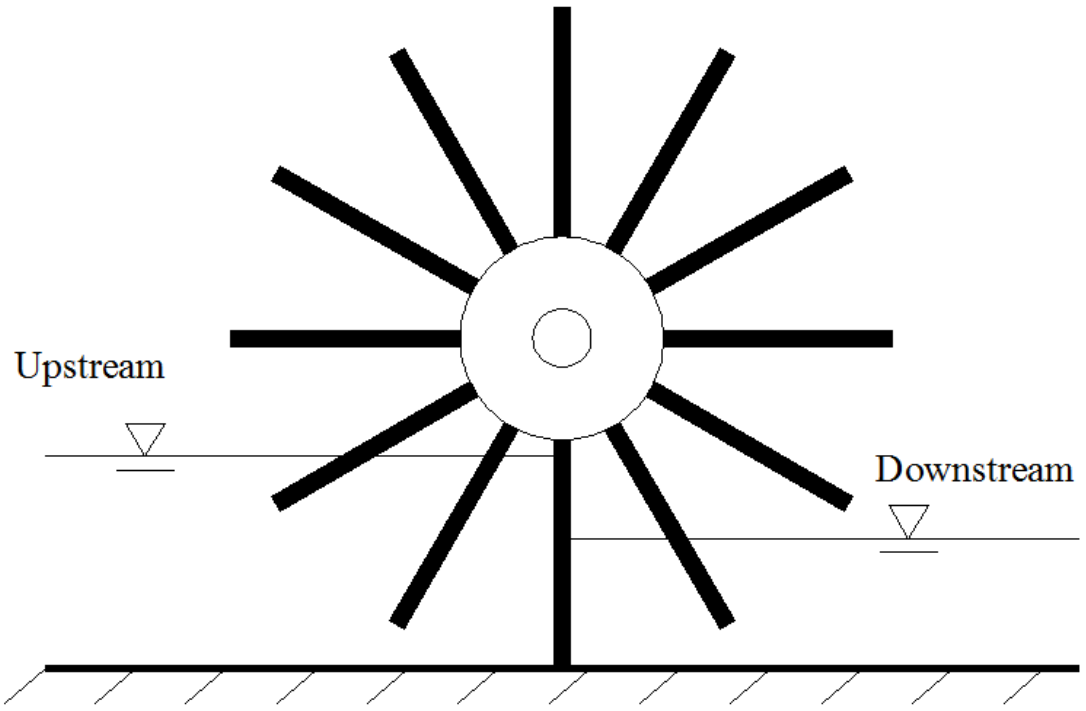

Figure 2.42: Undershot water wheel

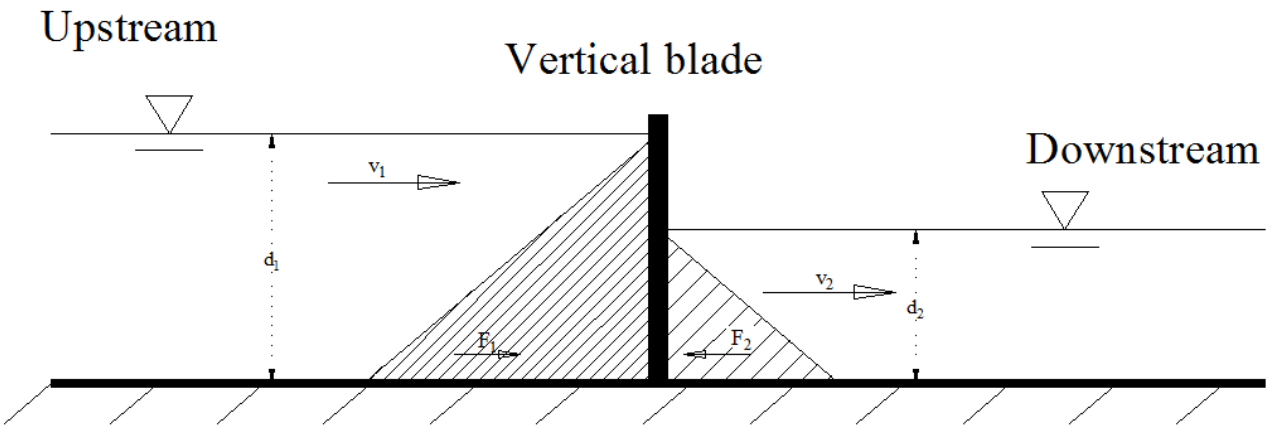

Figure 2.43: Type one force diagram

The total force in upstream is F_1, and formulated as

$$F_1 = \rho\, g\, \frac{{d_1}^2}{2} w \qquad 2.2$$

Whereas the total force in downstream is F_2, and formulated as

$$F_2 = \rho\, g\, \frac{{d_2}^2}{2} w \qquad 2.3$$

The force F that acts at the blade is

$$F = F_1 - F_2 \qquad 2.4$$

$$F = \rho\, g\, \frac{{d_1}^2 - {d_2}^2}{2} w \qquad 2.5$$

Since in the case of type one, the blade is extended from the channel bed up to the upstream water level therefore the blade is moving with the same velocity as upstream water surface v_1. In this case, power output is calculated as

$$P_{out} = F\, v_1 \qquad 2.6$$

$$P_{out} = \rho\ g\ \frac{{d_1}^2 - {d_2}^2}{2} w\ v_1 \quad (2.7)$$

Power input P_{in} is formulated as

$$P_{in} = \rho\ g\ H\ Q \quad (2.8)$$

$$P_{in} = \rho\ g\ (d_1 - d_2)\ (v_1\ d_1\ w) \quad (2.9)$$

So the efficiency η of the machine is

$$\eta = \frac{P_{out}}{P_{in}} \quad (2.10)$$

$$\eta = \frac{\rho\ g \frac{{d_1}^2 - {d_2}^2}{2} w\ v_1}{\rho\ g\ (d_1 - d_2)\ (v_1\ d_1\ w)} \quad (2.11)$$

$$\eta = \frac{1}{2}\left(1 + \frac{d_2}{d_1}\right) \quad (2.12)$$

Fig 2.44 is the theoretical efficiency curve as a function of the flow rate. The flow rate *Q* is non-dimensionalized by dividing the flow rate with the maximum flow rate. This figure was plot based on the ratio between downstream water level d_2 and upstream d_1 water level of 0.75 ($\frac{d2}{d1} = 0.75$). This figure shows that the efficiency of the type one machine is constant 88% at any range of the flow rate. The efficiency value is changing as the ratio between downstream water level d_2 and upstream d_1 water level changes. The efficiency is only function of the ratio downstream water level and upstream water level d_2/d_1 as shown in equation 2.12. The efficiency is independent of volume flow rate *Q*.

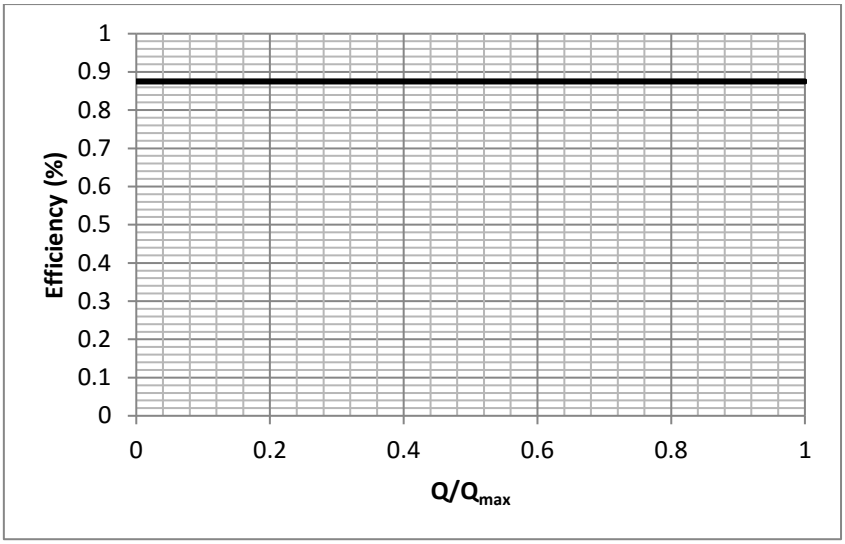

Figure 2.44: Theoretical efficiency of the type one machine

2.4.1.2 Type two HPC

The type two water wheel blade extends from the channel bed up to the downstream water surface level. Fig 2.45 is a typical example of the breastshot water wheel which width of the blade as *w*.

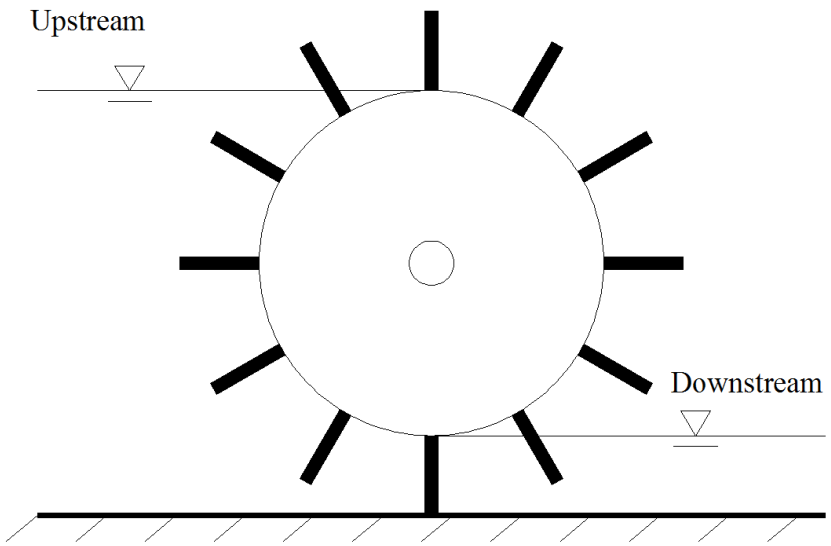

Figure 2.45: Breastshot water wheel

a. Constant width of the upstream and downstream water surface

The scheme and analysis for the case of constant width *w* of the upstream and downstream is shown in Fig 2.46 with control volume defined as a dashed line. Assume that the downstream water level is exactly on the lowest point of the hub. The force acts on this wheel with blade length *l* as shown in Fig 2.46. The forces that are involved in this calculation are F_1, F_2, F_3 and *F*. F_1 is the force that acts on the submerged hub. This force acts on the radial direction of the hub, as the generated force direction is perpendicular to the surface of the hub and this force is transferred to the shaft which then also give reaction force to this F_1 with the magnitude of F_{hub}. F_2 and F_3 oppose each other, which also cancel out each other. The only work that contributes to power production is hydrostatic force *F* which is acting on the blade. This force is then calculated as

$$F = \rho\, g\, H\, l\, w \qquad 2.13$$

$$F = \rho\, g\, (d_1 - c - (d_2 - c))\, l\, w \qquad 2.14$$

$$F = \rho\, g\, (d_1 - d_2)\, l\, w \qquad 2.15$$

The acceleration from v_1 to v_2 is accompanied by a drop in water surface level Δh as shown in Fig 2.46. This drop is calculated by applying the energy equation on both upstream and downstream surface, and formulated as

$$\Delta h = \frac{{v_2}^2 - {v_1}^2}{2g} \qquad 2.16$$

Dropping head reduces hydrostatic force *F* to be

$$F = \rho\, g\, (d_1 - d_2 - \Delta h)\, l\, w \qquad 2.17$$

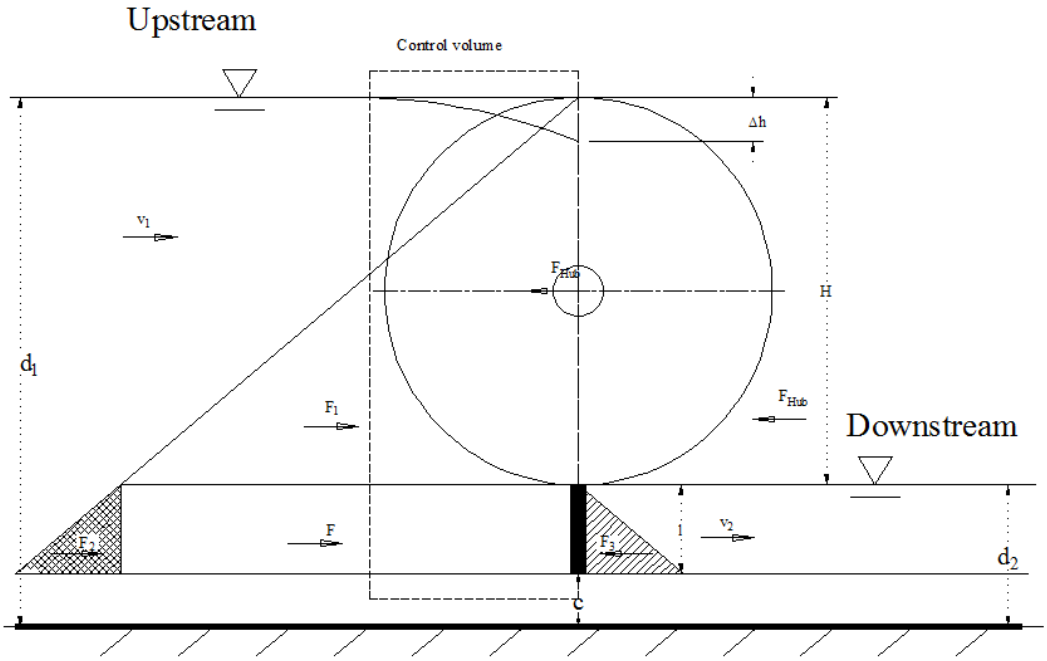

Figure 2.46: Type two force diagram

The acceleration from v_1 into v_2 also creates an inertial force which generates a reaction force which is opposed to the direction flow of the water. Applying Reynolds transportation equation at the case of momentum on the control volume (Fox et al. 2003), will get

$$F = F_s + F_b = \frac{\partial}{\partial t}\int_{cv} v\,\rho\,d\,d\forall + \int_{cs} v\,\rho\,v\,dA \qquad 2.18$$

$$F = F_s + F_b = \frac{\partial}{\partial t} v \int_{cv} \rho\,d\,d\forall + v\int_{cs} \rho\,v\,dA \qquad 2.19$$

Assumptions:

1. Steady flow
2. Incompressible flow
3. flow uniform at inlet and outlet of the control volume
4. No body Force
5. Surface force is reaction force F_t of the control volume

As the control volume being analyzed is limited until outer circle of the wheel, then the clearance *c* between blade to the base line can be neglected as shown on the control volume in Fig 2.47.

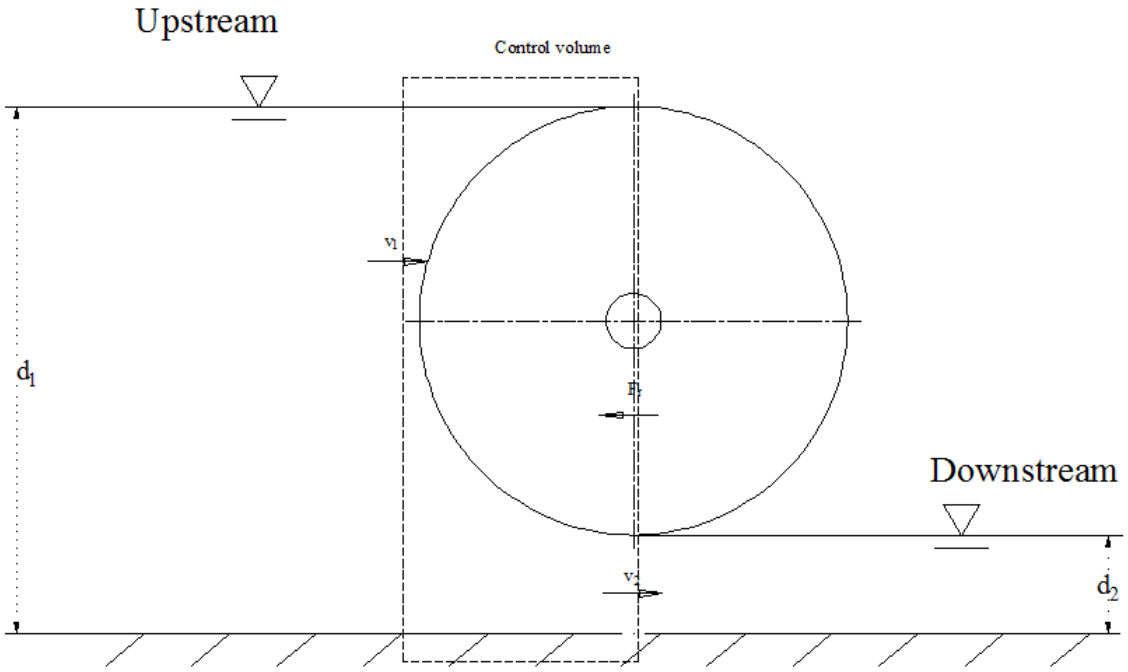

Figure 2.47: Control volume at the entering and exiting of the type two machine

From several assumptions above, then the control volume at Fig 2.47 is analyzed and the reaction force of the control volume which is F_r calculated as

$$F_r = \dot{m}(v_2 - v_1)$$

$$F_r = \rho\, Q\, (v_2 - v_1) \qquad 2.20$$

$$F_r = \rho\, d_1\, w\, v_1\, (v_2 - v_1) \qquad 2.21$$

The final force F_t acting on the blade is the hydrostatic force from previous calculation F subtracts to reaction force F_r and formulated as

$$F_t = F - F_r \qquad 2.22$$

In the case of type two, the blade is extended from the channel bed until downstream water level, as a consequence, the blade must move with the same velocity as downstream water movement v_2. So the power output is calculated as

$$P_{out} = F_t\, v_2 \qquad 2.23$$

$$P_{out} = (F - F_r)v_2 \qquad 2.24$$

Since the power input is similar to the power input formulation in the case of type one, therefore the efficiency is formulated as

$$\eta = \frac{P_{out}}{P_{in}} \qquad 2.10$$

$$\eta = \frac{(F-F_r)v_2}{\rho\, g\, (d_1-d_2)\, (v_1\, d_1\, w)} \qquad 2.25$$

The curve of theoretical efficiency of the type two machine is presented in Fig 2.48. Theoretical flow rate Q is dimensionalized with maximum theoretical flow rate Q_{max}

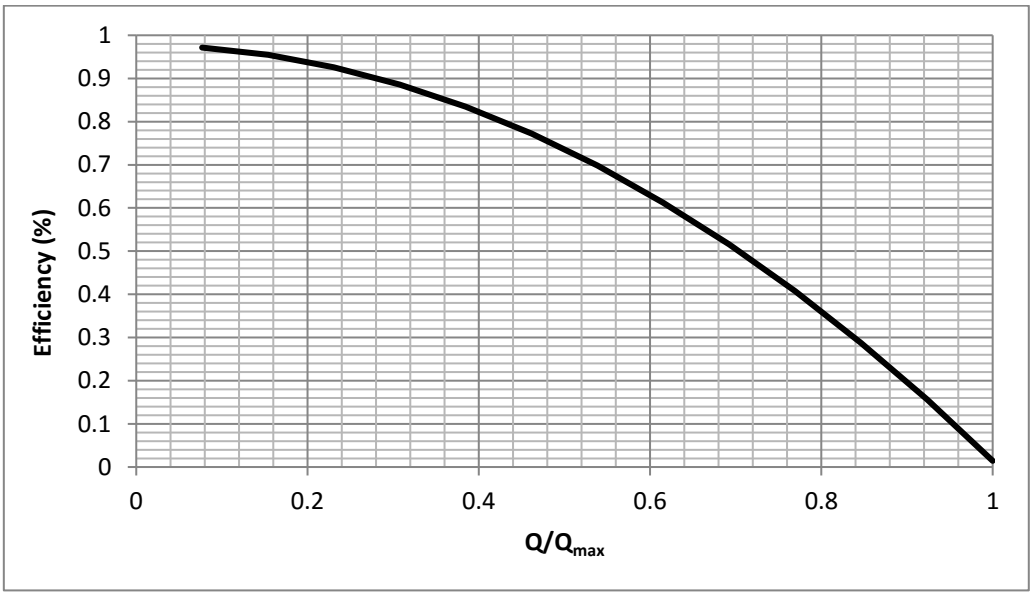

Figure 2.48: Efficiency curve of the type two machine

James Senior noted that the losses came from leakage and turbulence. Fig 2.49 is the graph of efficiency vs flow rate of type two water wheel from James Senior thesis.

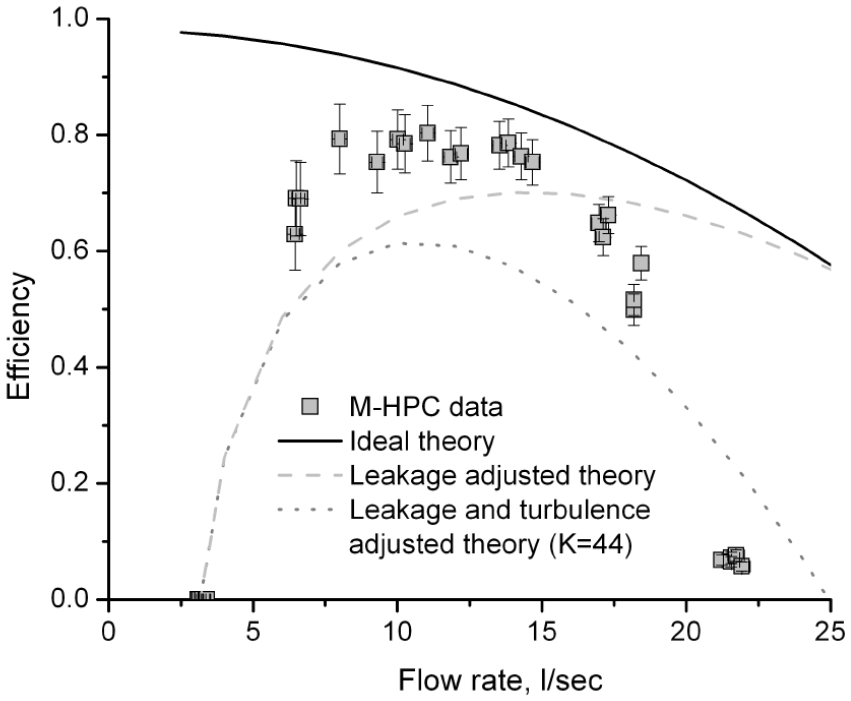

Figure 2.49: Efficiency with leakage and turbulence correction (Senior 2009)

2.4.2 Research on hydrostatic pressure machine (HPM)

Nick Linton conducted research on a HPM machine. He developed a theory to calculate power output using alternative method to James Senior. Instead of calculating power output based on the pressure force times downstream velocity as stated by Senior, he calculated the power output from a torque analysis perspective. In addition he also proposed further loss mechanisms that occurs with the HPM.

Pressure that acts on the blade from both the upstream and downstream side contributes to power output as shown in Fig 2.50 below. The power output is calculated based on the torque calculation.

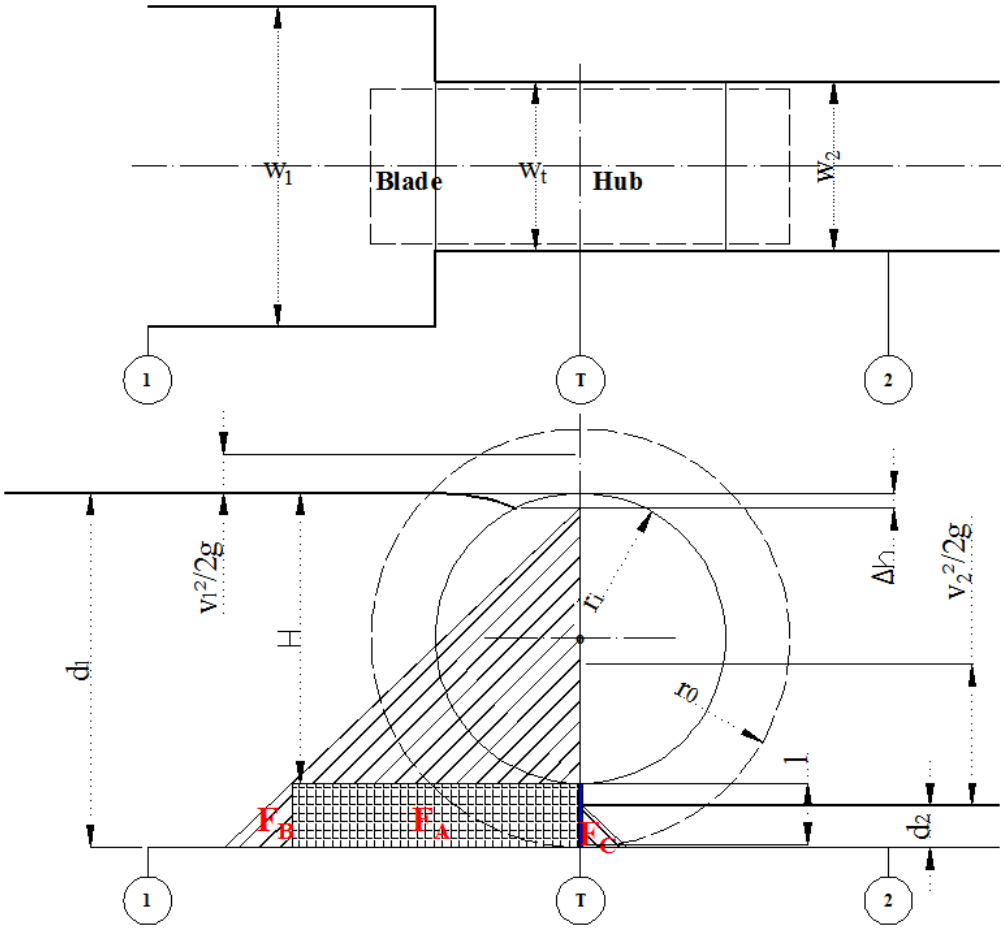

Figure 2.50: Blade force pressure component

The force that acts from upstream creates torque with direction counter clock wise (CCW).

$$T_A = F_A R_{mean} \qquad 2.26$$

Where F_A is the force that acts at area A and can be defined as hatched area A

$$F_A = \rho\, g\, (d_1 - \Delta h - l)\, l\, w_t \qquad 2.27$$

R_{mean} is the mean radius of the force that act

$$R_{mean} = \frac{r_0 + r_i}{2} \quad 2.28$$

T_B is the torque because of the F_B

$$T_B = F_B R_b \quad 2.29$$

Which F_B is the force that acts at area B and can be defined as area B calculated as

$$F_B = \frac{\rho\, g}{2}\, w_t\, l^2 \quad 2.30$$

R_b is calculated as

$$R_b = r_i + \frac{2}{3} l \quad 2.31$$

There is another torque which rotates at clock wise (cw) this torque is T_c

$$T_c = F_c R_c \quad 2.32$$

F_c is the force that acts at point c and defined as area C, calculated as

$$F_c = \frac{\rho\, g}{2}\, w_t\, {d_2}^2 \quad 2.33$$

R_c is the centre of F_c act, and calculated as

$$R_c = r_0 - \frac{1}{3} d_2 \quad 2.34$$

Thus total torque at o is calculated as

$$T = T_A + T_B - T_c \quad 2.35$$

As ω is angular speed of the water wheel, therefore power output is formulated as

$$P_{out} = T\omega \quad (2.36)$$

Where omega is angular velocity of the wheel, and calculated as equation 2.55

$$\omega = 2\,\pi\,f \quad (2.37)$$

Which *f* is rotational speed of the wheel per second.

All losses were reviewed by Linton and he stated that several losses occur on the HPM machine. For specific detail please refer to (Linton 2014). He defines that the losses that occurs within the HPM machine consist of *inflow acceleration losses, exit acceleration losses, partially vented losses, and turbulent losses.* Fig 2.51 is the plot of his theory against his experimental result. The figure shows rotational speeds against power output. The dimension of the machine that he uses to plot his theory is shown in Fig 2.52. The plot is staring from "*ideal power output-inflow acc losses*" then followed by "*ideal power output-inflow acc losses-exit acc losses*" until "*ideal-inflow acc losses-exit acc losses-turbulent losses-partially vented losses*". The theory match well at relatively low speed until 5.6 rpm and then deviates as the speed increases.

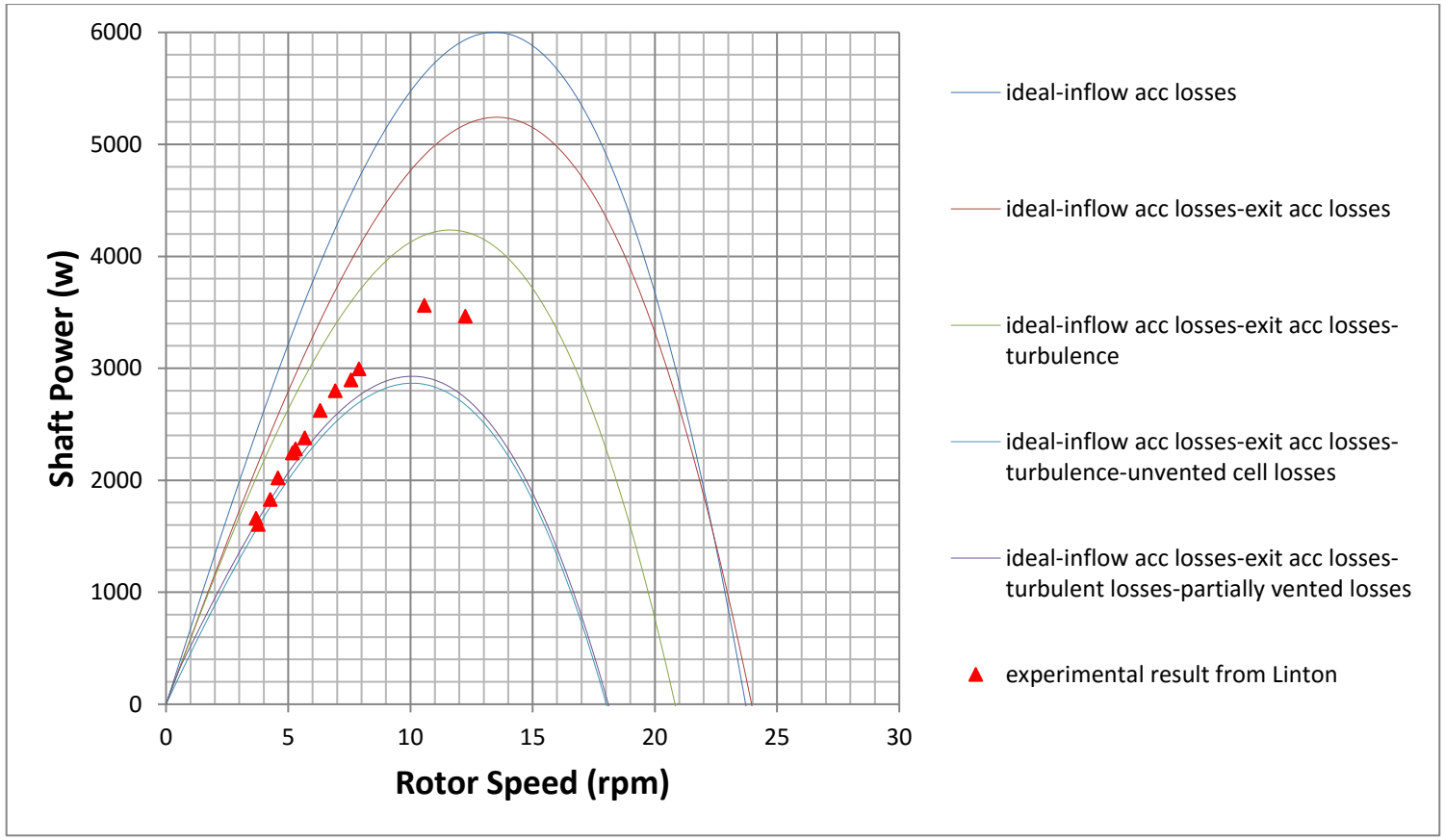

Figure 2.51: Theorethical shaft power (the graph was built based on the data from Linton thesis)

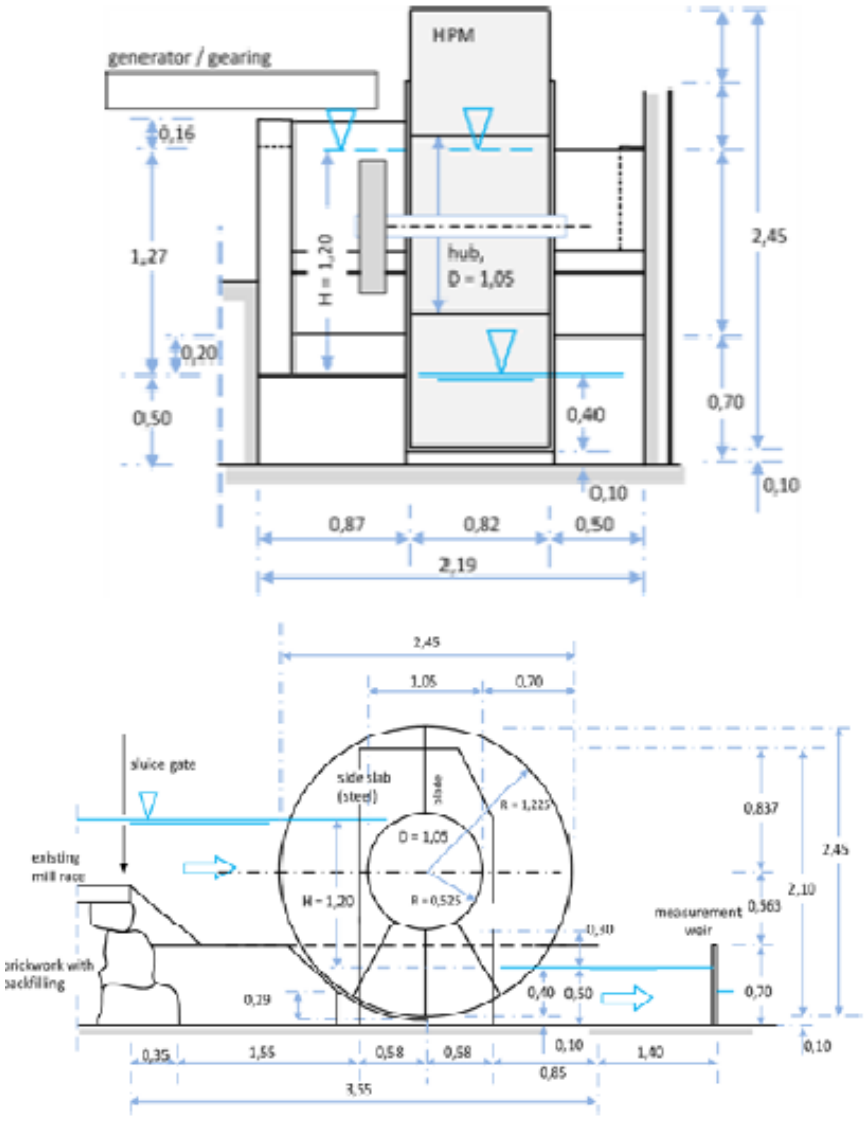

Figure 2.52: Nick Linton's HPM Machine (Linton 2014)

2.5 Relevance of previous theory to the current research

The machines that have been built by Senior and Linton have no shroud. The existence of the shroud potentially causes confusion between a hydrostatic machine and a potential machine. To begin with, it will be good to understand theory of potential machine.

2.5.1 Potential machine

An ideal potential machine is a machine that energy generation occurs due to gravity. For example on a cell-shaped box filled with water then moves vertically along the y as shown in Fig 2.53.

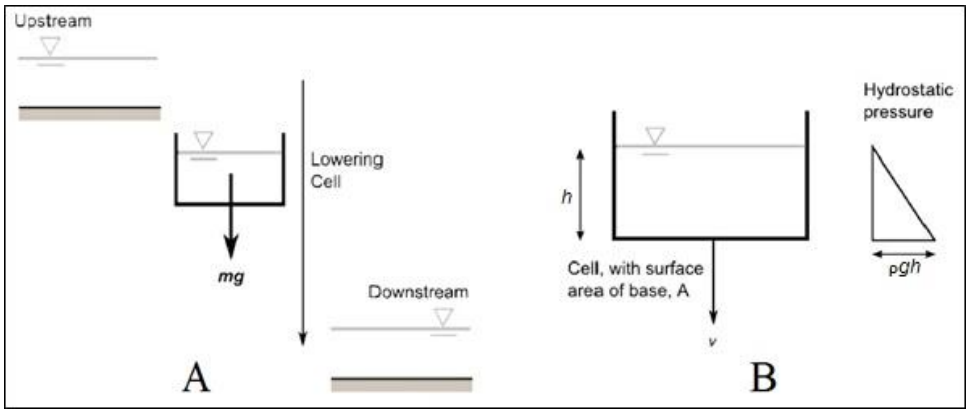

Figure 2.53: ilustration of potential machine A (weight analysis) B (pressure analysis) (Senior 2009)

In Fig 2.53A, the vertical downward force of the cell is the mass of water inside the cell multiplied by the acceleration due to gravity. It would be interesting to see further the relationship between the hydrostatic pressure in the cell against potential force arising in the cell. In the picture B, water pressure in the cell will be enlarged linearly from the free surface to the bottom surface of the cell. The magnitude of the increase in pressure as shown in the Fig 2.53B. The amount of pressure that works in all directions is

$$p = \rho\, g\, h \qquad 2.38$$

The pressure arising in the cell is actioned to any direction to the cell. The pressure acting on the base of the cell causes vertical force on the cell in the form of weight.

$$W = p\,A \tag{2.39}$$

$$W = \rho\,g\,h\,A \tag{2.40}$$

If the cell moves vertically with the speed of *v* within a certain distance due to weight or due to force (which generated because of hydrostatic pressure in the vertical direction), then the cell is already doing work. Amount of work done by cell per time unit is said as power

$$P = W\,v = \rho\,g\,h\,A\,v \tag{2.41}$$

This principle is quite relevant when applied to a overshot water wheel that a bucket shaped cell. The overshot water wheel does not require shroud to retain water.

The force obtained from the pressure only causes work in the vertical direction which is obtained from the pressure acts on the base of the cell, while the pressure in the lateral direction of the bucket does not result in work.

In the case of the overshot water wheel, the area behind the base of the cell is an open area, which is only surrounded by air at atmospheric pressure. Hence the pressure difference that occurs on the base of the cell is only due to the weight of the water inside the cell.

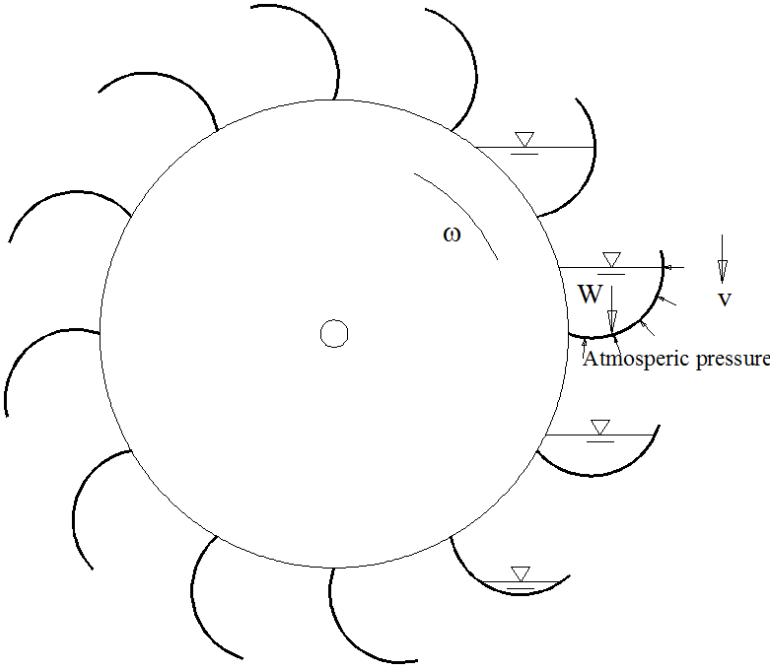

Figure 2.54: ilustration of overshot water wheel.

2.5.2 Water wheel with lower shroud

Fig 2.55 is an illustration of a water wheel with a shroud. Pressure acting on cells work on the entire surface of the field in that cell. The pressure acting on the shroud does not produce the force that generates power, because the shroud is stationery. Pressure that produces power is only a pressure acting on the blade and perpendicular to the blade surface. The resulting force, tangential to the direction of wheel rotation. To simplify the analysis, consideration should be given to the area covered by the red dotted line in Fig 2.55. For cases of middleshot waterwheel, assuming the area covered by the red dotted line is fully filled with water. Hence the pressure on each point inside the red dotted line area can be calculated with concepts hydrostatic equation as stated in equation

$$p = \rho\, g\, h \qquad 2.42$$

Where p is the pressure, g is the acceleration due to gravity and h is the depth of the water.

Assuming that the red dotted line isolates the water in the shroud, and considering the entire cell is filled with water, then the distribution of the pressure experienced by the blades A, B, C and D is shown in Fig 2.55. Blade A starts to experience pressure distribution on the blade, although the pressure acting on the blade is small, due to the shallow depth of water. Since the pressure is in all directions and it is also acting on a thin blade, then the distribution of the pressure experienced by the blade from the lower side is equal to the pressure received from the upper side, just the direction is oppose each other. The same effect was experienced by the blade B, C, D, and E but with a greater pressure magnitude, as the water deepens. Pressure experienced by blade C is uniform because the blade is in horizontal position.

In the case of blade F, because the downstream section is not isolated, then the water downstream is exposed to atmospheric pressure, hence the distribution of the pressure experienced by blade F is not like blade A, B, C, D and E. There is a difference of pressure distribution on both sides of blade F. The pressure distribution upstream is higher than downstream, due to the water depth upstream being greater than downstream. The differences in pressure eventually leads to a force difference between the upstream and downstream sides of the blade. Therefore this resultant force is capable of providing torque to spin the wheel. With this simple analysis, indicates that a water wheel equipped with a shroud also works on the principle of hydrostatic pressure difference between upstream and downstream as developed by James Senior and Nick Linton. It can also be seen evidently that the blades inside the shroud do not contribute to power generation, due to the pressure difference between the two blades is zero. A blade that plays a role in the generation of power is simply a blade that is directly affected by the downstream water level, because of the interaction with atmospheric pressure. In addition, the number of blades does not have any relationship to the power output of the machine. This assumption is proved in the experimental work as explained in subchapter 4.6.3.

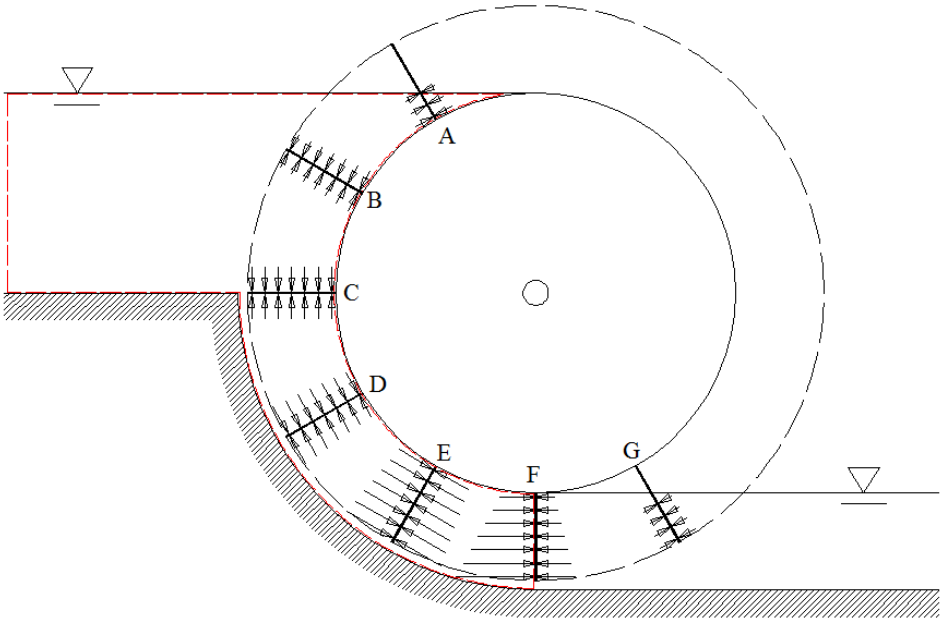

Figure 2.55: The pressure acting on the blades for water wheel with lower shroud

Based on the discussion above, we can conclude that the principal of power generation defined in the hydrostatic machines can also be applied for the turbine wheel, although the turbine wheel is equipped with a shroud.

2.5.3 Torque analysis discussion

Another approach to calculating the power output of the water wheel that is quite interesting is the research that was carried out by (Denny 2004). He was applying the governing equation of motion to develop the power output from the overshoot water wheel. He derived an equation of motion to predict power output using torque. For more detail please refer to (Denny 2004). In this thesis the approach that was undertaken by Denny is also considered. In this thesis the equation of motion approach was considered, however there are problems which make it difficult to use this approach to calculate the practical power output. To simplify the use of the equation of motion approach, this equation was derived based on a straight blade, then a curved blade which is used on the Zuppinger machine. The detail analysis of the equation of motion is presented in subchapter 2.5.3.1 and 2.5.3.2.

2.5.3.1 Case of simple blade

Acccording to the equation of motion, the mathematical equation of the wheel could be written as

$$I\,\dot{\omega} = \sum T \tag{2.43}$$

Considering at a instant situation where the machine is in the condition as shown in fig 1 in order to make it simple to analyse. In the case of simple blade as shown in fig 2.56, the torque that is involved in this system could be elaborated as

- T1 (the torque due to the force from hydrostatic pressure upstream)
- T2 (the torque due to the force from weight of the water inside the shroud)
- T3 (the torque due to force from hydrostatic pressure downstream)
- T_w (the torque due to the load that produce power output)

Total torque is the summation of all torque, which are T1, T2. The opposite torque is T3 and output torque T_w , then Equation of motion become

$$I\,\dot{\omega} = T1 + T2 - T3 - T_w \tag{2.44}$$

By assuming that the steady state angular speed, therefore $\dot{\omega} = 0$, then the output torque is calculated as

$$T_w = T1 + T2 - T3 \tag{2.45}$$

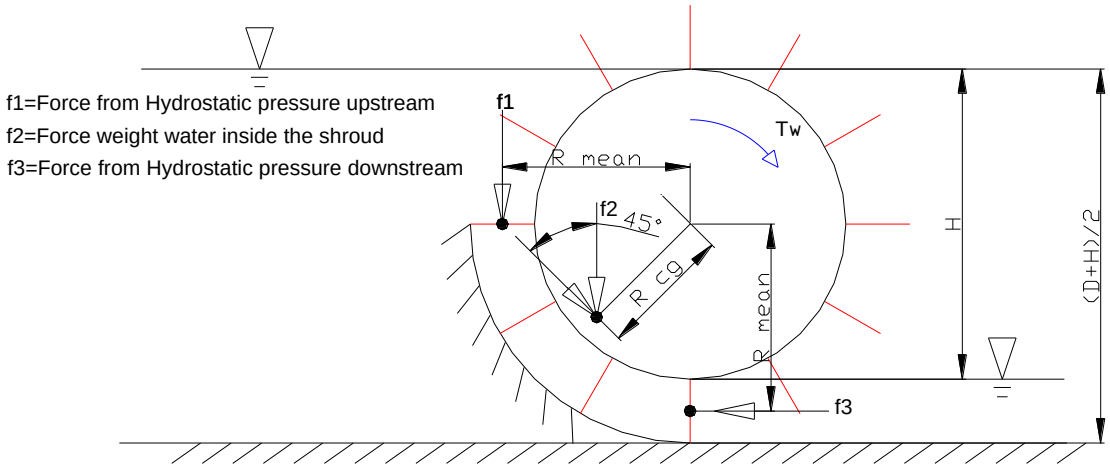

Figure 2.56: Torque and force that involved

Assuming

w=blade width

b=blade length=$\frac{D-H}{2}$

A. Consider f1 (force from hydrostatic pressure upstream) generate Torque 1 (T1)

$$f1 = P1 \cdot A \tag{2.46}$$

$$f1 = \rho . g . \frac{1}{2} . H . b . w \tag{2.47}$$

This force works at the R_{mean}, where R_{mean} is

$$R_{mean} = \frac{H+D}{4} \tag{2.48}$$

So Torque 1 (T1) is calculated as

$$T1 = f1 . R_{mean} = \rho . g . \frac{1}{2} . H . b . w . \left(\frac{H+D}{4}\right) \tag{2.49}$$

$$T1 = f1 . R_{mean} = \rho . g . \frac{1}{2} . H . \left(\frac{D-H}{2}\right) . w . \left(\frac{H+D}{4}\right) \tag{2.50}$$

$$T1 = f1.R_{mean} = \frac{1}{16}\rho.g.H\ .w.(D-H)\ .(H+D) \quad (2.51)$$

B. Consider f2 (force from weight of the water inside the shroud) generate Torque 2 (T2)

$$f2 = m.g \quad (2.52)$$

$$f2 = V \cdot \rho \cdot g \quad (2.53)$$

$$f2 = \frac{1}{4}.\left(\frac{1}{4}.\pi.D^2 - \frac{1}{4}.\pi.H^2\right).w.\rho.g \quad (2.54)$$

$$f2 = \frac{1}{16}.\pi.w.\rho.g(D^2 - H^2) \quad (2.55)$$

This weight works at the centre of gravity of the mass of water inside the shroud. With the total cross sectional area divided into sections, which are A_1 and A_2, so the relationship between cross sectional area to the centre of gravity can be calculated as

$$R_{cg}\ .A_{Total} = R_1\ .A_1 + R_2\ .\ A_2 \quad (2.56)$$

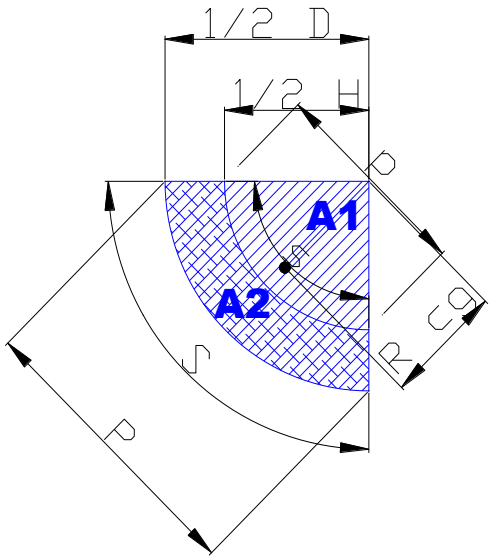

Figure 2.57: Schematic of determining centre of gravity water inside the shroud in the case of straight blade

Total cross sectional area is calculated as

$$A_{Total} = \frac{1}{4}.\frac{1}{4}\pi.D^2 = \frac{1}{16}\pi.D^2 \quad (2.57)$$

R_{cg} is the centre of gravity total cross sectional area which are formulated as

$$R_{cg} = \frac{2}{3}.\frac{1}{2}D.\frac{P}{S} = \frac{D.P}{3S} \quad (2.58)$$

$$R_{cg} = \frac{2}{3}.\frac{1}{2}D.\frac{\frac{1}{2}D\sqrt{2}}{\frac{\pi.D}{4}} = \frac{2\sqrt{2}.D}{3\pi} \quad (2.59)$$

R_1 is the centre of gravity part 1, which calculated as

$$R_1 = \frac{2}{3}.\frac{1}{2}H.\frac{p}{s} = \frac{H.p}{3s} \quad (2.60)$$

$$R_1 = \frac{2}{3}.\frac{1}{2}H.\frac{\frac{1}{2}H\sqrt{2}}{\frac{\pi.H}{4}} = \frac{2\sqrt{2}.H}{3\pi} \quad (2.61)$$

Cross sectional area of the part 1 is calculated as

$$A_1 = \frac{1}{4}.\frac{1}{4}\pi.H^2 = \frac{1}{16}\pi.H^2 \quad (2.62)$$

Cross sectional area of the part 2 is formulated as

$$A_2 = \frac{1}{4}.\left(\frac{1}{4}\pi.D^2 - \frac{1}{4}\pi.H^2\right) = \frac{\pi}{16}.(D^2 - H^2) \quad (2.63)$$

By rearranging all equation we can get

$$R_{cg}\,.A_{Total} = R_1\,.A_1 + R_2\,.\,A_2 \quad (2.64)$$

$$\left(\frac{2\sqrt{2}.D}{3\pi}\right).\left(\frac{1}{16}\pi.D^2\right) = \left(\frac{2\sqrt{2}.H}{3\pi}\right).\left(\frac{1}{16}\pi.H^2\right) + R_2\,.\left[\frac{\pi}{16}.(D^2 - H^2)\right] \quad (2.67)$$

So we will get

$$R_2 = \frac{\left(\frac{2\sqrt{2}.D}{3\pi}\right).\left(\frac{1}{16}\pi.D^2\right)-\left(\frac{2\sqrt{2}.H}{3\pi}\right).\left(\frac{1}{16}\pi.H^2\right)}{\left[\frac{\pi}{16}.(D^2-H^2)\right]} \quad (2.68)$$

$$R_2 = \frac{\left(\frac{2\sqrt{2}}{3\pi}\right).[(D^3)-(H^3)]}{[(D^2-H^2)]} \quad (2.69)$$

Torque 2 (T2) is calculated as

$$T2 = f2.Cos\ 45.R_2 = \frac{1}{2}\sqrt{2}\left[\frac{1}{16}.\pi.w.\rho.g(D^2-H^2)\right].\left[\frac{\left(\frac{2\sqrt{2}}{3\pi}\right).[(D^3)-(H^3)]}{[(D^2-H^2)]}\right] \quad (2.70)$$

$$T2 = \frac{1}{2}\sqrt{2}\left[\frac{1}{16}.\pi.w.\rho.g\right].\left(\frac{2\sqrt{2}}{3\pi}\right).[(D^3)-(H^3)] \quad (2.71)$$

$$T2 = \frac{1}{2}\sqrt{2}\left[\frac{\sqrt{2}}{24}.w.\rho.g\right].[(D^3)-(H^3)] \quad (2.72)$$

$$T2 = \left[\frac{1}{24}.w.\rho.g\right].[(D^3)-(H^3)] \quad (2.73)$$

C. Consider f3 (force from Hydrostatic downstream) generate Torque 3 (T3)

$$f3 = P3 \cdot A \quad (2.74)$$

$$f3 = \frac{\rho.g.b}{2}.b.w = \frac{\rho.g.b^2.w}{2} \quad (2.75)$$

$$f3 = \frac{\rho.g}{2}.\left(\frac{D-H}{2}\right)^2.w = \frac{1}{8}\rho.g.w.(D-H)^2 \quad (2.76)$$

$$R_3 = \frac{1}{2}H + \frac{2}{3}b = \frac{1}{2}H + \frac{2}{3}\left(\frac{D-H}{2}\right) = \frac{H+2D}{6} \quad (2.77)$$

So Torque 3 (T3) is calculated as

$$T3 = f3.R_3 = \left[\frac{1}{8}\rho.g.w.(D-H)^2\right].\left[\frac{H+2D}{6}\right] \quad (2.78)$$

$$T3 = \left[\frac{1}{48}\rho.g.w.(D-H)^2\right].[H+2D] \quad (2.79)$$

Substituting equation 9, 29 and 35 into equation 3, then, the output torque become:

$$T_w = \left\{\frac{1}{16}\rho.g.H.w.(D-H).(H+D)\right\} + \left\{\left[\frac{1}{24}.w.\rho.g\right].[(D^3)-(H^3)]\right\} - \left\{\left[\frac{1}{48}\rho.g.w.(D-H)^2\right].[H+2D]\right\} \quad (2.80)$$

Power output (P_{output}) is defined as mean angular velocity $\bar{\omega}$ times output torque T_w. Whereas mean angular velocity $\bar{\omega}$ is is formulated as

$$\bar{\omega} = 2\,\pi\,f \quad (2.81)$$

which *f* is rotational speed of the wheel per second.

So the Output power is formulated as

$$P_{Output} = T_w.\bar{\omega} \quad (2.82)$$

2.5.3.2 Case of curving blade

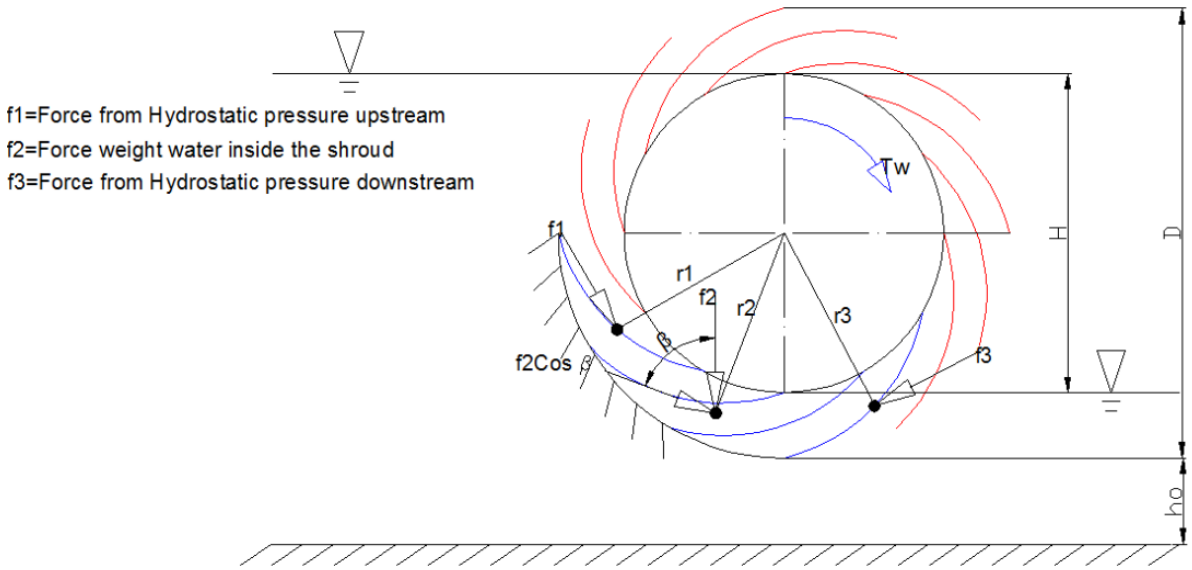

Figure 2.58: Schematic of determining centre of gravity water at the blade in the case of the curving blade

Assuming

w=blade width

b=blade length=$\frac{D-H}{2}$

It is very difficult to do undertake torque analysis on the curved blade tested. The problems associated with the torque analysis of this type of blade are listed below:

1. It is difficult to determine the position of centre of pressure of the force from hydrostatic pressure upstream (in this case is r1).
   In the case of the straight blade, determining the centre of upstream pressure position is easy to do. However it is very difficult to determine the position of the centre of pressure of the upstream hydrostatic force I the case of a curve blade. This position of the centre of pressure is important to determine the radius of the force. As this radius will be used to calculate the torque due to this upstream hydrostatic force.

2. Determining of the mass of the water inside of the shroud is also another problem in the case of the curved blade.
   As the form of the blade is curved, therefore it is also very difficult to calculate the mass/volume of the water inside the shroud. Even though the volume can be determined by a graphical method, however the general equation to determine the mass/volume area enclosed by lower shroud is still not possible.
3. It has proved difficult to determine the position of the centre of gravity of the mass inside the shroud.
   The position of the centre of gravity of the water inside the shroud is important because it is used to determine the lever arm (r2) of the mass, in which this lever arm is needed to determine the torque.
4. Determining the position of the centre of downstream hydrostatic pressure where the downstream force is working has also proved difficult to determine (in this case is r3).

Considering several problem above, it is easier to analyse and build theory of the Zuppinger model through hydrostatic analysis. The lossses shown are due to turbulence. The magnitude of this losses will be dependent upon the curve of the blade.

CHAPTER 3

EXAMINING THE EFFECT OF THE UPPER SHROUD TO THE PERFORMANCE OF WATER WHEEL.

The turbine wheel machine comprises of a lower shroud and upper shroud. Briefly, the experiments were conducted in the Hydraulics Laboratory, University of Southampton. The 12 m long, 30 cm width and 40 cm depth flume facility was used to support these experiments. In this initial study the turbine wheel physical appearance and dimensions was designed based on the drawing from *(Delabar 1855)*. In order to find out what is the effect of this upper shroud on the performance of the wheel, this preliminary experiment was undertaken and the effect of the upper shroud was investigated.

3.1 Testing Model

The testing model is a turbine wheel as shown in Fig 2.16. This turbine wheel was tested in two variations; with upper shroud and without upper shroud as shown in Fig 3.1 and 3.2 respectively. In this experiment, the outer diameter is 240 mm, whereas hub diameter is 160 mm. The blade width is 40 mm, and the wheel consists of 2 wheel which are separated by 4 mm thickness rim which the diameter the same as outer diameter of the outer wheel. Each side of the wheel consists of 12 blades.

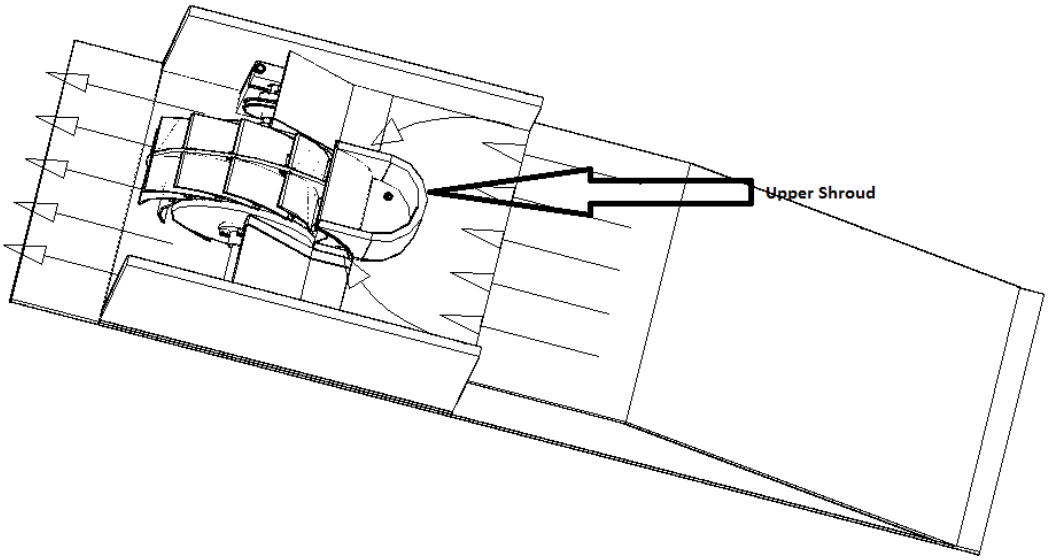

Figure 3.1: Three (3)-D Drawing of the experimental model with upper shroud

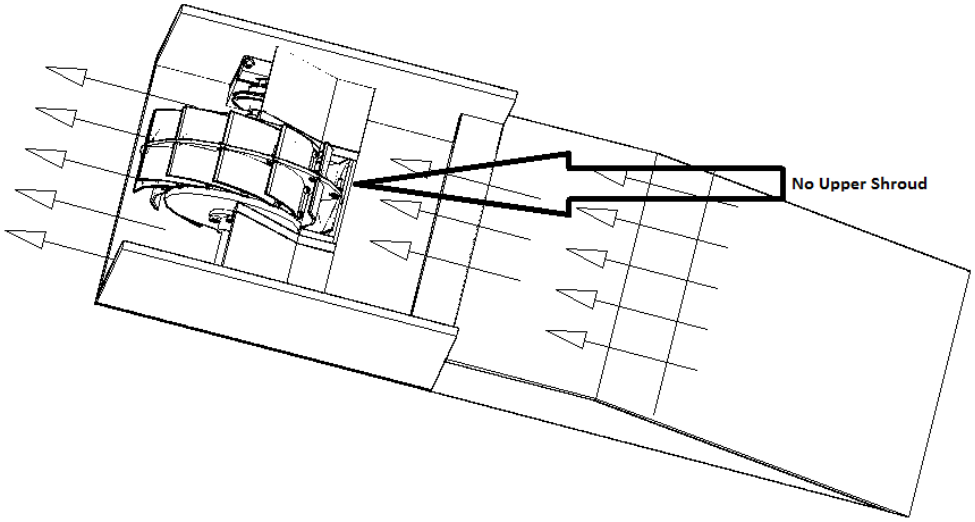

Figure 3.2: Three (3)-D Drawing of the experimental model without upper shroud

In order to give a clear overview of the dimension of the testing model, the 2D drawing accompanied with the dimensions of the model is shown in Fig 3.3. A picture of the model is presented in Fig 3.4

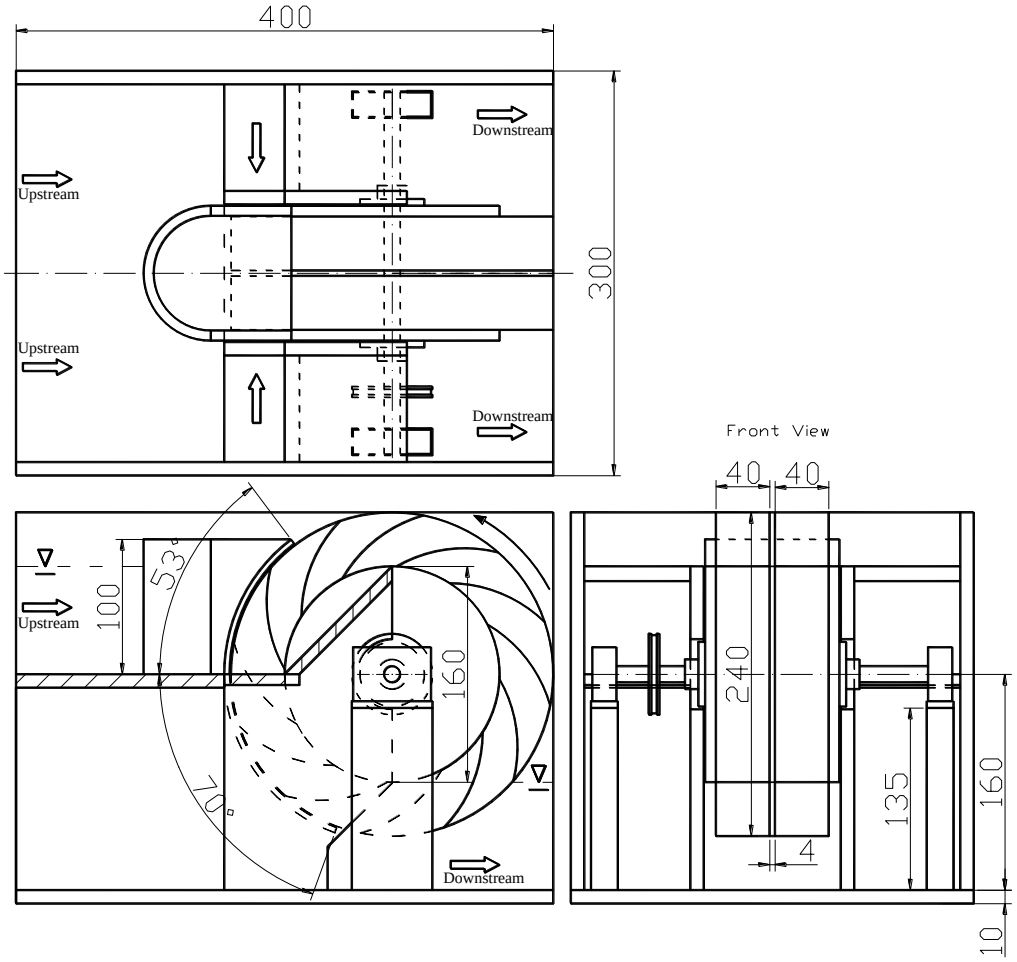

Figure 3.3: 2D drawing of the testing model (units in mm)

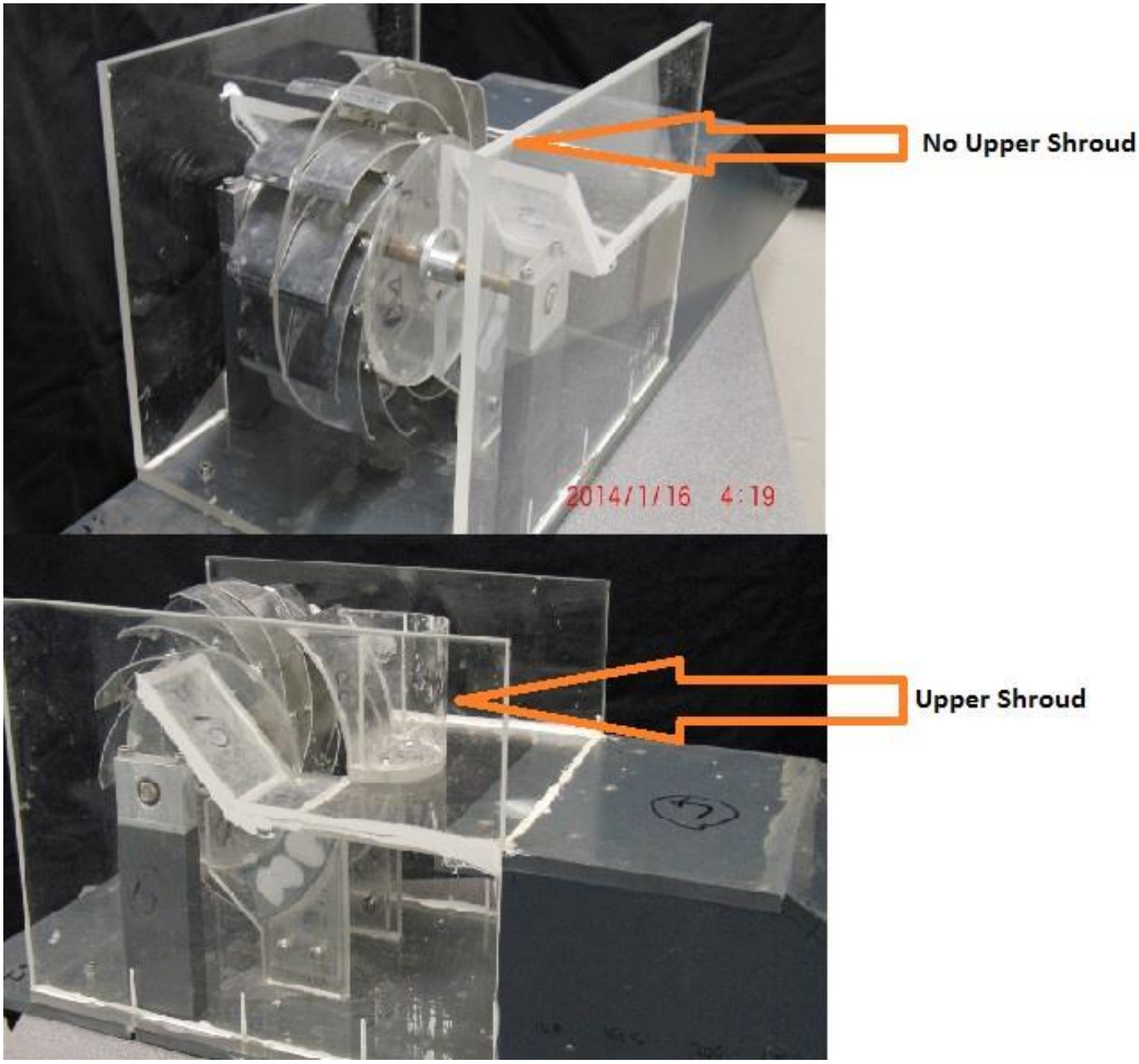

Figure 3.4: Photograph of the testing model, upper side : without shroud , lower side : with shroud

3.2 Determining blade dimension

The blade forms an arc, which is formed from circle that intersects the circle of the outer diameter D_{out} and hub circle D_{in}. Investigations in to turbine wheel blade design have shown that there appears to be no published detail designed information available. Therefore it can

be surmised that the blade was curved by hand. However, based on the information shown in his drawing, then the blade form can be predicted. By redrawing his original machine, the method for designing his blade can be explained as follows, whereas the shaping diagram of the blade is shown in Figure 3.5:

1. Draw circle with outer diameter D_{out} as diameter.
2. With the same circular centre, draw hub with diameter D_{in}
3. then draw straight line O-A
4. draw another line with angle 53^o in respect to previous line
5. connect two point, which are A and E.
6. draw line O-B which form 45^o in respect to line O-A
7. draw line C-D which perpendicular to line A-E and divide line A-E with the same length, this line must attain line O-B
8. draw circle from point D to form circle.
9. Arc A-E is the blade arc which forms the blade.

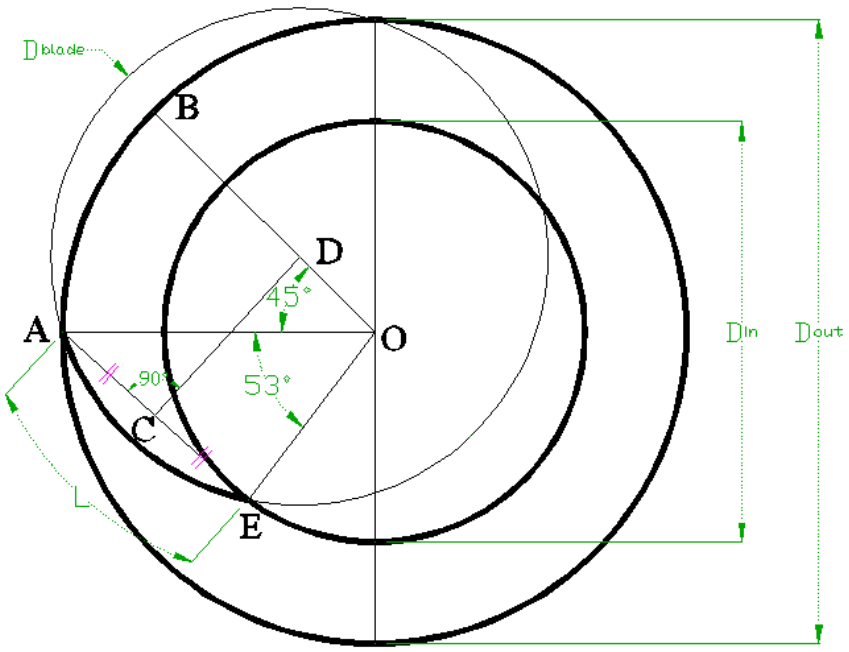

Figure 3.5: Shaping diagram of the blade

The methodology of forming the blade as explained above gives a reasonable accurate reproduction of the original blade that can be seen from Fig 3.6. The red blade is the blade

which is formed from the methodology as explained above. This overlays the original turbine wheel which is behind it.

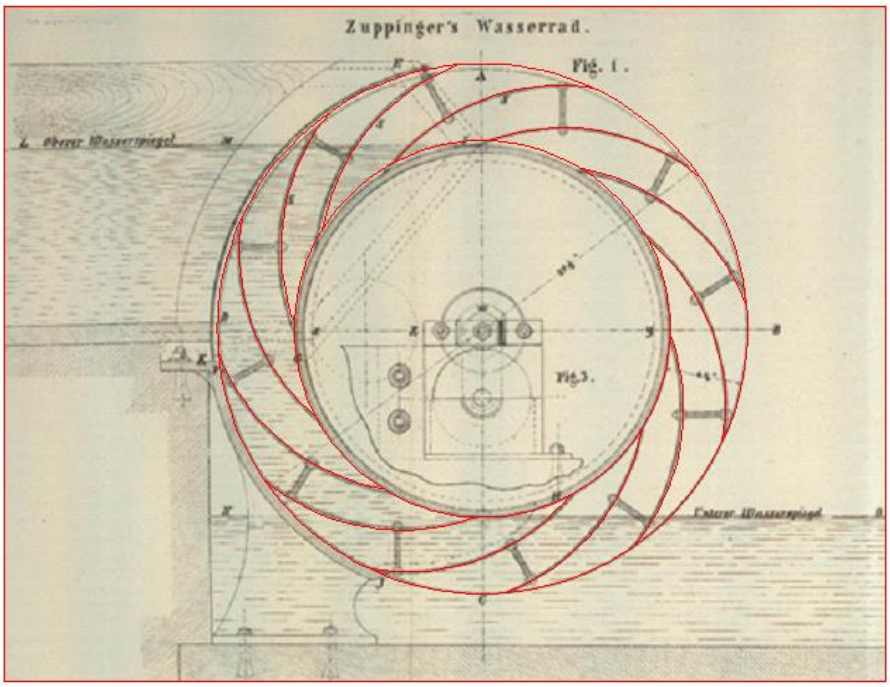

Figure 3.6: Matching between the original turbine wheel machine to the blade forming method

3.3 Equipment and facility

The experiments were conducted in the recirculating flume at Hydraulics Laboratory University of Southampton. Fig 3.7 shows a schematic diagram of the flume. The water from sump is pumped to the working section. The flow rate Q and head level H is controlled by using a control valve and the downstream weir.

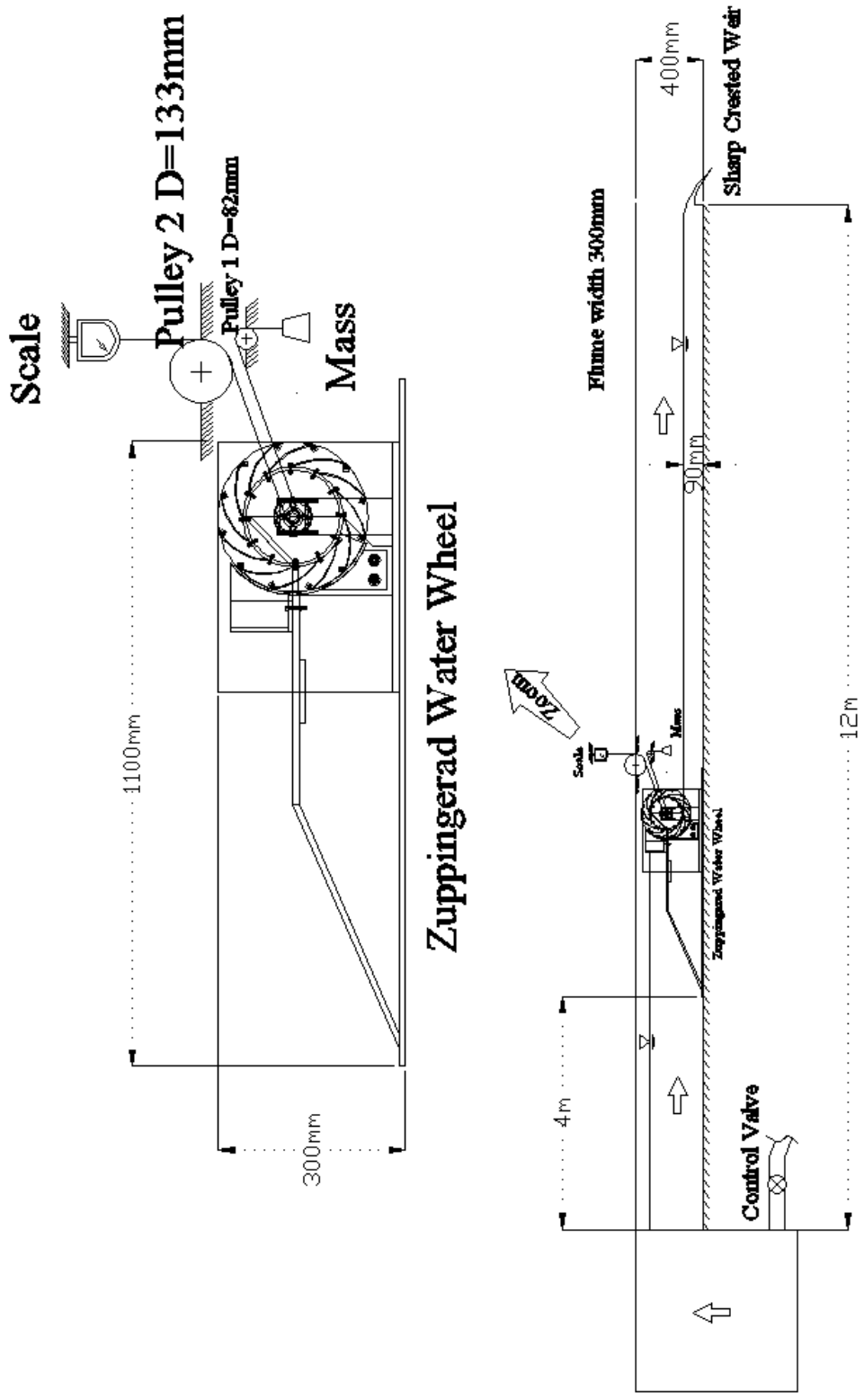

Figure 3.7: Schematic diagram of the flume

Some equipment that was used in this experiment will be elaborated. The tools are listed as below :

1. Prony brake

A Prony was used to measure the torque from the water wheel. The power is calculated by multiplying torque *T* by rotational speed *f*, as derived in equation 3.1. Free body diagram of the force on the Prony brake is presented in Fig 3.8. The friction wheel that was used is the disc which has gully as track for rope to wrap which has radius *r*= 26 mm.

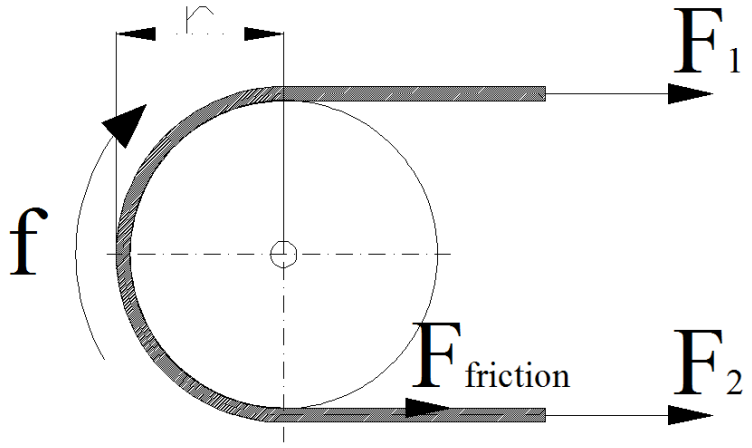

Figure 3.8: Free body diagram of the force on the rope

$$P = T \cdot 2\pi \cdot f \qquad 3.1$$

Where *T* is the torque, produced from friction force $F_{friction}$ times radius of the Prony brake *r* as stated on equation 3.2

$$T = F_{friction} \cdot r \qquad 3.2$$

Friction force $F_{friction}$ is the subtraction between strength on the edge of the rope

$$F_{friction} = F_1 - F_2 \qquad 3.3$$

Rope

The rope was used to wrap on the Prony brake, and then both ends were connected to the digital scale and weight.

Pulley

Two ball bearing pulleys were used in order to reduce friction effect in transmission. Which has diameter 82 mm for pulley 1and 133 mm for pulley 2.

Digital scale

A digital scale was used to measure the force in the rope, and the resulted data will be used to calculate the power. In this experiment, a 15 kg max scale and with a accuracy of 0.01 kg was used.

Mass

The loads that were used in this experiment are the mass with 50 gr each, and attached to the holder which connected to the end of the rope.

3.4 Experimental Parameters

This research is conducted by flowing water through model testing and maintaining water head H constant 0.166 m. The load/mass was hung through a rope which wraps two pulleys and friction wheel as shown in diagram. At the other edge, rope was connected to scale balance, and the scale on the balance was considered as output. The load/mass was started at 1800 gr and then decreased incrementally 50gr until 0. Then the counterweight mass/ scale balance response M_C (kg), flow rate Q (m^3/s) rotational speed f (rev/sec) are considered as output that need to be evaluated. Some output data are further calculated based on the measurement results as elaborated below.

1. Power Output

The measurement is made by wrapping a rope around Prony brake/friction wheel, and measuring the force transferred to the rope through friction. One end of the rope is connected to the weight through a pulley, whereas another end is attached to the digital scale also through a pulley. The difference between the weight and the reading at the digital scale then multiplied by the radius of the friction wheel which is equal to the torque. The speed of the friction wheel is calculated by recording the times needed for the drum to revolve 10 times. The schematic diagram of the Prony brake measurement can be seen at Fig 3.7. The equation that was used to calculate power output $P_{out\ measured}$ is written in equation 3.4 and 3.5. which derived from equation 3.1

$$P_{out\ measured} = (F_1 - F_2)\, r \cdot\ 2\pi \cdot\ f \qquad 3.4$$

$$P_{out\ measured} = \left(M_{measured\ from\ balance} - m_{mass}\right) g\ \cdot r \cdot\ 2\pi \cdot\ f \qquad 3.5$$

$$f = \frac{number\ of\ revolutions}{time(s)} \qquad 3.6$$

Water flow rate within the water wheel

The water flow rate can be measured using a sharp crested measurement weir which is placed downstream of the model being tested. The flow rate is measured by using the standard equation used in conjunction with the sharp crested weir to calculate the flow rate (Chanson 2001), as stated on the equation 3.7 and 3.8, where t_1 and ΔZ are the water depth and weir height as shown in Fig 3.9.

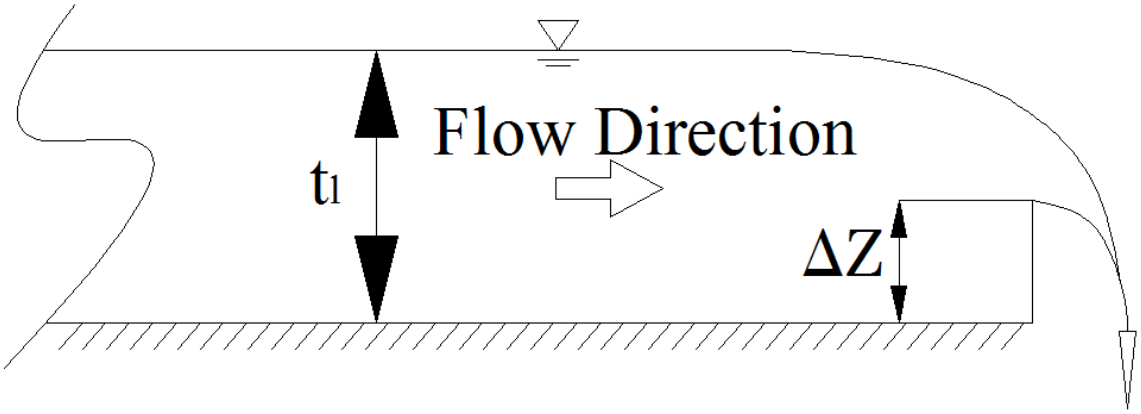

Figure 3.9 : Sharp crested measurement weir

$$Q_{sharp} = \frac{2}{3} C \sqrt{2\ g\ (t_1 - \Delta Z)^3} \qquad 3.7$$

Where

$$C = 0.611 + 0.08 \frac{t_1 - \Delta z}{\Delta z} \qquad 3.8$$

In addition, the theoretical water flow rate through the wheel is also considered in this thesis. This theoretical water flow rate is the flow rate that will be used as a basis to calculate the efficiency of the machine tested in these experiments. The reason for choosing theoretical water flow rate as a basis to calculate the efficiency of the water wheel will be discussed on subchapter 3.5.2. The equation to calculate theoretical water flow rate through water wheel is based on the equation 3.9

$$Q_{th} = \frac{\left((D_{out})^2 - (D_{in})^2 - n.l - n.t\right) \pi \cdot 2\ b \cdot f}{4} \qquad 3.9$$

Where D_{out} is the outer diameter of the water wheel, D_{in} is the inner diameter of the water wheel, n is number of blades, l is the length of the blade and t is the blade thickness. Whereas b and f is the blade width and rotational speed respectively. Equation 3.9 refers to Fig 3.10.

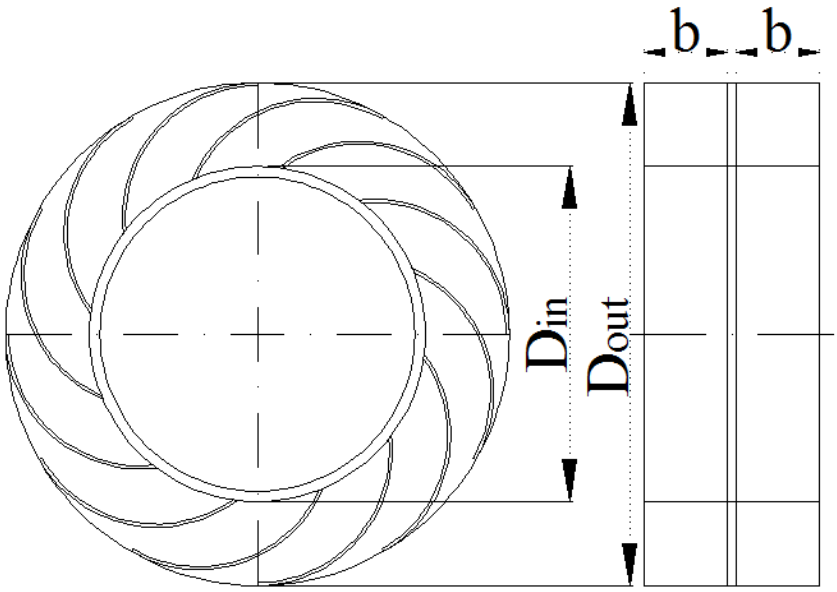

Figure 3.10: Water Wheel and the dimension

Hydraulic power available according to flow rate in blade of water wheel

Hydraulic power available according to flow rate in blade of water wheel can be calculated based on the water flow rate passes through water wheel blade's P_{mi} by equation 3.10

$$P_{m\,i} = \rho_{water} \cdot Q_{th} \cdot g \cdot H \qquad 3.10$$

Efficiency

The efficiency in this case is the ratio between output power $P_{out\ measured}$ and the hydraulic power available according to flow rate in blade of water wheel which is calculated based on the water flow rate passes through water wheel blade's P_{mi}. This efficiency is then called as efficiency exclude leakage η_{wl}. This efficiency η_{wl} is formulated as in equation 3.11.

$$\eta_{wl} = \frac{P_{out\ measured}}{P_{mi}} \qquad 3.11$$

Tangential velocity of the water wheel

Tangential velocity of the water wheel can be written as equation 3.12

$$v_{tan} = \frac{(D_{out}+D_{in})\,\pi \cdot f}{2} \quad 3.12$$

Maximum possible velocity

The maximum possible velocity of the water is free fall velocity of the water on the certain distance which is the head *H* of the water wheel or the hub diameter.

$$v_{max} = \sqrt{2 \cdot g \cdot H} \quad 3.13$$

Leakage

Leakage was measured in this research. The leakage was determined from the differences between the water flow rate passing over the sharp crested weir Q_{sharp} and the theoretical water flow rate Q_{th} as shown in equation 3.14.

$$Q_l = Q_{sharp} - Q_{th} \quad 3.14$$

3.5 Result

3.5.1 Measured Power vs Rotational Speed

Fig 3.11 shows measured power vs rotational speed of the water wheel. Measured power is calculated as refer to equation 3.5, whereas the speed is the rotational speed per minute *rpm*. It reveals that the water wheel with upper shroud provides higher power in comparison with the water wheel without upper shroud. The differences in power output are more obvious in higher speed. The graph also shows that the power output is decreasing as the speed increases. More over the maximum power output for water wheel with upper shroud is 2.5 Nm/s at the speed of 67 rpm, whereas in the case of without upper shroud the maximum power is 1.7 Nm/s at the speed of 60 rpm. At speeds of more than 46 rpm, the power output from the water wheel with an upper shroud is consistently higher than the power output of the water wheel without an upper shroud. Yet at speeds lower than 46 rpm, the power output trend is not as consistent as with speeds greater than 46 rpm. The power output of both wheels seems to overlay each other and has no pattern. This data indicates an error has occurred. This error is due to the methodology of measurement, by using the clasical prony

brake which relies on the friction between the rope and the prony wheel. At low speeds (high torque), sliding occurs between the rope and the prony wheel which causes an inacurate measurement of the power output. This problem is also identified from the efficiency curve, which will be elaborated in subsection 3.2

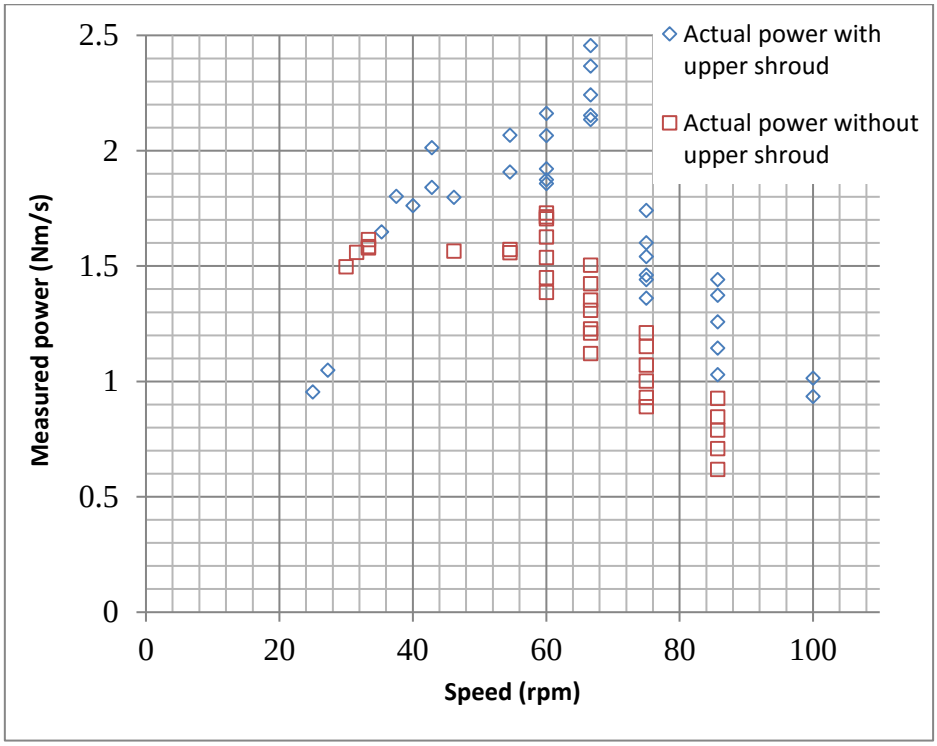

Figure 3.11: Power vs speed

3.5.2 Leakage

Leakage is a problem that is difficult to avoid in this research. The slowest speed which leakage was measured is at the speed of 25 rpm. This is the slowest speed where the machine can be set up. Since the leakage increases as the rotational speed increases, therefore the static leakage measurement (the leakage where measured at a rotational speed of zero) was not carried out. Fig 3.13 shows the percentage of leakage. It shows that the percentage of leakage decreases as the speed increases. In addition, the percentage of leakage is significant, which almost 140% at the speed of 25 rpm and around 22% at the speed of 67 rpm.

Considering this high percentage of leakage, therefore the water flow rate is calculated based on the theoretical water flow rate through water wheel.

As an example to show a source of leakage that can occur, then Fig 3.12 below indicates the clearance between the hub and the side plate. The clearance between these two parts is 3 mm for each side. This tolerance is required to avoid friction between the hub and the side plate.

The sources of friction between the hub and the side plate are as follows:

1 The wheel hub and side plate are constructed from Perspex. This material as supplied is not totally flat (typical tolerance ±1 mm across surface), therefore a clearance has to be allowed between these two parts to accommodate the flatness tolerance.

2 Under high load there is a tendency for the shaft to twist, which causes the wheel itself to skew and rubbing between the side plate and the hub can occur.

In order to overcome this problem, it was made a wide clearance between the hub and the side plate. In addition the gaps between the flume and the water wheel structure also are sources of leakage.

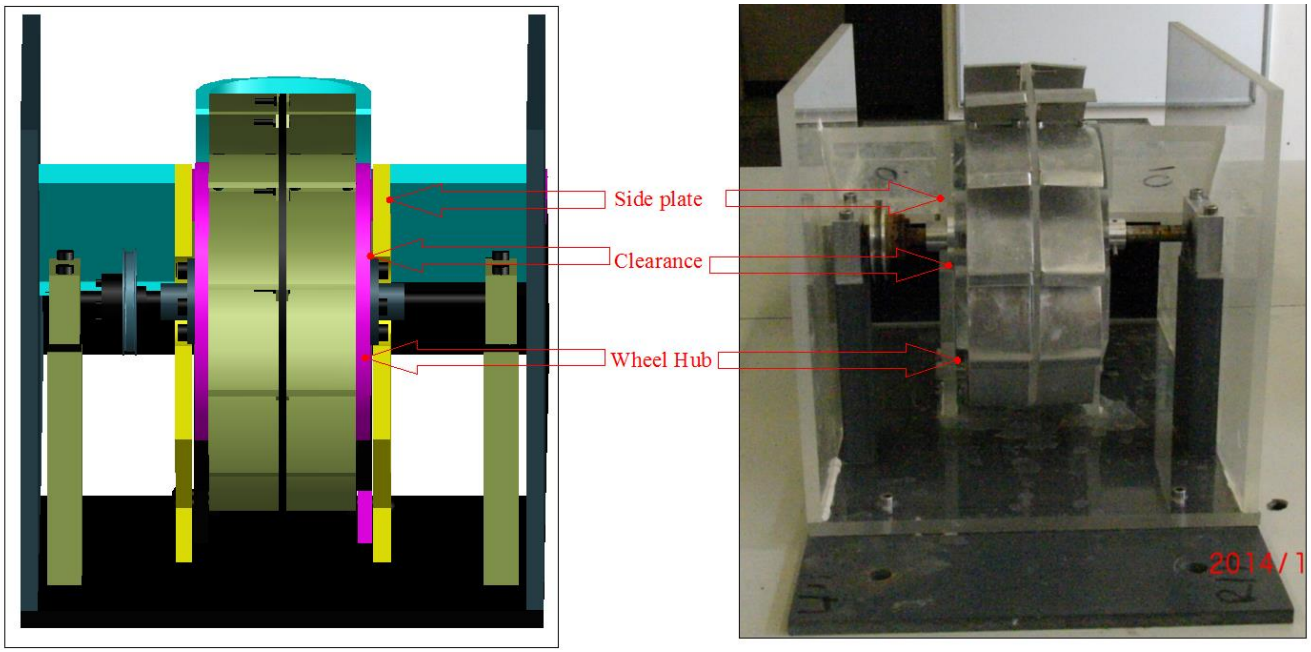

Figure 3.12: An example source of leakage (the clearance is 3 mm with the blade width 40 mm)

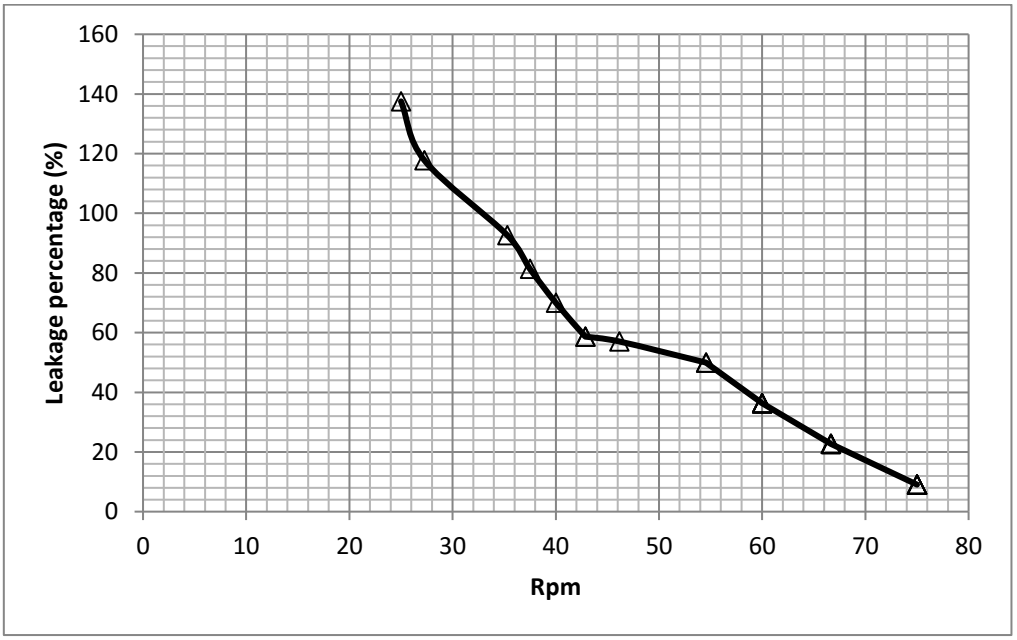

Figure 3.13: Rotational speed VS Leakage percentage

Fig 3.13 shows that the leakage trend is decreasing as the rotational speed increases. Leakage occurs due to the clearance between an unmovable part and a movable part. In addition, it is also due to the pressure difference between upstream and downstream. The pressure difference is caused by the water surface difference between upstream and downstream. In parallel with the increasing rotational speed of the wheel, an increase in upstream head drop occurs due to increasing rotational speed of the wheel. This head drop causes a reduced water surface difference between upstream and downstream, which also lead to a reduce pressure difference between upstream and downstream. A reduction in this pressure difference also reduces leakage as the rotational speed of the wheel increases.

3.5.3 Efficiency vs Tangential Velocity

Fig 3.14 represents the efficiency vs tangential velocity of the water wheel. The tangential velocity is non-dimensionalized by dividing it with the maximum possible velocity of the water (see equation 3.13). The effect of the upper shroud on the efficiency of the water wheel is being compared. The efficiency in this case is the ratio between measured powers

$P_{out\text{-}measured}$ to hydraulic power available P_{mi} as stated at equation 3.11. Most of the data indicates that the efficiency of the turbine wheel with an upper shroud is higher than the turbine wheel without an upper shroud. For example at v_{tan}/v_{max} 0.39, the efficiency of the turbine wheel with upper shroud is in the range of 60-67%, whereas the efficiency of the turbine wheel without upper shroud is in the range of 32-42%.

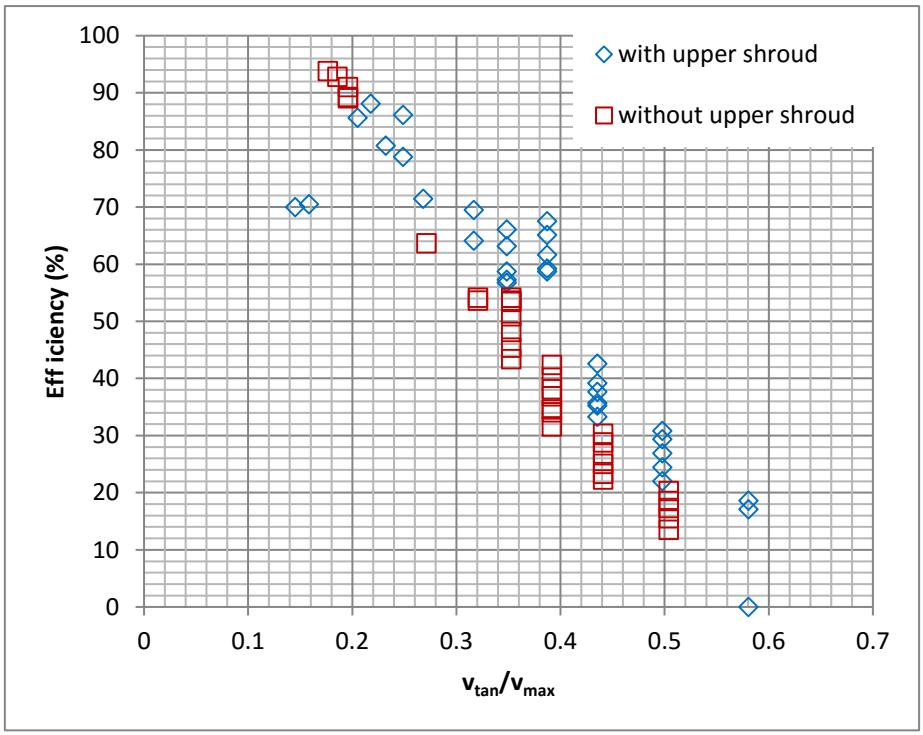

Figure 3.14: Efficiency vs non dimensionalized tangential velocity

3.6 Discussion on preliminary test

The experimental result shows that the turbine wheel with an upper shroud gives better performance in comparison to turbine wheel without an upper shroud. This is more obvious at higher speed. At Fig 3.11, shows that at a speed of more than 33 rpm, power output from the turbine wheel with an upper shroud is consistently higher than the turbine wheel without an upper shroud. More over Fig 3.14, shows that the efficiency of the turbine wheel with an upper shroud is also mostly higher than the turbine wheel without an upper shroud. At

v_{tan}/v_{max} more than 0.21, the efficiency of the turbine wheel with an upper shroud is always higher than the turbine wheel without an upper shroud. The difference in performance between these two turbine wheels might be related to the losses of power at the entrance of the machine. In the case of the wheel without an upper shroud, the blade hits the incoming water and creates splashing. This is what is called by (Linton 2014) as 'water slamming'. Water slamming is the event where the blade hits the body of the water at the cell inlet. This situation generates additional losses especially at high rotational speed. This water slamming occurs in the case of turbine wheel without an upper shroud, whereas in the case of turbine wheel with an upper shroud this situation does not occur.

The comparison performance between RHPM machine to the turbine wheel with upper shroud is shown at Fig 3.15. This graph shows that turbine wheel have chance to achieve certain efficiencies with higher tangential speed rather than middle shot hydrostatic machine. For example in the case of the efficiency ≈70%, where the turbine wheel machine can reach this 70% at $v_{tan}/v_{max} \approx 0.32$, whereas for the case of middle shot hydrostatic machine this 70% efficiency could be reached at $v_{tan}/v_{max} \approx 0.25$. This means that at given performance, turbine wheel machine can rotate at higher speed in comparison with RHPM. This graph also shows that turbine wheel machine have possibility to rotate at higher speed in comparison with RHPM, as result it can absorb more power and deliver more power. In addition the higher rotational speed of the turbine, the better it is from a transmission stand point, since the generator needs high speeds in order to produce electricity. It needs around 50 Hertz of rotational speed for the generator to produce electricity.

In Fig 3.11 can be seen at the rotational speed of 54rpm, which corresponds to $v_{tan} = 0.571$ m/s or $v_{tan}/v_{max} \approx 0.32$ the power output is 2.07 W. This power output is fairly high in comparison to other rotational speed variations. In addition, the efficiency of the turbine wheel with an upper shroud is at this $v_{tan}/v_{max} \approx 0.32$ is about 70%, which is fairly high as well. Furthermore this $v_{tan}/v_{max} \approx 0.32$ shows better performance (20% difference at $v_{tan}/v_{max}=0.3$) in comparison with a rotary hydrostatic machine (RHPM) as shown in Fig 3.15. Therefore it will be interesting to pay attention to this range of speed for further investigation. More over, the draw back that can be seen from the Prony brake method is that at a certain of speed, the data shows a variations in the recorded power output. This is the weakness of this

measurement methodology, where the data that was taken based on visual recording of the output from a weight scale display. This method could result in more than one data of power output at particular rotational speed being recorded, which will give a less accurate measurement of power output. A further drawback of the Prony brake method is the limited capability to measure power output at low speed due to the mechanism of measurement relies on the friction force between the rope and the Prony wheel. This statement is supported by the fact, where the efficiency drops at a speed v_{tan}/v_{max} of less than 0.22 rpm in the case of a turbine wheel with an upper shroud, this can be shown in Fig 3.14. Therefore an alternative method needs to be developed to overcome this problem.

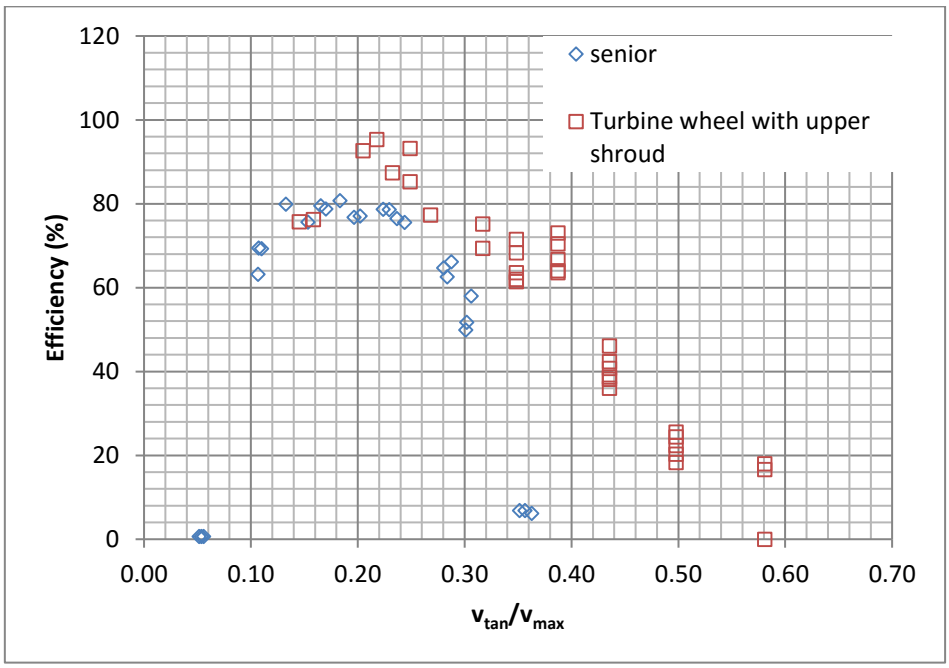

Figure 3.15: Comparison between turbine wheel machine to the RHPM shown by (Senior 2009)

3.7 Summary from preliminary test

As a preminilary test, it shows that the turbine wheel shows an interesting result incomparison to the RHPM. In addition, a water wheel with an upper shroud gives higher power output efficiency rather than water wheel without upper shroud. In hindsight, methodology of measuring power output by using Prony brake need to be improved. In

addition some modification on the machine is needed and the effect of the modification to the performance of the water wheel is still need to be investigated.

CHAPTER 4

ELECTRIC POWER TAKE OFF AND MODIFICATION OF THE TURBINE WHEEL

4.1 Experiments to improve performance of turbine wheel

In the chapter 3, the preliminary research on the original turbine wheel has been described. The power output was measured by using the Prony brake method. In this sub section the following work which the methodology of measuring power output will be improved by using an electric power take off (PTO). As previously mentioned from subsection 3.5, the Prony brake has a drawback in gaining accurate data, since the data was accrued by eye from weight scale displays. In addition the Prony brake also did not function particularly well at low speed. The Prony brake system measures power output based on friction force between rope and the Prony wheel as shown in equation 3.1 to 3.5. At condition where the mass balance is large enough and the friction coefficient of the surface of the Prony wheel is not enough to create friction force, then the interaction between rope and Prony wheel is sliding. Therefore the friction force that will be used to calculate power output is not reliable any more. This situation occurred at conditions of low speed, large mass balance and high torque. The following target is to investigate further design improvements on the turbine wheel to improve the efficiency. During this work there were multiple geometric parameters of the turbine wheel that required optimisation. Detailed below are short descriptions of the work undertaken to solve these optimization problems:

1. Assess the effect of changing the hub diameter

The hub diameter is varied in this research, since the performance of the water wheel could either improved or deteriorated. The larger the hub size, the higher the head differences, which potentially could result in a higher power output. However, this also means reducing the cell area, which potentially could reduce power output. Which factor will contribute more to the power output will be investigated by varying the hub diameter. The hub diameter set to

vary from 100 mm, 170 mm and 250 mm. The pulley which attach on the wheel is connected to the other pulley. The last pulley is attached on the DC motor. This DC motor is acts as load where the load level is controlled by using potentiometer (see Fig 4.4).

2. Assess the effect of varying blade numbers

Previous research undertaken by (Linton 2014) stated that the HPM with 6 blades, potentially will give a better power output in comparison to a 12 bladed wheel. However his claim is just based on the measured moment bending at a single blade, and did not measure the power output of the machine. In this test the power output of the 6 bladed wheel and 12 bladed wheel will be compared.

3. Assess the effect of the inlet baffle on the performance of the machine

The entrance of the water wheel will be improved by using baffles. However the effect of these baffles on the performance will be studied. Does it really improve or deteriorate the performance of the machine?

4. Capture visual images of the interaction between water in the cell and the blade

The interaction between water and the blade is an interesting point, since the mechanism of losses and the mechanism on how power produced is derived from this interaction. In order to get an idea on how the mechanism occurs, a high speed camera was used.

4.2 Cut-in half wheel

The interaction between water and the blade plays a prominent role in the mechanism of power production and power losses. In order to visualize the interaction between the blade and the water as the wheel rotates, the cut-in half turbine wheel was produced. This cut-in half turbine wheel as shown in Fig 4.1. This turbine wheel was tested in 5 variations as tabulated in table 4.1. In this experiment, the outer diameter is 337 mm, whereas hub diameter varies as follows 100 mm, 170 m and 250 mm. The hub with 250 mm diameter is used as a benchmark, since this ratio between the outer diameter to the hub diameter is almost similar to the original machine that was built by Zuppinger. As can be seen from the original

machine, the dimension of the turbine wheel is presented in the Fig 2.16 where the outer diameter D_{out} is 755.65 mm, hub diameter H is 539.75 mm and two side blade with 120.65 mm wide each. Considering that the outer diameter of the current machine is 337 mm, so the hub diameter of the current machine Hub_{cm} should be calculated as

$$\frac{D_{out}}{Hub} = \frac{755.65}{539.75} = 1.4 = \frac{337}{Hub_{cm}} \quad 4.1$$

So Hub_{cm} is 240.71 mm, due to availability a 250 mm hub size has been chosen. The other sizes of hub are used as a comparison and the effect of changing the hub diameter will be investigated. The blades are made of aluminum plate, of a thickness of 1.5 mm, and a width of 100 mm. The blade is attached at the outer rim where the thickness is 10 mm and also attached to the hub. The clearance between the outer rim and the wall flume is 1.5 mm. The water inflow enters the machine via the side of the wheel, so water from upstream enters axially, guided by the upper shroud and exits underneath downstream. The downstream water level is held at the lowest point of the hub. The blade was shaped curve as explained in subsection 3.2.

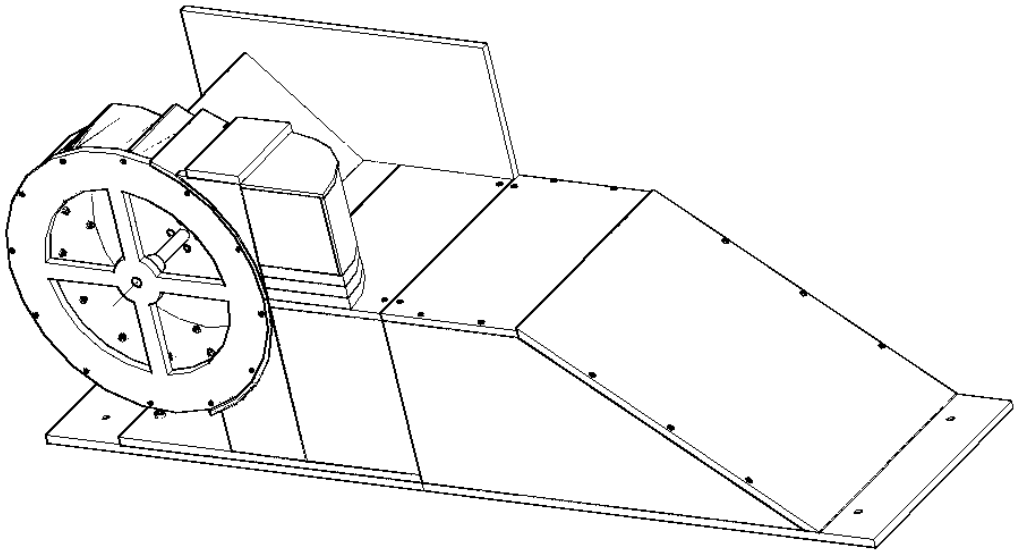

Figure 4.1:Three (3)-D Drawing of the half turbine wheel.

In order to give a clear overview of the dimension of the testing model, the 2D drawing accomplished with the dimension of the model is shown in Fig 4.2. The unit at this drawing is mm. The complete picture of the model is presented in Fig 4.3

Table 4.1: Experimental variations

No	Hub Diameter	No blade	note
1	250	12	
2	250	6	
3	250	12	baffle
4	170	12	
5	100	12	

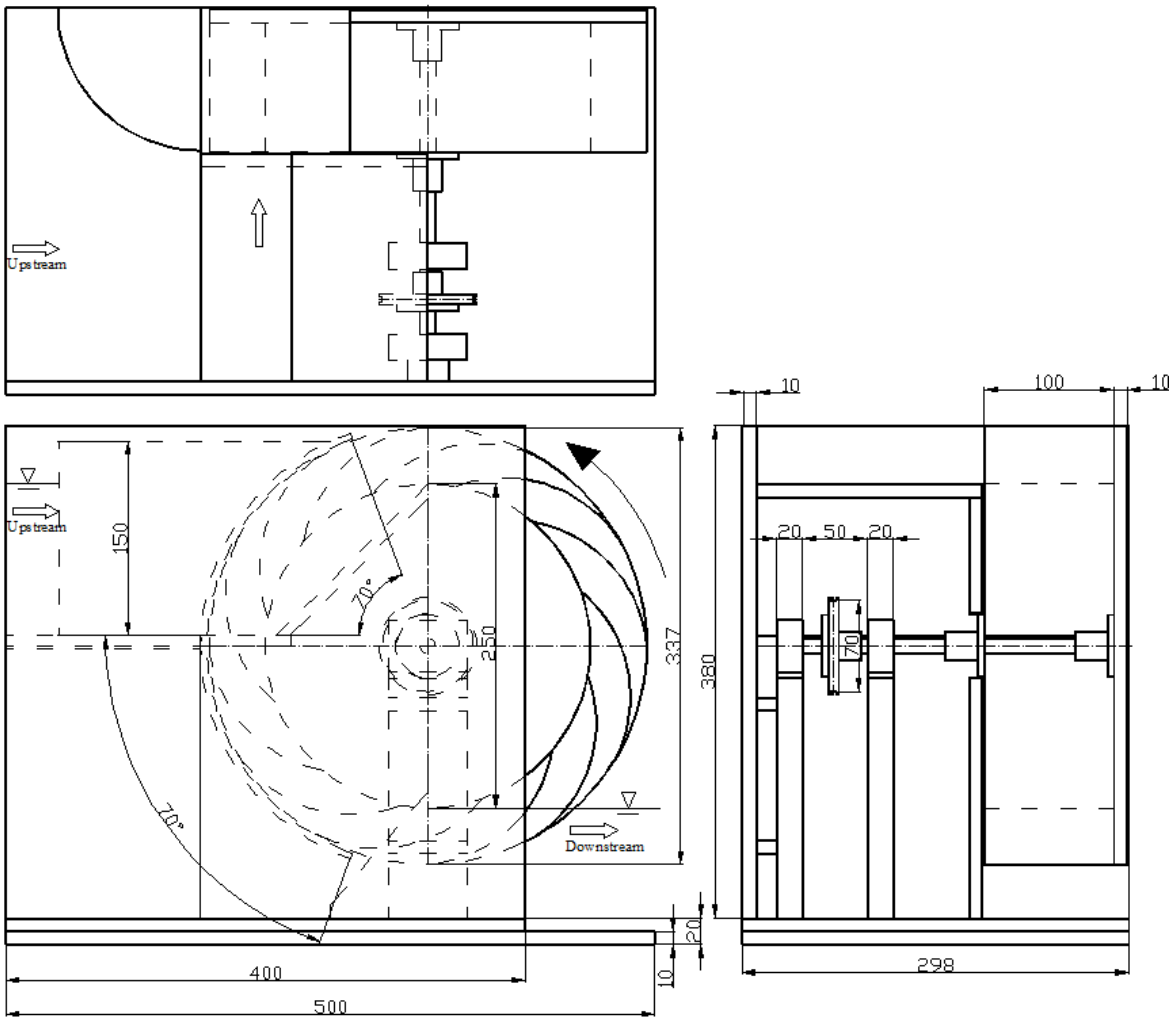

Figure 4.2: 2D drawing of the cut-in half turbine wheel for hub 250 mm.

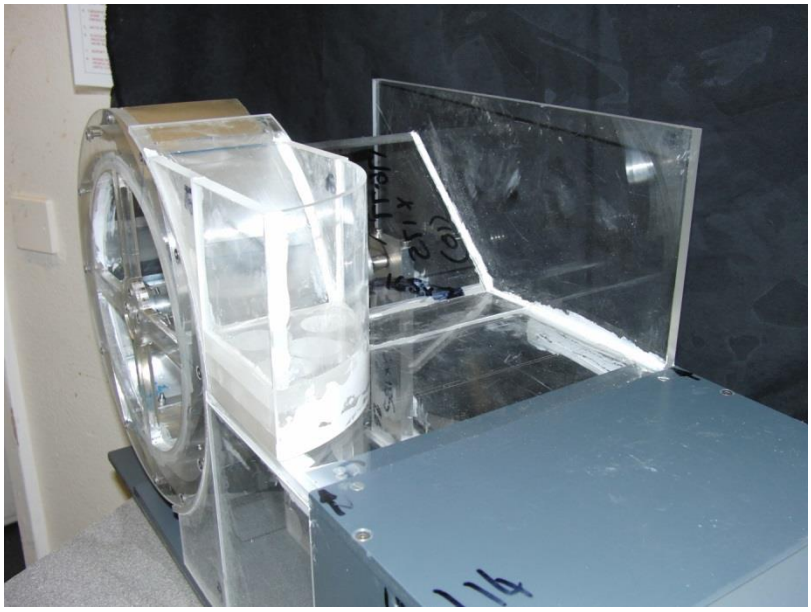

Figure 4.3: Photograph of the testing model of hub 250 mm

4.3 Preliminary research findings and their impact on the following research

The work in chapter 3 was done in order to get an initial assesment of the turbine wheel. From this preliminary research, which the head of the machine is 0.16m, it has been known that the optimum power output is around 2.07 W. The design maximum tangential velocity is about 0.571 m/s, with the outer diameter 240 mm and hub diameter 160 mm. The information from the preliminary research is used to predict maximum power output and the rotational speed of the machine. In addition this information will be used to determine the DC motor specification that will be used as a brake to measure power output.

Froude scaling is used in order to predict the performance of the large scale machine than the model scale. The scaling technique is allowed if the flow conditions between scaled model and large model are shows similarity in geometric, kinematic and dynamic as formulated in equation 4.2-4.4. Symbols l, v and F refer to length, velocity and force. Whereas subscript symbol $_p$ and $_m$ refer to prototype and model of the machine. In this case, model is refer to preliminary machine.

$$Geometric\ similarity = l_r = \frac{l_p}{l_m} \quad 4.2$$

$$Kinematic\ similarity = v_r = \frac{v_p}{v_m} \quad 4.3$$

$$Dynamic\ similarity = f_r = \frac{F_p}{F_m} \quad 4.4$$

However, some of the formula can be express as equation 4.5-4.6 below:

$$velocity = v_r = \frac{v_p}{v_m} = \sqrt{l_r} \quad 4.5$$

$$Power = P_r = \frac{P_p}{P_m} = {l_r}^{3.5} \quad 4.6$$

$$Flow\ rate = Q_r = \frac{Q_p}{Q_m} = {l_r}^{2.5} \quad 4.7$$

Data from preliminary experiment which the machine is considered as a model is tabulated on the table 4.2 below

Table 4.2: Data from previous experiment

l_m	160 mm
v_m	0.571 m/s
P_m	2.07 w

The machine that will be tested for the current experiment is considered as the prototype. Further, the predicted power output for the current experiment is calculated, based on the biggest hub of the current machine. Since the hub of the biggest current machine is l_p=250mm and the previous machine is l_m=160 mm, so l_r is calculated as $l_r = \frac{l_p}{l_m} = \frac{250}{160} = 1.562$.

The predicted velocity is calculated as $velocity = v_r = \frac{v_p}{v_m} = \sqrt{l_r} = \frac{v_p}{0.571\text{m/s}} = \sqrt{1.562}$, and v_p=0.714 m/s. The outer diameter of the current wheel is 337 mm, whereas the hub diameter is 250, this fact results the average radius of the wheel as $r = \frac{\frac{337\ mm}{2}+\frac{250\ mm}{2}}{2} = 146.75\ mm = 0.14675\ m$

based on the data above, the angular velocity of the current model ω is calculated as $\omega = \frac{v_p}{r} = \frac{0.71436\ \text{m/s}}{0.14675\ \text{m}} = 4.868\ rad/sec$. The rotational speed of the current machine also can be stated as rotation per-minute/rpm. This can be stated as $n = \frac{\omega}{2\pi} = \frac{4.868\ rad/sec}{2\pi} = 0.774\ rps = 46.489\ rpm$.

Power output also can be predicted from data provided above. Since the larger machine is designed as half machine, so the power per-m width is defined as $P_r = \frac{P_p}{p_m} = \frac{0.5 \cdot {l_r}^{3.5}}{b\ l_r} = \frac{0.5 \cdot 1.562^{3.5}}{0.08 \cdot 1.562}$. This calculation results predicted power output per-m width for prototype as P_p=39.419 W/m. Further, the predicted power output for the current machine is calculated as $P = P_p \cdot b = 39.419 \frac{\text{W}}{\text{m}} \cdot 0.1\ m = 3.941\ \text{W}$. The predicted power output and the rotational speed is the base of the consideration to determine DC motor as brake to measure power output as discussed in section 4.4.

4.4 Equipment and Facility for cut-in half water wheel

The experiments were conducted in the Hydraulics Laboratory of the University of Southampton. The model was placed in the 12 m long, 30 cm wide and 40 cm deep flume. Fig 4.4 shows a schematic diagram of the flume. The system consists of the cut-in half water wheel, with the pulley A attached on the shaft where the wheel is also attached on it. This pulley A is then connected to pulley B. This pulley B is connected to the DC motor. This motor will determine how much a load is applied to the machine. The load on the system is controlled using the resistance that is applied on the DC motor which is adjusted by using potentiometer. The motor is also attached on to the vertical bar as can be seen from Fig 4.4. At the lower side of the vertical bar, a hinge H is attached, therefore the vertical bar can pivot and the hinge also acts as the centre of the pivot of the vertical bar. At the upper edge of the vertical bar a wire is attached at point **a** which will connect the upper edge of the vertical bar to the force transducer/load cell. This load cell will give information about force applied on the point **a** to the module that transmits the signal to the computer to be displayed. As the wheel rotates CCW (counter clock wise), then pulley B which the DC motor is also attached via its shaft is rotating CCW as well. Then the vertical bar which the motor and the pulley B are attached also will pivot on the hinge H. The movement of this vertical bar will pull the

wire at point **a** and lead to a force measurement signal at the load cell. The mechanism on how the system work will also be explained in part 4.5.

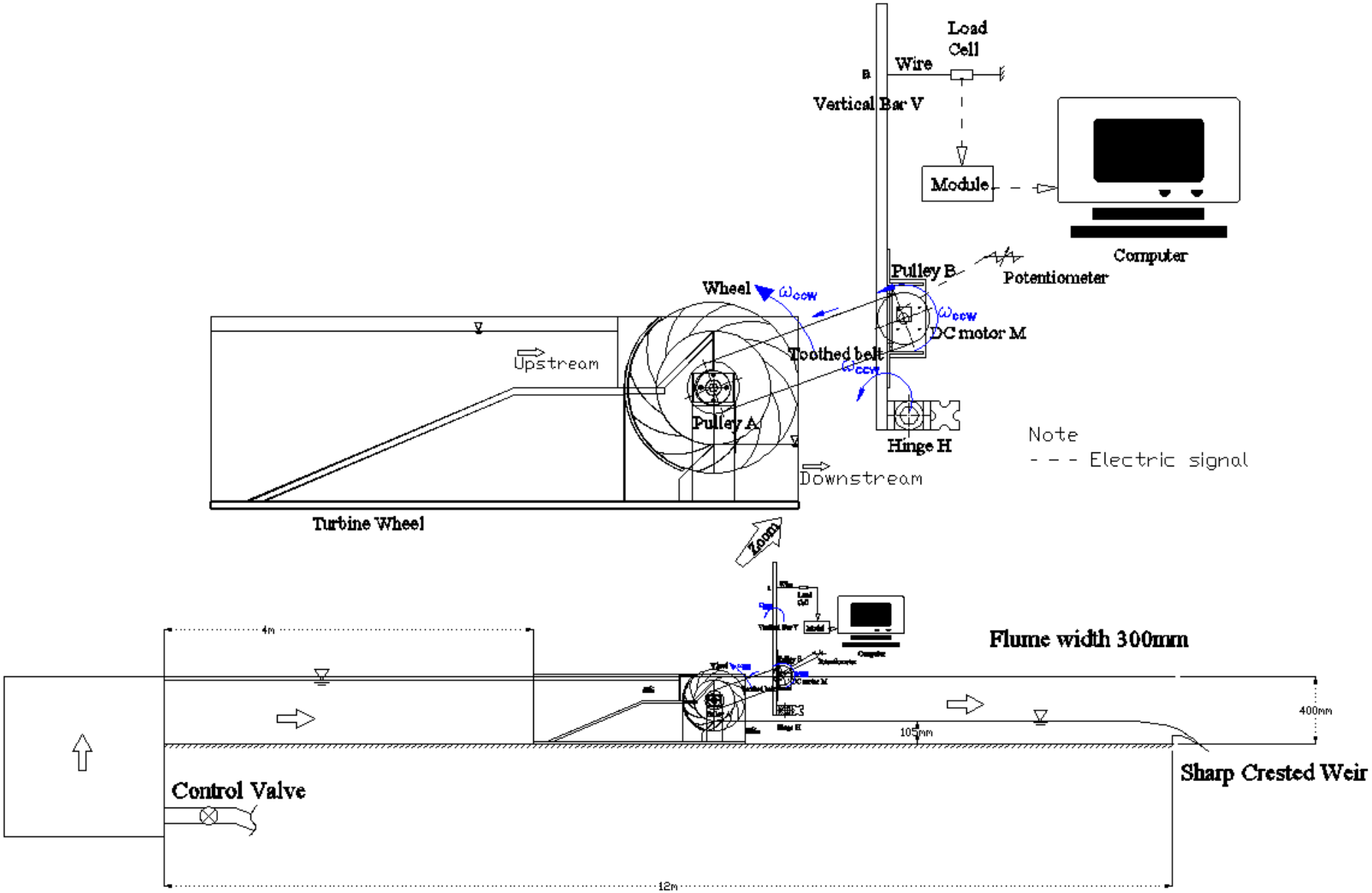

Figure 4.4: Schematic diagram of the flume

Some equipment that were used in this experiment will be elaborated. The tools are listed as below:

- *Pulley*

Two Aluminum Timing Belt Pulleys had been used as power transmission from the wheel to the motor. The detailed data of the pulley is presented in table 4.3. The bore diameter of the pulley that attach at the shaft of the wheel is enlarge from 8 m into 12 mm, since the shaft diameter is 12 mm. Whereas the bore of the pulley that attach on the motor also enlarge, in order to fit another cylinder to make it fix with the motor shaft. Also the bulge at the pulley was being milled since it is not needed. The pitch diameter of the pulley is 76 mm.

Figure 4.5:Power transmission device (uk.rs 2014b)

- *Belt*

The belt was used to wrap on the both pulley to transmit power from wheel to the motor.

Table 4.3: Detailed data of the Pulley

Bore	8 mm
Hub Diameter	38 mm
Material	Aluminum
Maximum Bore Diameter	26 mm
Number of Teeth	48
Pitch Diameter	76 m
Pitch	5 mm
To Suit Belt Width	15 mm

Figure 4.6:Timing belt that was used (uk.rs 2014a)

Table 4.4: Detailed data of the Belt

Length	800mm
Material	Polyamide
Maximum Operating Temperature	+100°C
Maximum Speed	50 m/s
Number of Teeth	160
Pitch	5 mm
Tooth Height	2.1 mm
Width	15 mm

- *Hinge*

Machine building system "ITEM" hinge 40x40, heavy-duty was used in the end of the bar. This hinge makes bar free to rotate. Picture of the hinge is presented in Fig 4.7

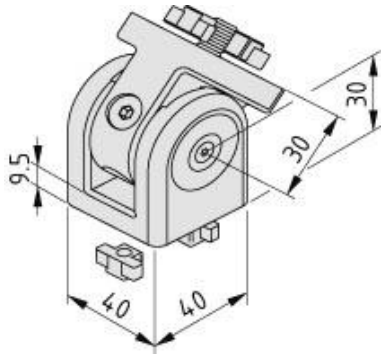

Figure 4.7:Hinge 40x40 that was used

- *Vertical Bar*

Two aluminum bars were arranged vertical and used to hold the motor, also acts as arm of the force which is transfer to the load cell. The bars and also how it was located on the frame is presented in Fig 4.8

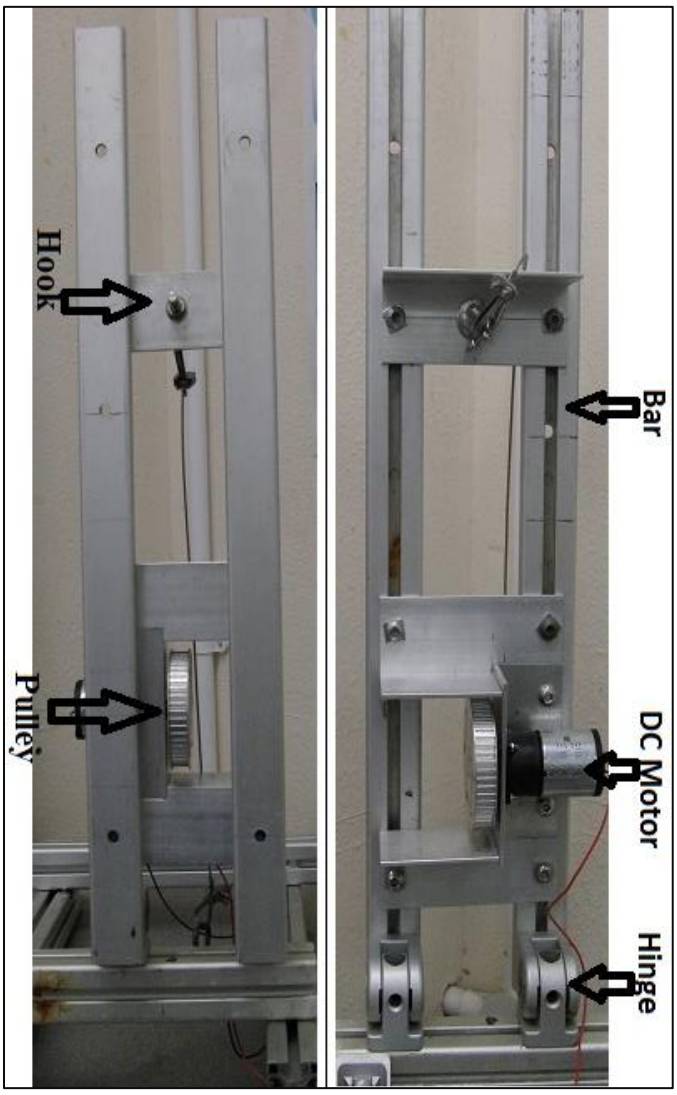

Figure 4.8: Vertical bar and the frame of the measured equipment

- *DC Motor*

A gearing DC motor was used as load. DC motor specification was determined based on the predicted power output and the rotational speed as discussed in part 4.3, which state the predicted power output is 3.394 W≈4 W and the max rotational speed is 46.489 rpm≈42 rpm. Based on commercial availability, the DC motor as detailed in the table below has been selected. The specification of this motor is detailed in table 4.5, whereas the picture of the motor is presented in Fig 4.9.

Table 4.5: Detailed data of the gearing DC motor

manufacturer	RS company
Core Construction	Ironless
DC Motor Type	Brushed
Gearhead Type	Spur
Length	38 mm
Maximum Output Torque	60 Ncm
Output Speed	42 rpm
Power Rating	4 W
Shaft Diameter	6 mm
Supply Voltage	24 V dc

Figure 4.9: A gearing DC motor that was used

- *Potentiometer*

The load that acts on the motor is controlled by using the potentiometer. If the two poles of the dc motor are connected directly (short), which is the same condition as putting a very low resistance on the DC motor, which results in an infinite load. In reverse, if the two poles are not connected to each other, this results in a very high resistance and there will be no load on the dc motor. This characteristic is used to control the load. Since the chosen motor is 4 W

DC motor and the supply voltage for the motor is 24 V, so the resistor must be above 4 Watt, to prevent overheating. In addition, the resistor also acts as a load supplier to the motor which can work within the range of 4w and a voltage of 24 V. To determine the resistor value, the simple calculation is needed.

$$R_s = \frac{v^2}{P} = \frac{24^2}{4} = 144\ \Omega \qquad 4.8$$

The calculation shows that the resistor that needed is 144 Ω ≈150 Ω.

From the calculation, so 10 W and 150 Ω resistor is chosen. The picture of the potentiometer is presented in Fig 4.10.

Figure 4.10: A Potentiometer that was used

- *Load Cell*

A load cell is a transducer that is used to create an electrical signal whose magnitude is proportional to the force being measured. For this particular application a waterproof bend beam load cell type was used, where the rating of the transducer is 0-5 kg. Calibration undertaken on the load cell prior to each application. The calibration software as supplied by the load cell manufacturer, only allows for two points to be inputted for calibrations. Then the three data point checking is undertaken to see the relationship between the measured force and the voltage generated on the transducer. The mass that was used on this test was verified on a calibrated scale. Then the three data point that shows the relationship between force measured and voltage generated is shown in table 4.6 and Fig 4.11.

Table 4.6 is the calibration table of the load cell.

Table 4.6: calibration table of the load cell

No	Weight scale	Reading on the force transducer mv/v
1	0	0.02
2	2	0.83
3	5	2.04

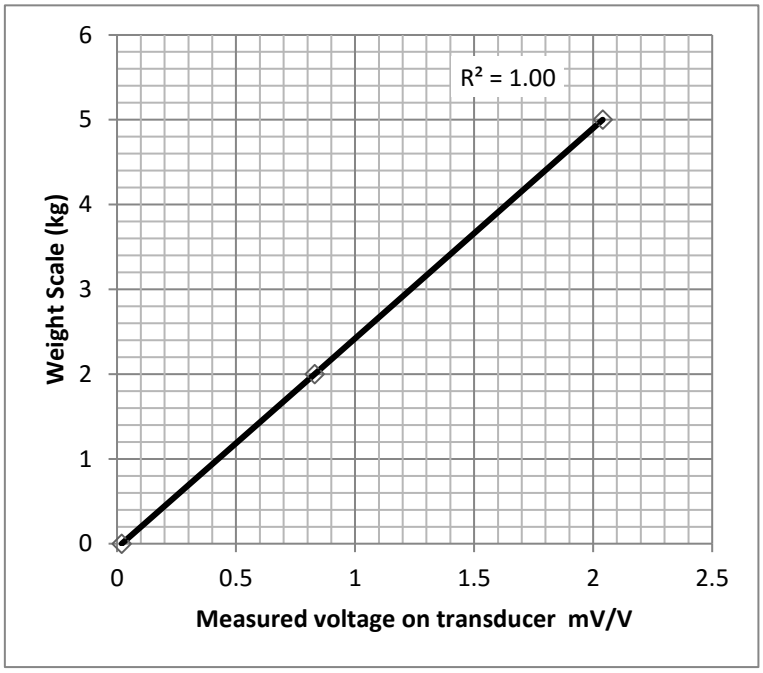

Figure 4.11: A Calibration graph of the force transducer

Figure 4.12: The load cell that was used

The checking of the load cell was conducted in order to confirm the accuracy of the measurements, by using three known weights. Three weights, 0 kg, 2 kg and 4.1 kg were attached to the load cell. The results of the load cell showed 0.003 kg, 2.087 kg and 4.097 kg

respectively. Furthermore to confirm whether "drifting" maybe an issue the weights were left on the load cell for 3 hours, the load cell was then reinitiated with the same calibration and retested again with the result showing 0.003 Kg, 2.087 Kg and 4.095 Kg respectively. The differences between the known weight and the measurements were within tolerance from the effects of drifting or inaccurate readings. There is a slight difference in the measurement of the 4.1 Kg load where, a 2 gr difference between the initial reading and the final reading is displayed. However this value is beyond the range of measurement since the highest force value measured is 2 Kg.

Table 4.7: drifting test of the load cell

Load (Kg)	Initial reading (kg)	Final reading (kg)	Differences (kg)	Differences (gr)
0	0.003	0.003	0	0 gr
2	2.087	2.087	0	0 gr
4.1	4.097	4.095	2.10^{-3}	2 gr

From load test drifting test, it is quite confident there is no drifting on this transducer.

- *Data Acquisition (DAQ)*

Data acquisition is the process of sampling signals that measure real world physical conditions and convert the resulting samples into digital numeric values, that can be manipulated by a computer. Data acquisition systems (abbreviated with the acronym **DAS** or **DAQ**) typically convert analog waveforms into digital values for processing. The sampling rate in this test is 2000 Hz. In this experiment, the National Instruments 9237 DAQ was used.

Figure 4.13: The DAQ module that was used

- *Computer*

A desktop computer was connected to the DAQ. National Instrument Labview 2014 was used to communicate with the DAQ and files saved to the computer. This DAQ calculates the force that acts on the load cell and records this data.

- *Flow direction tracker*

A further set of experiment that was undertaken investigating the effect of the guide vane/baffle to the performance of the machine. The baffle/guide vane is a formed plate that is placed at the entrance of the machine. The purpose of this baffle is to guide the flow of the water to the cell of the wheel. This baffle is formed based on the streamline of the water at the entrance. In order to determine the streamline of the water at the entrance, a flow direction tracker is placed at the entrance of the wheel. The streamline is tracked prior to inserting the baffle at the entrance. The flow direction is tracked by using a yarn which is attached to a rod, accompanied by a protractor to measure flow direction angle. The picture of the tool is shown in the Fig 4.14

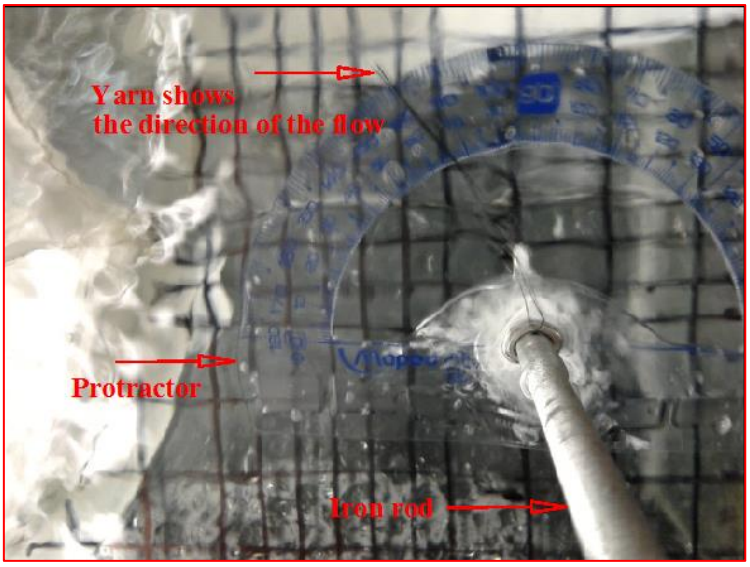

Figure 4.14: flow direction tracker that was used (top View)

- *High speed camera.*

In order to get a more detailed visualization of the flow on the wheel, a high speed digital camera, Casio EX-F1 with a frame rate of 30 fps was installed during the experiment. This camera was used to record all the events that took place, during draining and filling of the cell.

4.5 Experimental Parameters and Set-up

- *Power output measurement*

Power output of the water wheel is measured by using the system which is arranged as shown in Fig 4.15.

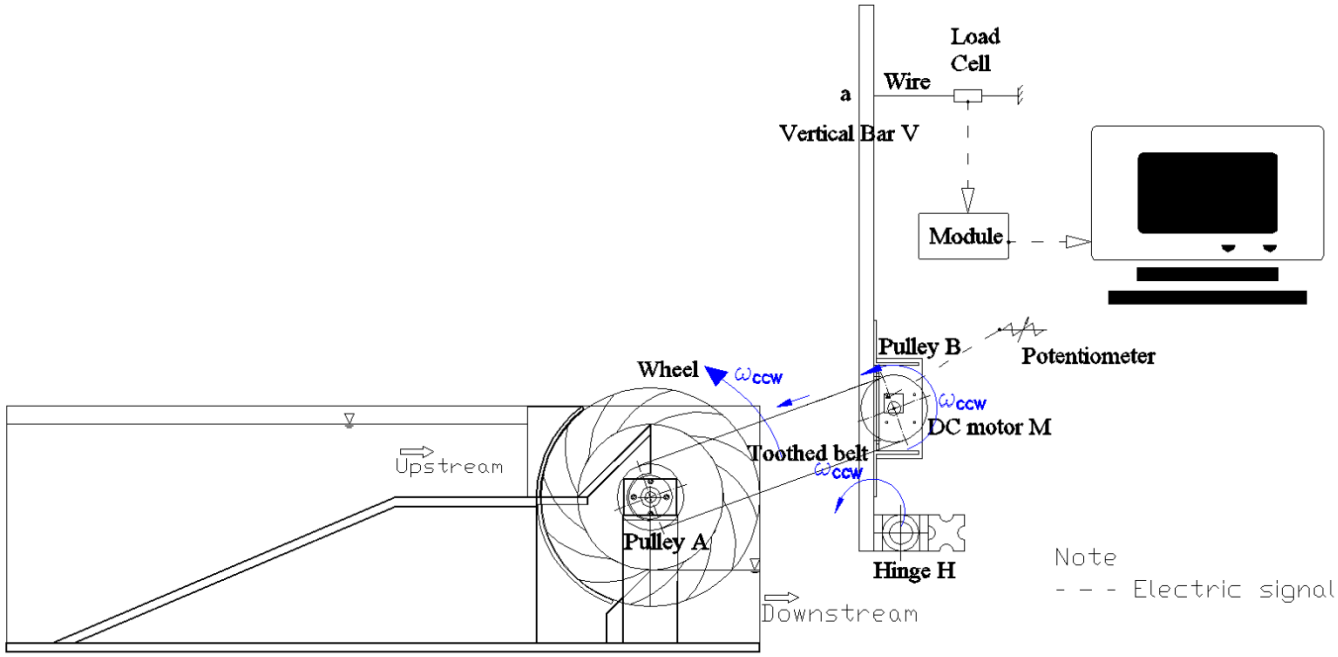

Figure 4.15: Power output measurement setup.

The wheel is fastened onto the shaft. To this shaft, the pulley A which pitch diameter = 76 mm is connected. A toothed belt is attached to pulley A, then connected to pulley B. The shaft of pulley B is connected to a DC motor M. This system starts to work as water fills the cell of the wheel. This condition starts the wheel to rotate CCW (counter clock wise). As the wheel rotates CCW, pulley A also starts to rotate CCW and the produced torsion is then transmitted through the toothed belt to pulley B, which rotates CCW as well. This situation causes the vertical bar V to pivot at the hinge H which induces a forward/backward motion which is reacted against by the wire which is connected to the load cell. The hinge H is fixed to the static frame. The data from load cell displays and records the force generated at point **a**. The potentiometer, which is connected to the DC motor, is acting as a load controller. The smaller the resistance, the slower is the rotational speed of the wheel which results in a higher load at pulley B. Consequently a larger torque will be produced, which will increase the force being recorded at point **a**. In order to simplify the calculation of power output of this system, it will be more convenient to make a free body diagram analysis.

The data analysis sequence is arranged as below:

1. Calculating balancing Forces $\overline{P}$ at point a because of the weight of the motor and vertical bar

At the initial condition, where the wheel is not rotating the schematic of the measurement system is shown in Fig 4.16. A pretension force P_{im} is applied at point **a** on the vertical bar. This pretension force P_{im} is recorded on the computer. A proportion of this pretension force balances to the weight of the vertical bar W and weight of the motor N and does not contribute to load measurement. This proportion of force is then called a balancing force $\overline{P}$. From moment balance equation at hinge H, the value of this balancing force $\overline{P}$ is calculated as equation 4.9

$$\overline{P} = \frac{W \cdot Z + N \cdot X}{L} \qquad 4.9$$

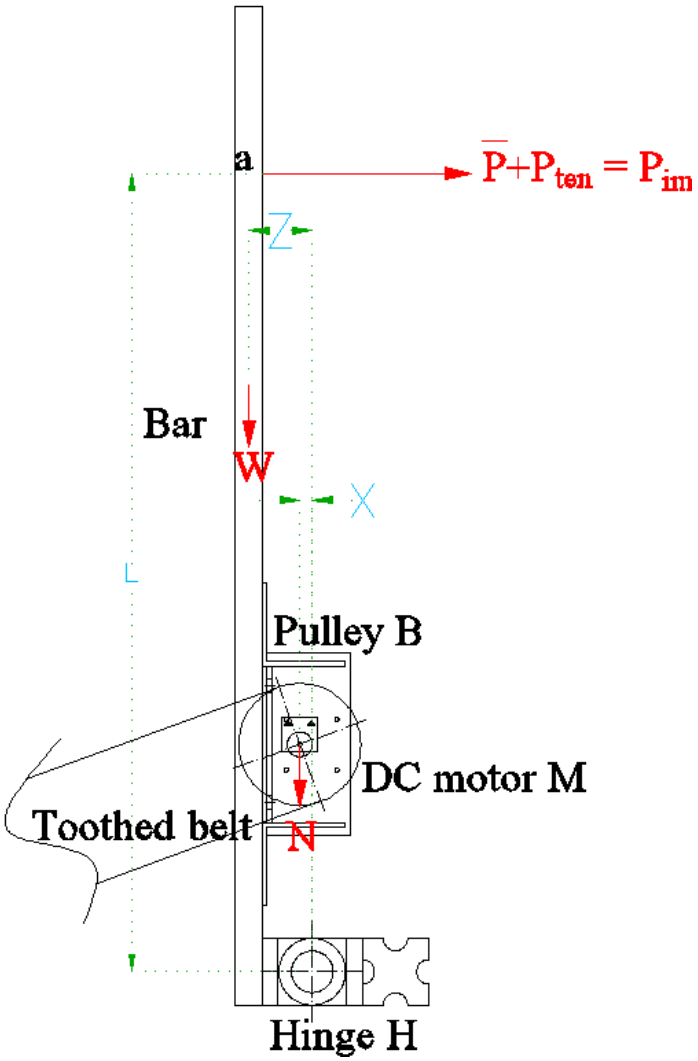

Figure 4.16: pretension condition where weight of the bar and motor is involved.

2. Calculating initial tension on the upper and lower chord of the belt.

Applying pretension at point **a** of the vertical bar will create a tension in both the upper and the lower chord of the belt, which are P_1. This also means some portion of pretension force P_{im} at point **a** of the vertical bar contributes to the value of the tension force on the upper and lower chord. This force is then called as P_{ten} and calculated as equation 4.10

$$P_{ten} = P_{im} - \overline{P} \qquad 4.10$$

The moment balance equation at the hinge is then applied, which involves P_{ten}, and P_1. From free body diagram force in Fig 4.17, the tension force P_1 can be calculated as equation 4.12

$$P_{ten}.L = P_1(Y + R) + P_1\,(Y - R) \qquad 4.11$$

$$P_1 = \frac{P_{ten}.L}{2\,Y} \qquad 4.12$$

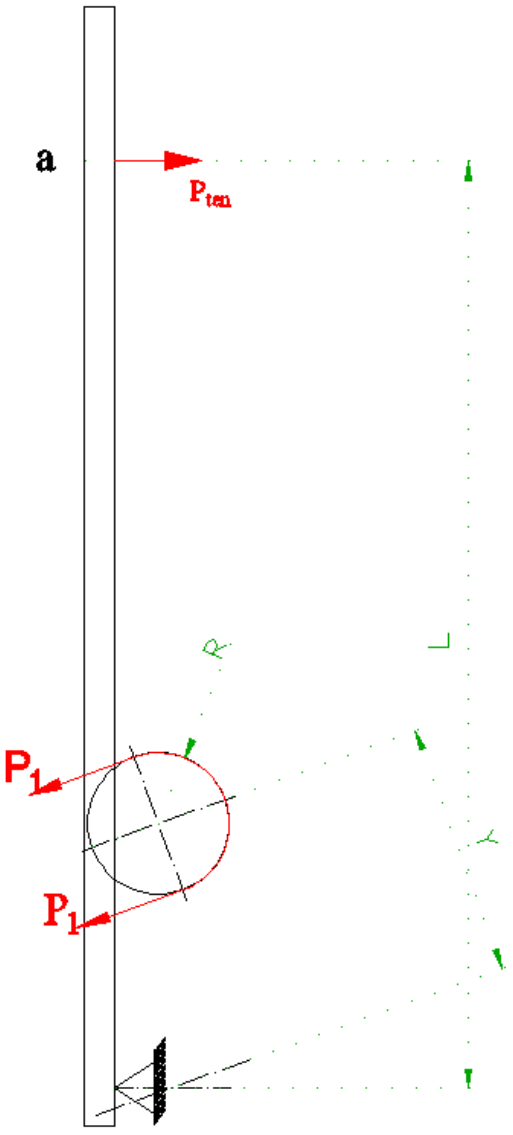

Figure 4.17: Free body diagram of the system when P_{ten} is applied.

3. Calculating force at point **a** of the bar as lower chord slack

Initially, both the upper and lower belts are in tension. As the torque on pulley A increases, the tension in the upper chord increases, whilst the tension in the lower chord is reduced. When the force created by the pulley A reaches P_1 in the lower chord, the belt slackens as shown on the drawing in Fig 4.18, and it can not transmit any force. At this condition, the situation on the belt and pulley is shown in Fig 4.19a.

The moment m_w causes the lower chord to slacken. This moment m_w occurs as the torque that is being transmit from pulley A. This torque also induces a force, which at certain torque values, causes the lower chord to slacken as shown in Fig 4.19b which is P_1 . The moment m_w is calculated as equation 4.13

$$m_w = P_1 R \qquad 4.13$$

When this moment m_w occurs at pulley B, the force F_{m1} produced at point **a** results in moment m_v in respect to hinge H. Therefore, the moment balance can be formulated from this situation as equation 4.14

$$m_w = m_v \rightarrow F_{m1} L = P_1 R \qquad 4.14$$

$$F_{m1} = \frac{P_1 R}{L} \qquad 4.15$$

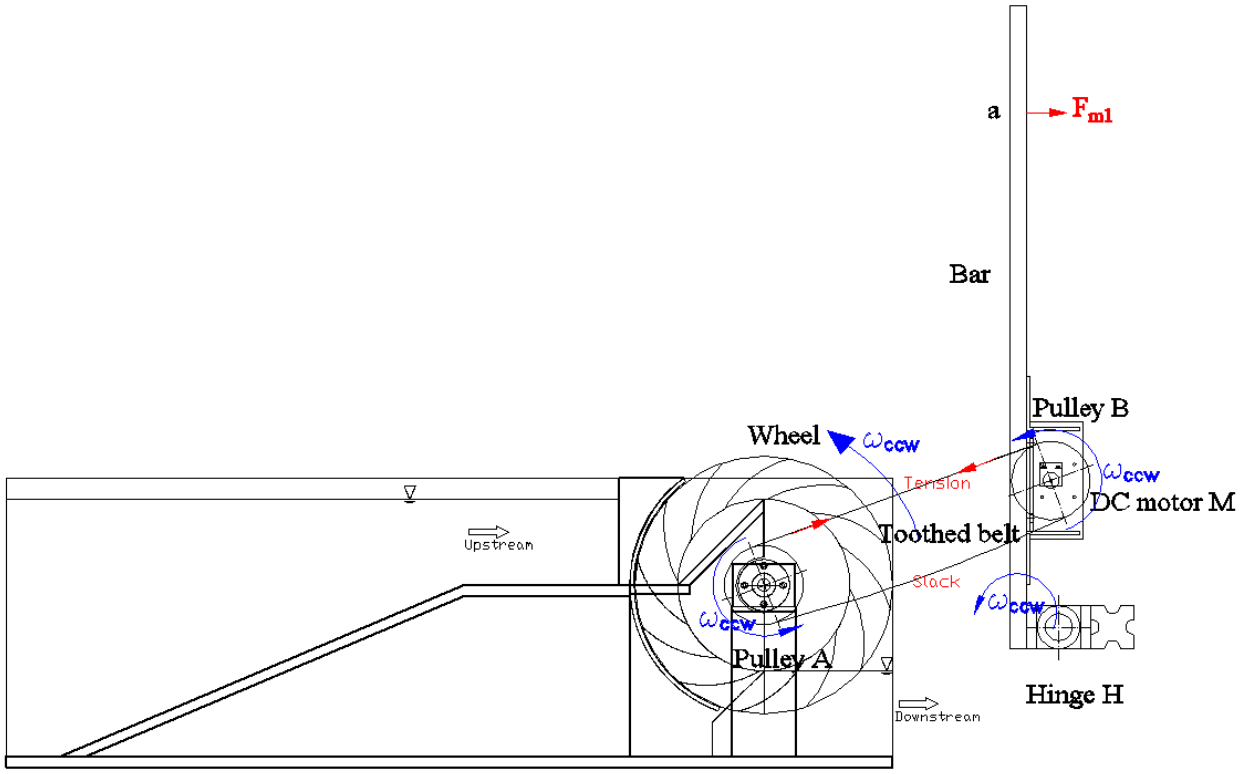

Figure 4.18: Experiment setup at situation where lower chord is slack..

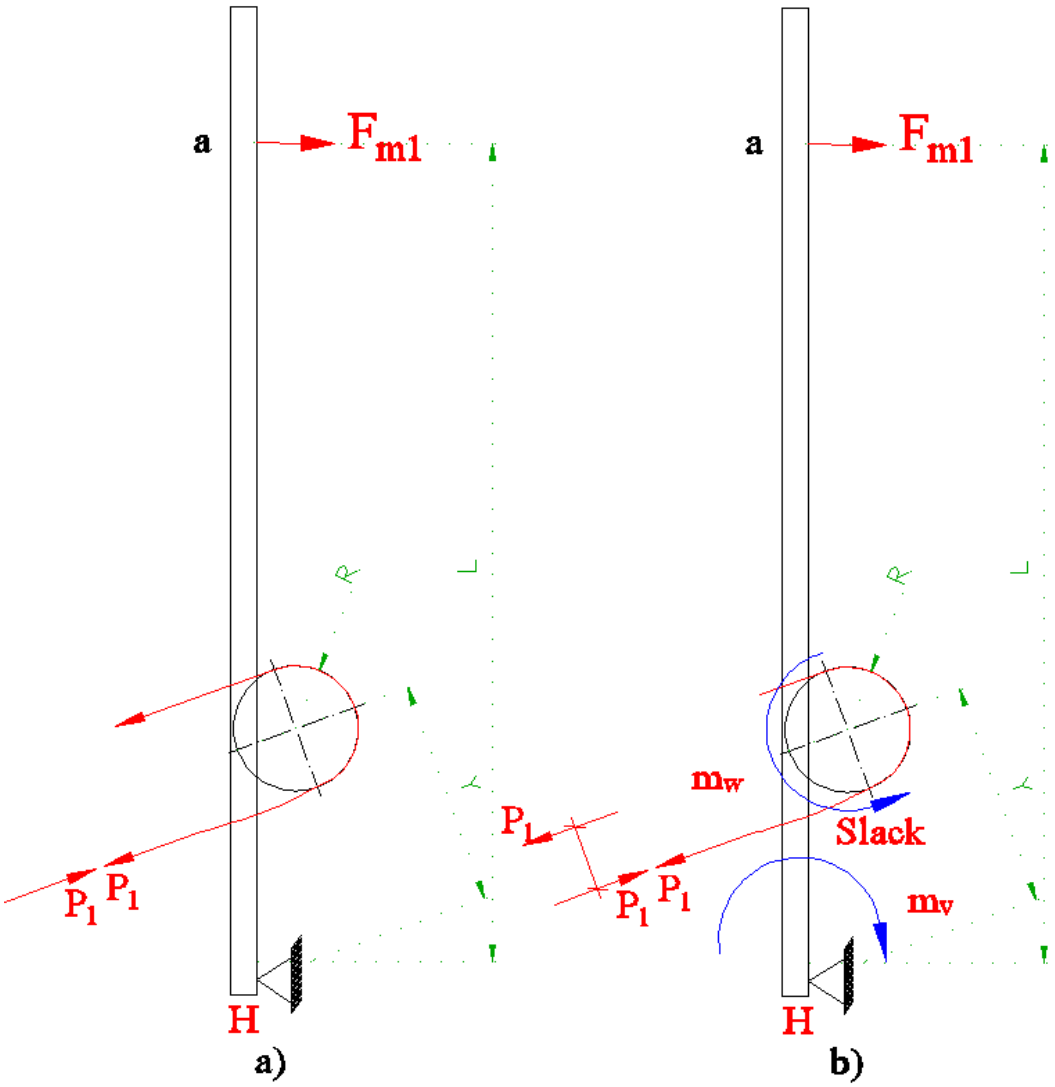

Figure 4.19: Free body diagram at condition where slackens lower chord

The nett force measured F_m from pretension condition until water fills into the cell of the wheel is calculated as the difference between final measured force P_{fm} and initial measured force/pretension P_{im}

$$F_m = P_{fm} - P_{im} \qquad 4.16$$

The actual force that acts at point **a** of the bar due to the torque applied on the pulley is F_{m2}. This F_{m2} results from the nett force measured F_m subtracted from the force at point **a** of the bar due to the slack condition F_{m1}

$$F_{m2} = F_m - F_{m1} \quad 4.17$$

At the condition where torque is generated and the machine start producing power, the lower chord is also in a slack condition. The moment balance over the hinge as shown in Fig 4.20 results equation as 4.18 and 4.19

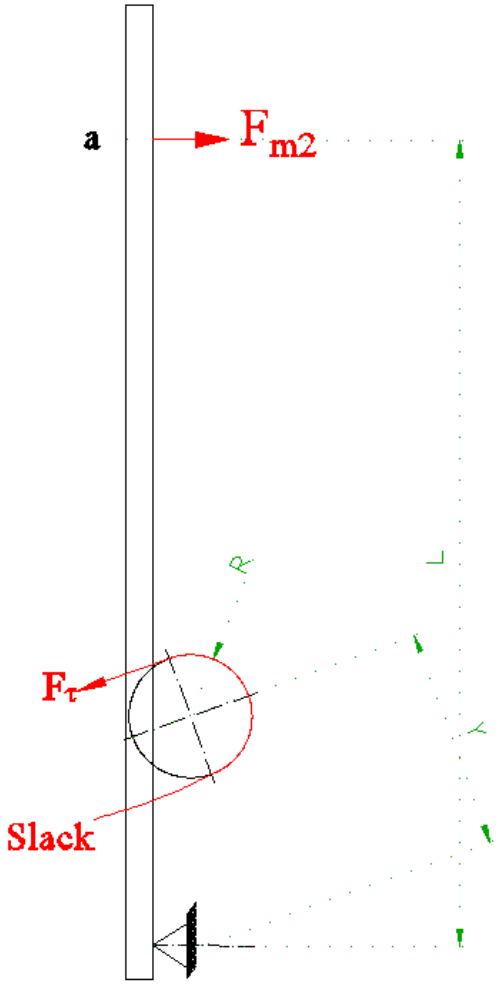

Figure 4.20: Free body diagram at condition pulley is rotating

$$F_\tau\,(Y + R) = F_{m2}\,L \quad 4.18$$

$$F_\tau = \frac{F_{m2}\,L}{(Y+R)} \quad 4.19$$

Where F_{m2} is the actual force that acts at point **a** of the bar due to applied torque, and F_τ is the tension force in the upper chord. So the total torque produced T is the sum of the tension force at the upper chord F_τ and the pretension force P_1, then multiplied by the radius R of the pulley B. The free body diagram of this force can be seen from Fig 4.21.

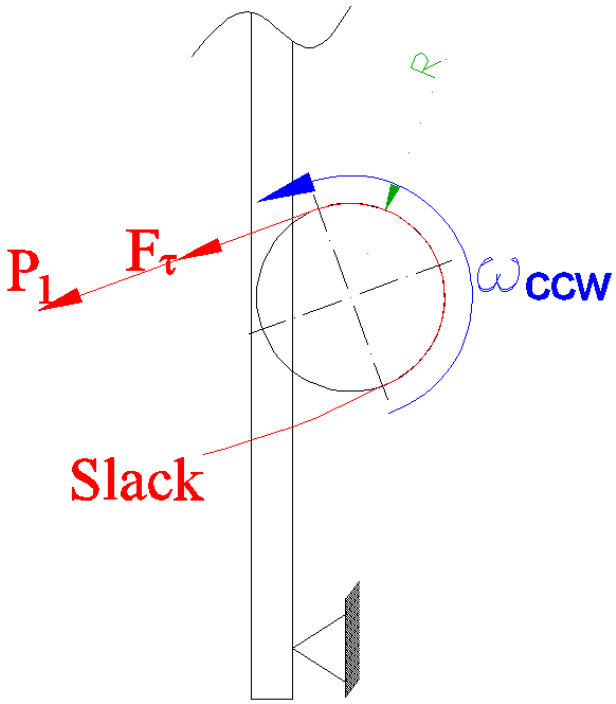

Figure 4.21: Total force that contribute to the torque produced at pulley

$$T = (F_\tau + P_1)R \qquad 4.20$$

Power output P_{out} is stated as

$$P_{out} = T \,.\, \omega \qquad 4.21$$

- *Theoretical water flow rate on the water wheel*

Water volume flow passing through the water wheel can be calculated theoretically. The mathematical equation to calculate water flow rate pass through water wheel Q_{th} is calculated based on the equations 4.22 to 4.28. D_{out} is the outer diameter of the water wheel, and D_{in} is the inner diameter of the water wheel, whereas b and f is the blade width and rotational speed

respectively. Equation 4.22 to 4.28 refer to Fig 4.22 and 4.23 and also the other symbol is refer to symbol list .

$$Q_{th} = Q_c - Q_{bl} - Q_{ho} - Q_{bh} - Q_{rbr} - Q_{nr} \quad 4.22$$

Q_c is water flow rate inside the cell, and calculated as

$$Q_c = \frac{\left((D_{out})^2 - (D_{in})^2\right)\pi \cdot b \cdot f}{4} \quad 4.23$$

Q_{bl} is the volume of the area that is covered by the blade as the wheel rotates, and calculated as

$$Q_{bl} = 12 \cdot t \cdot l \cdot b \cdot f \quad 4.24$$

Q_{ho} is the volume of the area that is covered by the hook as the wheel rotating, and calculated as

$$Q_{ho} = 12 \cdot t \cdot lh \cdot wh \cdot f \quad 4.25$$

Q_{bh} is the volume of the area that is covered by bolt hub as the wheel rotating, and calculated as

$$Q_{bh} = 2 \cdot 12 \cdot h_{bo} \cdot \frac{\pi \cdot {D_{bo}}^2}{4} \cdot f \quad 4.26$$

Q_{rbr} is the volume of the area that is covered by rod bolt rim as the wheel rotating, and calculated as

$$Q_{rbr} = 12 \cdot h_{rbr} \cdot \frac{\pi \cdot {D_{rbr}}^2}{4} \cdot f \quad 4.27$$

Q_{nr} is the volume of the area that is covered by nut rim as the wheel rotating, and calculated as

$$Q_{nr} = 12 \cdot h_{nr} \cdot \frac{\pi \cdot {D_{nr}}^2}{4} \cdot f \quad 4.28$$

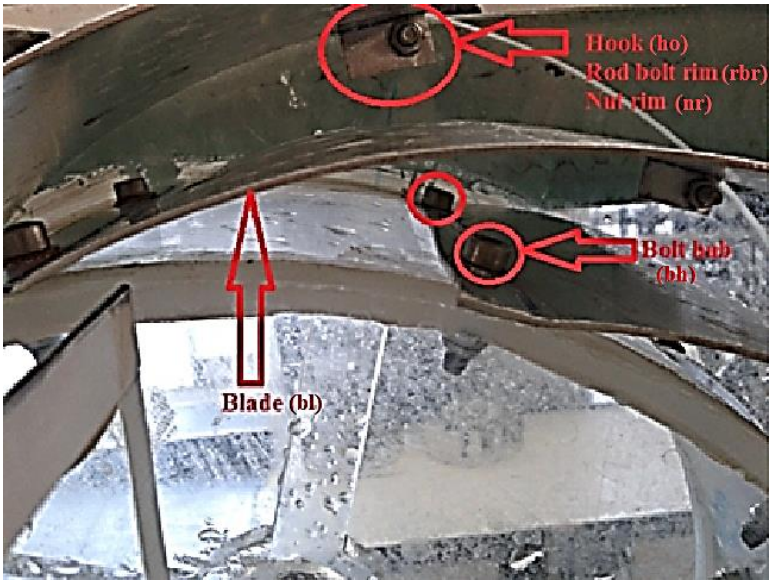

Figure 4.22: Picture of the cell

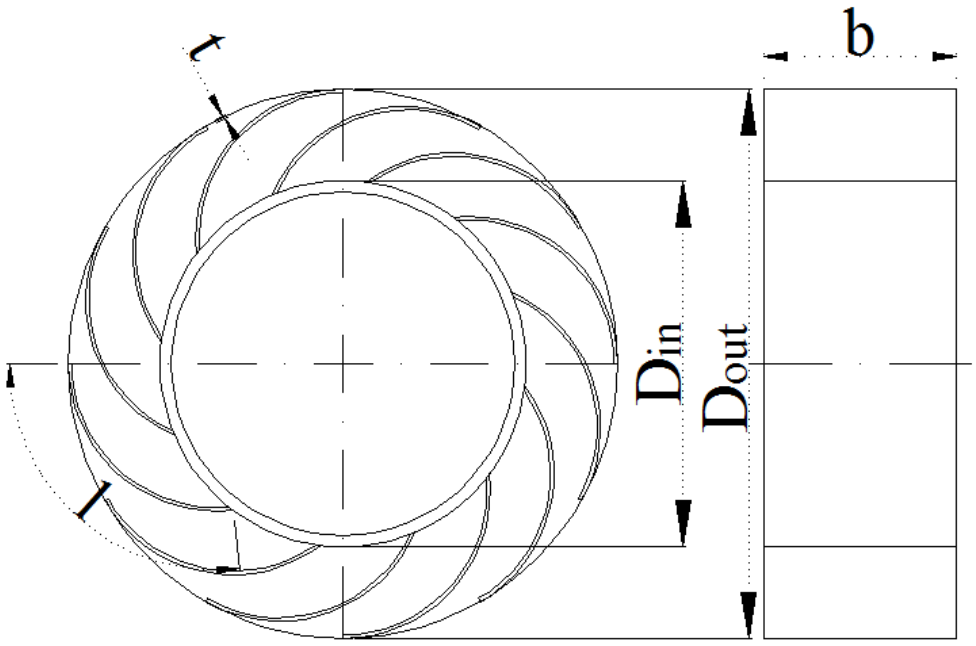

Figure 4.23: Water Wheel and the dimension

- *Hydraulic power available according to flow rate in blade of water wheel*

The hydraulic power available can be calculated based on the water flow rate passing through water wheel blade's P_{mi} as stated in equation 3.7, and rewrite below

$$P_{mi} = \rho_w \cdot Q_{th} \cdot g \cdot H \qquad 3.7$$

- *Efficiency*

The efficiency in this calculation is the efficiency without leakage. Leakage is the water flow that passes through the machine without power extracted. This water flow occurs between movable part and a static part. The efficiency without leakage η_{wl} is the ratio between output power P_{out} and the hydraulic power available P_{mi} which is calculated based on the water flow rate passes through water wheel blade's. The efficiency without leakage η_{wl} is formulated as in equation 3.8 and rewrite below

$$\eta_{wl} = \frac{P_{out}}{P_{mi}} \qquad 3.8$$

- *Blade velocity of the water wheel*

Peripheral velocity of the water wheel basically is the velocity in the centre of the cell, which can be written as equation 3.9 and rewrite below

$$v_{tan} = \frac{(D_{out}+D_{in})\,\pi \cdot f}{2} \qquad 3.9$$

- *Maximum possible velocity*

The maximum possible velocity of the water for a given head difference H is calculated as equation 3.10 and rewrite below

$$v_{max} = \sqrt{2 \cdot g \cdot H} \qquad 3.10$$

4.6 Result and Discussion

Experimental results are presented in this chapter, where the force signal from the force transducer appears on the computer screen. This data is shown as an amplitude signal as can be seen in Fig 4.24. Fig 4.24 is the signal output from the transducer for a hub diameter of 250 mm, no baffle, 12 blades at the speed of 60 rpm. The horizontal axis is time, whereas the vertical axis is amplitude which equates to force. This signal is then averaged in order to get the force that is generated.

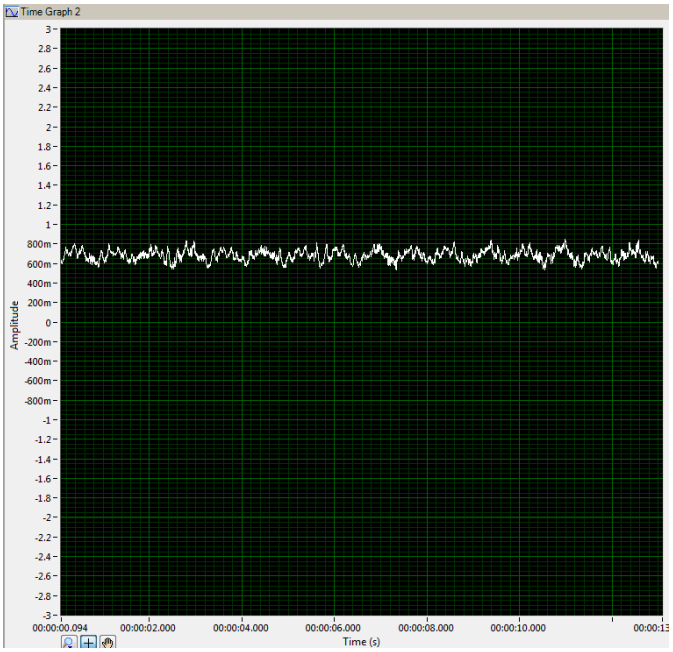

Figure 4.24: Force signal output resulted from hub250 mm, no baffle , 12 blades, 60 rpm.

In order to examine the detail of each experimental variation, all the data were then compiled and presented in several parts, which are:

1. Comparison between the electric power take off and the Prony brake method
2. The effect of the hub diameter on the performance of the water wheel
3. The effect of the number of blades on the performance of water wheel
4. The effect of the baffle on the performance of the water wheel

4.6.1 Comparison between the electric power take off and the Prony brake method

The electric power take off method is proposed because of its ability to control a wider range of rotational velocity, especially at low speed/high torque. In addition the electric PTO provides more accurate data, since the data was taken by using a force transducer and accrued by using a computer. In order to ascertain the reliability of the electric power take off method, a comparison was taken of the PTO measurement result against the Prony brake measurement result. In this experiment, the comparison is taken from the small water wheel which was tested for preliminary test. This water wheel has an outer diameter of 240 mm and hub diameter of 160 mm. The power measurement results are shown in Fig 4.25. In terms of trend, it shows that both methods show similarity, whereas at slow rotating speeds, the power output is small and then increases at a certain rotational speed, followed by smaller power output as the rotational speed increases. In term of magnitude, it shows a slight difference between both results. The Prony brake method shows a higher magnitude in comparison to the electric power take off method. A possible answer for this occurrence might be because of the value that was taken from electric PTO is the average of the fluctuating signal which is captured by the force transducer. Whereas the value that was taken from the Prony brake is the highest value that can be visually acquired from the display of the scale. During measurement, the value that appear on the scale display is constantly changing. It is assumed that the variations of the displayed value are caused by rubbing since it is very difficult to deal with the rubbing problem. So the highest value that appeared on the display was assumed to be the correct data. This inaccuracy causes a potential problem with data collected using the Prony brake method. Rubbing is caused when the movable part (wheel hub) comes into contact with the unmovable part (side plate) as can be seen from fig 3.12. This causes friction to occur which lead to a lower scale reading. Whereas when no contact occurs between a movable part and an unmovable part no friction occurs therefore a higher scale reading is viewed. For this reason, low scale reading might be inaccurate, whereas high scale reading should be of a greater accuracy. Hence the reason for using high scale values when using the classic prony brake method. The differences between the data collection set of the classic prony brake and the electric method can be explained by the reason as mentioned above.

In addition, since the electric PTO uses a timing belt, probably the timing belt is potentially absorbing some power from the pulley that attaches on to the wheel shaft (pulley A) and also to the pulley that is attached to the measurement bar (pulley B) refer to Fig 4.15, hence causing potential loss.

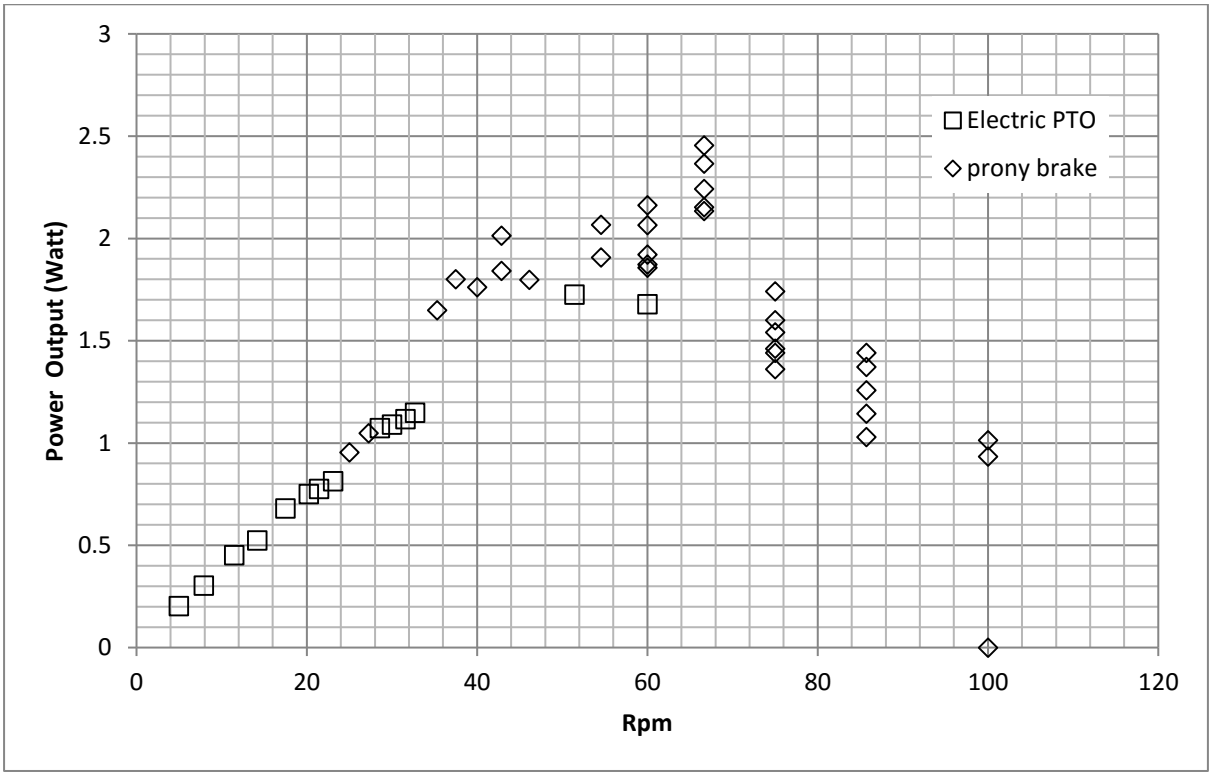

Figure 4.25: The comparison of the measured power output from Prony brake method and electric power take off method in the case of hub 160 mm and outer diameter 240 mm.

The efficiency curve is shown in Fig 4.27. The result shows that the efficiency is high at low speed and low at high speed. The efficiency trend that appears from the Prony brake method and electric PTO is similar. Nevertheless the efficiency of the Prony brake is slightly higher than the electric PTO. Again this occurrence is possibly due to the same problem that occurs with the power output as described in the previous paragraph.

The drawback of this electric PTO data is that the potentiometer resistance value that was used during this test was too small. The selection of this potentiometer value causes problems with accruing data at high speed ($v/v_{max} > 0.37$, which is correspond to 60 rpm). The small resistance values causes the breaking effects to only work at low speed (high torque), whereas at high speed (low torque) there is no breaking effect. As consequences the data for high speed (low torque) can not be collected. This problem can be potentially solved by adding several potentiometer and arranging them in series configuration.

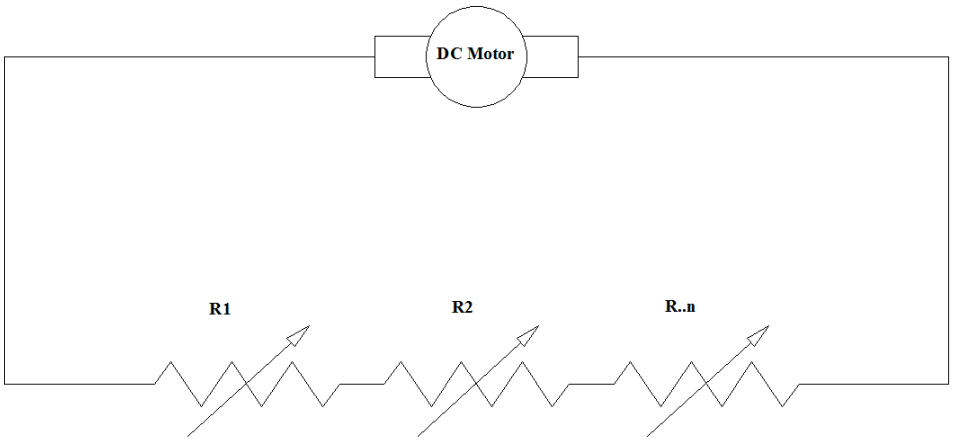

Figure 4.26: serial arrangement of some resistors which acts as load controller

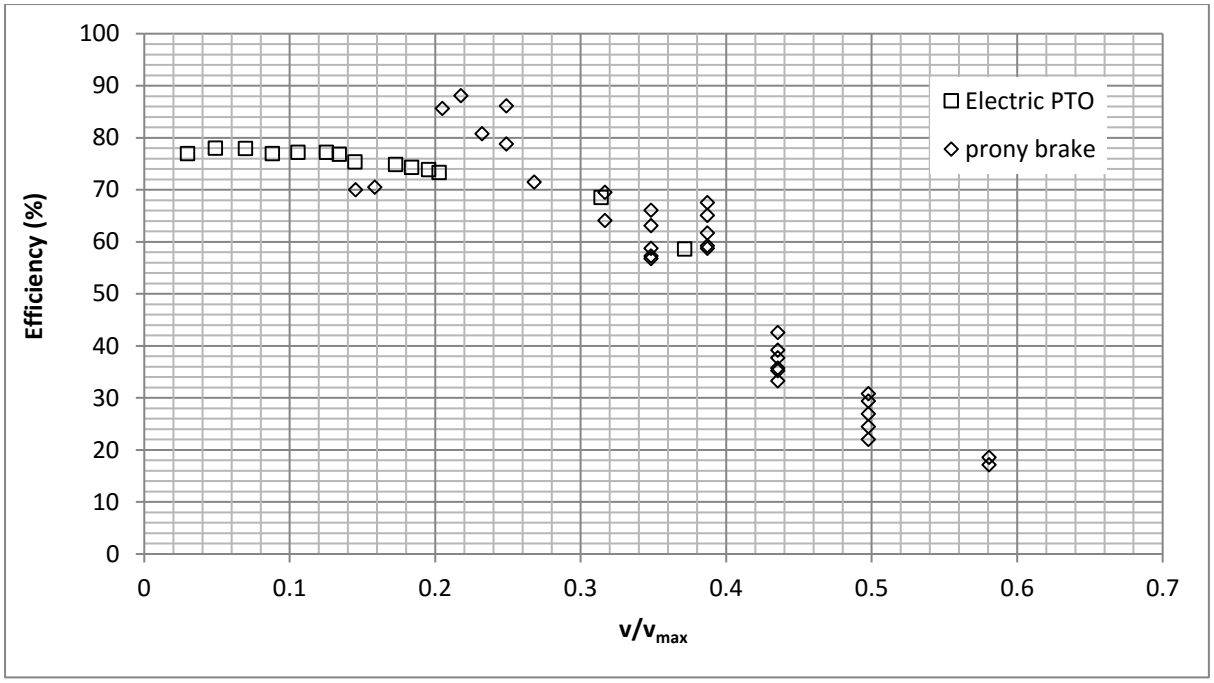

Figure 4.27: The comparison of the efficiency of the machine from Prony brake method and electric power take off method in the case of hub 160 mm and outer diameter 240 mm.

4.6.2 The effect of the hub diameter on the performance of the water wheel

The effect of the hub diameter was investigated. The hub diameter was varied between 250 mm, 170 mm and 100 mm, whereas the outer diameter remaining constant at 337 mm. The number of blades for each wheel was twelve. The power output result is shown in Fig 4.28. In terms of trend, the power output curve shows a similar pattern with several results from previous research undertaken on water wheels, as shown in Fig 4.29 as an example.

A rotational speed of 26 rpm increasing, the water wheel with a hub diameter of 250 mm always produces a higher power output, whereas for a hub diameter of 100 mm, the power output is steadily lower than the others. At a rotational speed from 15 rpm to 24 rpm, the power output from a hub diameter 170 mm is slightly higher than with a hub diameter of 250 mm. The highest power output resulted from the 250 mm diameter hub which is 3.31 W at 37.5 rpm, whereas for the 170 mm hub, the maximum power output is 2.88 W at 24 rpm.

In addition, in the case of the 100 mm hub, the maximum power output is 0.81 W at 10.7 rpm.

This graph shows that the effect of the head difference is much more important than the effect of the flow rate. For example in the case of a rotational speed of 15 rpm, in which the power output of the machine using 100 mm hub is 0.43 W, using 170 mm hub is 1.9 W, and using 250 mm hub is slightly smaller than 1.9 W (since the power output of hub 250 is not provided, it is predicted from the graph trend). In the graph can be seen that for rotational speed of 15 rpm, the volume flow rate of the 100 mm hub is much higher than 250 mm hub and 170 mm hub, however the power output is much smaller than 170mm and 250mm hubs. The power output from 170 mm hub is slightly higher than the predicted power output of the 250 mm hub, however the differences is small, therefore, even though the 170 mm hub gives a higher power output than 250 mm hub, yet the differences is small. To sum up this fact shows that the effect of the head is more important than the effect of the flow rate in order to get higher power output.

Fig 4.28 also shows that the 250 mm hub can reach a higher velocity in comparison to the 170 mm and 100 mm hubs. In the case of the 100 mm hub, at the rotational speed of 10 rpm, the power output decreases, whereas in the case of 170 mm hub, the power output decreases at the speed of 24 rpm. However in the case of 250 mm hub, at the rotational speed of 37.5 rpm, the wheel does not reach maximum rotational speed yet. This fact shows that the 250 mm hub has the possibility to reach higher speed at maximum power output than the 170 mm and 100 mm hubs. It is also reflect that the higher the hub the higher the rotational speed can be achieved at maximum power output. This fact reflect that the bigger the hub diameter the wider the speed range of the wheel. As the wider the speed range, therefore the higher the rotational speed at the maximum power output. This fact shows that the effect of the hub/head is very crucial for this machine. For the case of water which passes from upstream to downstream, there will be head drop which causes losses. This head drop becomes more important as the head reduces. This might be the reason why for hub 100mm (the smallest diameter) has the narrowest speed range due to the small head difference occurring. Whereas for hub 250mm even though a head drop occurs, since the head difference is quite large, the effect of the head drop is not significant. The same effect that occurs with the 100mm hub will also occurs with the 250mm hub yet at higher speed.

The effect of the hub diameter to the torque output is shown in Fig 4.31. At a speed between 15 and 24 rpm, the torque output for the hub 170 mm diameter hub is higher than the 250 mm diameter hub. The highest torque output from 170 mm hub is 1.29 Nm at 20 rpm, whereas for 250 mm hub, the maximum torque output is 1.12 Nm at 14.3 rpm. At the rotational speed greater than 25 rpm, the torque output for the 250 mm hub was constantly higher than 170 mm hub. In the case of the 100 mm hub, the torque produced is always lower than the others, with the highest recorded torque is 0.84 Nm at 8.8 rpm. Fig 4.31 shows that the torque is essentially high at low speed. This occurs in all variations of hub. This torque graph support the explanation on the power graph as shown in fig 4.28. Power is the result of the multiplication between torque and rotational speed. For the same speed, if the output torque is bigger, then the power is bigger as well. Interestingly, the torque output in the range of 15-24rpm, with the 170mm hub is greater than 250mm hub, which is also shown on the power graph fig 4.28. On the rotational speed bigger than 24 rpm, power output and torque of the hub 170mm is decreasing. Power output of a water wheel is a combination between flow rate and water surface difference as explained in equation 2.1. With increasing rotational speed (also flow rate increase) efficiency decreases due to head drop. This head drop makes reducing water surface difference. In the case of the 170mm hub, within the rotational speed range of 15-24rpm, decreasing head also occurs as with 250mm hub, but the combination of flow rate and the head difference of the hub 170 mm is larger than the hub of 250 mm hub. Therefore the torque and power output is bigger.

The interesting fact is the drop of the torque in 170 mm hub and 100 mm hub is much steeper than the 250 mm hub. Fig 4.31 shows that 250 mm hub has a shallower torque drop gradient than the other two. So it can be said that the torque produce in the case of 250 mm hub is relatively more constant than others. This graph shows that 250mm hub experiences head drop. Yet the effect of this head drop is not significant to reduce the torque and power output of this 250mm hub. Meanwhile with the hub 100mm and 170mm, decreasing head has significant effect on the torque and power output. As a consequence the decreasing torque and power is becoming significant, and the power and torque curve also drops steeply.

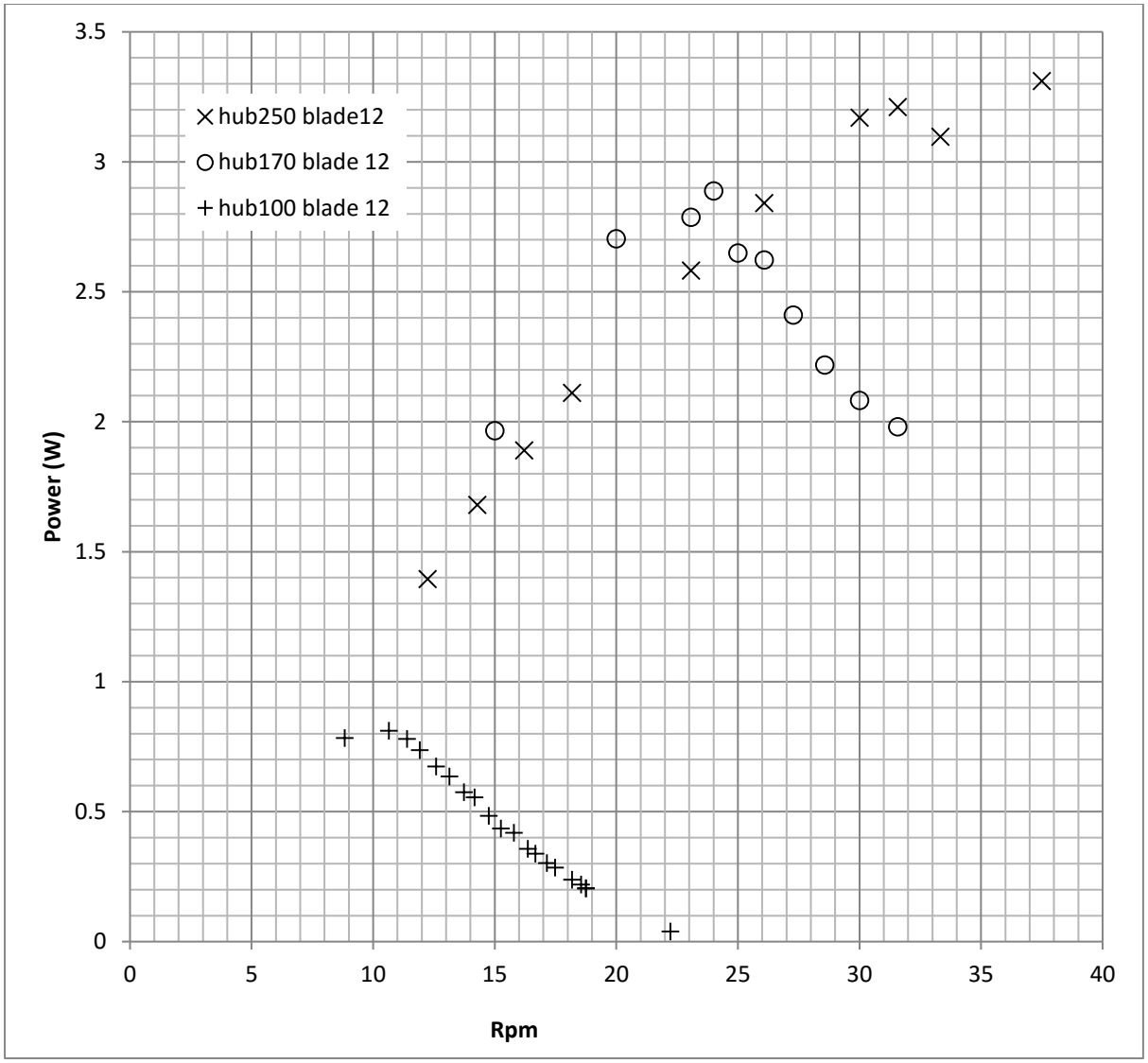

Figure 4.28: power output with the hub diameter varies

Furthermore, in the case of 250 mm hub, the torque drop is not as low as the other two hub as the rotational speed increases, so the power output result from the 250 mm hub is higher than the others variations of hub since power is the product of Torque T and rotational speed ω. Nevertheless in the case of 100 mm hub, both the torque and the power output are consistently lower than 250 mm hub and 170 mm hub. This fact might be because of the head difference for this variant is too small in comparison to the other two hubs. Even though the frontal area of the blade (refer to Fig 4.30) for the 100 mm hub is bigger than 250 mm hub

and 170 mm hub, but since the head difference is too small in comparison to other variations, so the power output and torque produced is the smallest eventually.

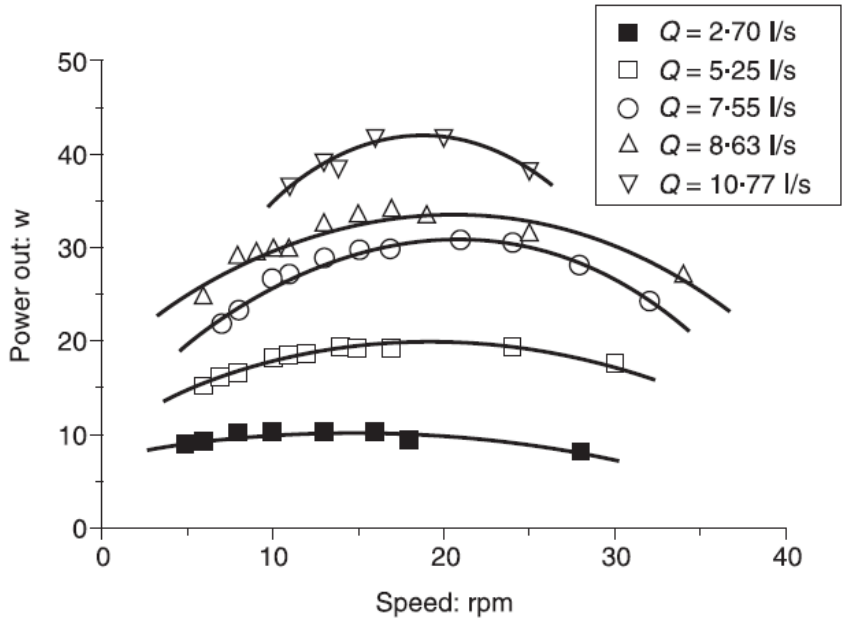

Figure 4.29: Power output pattern of the water wheel as function of speed and flow rate (Müller & Wolter 2004)

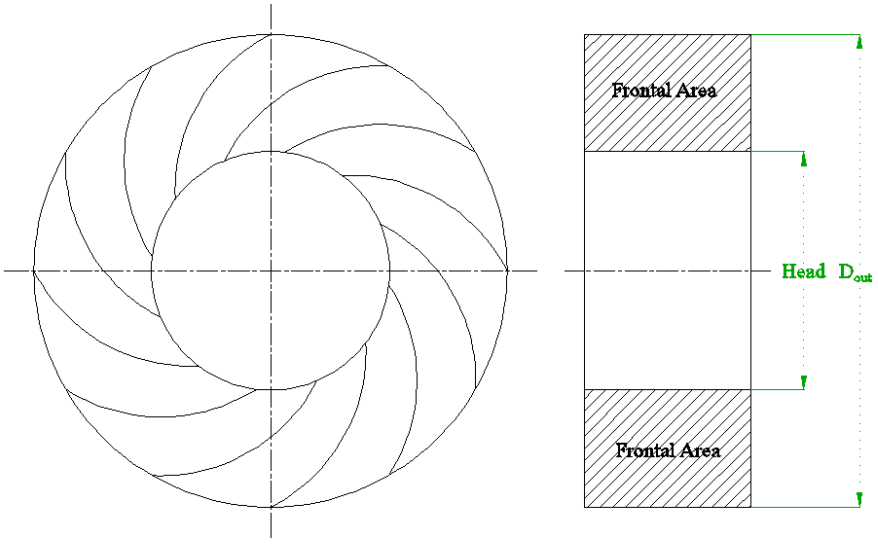

Figure 4.30: Frontal area and head of the turbine wheel

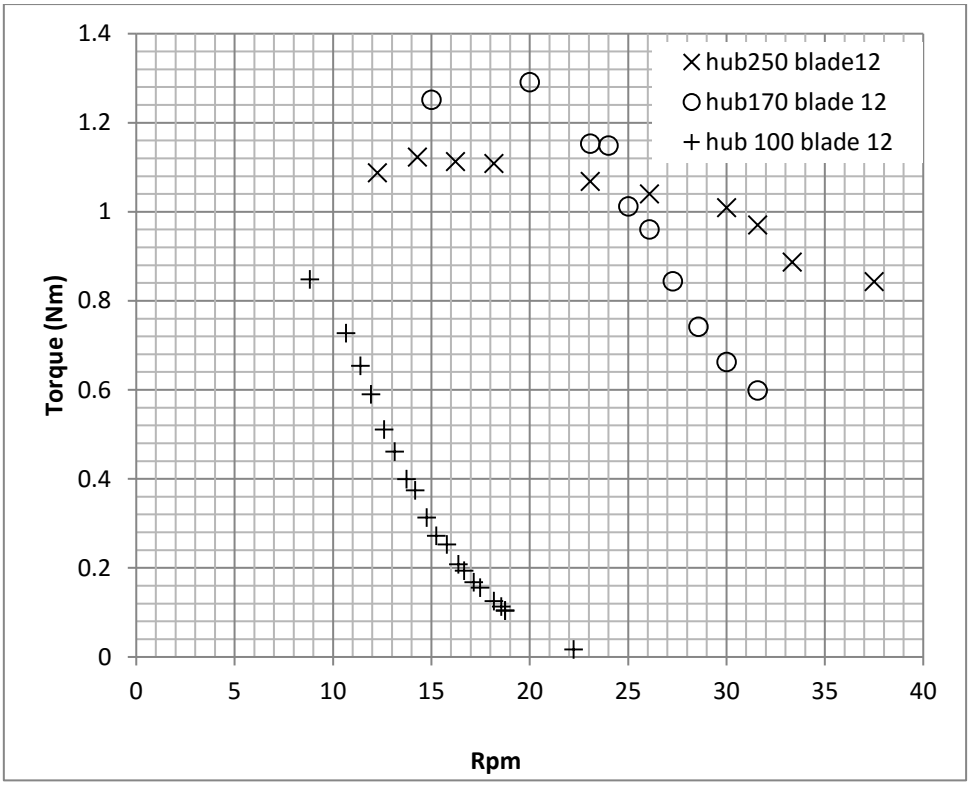

Figure 4.31: Torque output with the hub diameter varies

The efficiency of the machine as the hub diameter varies is shown in Fig 4.32. In this plot, three variations of hub diameter are presented into dimensionless, all these variations are then called as $\frac{D_{out}}{Hub}$ 1.34, 1.98 and 3.37 as representation of hub diameters 250mm, 170mm and 100mm respectively.

At rotational speed of $\frac{V_{tan}}{V_{max}}$ more than 0.2, the efficiency of $\frac{D_{out}}{Hub} = 1.34$ (hub 250mm) is higher than $\frac{D_{out}}{Hub} = 1.98$ (hub 170mm). At a rotational speed $\frac{V_{tan}}{V_{max}}$ lower than 0.2, the efficiency of the water wheel with $\frac{D_{out}}{Hub} = 1.98$ is slightly higher than water wheel with hub 250mm. However, for $\frac{D_{out}}{Hub} = 3.37$ the efficiency is always lower than the others.

The efficiency curve displays similar characteristics to the torque curve, as at a low speed the efficiency is high and tends to a lower value as the rotational speed increases. In addition, the efficiency curve also shows that the comparison between the outer diameter to the hub diameter $\frac{D_{out}}{Hub}$ plays an important role in term of the efficiency of the machine. The graph

shows that the efficiency of the $\frac{D_{out}}{Hub} = 1.34$ is lower than $\frac{D_{out}}{Hub} = 1.98$ only within a certain range (in this case at $\frac{V_{tan}}{V_{max}}$ less than 0.2), then the efficiency of both of them decreases as the speed increases. However the efficiency drop of the $\frac{D_{out}}{Hub} = 1.98$ is much steeper than $\frac{D_{out}}{Hub} = 1.34$. More over the graph also shows that the efficiency gradient is of the $\frac{D_{out}}{Hub} = 1.34$ is shallower in comparison to the others.

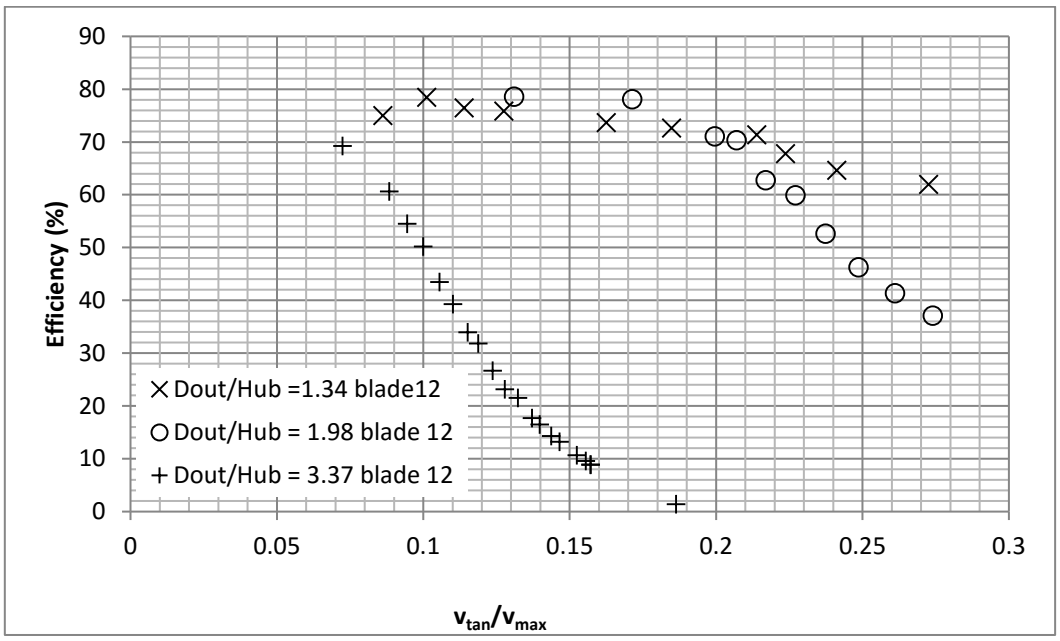

Figure 4.32: The efficiency of the machine at varies hub diameter

Figs 4.33 until 4.36 shows the interaction between the water and the blades of the wheel. Each figure was taken at the highest power output produced. The interaction between the water and the blades at maximum power output is an interesting point to discuss. The maximum power output and efficiency of each hub diameter variations is presented in table 4.8.

Table 4.8: Summary of maximum power output by varying hub diameter

Machine	Max power output (w)	Efficiency at max power output	Rotational speed (rpm)	v_{tan}/v_{max}
Hub250 blade 12	3.31	62 %	37.5	0.27
Hub170 blade 12	2.88	70.34%	24	0.21
Hub 100 blade 12	0.811	60.64%	10.65	0.09

At first glance, it can be seen from Figs 4.33, 4.35 and 4.36, there are some sources of losses that can be identified from this machine. The losses potentially come from turbulence in the cell, hydraulic head drop and elevation losses.

Fig 4.33 shows a figure which reveals the interaction between blade and water for the case of hub 250 mm 12 blade and 37.5 rpm. This figure shows the position of one blade (the blade with dot red on it) from very beginning of cell draining until completely draining. From this figure also indicates some sources of losses. In this case the power output is around 3.31W with the efficiency of 62%. Since the speed at this highest power output is essentially high, so the contribution of losses coming from turbulence, head drop and elevation losses are quite significant. From Fig 4.33a until 4.33e can be seen that the proportion of air bubbles in the cell is quite significant in comparison to the proportion of water in the cell. The enlarged view of Fig 4.33 is shown in Fig 4.34. These bubbles are generated by turbulence in the cell which becomes more significant as the speed increases (as shown in Fig 4.33b and enlarged in Fig 3.34). In addition, other loss also comes from elevation losses as a proportion of the water is not released from the cell as the edge of the blade leaves downstream water surface (as shown in Fig 4.33e and detailed in Fig 4.34). This occurs because of the wheel rotation speed is relatively high, and the water does not have enough time to release from the cell. Another factor contributing to the losses comes from the hydraulic head drop from the water inlet to the receiving cell from the upstream flow (as shown in Fig 4.33a and detailed in Fig 4.34). This loss will also be discussed at a later point in this chapter as an explanation of Fig 4.37. To sum up, the most significant contributing factor in creating losses in the case of the 250mm hub is the relatively high rotational speed, which subsequently induces turbulent losses, elevation losses and hydraulic head drop. Downstream pressure losses can also be considered factor, however this loss is not so significant in the case of 250 mm hub, as the frontal area of the cell is not too large in comparison to other variants. Fig 4.35 shows the interaction between the water and the blades of the wheel in the case of 170 mm hub, with 12 blade and an operating speed of 24 rpm. Since the speed for this case is lower than the case of 250 mm hub at maximum power output, so essentially the losses for 170 mm hub with 12 blade mostly comes from downstream pressure which happens because the blade frontal area is larger than 250 mm hub. Nevertheless, the turbulence losses still occurs in the case of the 170 mm hub as can be seen in Fig 4.35a until 4.35e. The elevation loss is smaller than in the

previous case, as can be seen from Fig 4.35c, and then water drop at 4.35d and blade leaves downstream water surface cleanly at 4.35e. In short, most of the losses in this case comes from downstream pressure.

Fig 4.36 shows the interaction between the water to the blade in the case of the 100 mm hub, with a speed of 10.65 rpm. Essentially the contribution of losses due to turbulence is not significant, as can be seen from Fig 4.36 a until 4.36e, where the bubble proportion is less in comparison to the case of 170 mm and 250 mm hubs. In addition, the contribution of elevation losses are also small as can be seen from Fig 4.36d-e, in which the blade leaves the downstream water surface cleanly. So mostly the losses for the case of 100 mm hub comes from downstream pressure, as the frontal area of the blade is larger than the others.

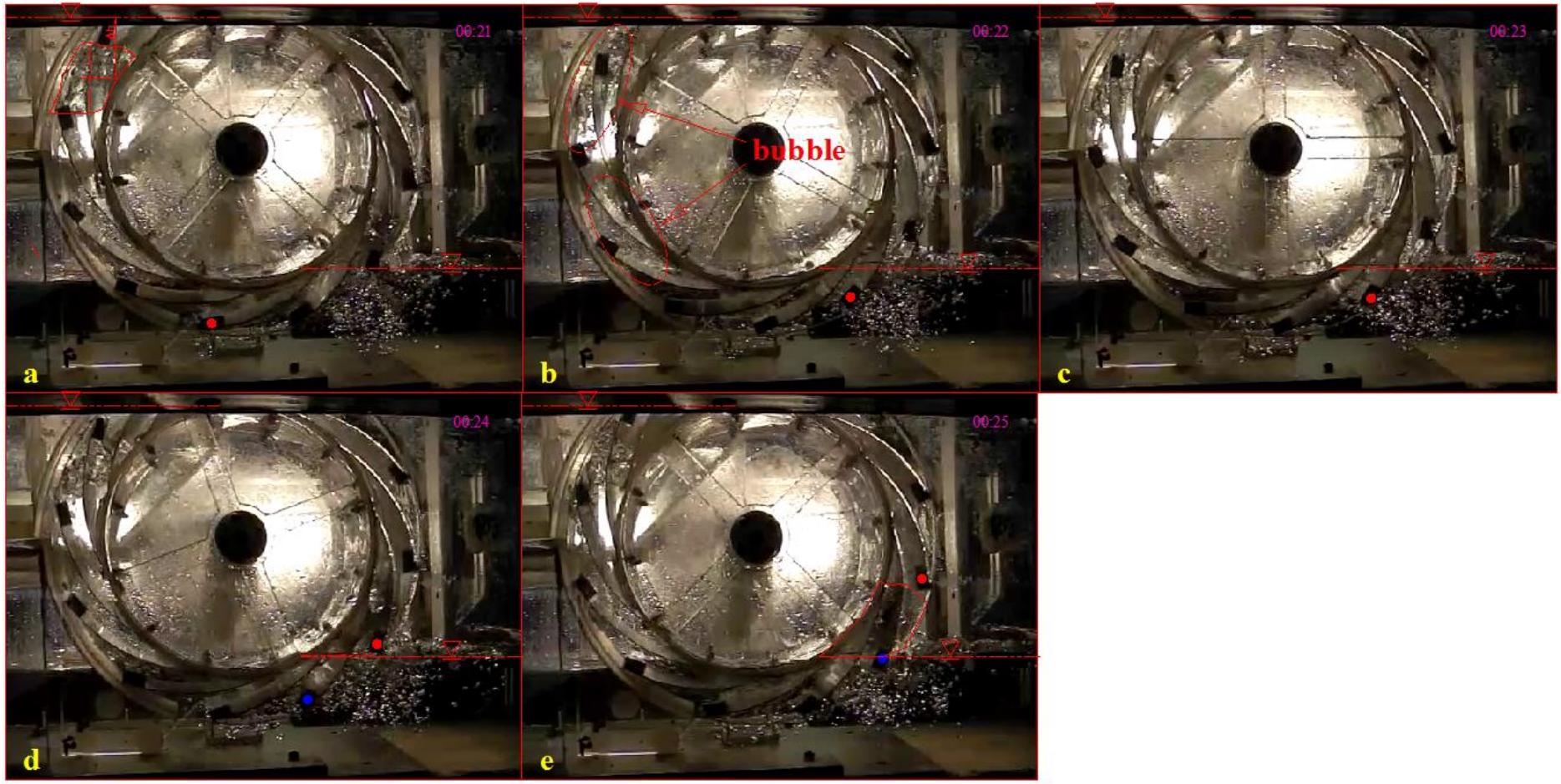

Figure 4.33: The interaction between water and blades for hub250 mm-12 blade-37.5 rpm

Figure 4.34: Enlarging view of Fig 4.33 a, b and e.

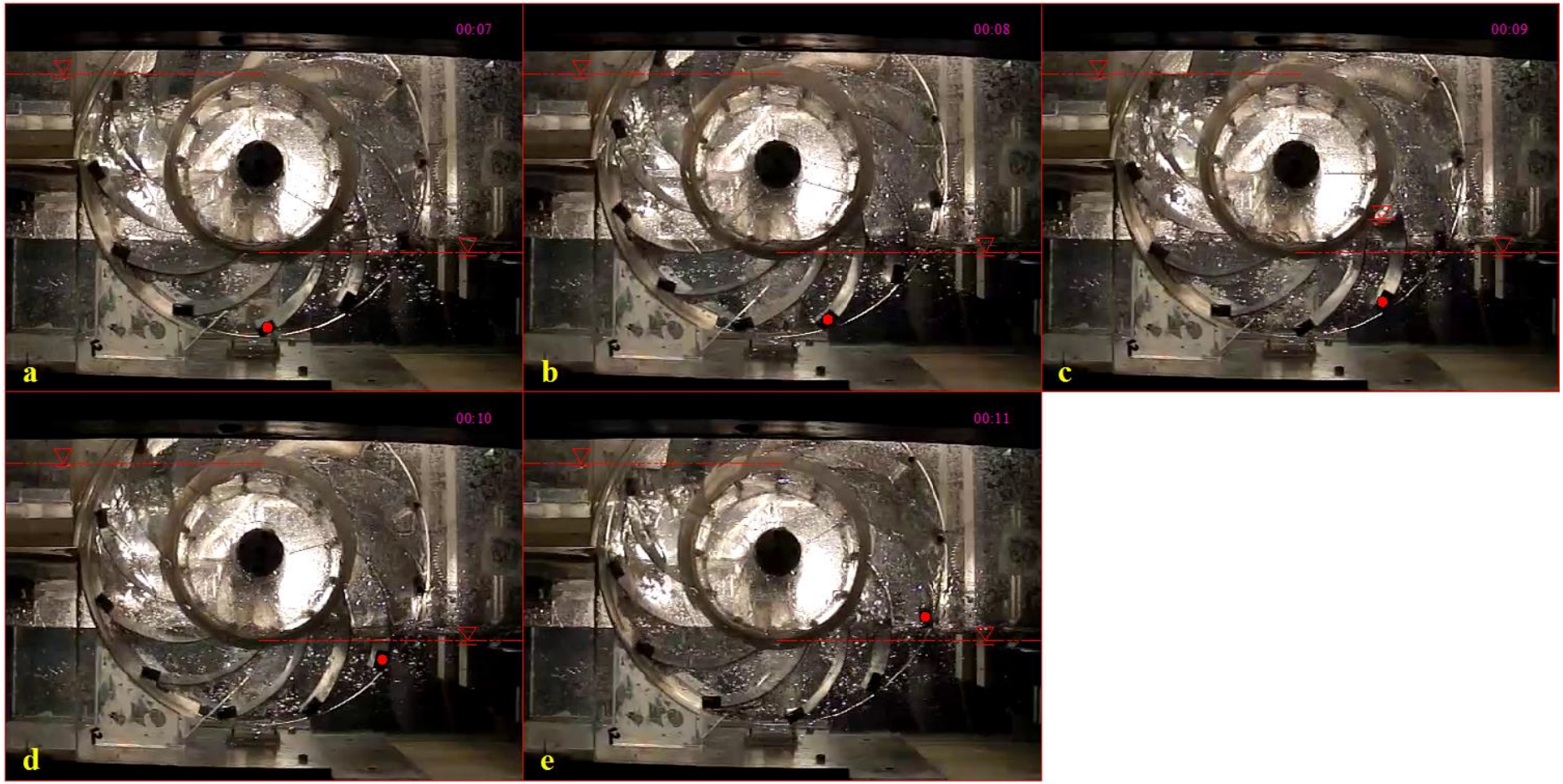

Figure 4.35: The interaction between water and blades for hub170 mm-12 blade-24 rpm

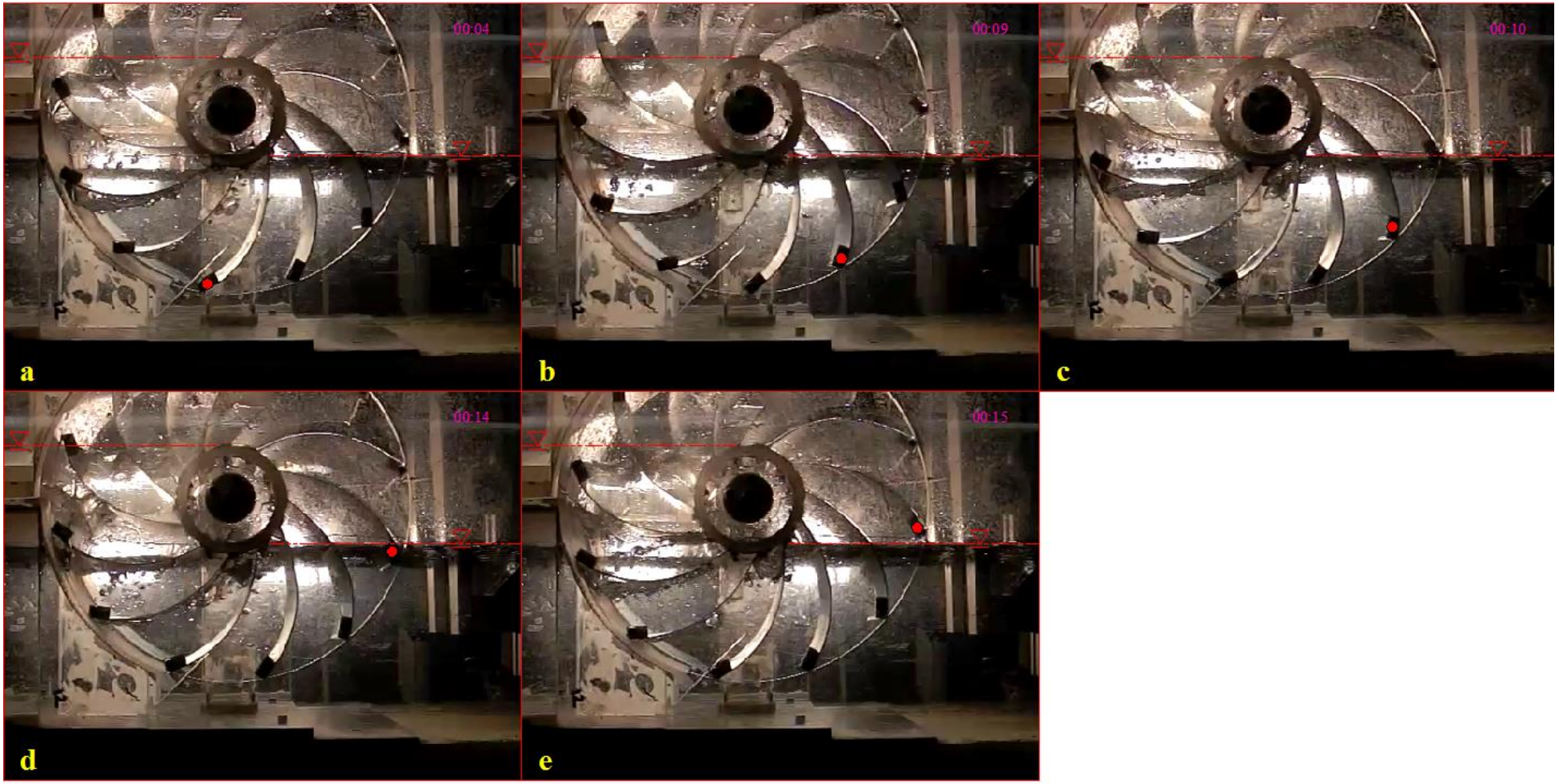

Figure 4.36: The interaction between water and blades for hub 100mm-12 blade-10.65 rpm

Fig 4.37 shows the picture of the inlet section of the turbine wheel. Fig 4.37a shows the inlet section of the machine for the 250 mm hub with a rotational speed of 37.5 rpm. At this relatively high speed, obviously there is a head drop of water occuring. This situation also occurs with the 170 mm hub diameter wheel at a speed of 24 rpm. From this picture, it is clear that the one factor that is creating significant losses at the maximum power output in the case of the 170 mm and 250 mm hubs is the head drop. In the case of the 100 mm hub, with a rotational speed of 10.65 rpm at maximum power output, the head drop is not clear, since the rotational speed of the blade is slow, so it can be said that the contribution of the head drop for the case of the 100 mm hub at maximum power output is small. The data shows that the higher the hub, the more possibility to get larger power output. In addition also there is possibility to get wider range of rotational speed in the case of hub 250 than 170mm hub and 100 mm hub

.

Figure 4.37: The inlet section for hub 250 mm, 170 mm, and 100 mm at max power output

4.6.3 The effect of the number of blades on the performance of the turbine wheel

The effect of blade number on power output is investigated. Test was conducted with 6 and 12 blades on the 250 mm diameter hub model. Power output as function of wheel speed is shown in Fig 4.38. The results show that the 12 bladed wheel provides a similar power output to the 6 bladed wheel. However for a rotational speed of 31.5rpm, the water wheel with 12 blades gives a power output that is higher than a 6 bladed wheel about 0.2 W. Unfortunately the data for velocities higher than 37.5 rpm is not provided, since this range is beyond the capabilities of the resistor that was used to control the speed of the motor. This problem is mitigated during the next experiment, whereby the methodology of measurement is improved. At the speed of less than 22 rpm, the 12 bladed wheel shows similar power output with 6 bladed wheel. This fact can be explained speculatively from Fig 4.39 for 12 blade and 4.40 for 6 blade. From Fig 4.39 it can be seen that the cell is essentially fully filled with water (very small amount of bubbles) at a low rotational speed. This situation occurs at every position of the blade (as can be seen from Fig 4.39 a-e). In the case of the 6 bladed wheel (Fig 4.40), the situation is similar to the 12 bladed wheel, when the cell is also fully filled with water at a low rotational speed. In addition, Fig 4.41 shows the inlet section of the 12 bladed and 6 bladed wheel. This figure also shows that at a low speed the cell is fully filled with water (no bubble at entrance), so the volume of water which occupies the cell is similar between a 12 and a 6 bladed wheel. As the cell is fully filled with water especially at low speed, then the pressure that acts on each of the blades does not make any contribution to the power output (this explanation is refer to subchapter 2.5.2). The blade that actually contributes to the power output is the blade that is in contact with downstream area. This data also strengthen the explanation of the subsection 2.5.2.

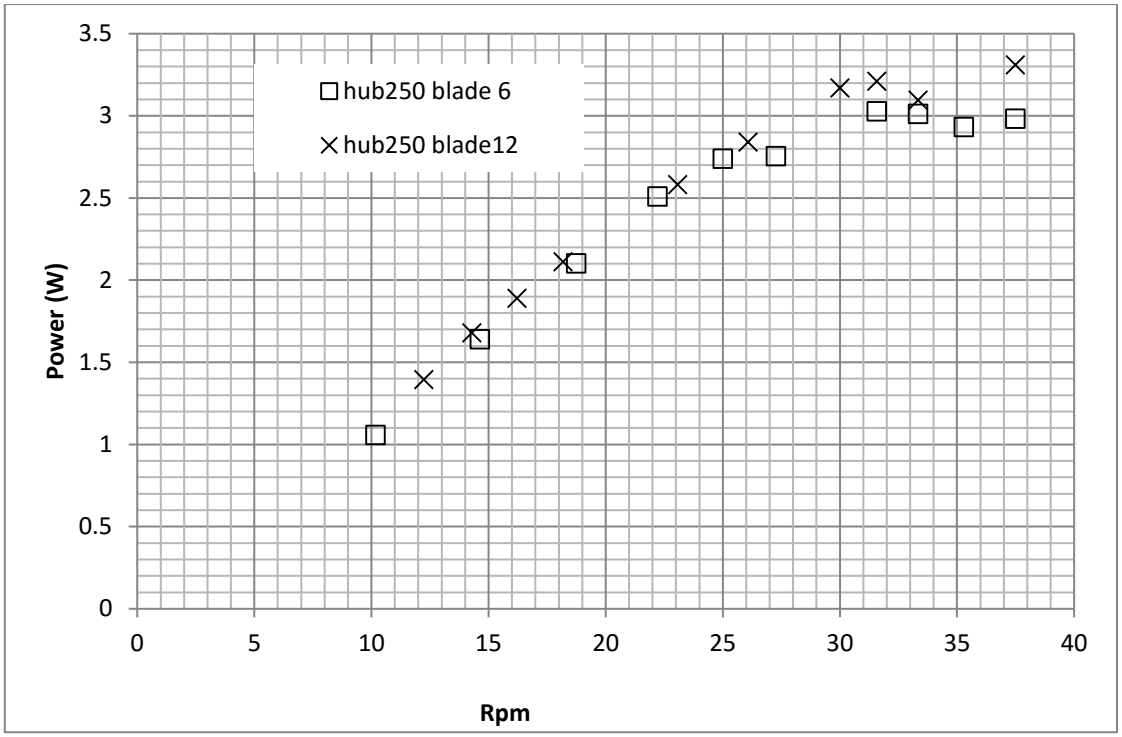

Figure 4.38: Power output of the machine at varies blade numbers for the 250 mm hub

.

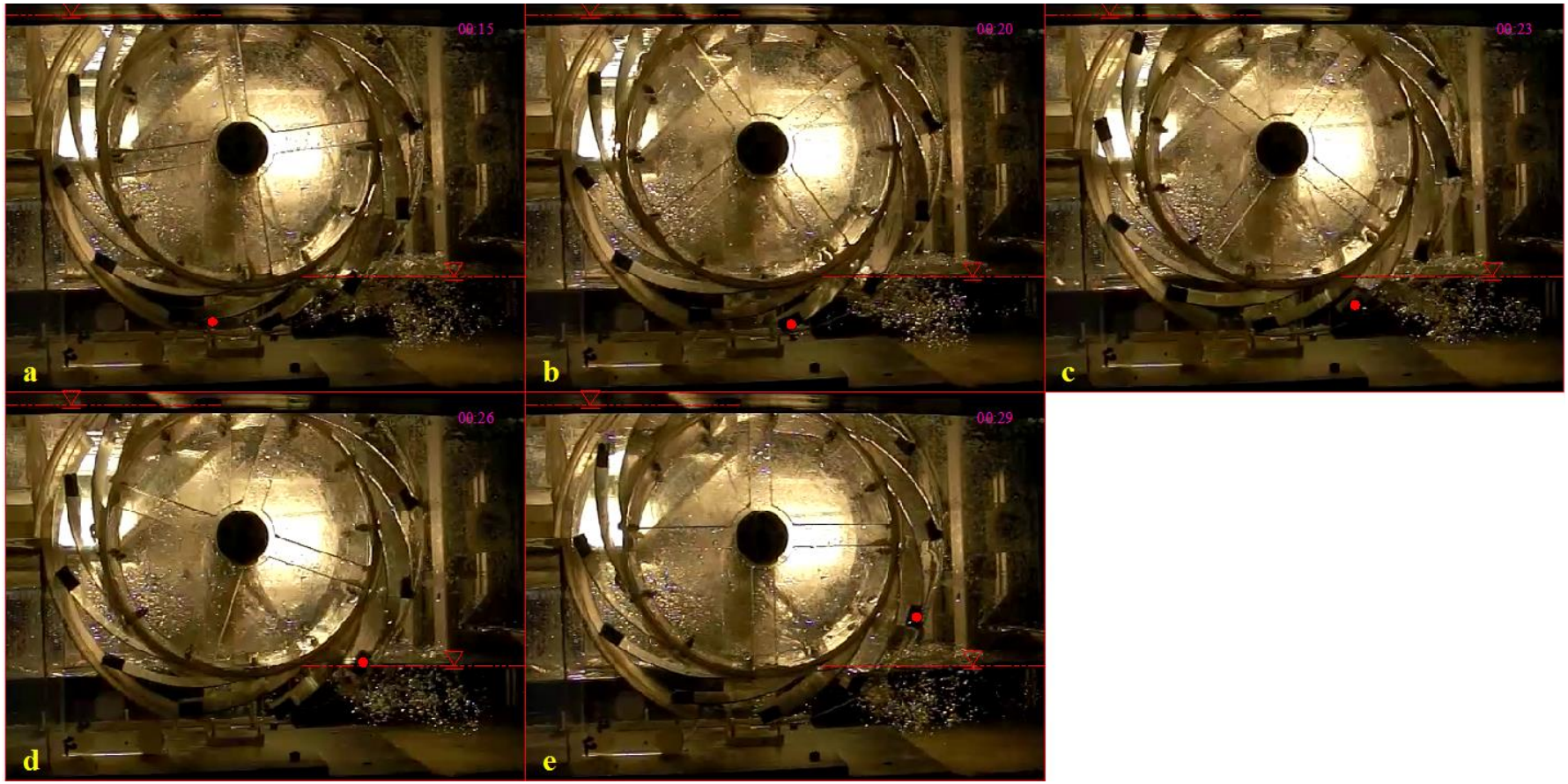

Figure 4.39: The interaction between water and blade for the 250 mm hub-12 blade-12.2 rpm

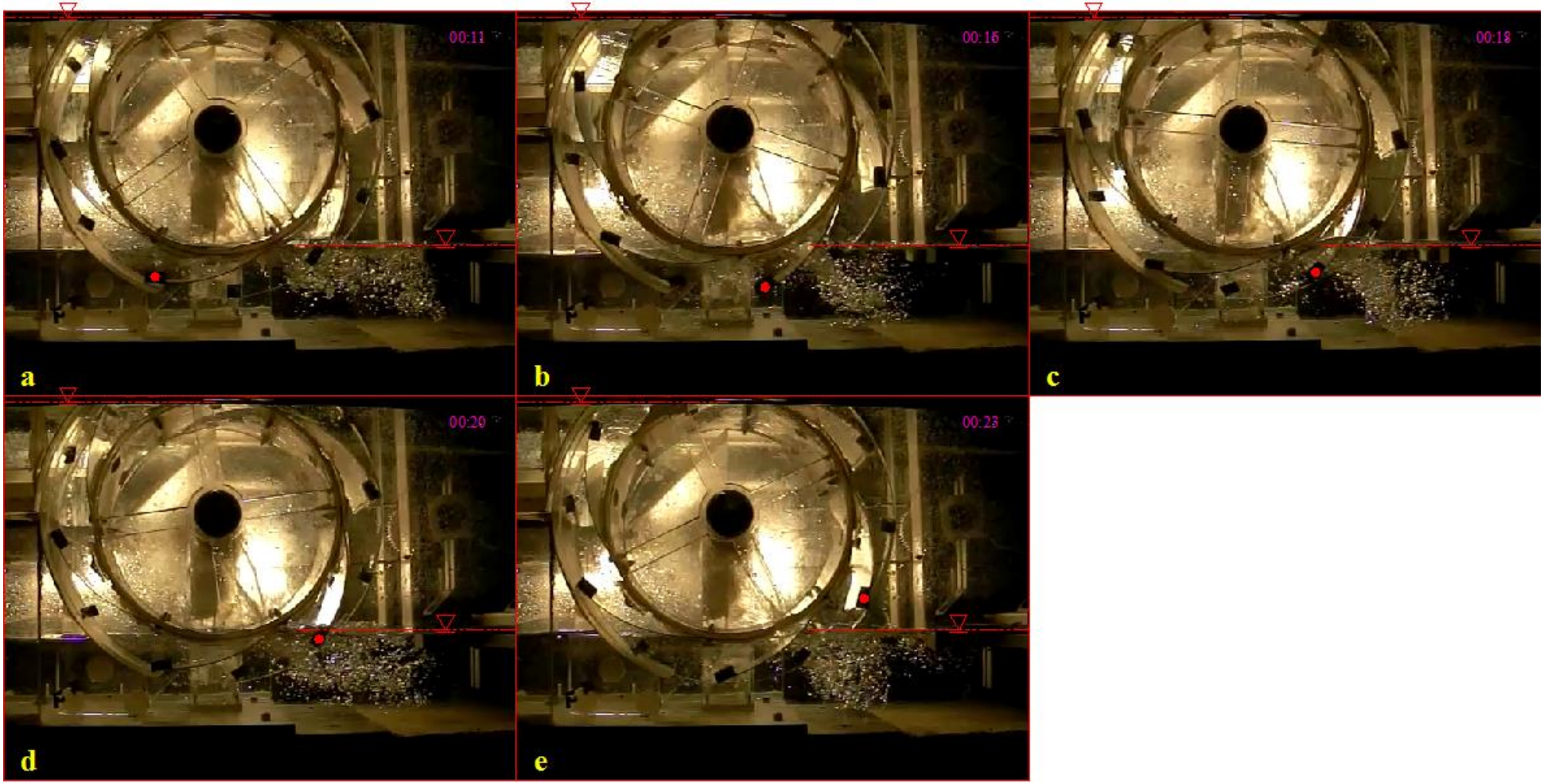

Figure 4.40: The interaction between water and blade for the hub 250mm hub-6 blade-10 rpm

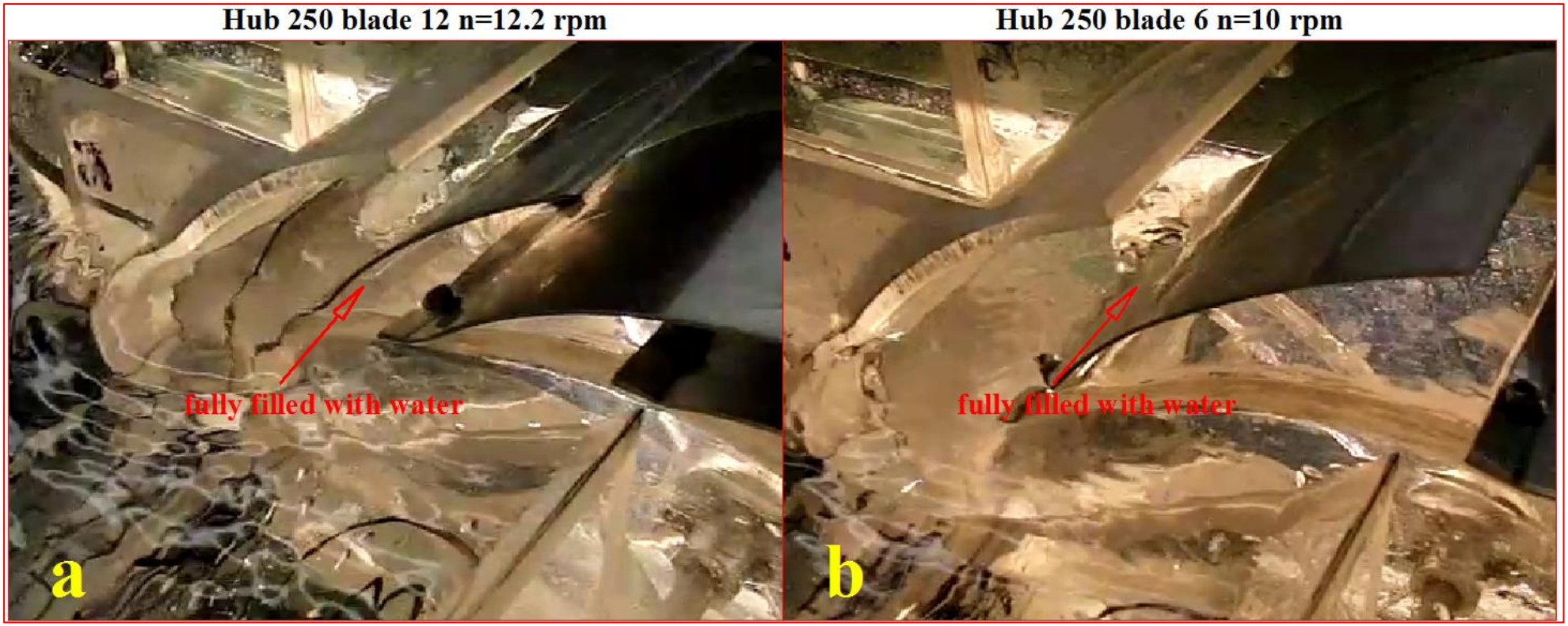

Figure 4.41: The inlet section for the 250 mm hub, 12 blade and 6 blade

Fig 4.42 shows the torque output for a water wheel with 250 mm hub diameter and an outer diameter of 337 mm with the blade numbers varying between 6 and 12. The magnitude is slightly similar at the rotational speed of 23 rpm, and then deviates.

However the deviation between them is quite close, for example at a speed of 31.57 rpm, the torque output for 12 bladed wheel is 0.97 Nm, whereas for a 6 bladed wheel it is 0.91 Nm. Logically the torque reaches its highest value as the speed reduces instead of decreasing as shown in the torque graph. From this graph essentially the author thinks there must be an uncertainty that makes the data at low speed deviate. The author believes that the torque produced at low speeds is similar with the 12 bladed wheel and the 6 bladed wheel. This theory is match with the explanation from subsection of 2.5.2, which states that the number of blades does not have any relationship to either the torque or the power output of the machine especially at low speed. This is confirmed by the experimental result. Furthermore, the efficiency values are also similar between a 6 bladed and a 12 bladed wheel as shown in Fig 4.43. However, at the $\frac{V_{tan}}{V_{max}} = 0.27$, the 12 bladed wheel shows higher efficiency. The issue that is noted in this experiment is that the range of speed that is being used, is too small. It is still possible to increase the wheel speed by using the potentiometer which has a higher range of resistance or by using several resistors with varying resistance as previously discussed in part 4.6.1.

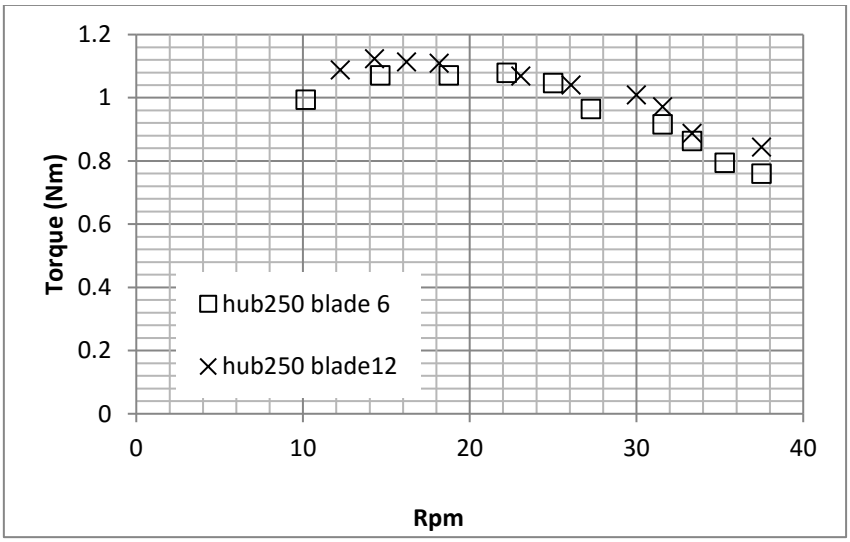

Figure 4.42: The Torque output for two different blade numbers for hub 250 mm

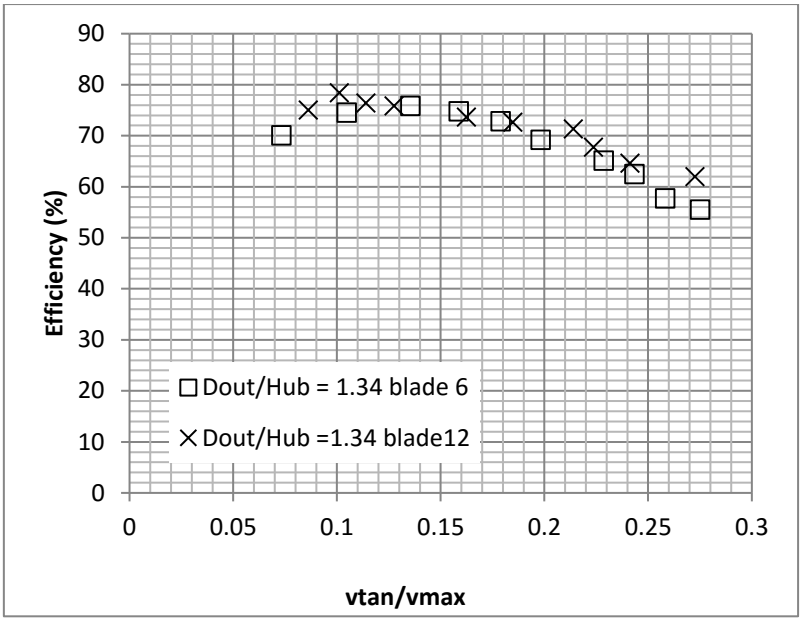

Figure 4.43: The efficiency of the machine for two different blade numbers for hub 250 mm $/\frac{Dout}{Hub} = 1.34$

4.6.4 The effect of the baffle on the performance of the water wheel

In this series of test, it was attempted to optimise the inflow geometry in order to reduce losses. The entrance of the wheel is suspected to create losses. On this entrance the flow direction is changes abruptly through 90° which potentially causes losses. It is very common in fluid dynamics where the flow passes through a 90° change in direction, then a guide vane/baffle is placed within the flow stream to reduce the losses. In order to reduce these losses, the idea of using the inlet baffle as a guide to the inflow water has evolved. The baffle/guide vane is a hand shaped plate that is located at the upstream inlet of the wheel which position the flow to give a streamline effect. The picture of the plate is shown in Fig 4.44

Figure 4.44: Guide vane/baffle at the inlet of the wheel

The effect of the baffle on the performance of the water wheel was only tested on the 250 mm hub. Initially, the flow directions at the inflow were visualised using a thread method, (see Fig 4.45). The baffles were then designed to match the streamline of the flow. The streamline of the flow is drawn, based on the result from flow path tracking. The flow path tracking method basically draws the flow streamline by using a yarn that is tied on to a rod that is placed in to the upstream flow. The yarn direction is measured by using a protractor that is attached below the yarn. The direction of the yarn is then drawn as an arrow to show flow direction (see Fig 4.45).

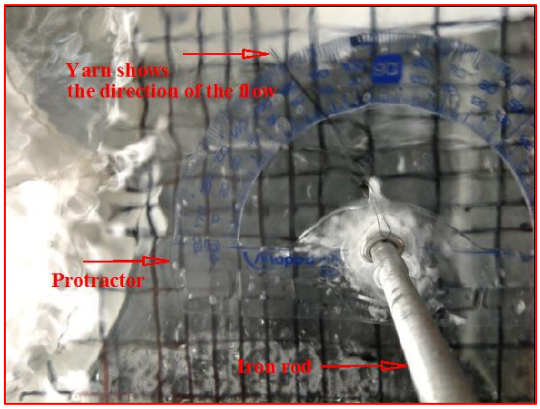

Figure 4.45: flow tracking results and baffle for hub 250 mm

The path tracking result is presented in this section. Fig 4.46 shows the flow direction and also the baffles for the 250 mm hub. From this flow direction result, the baffle is then designed based on the streamline that is drawn by making a line through the tangent of the arrow at several points.

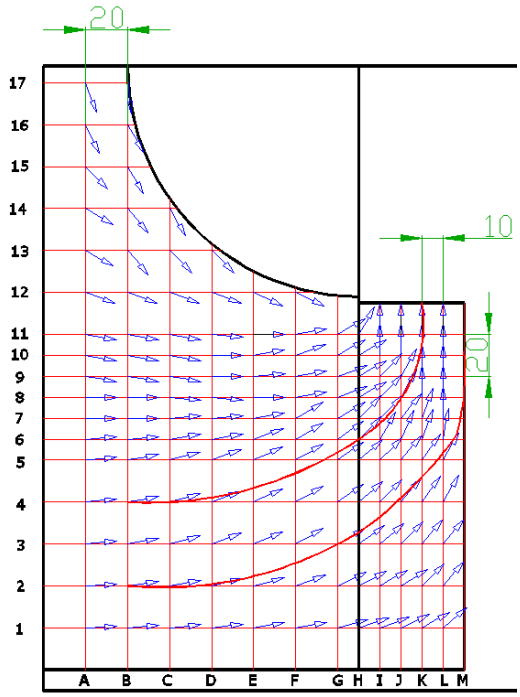

Figure 4.46: flow tracking results and baffle for hub 250 mm

The effect of the baffle to the performance of the water wheel is then compared to the same water wheel without baffle. Fig 4.47 shows the power output as function of the rotational speed and the effect of the baffles on it. In Fig 4.47, for low speeds, below 33 rpm, the power output is similar between a baffled wheel and a wheel without baffles. At a speed of more than 33 rpm, the baffled wheel shows 0.166 W higher power output than non-baffled wheel which is insignificant value. Unfortunately the numbers of recorded data are too small to draw a conclusion, since it is only two data points recorded after rotational speed of 33 rpm. This data shows that the baffle does not give a significant effect.

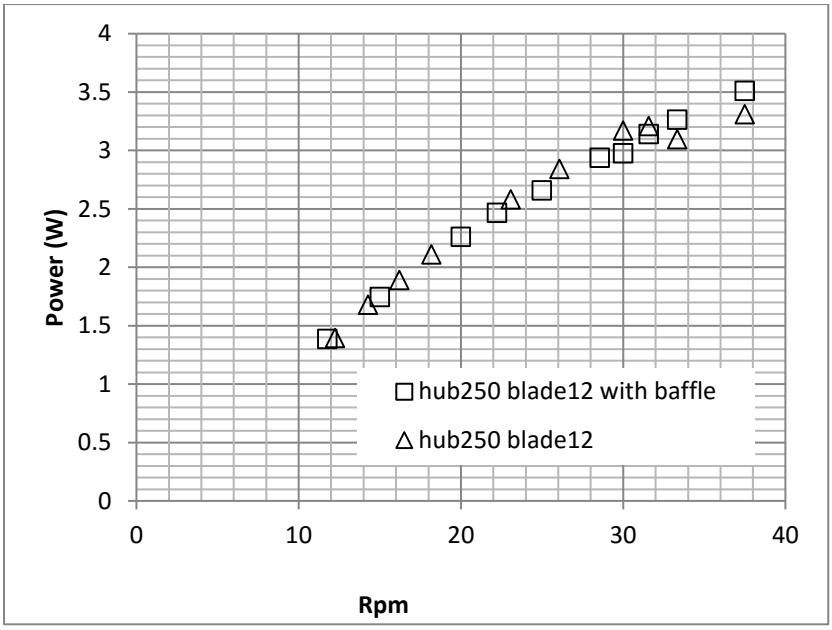

Figure 4.47: Power output graph water wheel with baffle and without baffle for hub 250 mm

The existence of the baffle on the torque output is also investigated in this experiment. As shown in Fig 4.48. In the case of the 250 mm hub the torque produced is similar for speed less than 33 rpm. Moreover the torque output for the baffled wheel operating at speed greater than 33 rpm, is slightly higher than the wheel operating without baffles.

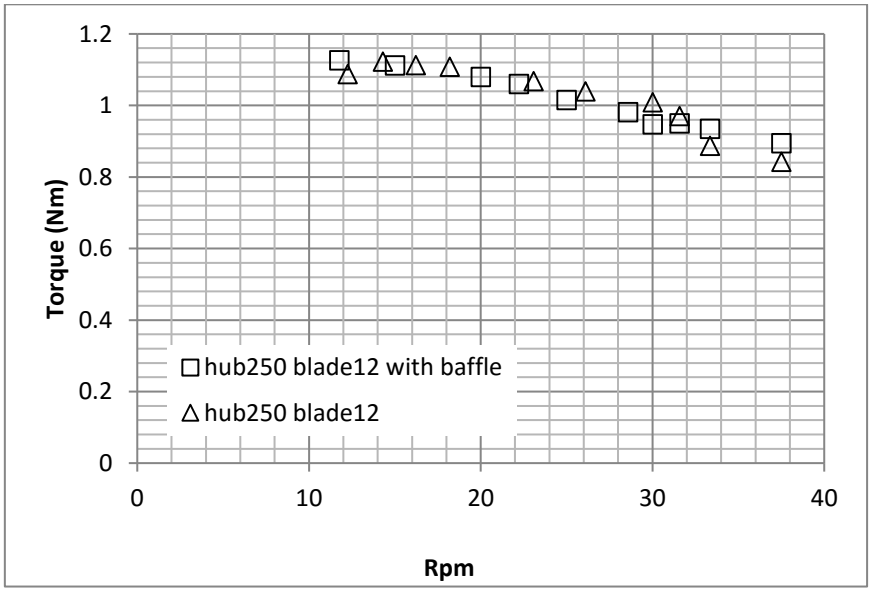

Figure 4.48: Torque output graph water wheel with baffle and without baffle for hub 250 mm

4.7 Discussion and conclusion

4.7.1 Discussion

The experimental result show that the best ratio between the outer diameter to the hub diameter $\frac{D_{out}}{Hub}$ is 1.34 for this set of experiments, results in the highest possibility to increase power output in comparison to $\frac{D_{out}}{Hub}$ 1.98 and 3.37. Actually this ratio is almost similar to the original machine (Zuppingerrad), which the comparison is $\frac{Dout}{Hub} = \frac{29\,3/4\,"}{21\,1/4\,"} = \frac{755.65\text{mm}}{539.75\text{mm}} = 1.4$

The data is not covered at high speed especially in the case of-the ratio between the outer diameter to the hub diameter $\frac{D_{out}}{Hub}$ 1.34. It only exists in the range of speed less than 37.5 rpm. This is not the probable speed that correlates to maximum power output. Since from the HPM power curve, the curve always trends close to a parabolic curve (Senior 2009), (Linton 2014). So after the rotational speed of the model reaches maximum power output, the power output will decrease as the rotational speed increases. This phase of decreasing power output is not found in this case at the $\frac{D_{out}}{Hub} = 1.34$ or 250 mm hub. It reflects that the range of the speed should be increased. This could be achieved by adding a series of potentiometer as controller or as series of resistors as discussed in section 4.6.1. The power output for the case of $\frac{D_{out}}{Hub}$ 3.37 is very low in comparison to the variants. This situation occurs at all ranges of speed from 8 rpm to 22 rpm. As described previously in section 4.6.2, this situation occurs because the hub diameter too small, so the head is small as well (as hub diameter=head). This occurrence also make the speed range of the $\frac{D_{out}}{Hub} = 3.37$ wheel small, since the sources of energy that are required to rotate the wheel comes from the head difference which is small, even though the frontal area is larger than other variants.

There is no different in performance between a twelve bladed and a six bladed wheel at low speed. However at higher speeds, the performance of the twelve bladed wheels shows a slightly higher power output. This result is contrary to (Linton 2014) who claimed that the six bladed wheel potentially displays an advantage in term of power output in comparison to the twelve bladed wheel.

The effect of the baffle on the performance of the wheel is not that clear at low speeds, even though there is a potential possibility to increase performance of the wheel at high speeds by adding baffles in the inlet. However there is a question mark as to whether this baffle contributes to increasing the performance of the water wheel. At any flow speed this baffle may act as a barrier to the flow, since this baffle was designed based on the 2D flow, whereas, the actual flow at the inlet is actually a 3D flow. In addition the velocity range at high speed also is too short to determine whether the baffle will have an effect on the performance of the water wheel.

4.7.2 Conclusion

The determined efficiencies reached 70-88% exceeding those reported in the historical literature which are 75-80%.

The ratio between the outer diameter to hub diameter $\frac{D_{out}}{Hub}$ 1.34 which almost matches the original machine ($\frac{D_{out}}{Hub}$ 1.4) gives the best performance with efficiencies of 71% for normalised speed ratio of 0.21.

There is no significant effect identified with either 6 or 12 bladed wheel on the performance of the turbine wheel, but at higher speeds, 12 blades tends to give a higher power output.

An optimised inflow with guide vanes does not give an obvious positive contribution for $\frac{D_{out}}{Hub} = 1.34$, eventhough at high speed (more than 33 rpm), it seems that the baffled wheel give a higher power output.

The electric PTO seems to be working well in measuring torque, however, it still needs to be improved, since it is not reliable for the measurement of power outputs at rotational speeds of more than 37.5 rpm.

CHAPTER 5

TORQUE METER MEASUREMENT METHOD AND UPSCALING TURBINE WHEEL

The experimental results from chapter 4 shows the effect of the ratio between the outer diameter to the hub diameter $\frac{Dout}{Hub}$, numbers of blades and also the effect of the baffle on the performance of the turbine wheel. An overview of the performance of the turbine wheel has been undertaken. The data from the experimental work in chapter 4 shows for a head of water of 250 mm or the machine with the ratio between the outer diameter to hub diameter $\frac{D_{out}}{Hub}$ 1.34 (which is closest to the original turbine wheel machine) shows the highest power output of all the other variants. However, the data was limited to a speed of less than 37.5 rpm. In addition the 250 mm hub with the ratio between the outer diameter to hub diameter $\frac{D_{out}}{Hub}$ 1.34 has the widest range of rotational speed in comparison to the other variants.

Based on this fact, then the third model was made as a testing model with the ratio between outer diameter to hub diameter of 1.4. The outer diameter is 490 mm and the hub diameter is 350 mm. The blade width of 80 mm makes this machine geometrically similar to the original machine of Walter Zuppinger. By upscaling the third test model from the previous one, it is expected that this test model will provide more accurate data, where the influence of leakage, friction and other external influences can be minimized. The 2D drawing of the third machine is shown in Fig 5.1

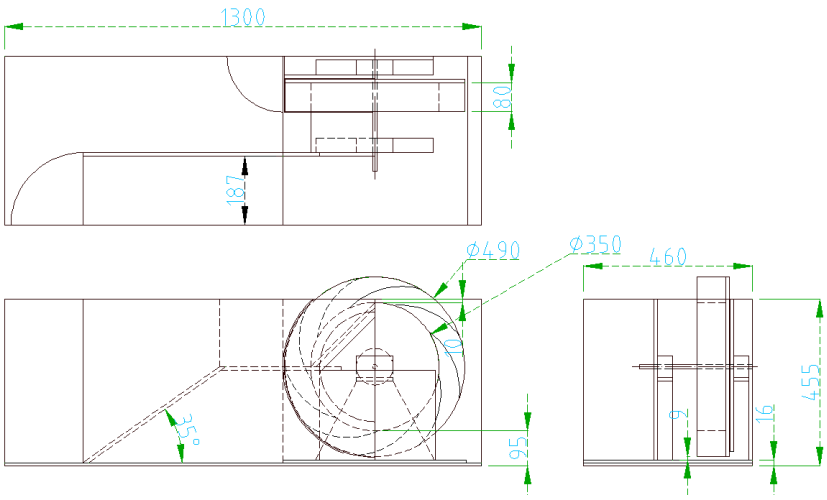

Figure 5.1: 2D drawing of the turbine wheel

This machine was tested in the wave tank of 460 mm (width) x 455 mm (depth) flume which was modified in to a recirculating flume in order to make it fit with the nature of the test. The 3D design of the third machine is drawn in Fig 5.2. The power measurement devices were installed on the left hand side of the machine.

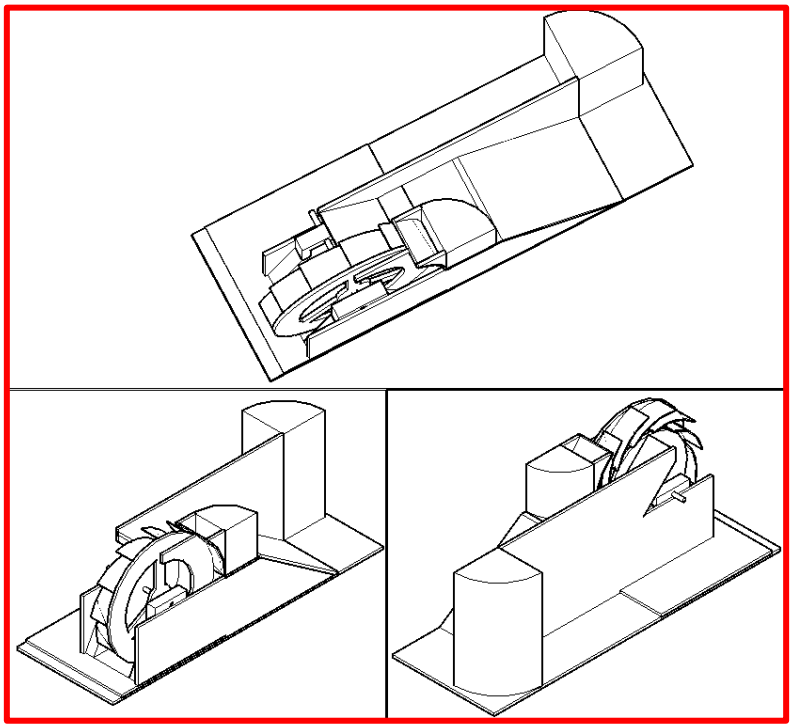

Figure 5.2: 3D drawing of the 3rd turbine wheel

5.1 Measuring Power output by using Torque meter

In chapter 4 as has been discussed an experiment was undertaken on several variations of the turbine wheel. In chapter 3 the effect of the upper shroud to the performance of turbine wheel has been discussed. The power output was measured by using the classic Prony brake. In chapter 4 other modifications to the wheel have also been undertaken, these were varying the inlet incorporating several baffles. Furthermore, it has also been discussed about the effect of the ratio between outer diameter to the hub diameter on the performance of water wheel. The drawback of the classic Prony brake method is that there was a slip between the belt and the disc brake especially at high torque, which eventually lead to inaccurate measurements. For more details on how the classic Prony brake operate please refer to section 3.3. Referring to this problem, the technique of measuring power output was improved during the 2nd machine test. In 2nd machine test, the measurement was improved by using the electric method. The load that applies on the water wheel is controlled by using a DC motor. A lever arm which is connected to the force transducer indicates the torque that is produced by the water wheel. For more detail please refer to subsection 4.5. Nevertheless this 2nd method also have some drawbacks which are:

- Losses might occur during the transmission of power from the water wheel to the pulley to which the DC motor is attached.
- The methodology of the power calculation always assumes that the belt is slack which always occurs at the lower chord. This potentially produces unreliable results at low torque/high speed. This is the reason why the data that was taken on this experiment was only at high torque/low speed.

In order to overcome some of the drawbacks mentioned above, the following measurement methodology is to use a torque meter to measure the torque produced and to calculate the power output in a more accurate way. The power output result from the third machine was measured using the torque meter, whereas, the load is generated from the DC motor, which is similar to the previous method. The view of the measuring method is shown in Fig 5.3.

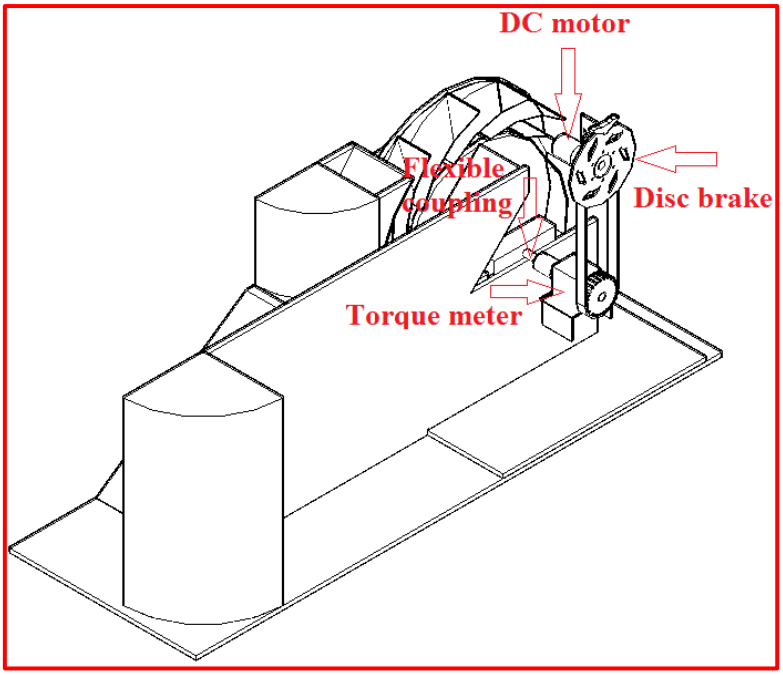

Figure 5.3: Measuring Torque output by using Torque meter

The measurement result from the torque meter provides a better result, which can be used as reference to build the theory of the turbine wheel.

5.2 Equipment and Facility

The experiment was conducted in the hydraulic Laboratory University of Southampton. The model was placed in the 455 mm x 460 mm recirculating tank. The length of the flume is 13m. A sump tank was used as reservoir of the water. Fig 5.4 give schematic diagram of the experimental set-up. The torque output was measured by using a torque meter transducer. The shaft from the water wheel is connected to the torque meter via a flexible coupling. The rotation of the water wheel is opposed by using a DC motor. Control of the load is applied via a DC motor by adjusting the resistance in the circuit of the DC motor. At very high torque, the speed of the wheel is decelerated by using a disc brake. The picture of the measurement system is shown in Fig 5.5.

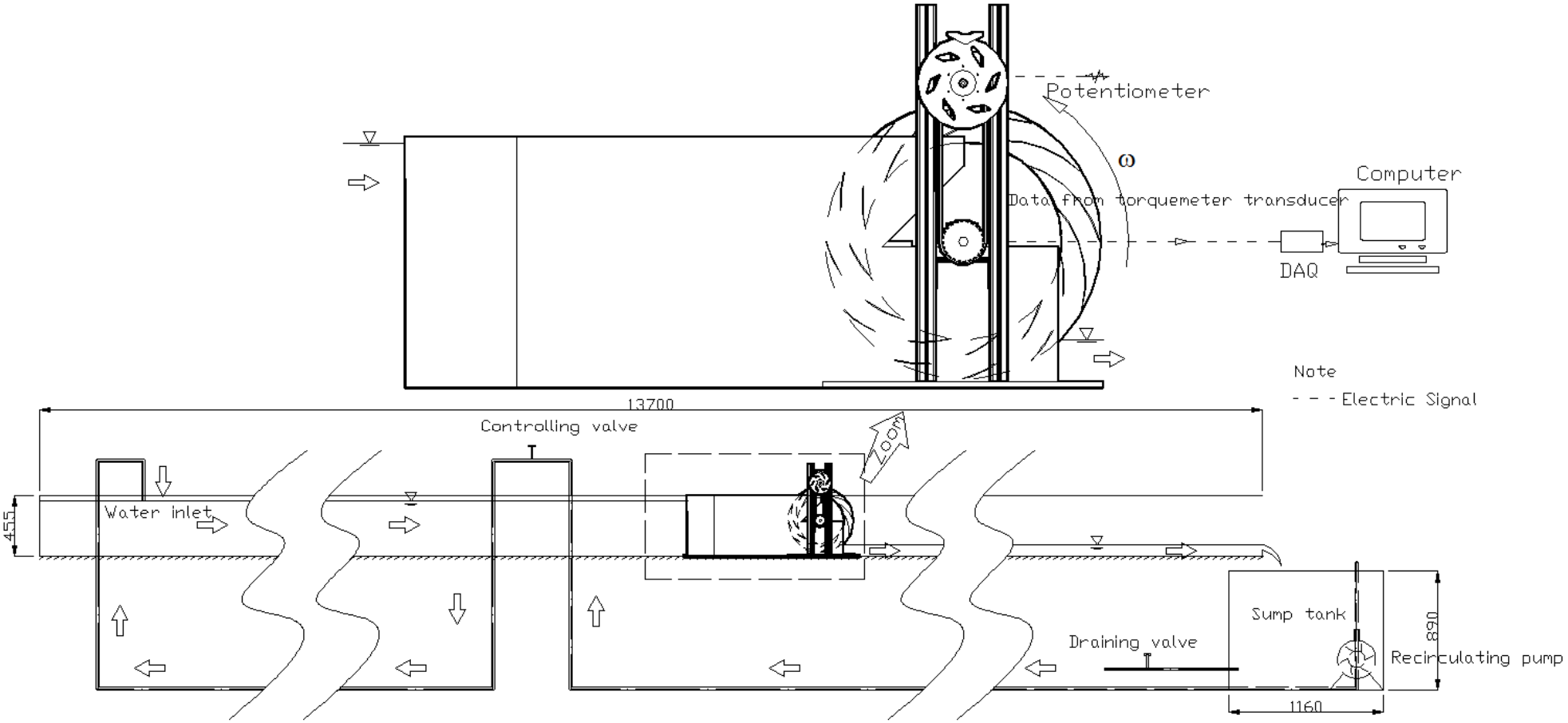

Figure 5.4: Schematic diagram of the experimental setup.

Figure 5.5: Depiction of the torqumeter, DC motor, disc brake and controoler of the load

The equipment that was used in this experiment is described as below:

1. Torquemeter

The output torque from the machine should be calculated in order to determine the specification of the torque meter. The explanation on how to predict torque output and the selection of a torque meter is shown in the appendix. From the torque prediction, it was decided that the torque meter should have a maximum torque measurement of 5 Nm. In this case, an AEP transducer was used. The AEP transducer is shown in Fig 5.6.

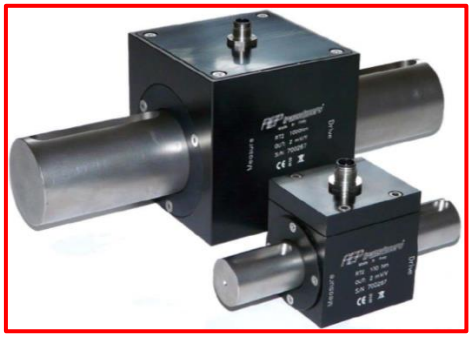

Figure 5.6: AEP Torque transducer

Calibration was undertaken to confirm the accuracy of this transducer. The calibration was conducted by putting a clamp on the shaft of the torque meter. The lever arm of the clamp L is known as 0.18 m. The actual torque is calculated as the weight w times lever arm L

$$T = w\,L \qquad 5.1$$

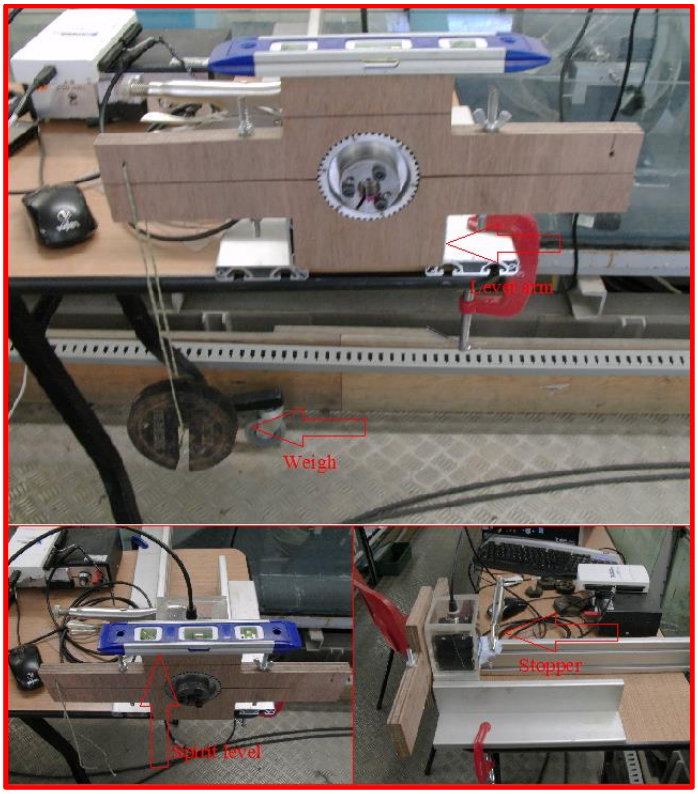

Figure 5.7: Calibration equipment

The torque output from torque transducer is then plotted against the actual torque. These values are then shown in the calibration curve, and shown as in Fig 5.8.

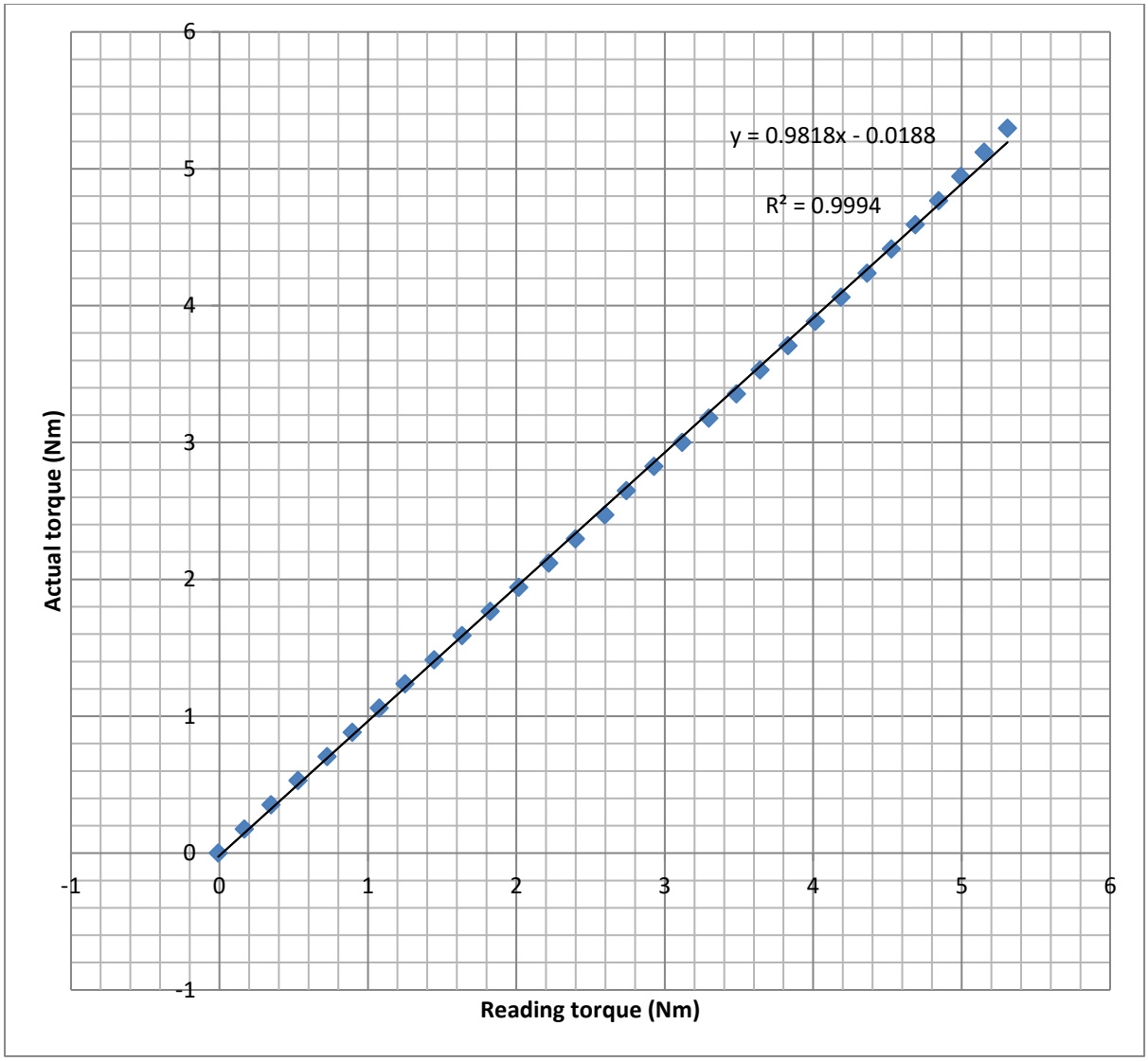

Figure 5.8: Calibration curve

2. DC motor

This DC motor was used as a brake, to oppose the rotation of the wheel. Predicted power output and rotational speed of the third water wheel is important, since this information will be used to determine the specification of the DC motor. Scaling up technique by using Froude scaling which is similar to what has been explained in sub chapter 4.3 is the method to estimate the power output and rotational speed of the third water wheel. Data from the preliminary experiment undertaken using the earliest machine is considered as a data model and is tabulated in the table 4.2. Determining the power rating of DC motor as a brake for this wheel is based on the predicted power output and rotational speed of the water wheel. The

machine that was being tested for the third experiment is considered as the prototype. Further, the predicted power output for the third experiment is calculated, based on the biggest hub of the third machine. Since the hub of the biggest current machine is l_p = 350 mm and the previous machine is l_m = 160 mm, so from geometric similarity equation, l_r is calculated

$$Geometric\ similarity = l_r = \frac{l_p}{l_m} = \frac{350\ mm}{160\ \text{mm}} = 2.19 \qquad 5.2$$

Power output of the water wheel can be predicted from data provided from the first model. The third machine is made as a half machine, so the power per-m width is defined as $P_r = \frac{P_p}{p_m} = \frac{0.5 \cdot {l_r}^{3.5}}{b\ l_r} = \frac{0.5 \cdot 2.19^{3.5}}{0.08 \cdot 2.19}$. This calculation predicts power output per-m width for prototype as *Pp*=91.42 W/m. Further, the predicted power output for the third machine which the width of 0.08m is calculated as $P = P_p \cdot b = 91.42 \frac{\text{W}}{\text{m}} \cdot 0.08\ m = 7.31$ W.

Rotational speed is also one of the criteria that needs to be considered in order to specify a DC motor.

The predicted velocity is calculated as $velocity = v_r = \frac{v_p}{v_m} = \sqrt{l_r} = \frac{v_p}{0.571\text{m/s}} = \sqrt{2.19}$, and v_p = 1.25 m/s. The outer diameter of the third wheel is 490mm, whereas the hub diameter is 350, this fact results the average radius of the wheel as $r = \frac{\frac{490\ mm}{2} + \frac{350\ mm}{2}}{2} = 210\ mm = 0.21\ m$

Therefore, based on the data above, the angular velocity of the third model ω is calculated as $\omega = \frac{v_p}{r} = \frac{1.25\ \text{m/s}}{0.21\ \text{m}} = 6.06\ rad/sec$. The rotational speed of the third machine also can be stated as rotation per-minute/rpm. This can be stated as $n = \frac{\omega}{2\pi} = \frac{6.06\ rad/sec}{2\pi} = 0.96\ rps = 57.89\ rpm$.

based on the consideration above, then MFA Como Geared DC motor being chosen as speed regulating device.

Figure 5.9: MFA Como Geared DC motor

Table 5.1: DC motor specification

Core Construction	Metal
Current Rating	0.99 A
Dimensions	32 Dia. x 80.5 mm
Length	80.5 mm
Output Speed	60 rpm
Power Rating	7.98 W
Shaft Diameter	6 mm
Supply Voltage	15 V
Width	32 mm

3. Resistor

   The resistor was used to control the rotational speed of the wheel through the DC motor. The methodology for calculating the resistance value for this experiment is the same as used in previous experiment as detailed in sub chapter 4.4. The design speed for the motor with a voltage input of 15 V predicts a maximum power output of 7.98 W, therefore the resistor should have a minimal resistance as shown below

$$R_s = \frac{v^2}{P} = \frac{15^2}{7.98} = 28.2\ \Omega \qquad 5.3$$

At this experiment, a series of three potentiometers each with a resistance value of 150 Ω, 10 W was used as load controller.

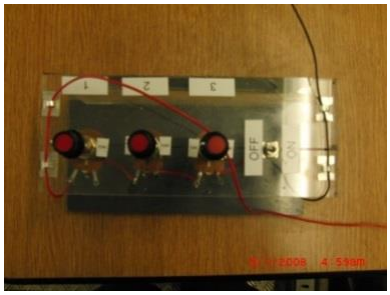

Figure 5.10: A series of three resistors that was used as controller

4. Wheel brake
   In certain situations, where the resistance on the DC motor circuit is infinitely small, therefore it fails to slow the wheel further. Yet, the rotational speed of the wheel still needs to be decreased. To achieve that, a disc brake was used to decelerate the wheel further. The placement of the disc brake is shown in Fig 5.5.
5. Timer
   A timer was used to measure the speed of the water wheel. The speed was measured by the time taken for the wheel to rotate 30 times.

5.3 Result

The used of the torque meter and the DC motor as a brake to measure torque and eventually to measure power output is the best method to establish the performance of the water wheel. This is the first time as far as the writer knows that this method has been used to measure the performance of a water wheel. The effect of the downstream water level on the performance of the machine is also then investigated. The downstream water level is varied four times. The downstream water level is set by adjusting the weir to a certain height. Since the downstream water level varies as the rotational speed of the wheel changes, therefore, the best way to present the data is showing weir height instead of downstream water level height. The data is then presented in several graphs, and discussed below.

5.3.1 Power VS RPM

Power output as a function of the rotational speed is shown in Fig 5.11. In term of the trend of the graph, it shows that all variations of the downstream level provide a similar trend. This trend is following most of power output vs rotational speed of the water wheel. At low speeds, the power is low, then this increases as the speed increases and then after it reaches a certain

point, the power drops as the rotational speed increases. The power output from weir heights of 10 mm, 30 mm, and 50 mm almost coincides. However for the weir heights of 120 mm (this weir heights relates to a downstream water level between 149 mm-161 mm), the power output is much smaller than the previous weir heights. The weir height of 50 mm is related to the downstream water level of between 78-87 mm. This 78-87 mm downstream water level is the closest water level to the lowest point of the hub, which is 95 mm (see Fig 5.1). In the case of weir height of 10 mm and 30 mm, obviously, the downstream water level is lower than lowest point of the hub (downstream water levels with the weir height of 10 mm and 30 mm are in the range of 35-45 mm and 60-70 mm respectively). This data indicates that when the downstream water level is higher than lowest point of the hub, will result in a lower power output for the same rotational speed. In the case of when the downstream water level is lower than the lowest point of the hub, this will result in the same power output at any rotational speed. When the downstream water level is higher than the lowest point of the hub, the power output is low, because of the torque produced at a certain rotational speed is being reduced. This occurs due to the water downstream producing pressure to the blade as well as the hub. This eventually leads to a reducing of the contribution of the upstream pressure . This situation is similar to reducing head differences between upstream and downstream. The torque produced at certain speed is lower the other variations. The graph of torque as a function of the rotational speed is shown in Fig 5.12. From this figure, it is very obvious that the torque produced at any rotational speed in the case of the downstream water level being higher than the lowest point of the hub is lower than other variations. This situation eventually leads to a lower power output. The torque produced from the wheel when the downstream water level is lower than the lowest point of the hub remains the same at the same rotational speed. The lower torque which eventually leads to a lower power output when the downstream water level is higher than the lowest point of the hub because some of the torque produced is opposed by the pressure of the water from downstream which acts on the hub of the machine. In the case of the weir height of 120 mm at the speed of lower than 13 rpm on the Fig 5.12, the torque drops. This is because of the reducing upstream water level. Maintaining a certain water level at low speed is very difficult to achieve, it could cause an overflow of water from the flume. For this reason, the lower upstream water level can be adjusted and in this case is lower than the others, which eventually leads to a lower torque as can be seen from Fig 5.12 on speeds of lower than 13 rpm.

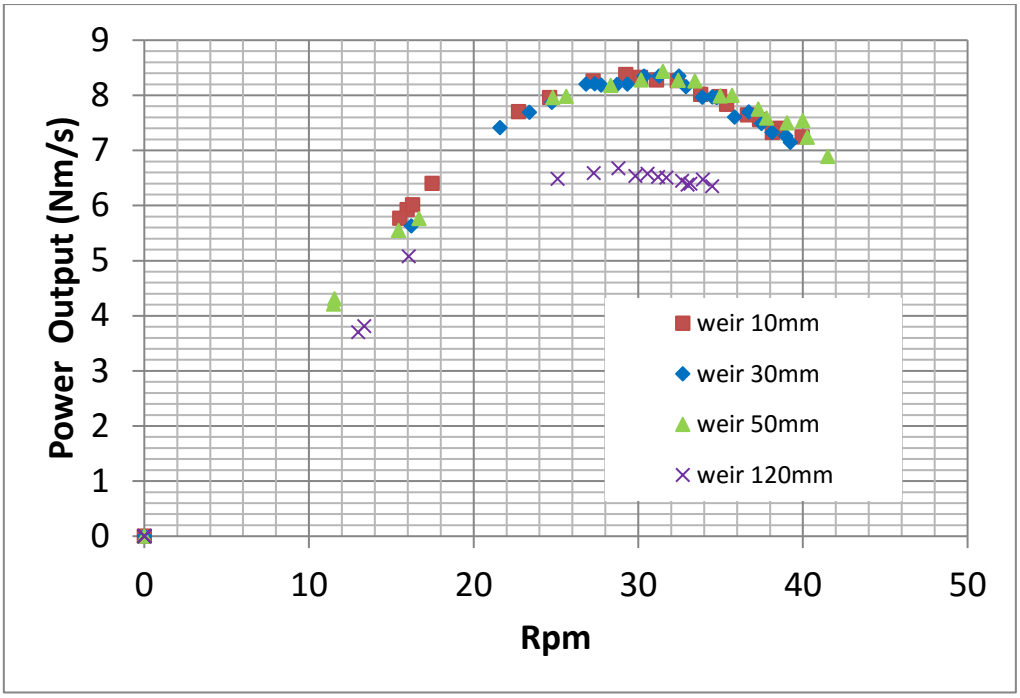

Figure 5.11: power output as function of rotational speed in the case of outer diameter 490 mm and hub diameter of 350 mm

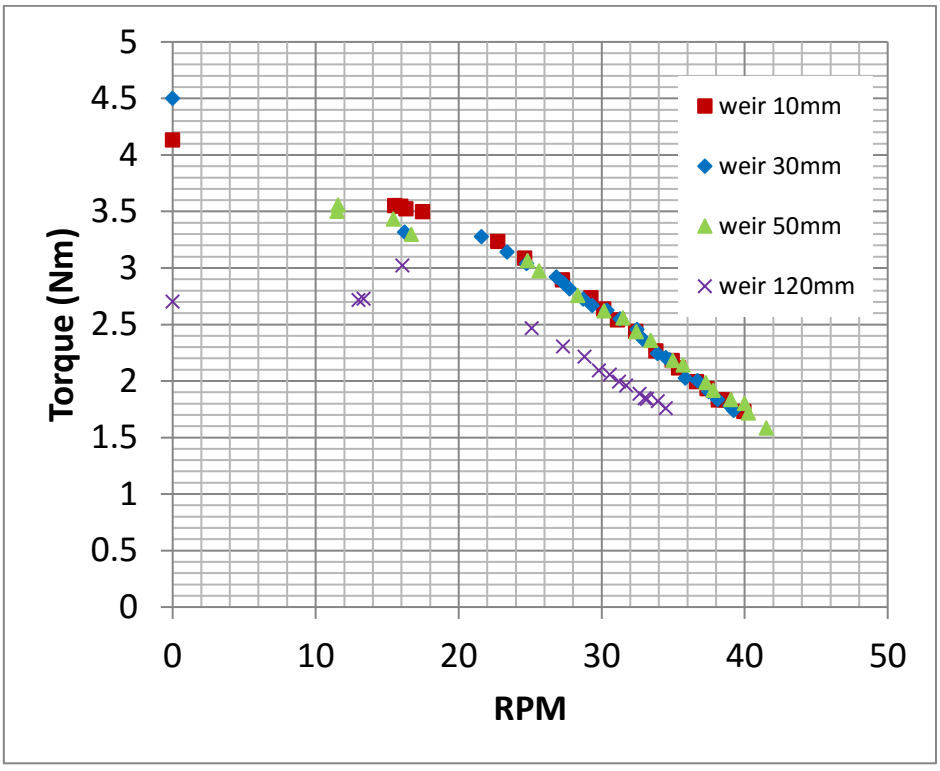

Figure 5.12: Torque as function of the rotational speed in the case of outer diameter 490 mm and hub diameter of 350 mm

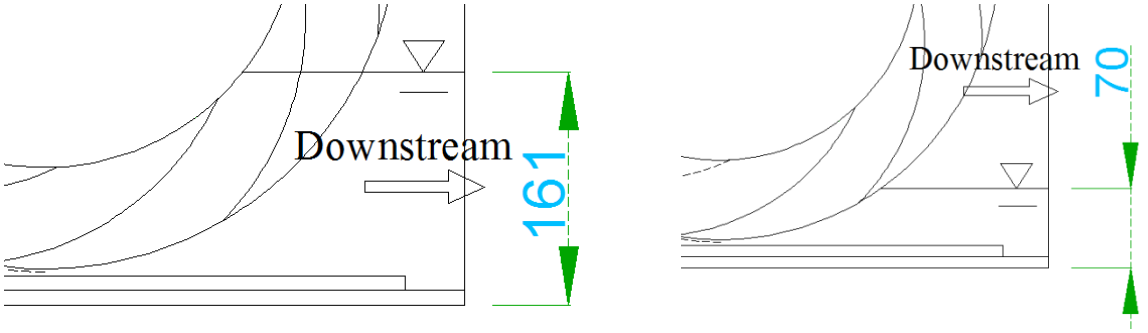

Figure 5.13: Situation on the downstream water level of 161 mm (weir of 120 mm) and 70 mm (weir of 30 mm)

5.3.2 Efficiency excluding leakage

The graph of efficiency excluding leakage is presented in Fig 5.14. In the case of a weir height of 50 mm, this shows the highest efficiency in comparison to other weir height setting. Weir heights of 30 mm and 120 mm show almost similar efficiency. A weir height of 10 mm provides the lowest value amongst the others. A weir heights of 50 mm provides the highest efficiency in comparison to others weir heights (recall this weir height is related to the downstream water level which is the closest to the lowest point of the hub). More over from Fig 5.11 and 5.12, a weir height of 50 mm provides larger values of power output as well as torque. The graph from Fig 5.11, 5.12 and 5.13 shows that the wheel with the downstream water level closest to the lowest point of the hub will give the best performance, as the power and the torque is at the maximum value, and the efficiency is the highest amongst the other weir height variations. In addition, in the case of the weir height of 10 mm, the power output and the torque provide higher values, however, the efficiency is the lowest amongst the other weir height as can be seen from Fig 5.14. Fig 5.14 shows that the weir heights of 10 mm and 30 mm give lower efficiency. This is because of the denominator of the equation to define the efficiency is larger. As the power input becomes higher, the downstream water level become lower. In the case of the weir height of 120 mm, the efficiency is also lower than the efficiency value of the weir height of 50 mm, this is due to downstream water level reducing some of the power output from the water wheel, which has been explained at the previous sub section 5.3.1.

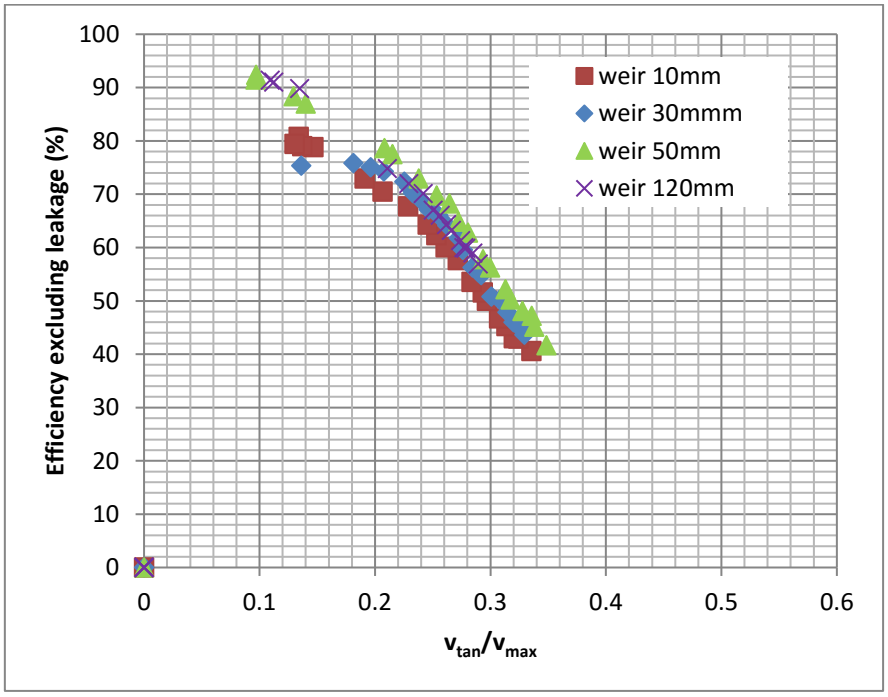

Figure 5.14: Efficiency excluding leakage vs non dimensionalized tangential velocity at various weir heights

5.3.3 Power vs Torque

Fig 5.15 shows the graph of power vs torque. The graph shows that the power vs torque coincides with the results from the weir height from 10 mm, 30 mm and 50 mm. Whereas in case of weir height of 120 mm, the power output is smaller than the other weirs height setting. In the case of weir height of 120 mm, the power output is smaller than the others, because the power is reduced the downstream pressure. This graph agrees with the efficiency graph as shown in Fig 5.14. The trend of power vs torque is that the power keeps increasing as the torque increases, and then after reach maximum power output, the power will decrease as the torque increases.

However from the experiment result, especially in the case of weir height of 120 mm, after torque of 3.02 Nm with the power of 5.08 Nm/s, the torque is reduced. This is because of the downstream water level is decreased. It is very difficult to maintain the upstream water level, especially at high torque and low speed, because it is very easy for the flume to over flow.

The reducing value of the torque in the case of a weir height 120 mm, is because of the lower upstream water level.

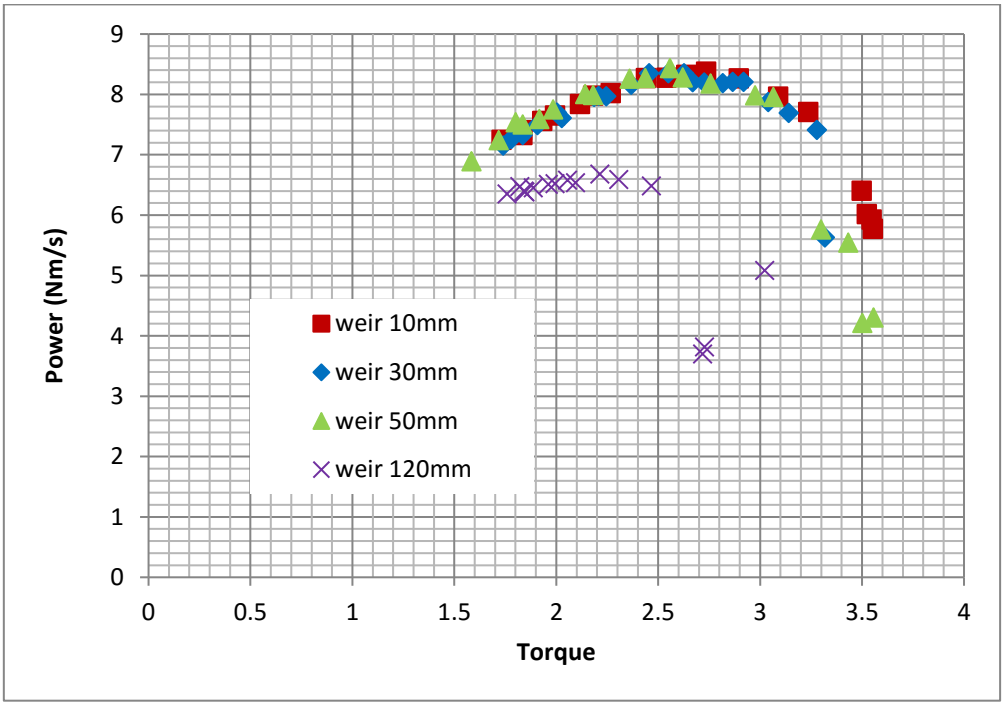

Figure 5.15: Power vs Torque at various weir high

5.4 Theoretical Power Output for turbine wheel

The mechanism of power output from a water wheel that has straight blades and include a lower shroud has been discussed in subchapter 2.5.2. Theoretical analysis of the pressure distribution on the blade indicates that the lower shroud means that the turbine wheel does not use the same operating machine principle as a gravitational machine. The machine still works with the concept of a hydrostatic pressure difference. A machine with curved blades such as the turbine wheel, the power production concept is also similar to the straight blade water wheel as described in subchapter 2.5.2. Consider a blade at Fig 5.16, projection of a curved blade on the vertical line is in the form of dotted lines a-b. Dotted line a-b is the surface where the hydrostatic pressure works on the wheel. This hydraustatic pressure creates

force on the a-b surface which which produces power eventually. Further the power analysis on the turbine wheel which has a curved blade can be assumed as the same power analysis as the straight blade.

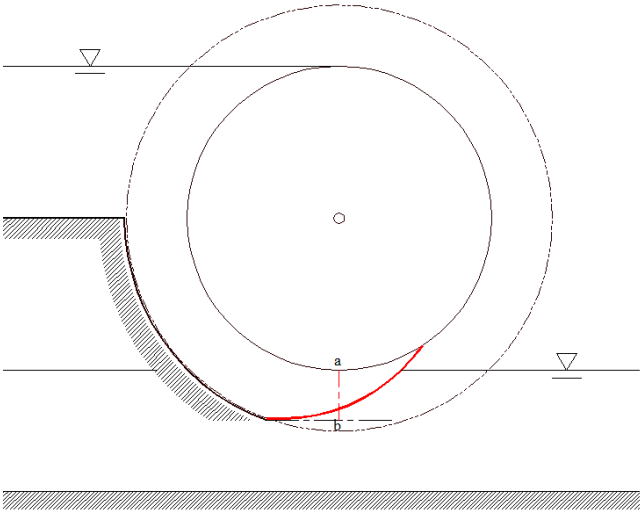

Figure 5.16: A curved blade on the turbine wheel

An explanation detailing the power output produced by the turbine wheel is detailed in the following discussion. Power output is the result of the pressure that acts at the blade in both upstream and downstream side as shown in Fig 5.17 Whereas the losses are due to turbulence losses.

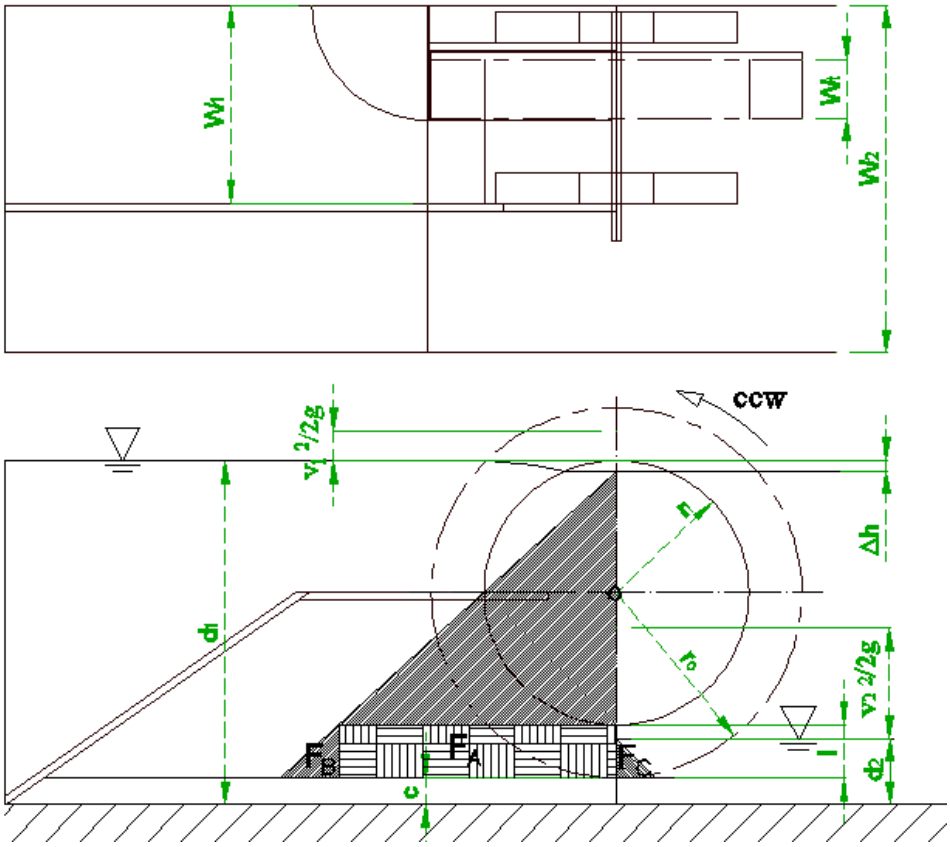

Figure 5.17: Blade force pressure component

The force distribution on the machine is shown in the Fig 5.17. The force that contributes to the power output is distributed as shown by F_A, F_B and F_C. The force distribution on the top part of F_A has no influence on the power production, because this force acts on the hub which acts as a weir and the hub just gives a reaction force. Basically the analysis is similar to subsection 2.4.2.1. However, it is repeated in this subsection.

F_A is the force that acts on the blade from upstream, which is calculated as

$$F_A = \rho\, g\, (d_1 - c - \Delta h - l)\, l\, w_t \qquad 5.4$$

F_B is also the force from upstream which can be calculated as

$$F_B = \frac{\rho\, g}{2}\, w_t\, l^2 \qquad 5.5$$

F_c is the force that acts from downstream, calculated as

$$F_c = \frac{\rho\, g}{2}\, w_t\, (d_2 - c)^2 \qquad 5.6$$

The force that acts from upstream creates torque with a counter clock wise (CCW) direction.

$$T_A = F_A R_{mean} \qquad 5.7$$

R_{mean} is the mean radius of the acting force

$$R_{mean} = \frac{r_0 + r_i}{2} \qquad 5.8$$

T_B is the torque because of the F_B

$$T_B = F_B R_b \qquad 5.9$$

R_b is calculated as

$$R_b = r_i + \frac{2}{3} l \qquad 5.10$$

T_c is the torque that is formed by force F_c which rotates clock wise (CW)

$$T_c = F_c R_c \qquad 5.11$$

R_c is the centre of F_c act, and calculated as

$$R_c = r_o - \frac{1}{3}(d_2 - c) \qquad 5.12$$

Thus total torque at o is calculated as

$$T = T_A + T_B - T_c \qquad 5.13$$

As ω is angular speed of the water wheel, therefore power output is formulated as

$$P_{out} = T\omega \qquad 5.14$$

$$P_{out} = \left((\rho\, g\, (d_1 - c - \Delta h - l)\, l\, w_t)\left(\frac{r_0 + r_i}{2}\right) + \left(\frac{\rho\, g}{2}\, w_t\, l^2\right)\left(r_i + \frac{2}{3}l\right) - \left(\frac{\rho\, g}{2}\, w_t\, (d_2 - c)^2\right)\left(r_o - \frac{1}{3}(d_2 - c)\right)\right)\omega \quad 5.15$$

Losses

In the subchapter 4.6.2 the losses that occur within the water wheel were briefly discussed. The possibility of losses stemming from the hydraulic head drop, turbulence and elevation losses (losses from water that is trapped within the cell) when the blade exits the downstream surface has been discussed. Linton proposed a theory of losses even though the results obtained between the theory and the experimental results were not close. It is very difficult to categorize and to quantify the losses as mentioned and indicated in subchapter 4.6.2. Therefore it is very difficult to develop a theory that can estimate the losses. However, all of these losses can be considered as a result of the turbulence caused by the interaction between the water and the water wheel. Thus, all the losses incurred are represented as turbulent losses. Turbulent power losses are calculated as $P_{tr} = \frac{1}{2} Cd\, \rho\, {v_t}^3\, l\, w_t$. where Cd is the empirical losses coefficient.

Efficiency

The efficiency of this machine can be calculated as

$$\eta = \frac{P_{out} - P_{tr}}{P_{input}} \quad 5.17$$

Graph plotting

A graph showing a comparison between the measured power output and the theoretical power output is shown in Fig 5.18. Whereas the efficiency curve is presented in Fig 5.19. The graph was plotted based on the *Cd* (turbulence coefficient) of 3.8. In addition, a torque comparison between the experimental and theoretical results is presented in Fig 5.20. All graphs show a good agreement between the theoretical and the actual data for either the power curve, the efficiency or the torque curve.

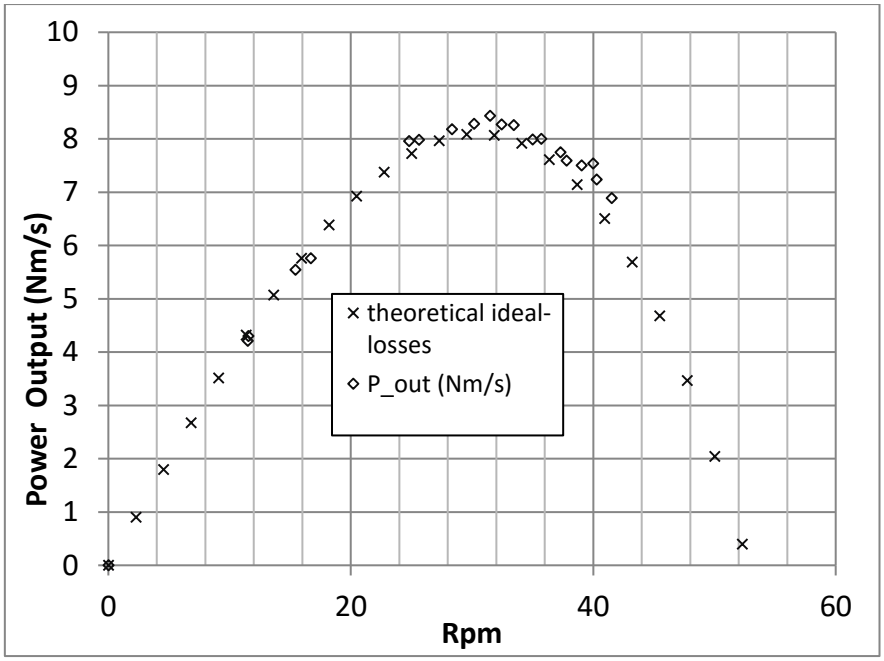

Figure 5.18: Comparison of measured power with theory in the case of downstream water level 78-87 mm

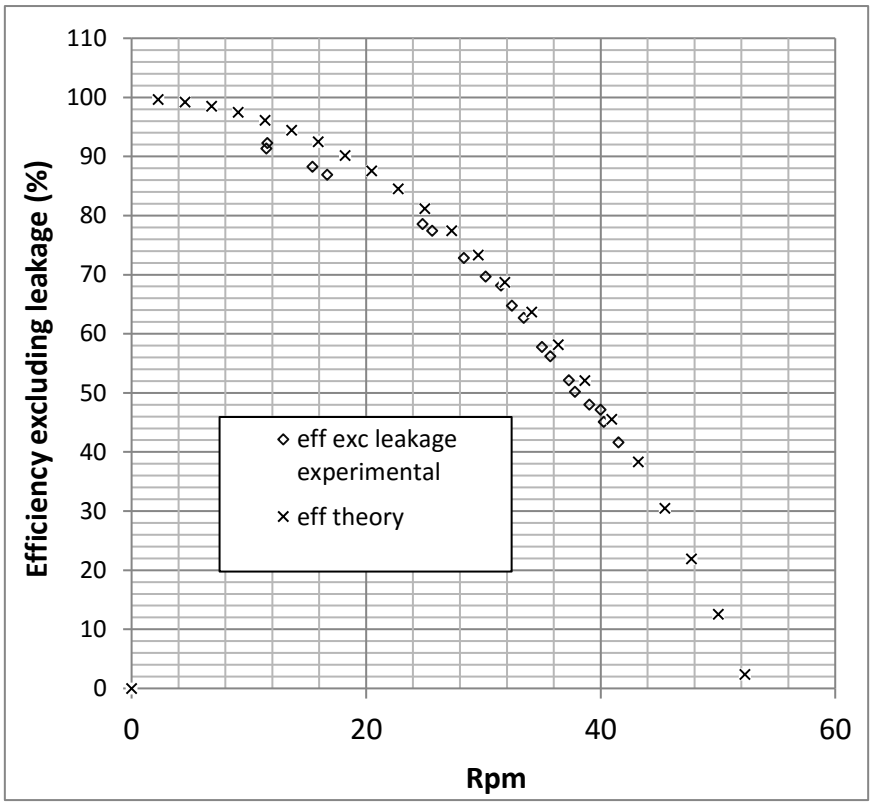

Figure 5.19: Comparison of measured efficiency excluding leakage with theory in the case of downstream water level 78-87 mm

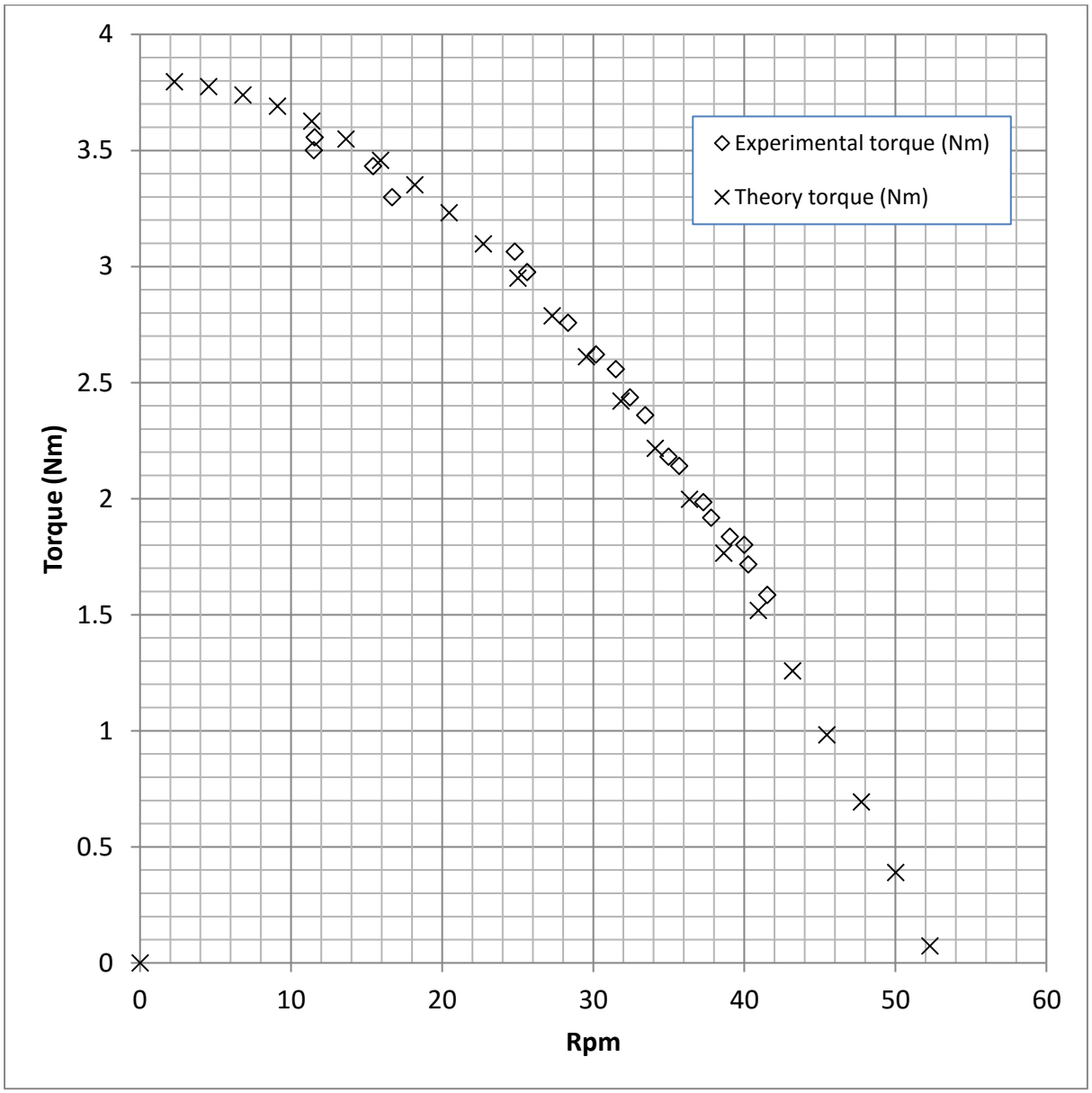

Figure 5.20: Comparison showing experimental torque and theoretical torque results with the downstream water level 78-87 mm

Fig 5.21 shows a comparison between the experimental data and the theoretical data of torque vs power. The data shows that the data match well, and supports the proposed theory.

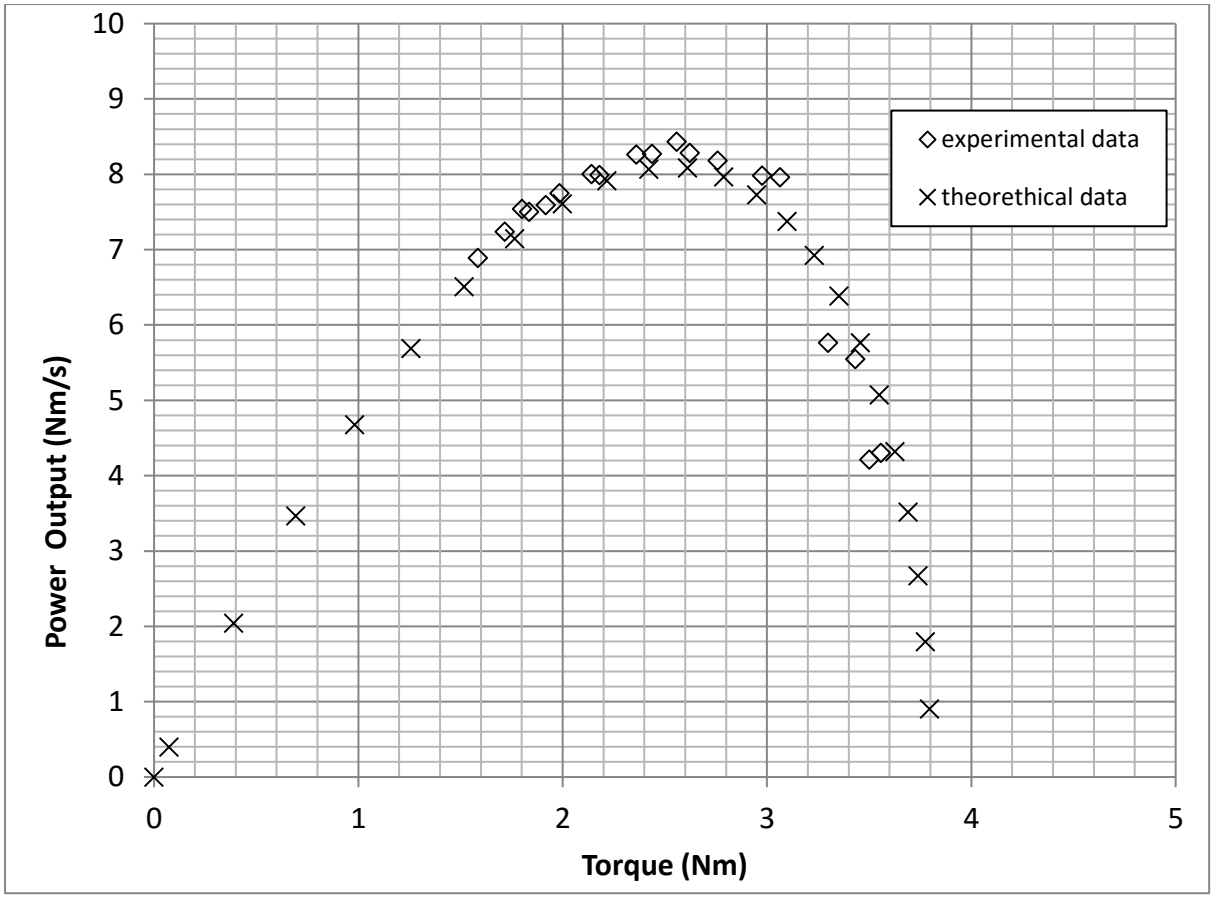

Figure 5.21: Comparison of experimental data and theoretical data for torque vs power with a downstream water level 78-87 mm

CHAPTER 6

DISCUSSION

The performance of the turbine wheel has been tested. From these tests, a theory for this machine has been proposed. In the next section, the comparison of these test results against the results submitted by James senior and Nick linton are discussed. In addition the real scale power output and flow rate are presented in this chapter.

6.1 Comparison between the turbine wheel and previous research

Fig 6.1 shows a comparison of the efficiencies of the turbine wheel, the RHPM water wheel developed by Senior and the HPM developed by Linton. Absis axis is the tangential velocity of the wheel which is non-dimensionlized with maximum velocity v_{max}. The maximum velocity v_{max} refer to equation 3.11. The graph shows that the methodology of power output measurement for this research (turbine wheel) is much improved than previous research, especially at low speed. The evidence for this claim is that the efficiency of the current turbine wheel keeps increasing as the speed reduces. In the case of the Linton experiment, the efficiency slightly decreases as speed reduces. This trend continuous in the case of Senior's machine, where the efficiency of his machine decays at the speed v/v_{max} of lower than 0.18. This problem can be explained due to sliding between the Prony wheel and the rope/belt, which mostly occurs at low speed/high torque. This is the reason the use of the electricity method measurement is prefer to the Prony brake method as has been explained in subsection 4.1. The graph also shows that the turbine wheel has a higher efficiency at higher speed comparison to both the Senior and Linton machines. As the speed increases, the efficiency drops steeply in both the Senior and Linton machine. Whereas in the case of the turbine wheel, the rate of efficiency drop is lower. The preliminary test which used the Prony brake measurement method has shown that on the range of v_{tan}/v_{max}=0.32, the machine shows a maximum power output of 2.07 W. The efficiency in this speed range was 70%. The result from this third machine seems to show consistency with the preliminary test. The third machine shows the efficiency at the maximum power output is 68.3%. The maximum power output is 8.43 Nm/s (refer to Fig 5.18) which is achieved at v_{tan}/v_{max}= 0.26 which correlates to

a rotational speed of n 31.5 rpm. The maximum power output which is achieved at the efficiency of 68.2% is correlated to the flow rate of 3.9 l/s.

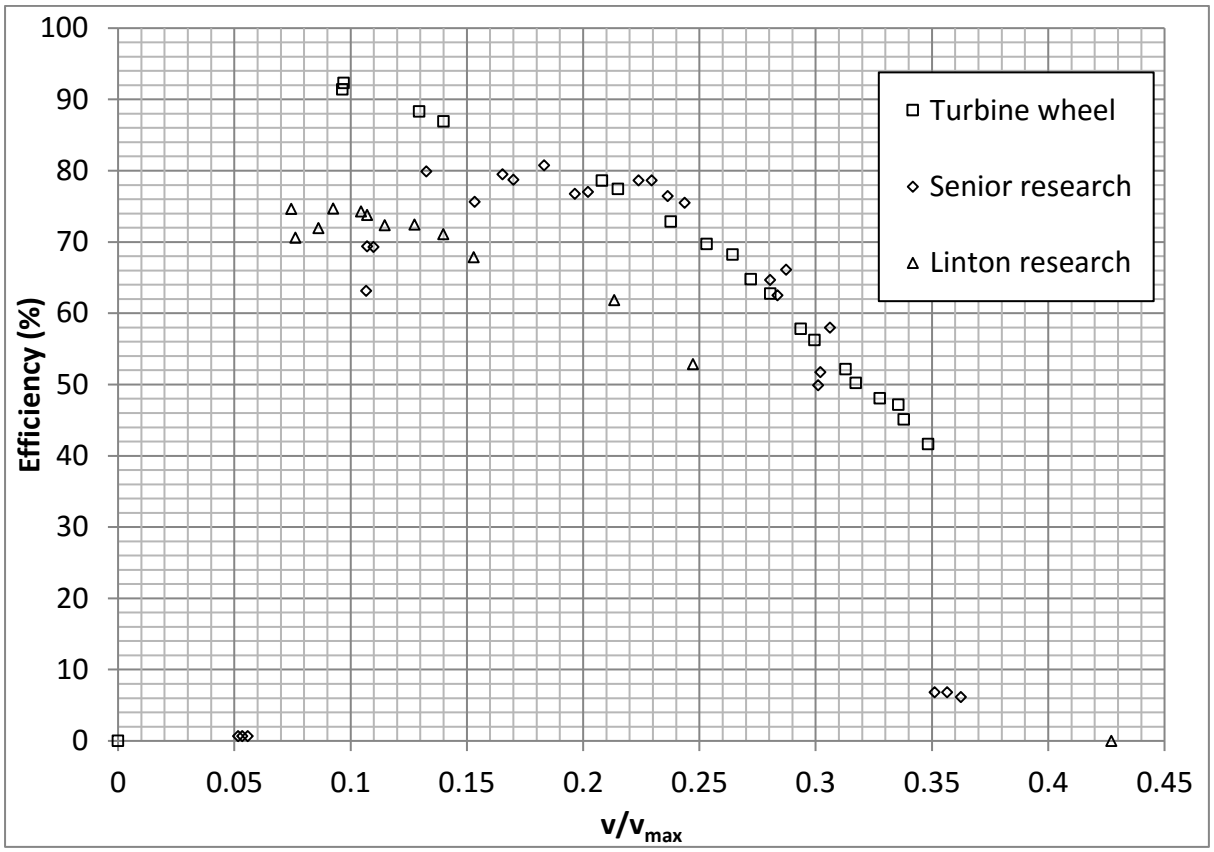

Figure 6.1: Comparison between Turbine wheel, RHPM (Senior) and HPM (Linton)

6.2 Scalling up of the turbine wheel

Froude scalling is used to predict the flow rate and power output of the real machine. Data from the third machine is used as a reference and will be considered in any future scaling up of this machine. In the case of the third model, the maximum power output P_{max} was 8.43 Nm/s, in which the rotational speed at this power output n was 31.49 rpm, where the efficiency excluding leakage η_{wl} was 68.3% and the flow rate at max power output Q_{max} was 3.9 l/s. This data and the dimensions of the third machine are then used as a reference to calculate the performance of the full scale machine by using Froude scaling law. The Froude

scalling law as explained in sub section 4.3 is also applicable in this calculation. The upscalling is undertaken from 2.5 m head up to 5 m head difference as provided in table 6.1. A fuller explanation on the Froude scaling approach is further detailed in Appendix B. In addition, the matching result between the theoretical approach and the Froude scaling is also presented in appendix B. This is the power curve presented in the case of a 2.5m and a 5 m hub.

Table 6.1: scaled estimation of the full scale turbine wheel.

Head (m)	**Scale**	**Q_{max} (m^3/s per m width)**	**P_{max} (kW per m width)**
2.5	7.14	1.85	28.74
3	8.57	2.43	45.33
3.5	10.00	3.07	66.65
4	11.43	3.75	93.06
4.5	12.86	4.47	124.92
5	14.29	5.23	162.56

CHAPTER 7

CONCLUSSION AND RECOMENDATIONS

7.1 Conclusion

- The existence of the upper shroud gives a positive contribution, in which it gives a higher efficiency result incomparison to a turbine wheel without an upper shroud.
  The existence of the upper shroud significantly prevents losses due to water slamming, whereas without the upper shroud, water slamming losses make the power output smaller.
- The best ratio between the outer diameter to the hub diameter is 1.34 which almost matches the original machine ($\frac{D_{out}}{Hub}$ 1.4).
- No significant effect was noted with varying blade numbers, with six or twelve blades showing the same power output.
  The blade that has the most significant effect in term of contributing to the power output is the last blade which comes into direct contact with the downstream water surface. Therefore the number of blades does not play a significant role in terms of power output.
- Guide vanes do not give any obvious positive contribution for $\frac{D_{out}}{Hub} = 1.34$.
  As the speed of the incoming water is slow (and this machine also designed for low flow rate) therefore the losses that might occur due to the 90° turn is not significant. This is the reason why the guide vane fitted to the incoming water shows no differences in comparison with no guide vane fitted.
- In order to achieve the best performance of the turbine wheel, the downstream water level needs to be adjusted to the lowest point of the hub.
- The turbine wheel is considered as a machine which works based on the hydrostatic pressure difference between upstream and downstream, where the losses shown merely come from turbulence with *Cd* (turbulence coefficient) of 3.8
- The experiment shows that the turbine wheel achieves maximum power output at the speed of v_{tan}/v_{max}= 0.27, with an efficiency at the maximum power output of 68.3%.

- The maximum power output for head differences of 2.5m is 28.74 kW per m width with the flow rate of 1.85 m^3/s per m width.
- The maximum power output for a head differences of 5m is 162.56 kW per m width with the flow rate of 5.23 m^3/s per m width.

7.2 Recommendations

- A study on the effect of the blade width still needs to be undertaken to find out the optimum blade width at a certain hub diameter of the turbine wheel.
- The effect of reducing the ratio between the outer diameter to the hub diameter needs to be investigated as to whether the ratio between the outer diameters to the hub diameter of 1.34 (standard size) is the best value. It is possible that a smaller value than 1.34 will give a better result.
- At the present time the rotational speed for maximum power output of the turbine wheel is 0.5 rps for a hub diameter of 350 mm. This rotational speed obviously still needs to be increased for electricity generation. In order to make it competitive in term of economics, a cheap power transmission system which can increase the rotational speed of an electric generator is required.

APPENDIX A

The output torque from the machine should be calculated in order to determine the specification of the torque meter. In the Fig A.1 it is shown where the cell fills up with water. Assuming that the water is in the region of KLMN. This assumption is obviously "safe" in order to determine amount of water in the cell, eventhough the amount of water inside the cell might be less than the area as covered by KLMN.

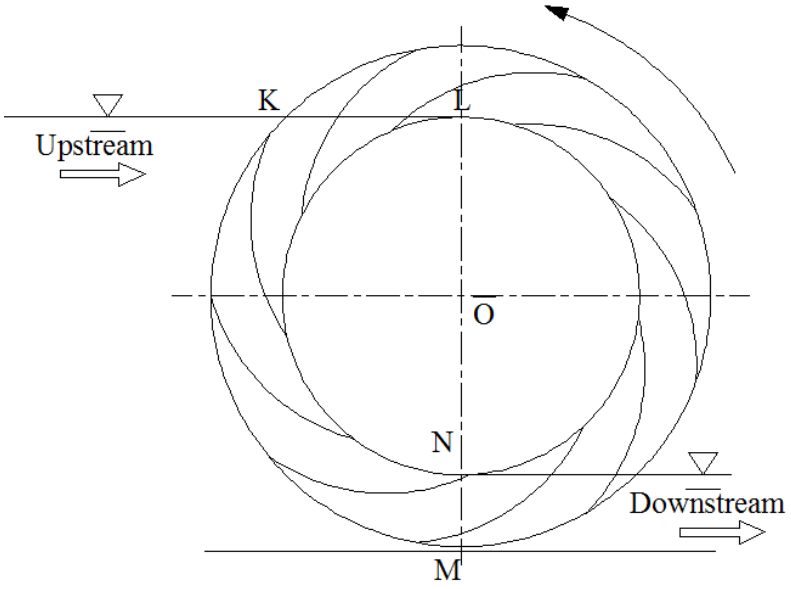

Figure A.1: the existence of the water on the water wheel

The area KLMN could be represented by hatched area as shown in Fig A.1

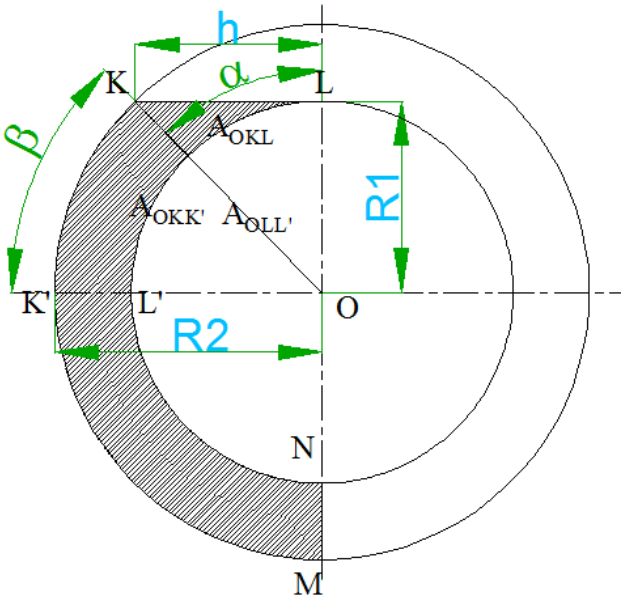

Figure A.2: hatched area where water fills in the cell

Shaded area actually is the sum of the extents of the KLK'L' and K'L'MN segment. K'L'MN area can easily be calculated by

$$A_{\mathrm{K'L'MN}} = \frac{90}{360}\,\pi\left({R_2}^2 - {R_1}^2\right) \qquad 1$$

$$A_{\mathrm{K'L'MN}} = \frac{90}{360}\,\pi\,(0.245^2 - 0.175^2) \qquad 2$$

$$A_{\mathrm{K'L'MN}} = 0.02m^2$$

Area KLK'L' $A_{KLK'L'}$ can be calculated by

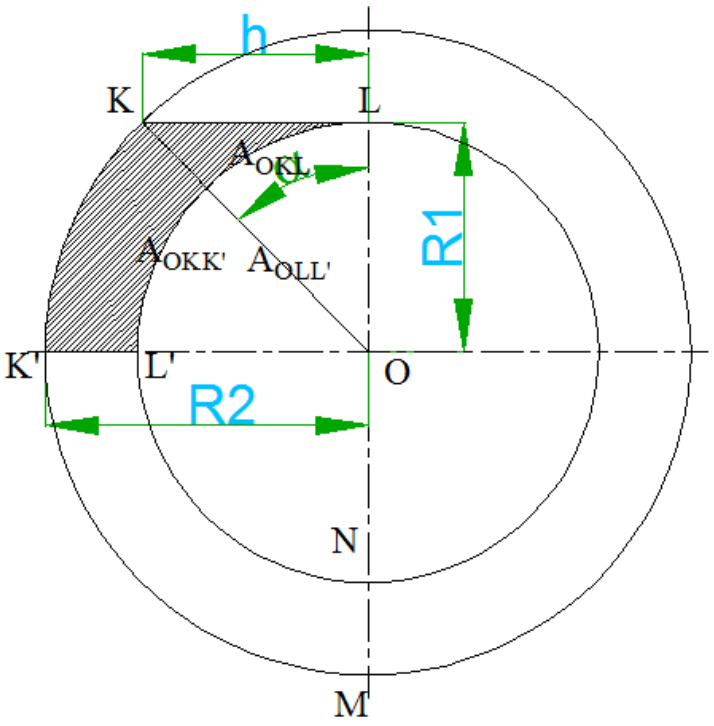

Figure A.3: segment KLK'L' on the cell

$$A_{KLK'L'} = A_{OKL} + A_{OKK'} - A_{OLL'} \quad (3)$$

$$h = \sqrt{{R_2}^2 - {R_1}^2} \quad (4)$$

$$A_{OKL} = \frac{1}{2} h \,.\, R_1 = \frac{1}{2} R_1 \left(\sqrt{{R_2}^2 - {R_1}^2}\right) \quad (5)$$

$$A_{OKK'} = \frac{\beta}{360} \pi \,.\, {R_2}^2 = \frac{\beta}{360} \,.\, \pi \,.\, {R_2}^2 \quad (6)$$

Where

$$\beta = 90 - \alpha \quad (7)$$

And

$$\alpha = \cos^{-1} \frac{R_1}{R_2} \quad (8)$$

Substitute β and α

$$A_{OKK'} = \left(\frac{90-\alpha}{360}\right) \pi \, . {R_2}^2 = \left(\frac{90-\cos^{-1}\frac{R_1}{R_2}}{360}\right) \pi \, . {R_2}^2 \quad 9$$

$$A_{OLL'} = \frac{1}{4}\pi \, . {R_1}^2 \quad 10$$

$$A_{KLK'L'} = \frac{1}{2} R_1 \left(\sqrt{{R_2}^2 - {R_1}^2}\right) + \left(\frac{90-\cos^{-1}\frac{R_1}{R_2}}{360}\right) \pi \, . {R_2}^2 - \frac{1}{4}\pi \, . {R_1}^2 \quad 11$$

$$A_{KLK'L'} = \frac{1}{2}\, 0.175 \left(\sqrt{0.245^2 - 0.175^2}\right) + \left(\frac{90 - \cos^{-1}\frac{0.175}{0.245}}{360}\right) \pi \, . 0.245^2 - \frac{1}{4}\pi \, . 0.175^2$$

$$A_{KLK'L'} = 0.01`m^2$$

Total area cell filled with water to produce maximum torque is

$$A_{KLMN} = A_{\mathrm{K'L'MN}} + A_{KLK'L'} \quad 12$$

$$A_{KLMN} = 0.02m^2 + 0.01m^2$$

$$A_{KLMN} = 0.03m^2$$

Volume of the water is calculated as

$$V_{water} = A_{KLMN}\, W_t \quad 13$$

$$V_{water} = 0.03m^2 \;\; 0.08m$$

$$V_{water} = 2.43\; 10^{-3} m^3$$

The weight of the water inside the cell is

$$W_{water} = V_{water}\ \rho\ g \quad (14)$$

$$W_{water} = 2.43\ 10^{-3} m^3\ \rho\ g$$

$$W_{water} = 2.43\ 10^{-3} m^3\ 999\ \frac{kg}{m^3}\ 9.81 m/s^2$$

$$W_{water} = 23.8N$$

So the max torque is calculated as

$$T_{max} = W_{water}\ R_{mean} \quad (15)$$

$$T_{max} = 23.8N\ \ 0.21m$$

$$T_{max} = 4.99\ Nm$$

In this experiment, the torque meter that was used is an AEP transducer, with a maximum torque measurement of 5 Nm.

APPENDIX B

Using of Froude scaling to predict power output of the upscaling water wheel.

The basic relevant parameters needed for any dimensional analysis of the hydraulic model, includes The flow properties which consist of velocity *v* (m/s) and the pressure difference ΔP (N/m^2), machine geometry which is characteristic length l (m) and fluid properties which consist of fluid density ρ (kg/m^3), acceleration of gravity g (m/s^2), and viscosity of the fluid μ (Ns/m^2). In practice, model tests are performed under controlled flow conditions. The pressure difference ΔP may usually be controlled. This enables ΔP to be treated as a dependent parameter, therefore the independent parameters are fluid density ρ, velocity *v*, characteristic length *D*, acceleration of gravity *g*, and viscosity of the fluid μ (Chanson 2001). Taking into account all basic parameters, dimensional analysis yields:

$$\Delta P = f(\rho, v, l, g, \mu)$$

It is now six basic parameters and the dimensions of them can be grouped into three categories which are: mass (M), length (L) and time (T). The Buckingham Π theorem implies that the quantities can be grouped into three (3 =6-3) independent dimensionless parameters:

$$\{ML^{-1}T^{-2}\} = f[\{ML^{-3}\};\ \{LT^{-1}\};\ \{L\};\ \{LT^{-2}\};\ \{ML^{-1}T^{-1}\}]$$

Choose repeating parameter ρ,*v*,*l*, then

$$\pi_1 = \rho^a v^b l^c \Delta P = \{ML^{-3}\}^a\ \{LT^{-1}\}^b\ \{L\}^c\ \{ML^{-1}T^{-2}\} = M^0L^0T^0$$

$M \implies a + 1 = 0 \implies a = -1$

$L \implies -3a + b + c - 1 = 0 \implies b + c = -2$

$T \implies -b - 2 = 0 \implies b = -2$

$b + c = -2 \implies -2 + c = -2 \implies c = 0$

$$\pi_1 = \rho^{-1} v^{-2} l^0 \Delta P = \frac{\Delta P}{\rho\, v^2}$$

$$\pi_2 = \rho^{d} v^{e} l^{f} g = \{ML^{-3}\}^{d}\,\{LT^{-1}\}^{e}\,\{L\}^{f}\,\{LT^{-2}\} = M^0 L^0 T^0$$

$M \implies d = 0$

$L \implies -3d + e + f + 1 = 0 \implies e + f = -1$

$T \implies -e - 2 = 0 \implies e = -2$

$e + f = -1 \implies -2 + f = -1 \implies f = 1$

$$\pi_2 = \rho^0 v^{-2} l^1 g = \frac{lg}{v^2}$$

$$\pi_3 = \rho^{g} v^{h} l^{i} \mu = \{ML^{-3}\}^{g}\,\{LT^{-1}\}^{h}\,\{L\}^{i}\,\{ML^{-1}T^{-1}\} = M^0 L^0 T^0$$

$M \implies g + 1 = 0 \implies g = -1$

$L \implies -3g + h + i - 1 = 0 \implies h + i = -2$

$T \implies -h - 1 = 0 \implies h = -1$

$h + i = -2 \implies -1 + i = -2 \implies i = -1$

$$\pi_3 = \rho^{-1} v^{-1} l^{-1} \mu = \frac{\mu}{\rho\, v\, l}$$

$$\pi_1 = f[\pi_2\,;\,\pi_3]$$

$$\frac{\Delta P}{\rho\, v^2} = f\left[\frac{lg}{v^2}\,;\,\frac{\mu}{\rho\, v\, l}\right]$$

Rearrange equation above result in

$$\frac{\rho\, v^2}{\Delta P} = f\left[\frac{v}{\sqrt{lg}}\,;\,\frac{\rho\, v\, l}{\mu}\right]$$

$$Eu = f[Fr\,;\,Re]$$

Result in three groups of dimensionless parameter, in which consist of Euler number *Eu*, Froude number *Fr*, and Reynolds number *Re*. *Eu* is the Euler number, proportional to the ratio of inertial force to pressure force. The Froude number *Fr*, characterizing the ratio of the inertial force to gravity force. The last dimensionless parameter is the Reynolds number *Re* which characterizes the ratio of inertial force to viscous force.

In most cases, only the most dominant mechanism is modelled. In fully-enclosed flows (e.g. pipe flows), the pressure changes are basically related to the Reynolds number *Re*. Hence, Reynolds number scaling is used: i.e. the Reynolds number is the same in both model and prototype. The Euler number is used in practice for the scaling of models using air rather than water: e.g. hydraulic models in wind tunnels, or a manifold system with water flow which is scaled at a smaller size with an air flow system. In open free-surface flows (i.e. flows with a free surface/open channel flow), gravity effects are always important and a Froude number is always significant and Froude number modelling is used (i.e. Fr_m=Fr_p) (Chanson 2001). As the water wheel is operated on the free surface/open channel flow, hence predicting power output of the prototype will be derived based on the Froude similarity.

For Froude Number Similarity,

$$Fr_m = Fr_p$$

$$\left[\frac{v}{\sqrt{l\, g}}\right]_m = \left[\frac{v}{\sqrt{l\, g}}\right]_p$$

Since gravitational acceleration *g* is constant, therefore the velocity ratio can be defined as:

$$\left[\frac{v}{\sqrt{l}}\right]_m = \left[\frac{v}{\sqrt{l}}\right]_p$$

As diameter of the water *D* wheel is length unit, therefore the velocity ratio can be defined as:

$$v_r = \frac{v_p}{v_m} = \sqrt{\frac{D_p}{D_m}} = \sqrt{l_r}$$

Mass ratio can be defined as

$$m_r = \frac{m_p}{m_m} = \frac{V_p\, g}{V_m\, g} = \frac{V_p}{V_m} = \frac{{l_p}^3}{{l_m}^3} = \left(\frac{l_p}{l_m}\right)^3 = {l_r}^3$$

Time ratio can be defined as

$$T_r = \frac{T_p}{T_m} = \frac{l_p/V_p}{l_m/V_m} = \frac{l_r}{\sqrt{l_r}} = \sqrt{l_r}$$

Acceleration ratio can be defined as

$$a_r = \frac{a_p}{a_m} = \frac{V_p/T_p}{V_m/T_m} = \frac{v_r}{T_r} = \frac{\sqrt{l_r}}{\sqrt{l_r}} = 1$$

Force ratio can be defined as

$$F_r = \frac{F_p}{F_m} = \frac{m_p\, a_p}{m_m\, a_m} = m_r\, a_r = {l_r}^3$$

Power ratio can be derived from dimensionless parameter above as

$$P_r = \frac{P_p}{P_m} = \frac{F_p\, v_p}{F_m\, v_m} = F_r\, V_r = {l_r}^3 \sqrt{l_r} = {l_r}^{3.5}$$

$$P_r = \frac{P_p}{P_m} = {l_r}^{3.5} = \left(\frac{D_p}{D_m}\right)^{3.5}$$

Comparison between Froude scaling methodology and theoretical approach

In addition, applying theory for upscaling machine also confirms the result. Fig 1 and 2 gives the plot for the upscaling machine from the theory mentioned in subchapter 2.5.2. Fig 1 shows the plotted result for the machine with a head of 5m (correlates to scaling ratio *lr* of

4.29), whereas Fig 2 shows the plotted result for the machine with a head of 2.5m (correlates to scaling ratio *lr* of 7.14). The graph in fig 1 shows that the maximum power output is 162kw/m width which is close to the Froude scaling result which gives 162.56 kw/m width. Fig 2 shows that the maximum power output is 28.09 kW/m width. This result also match to the Froude scaling result which gives 28.74 kW/m width.

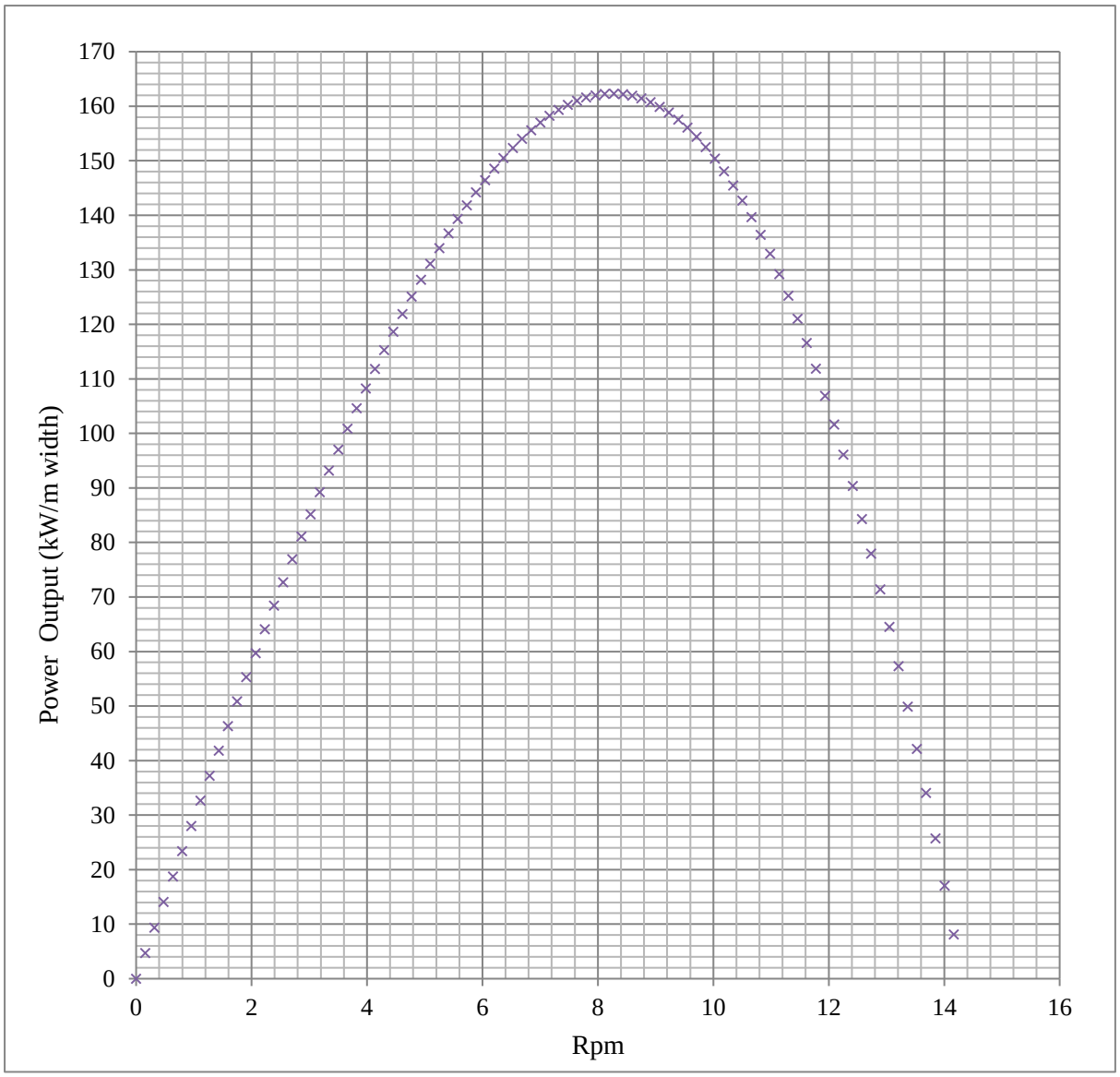

Figure B.1: Plotted power output vs rotational speed for upscaling in the case of hub 5m

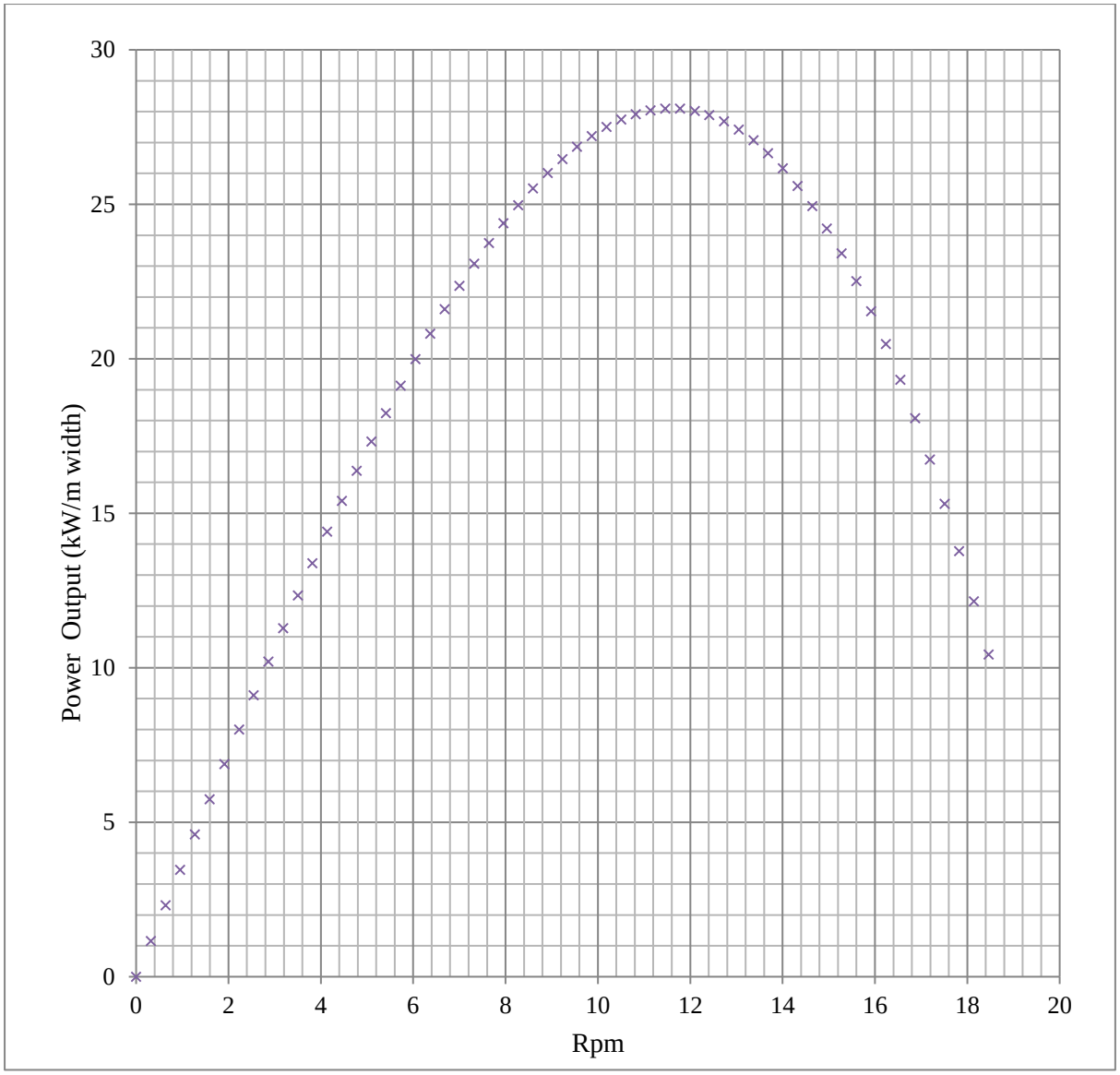

Figure B.2: plotted power output vs rotational speed for upscaling in the case of hub 2.5m

REFERENCES

Andritz vatech hydro, 2008. LOW HEAD HYDRO TURBINES. In *Small Hydro Power Schemes in the North West of England: Overcoming the Barriers*. Available at: http://www.engineering.lancs.ac.uk/lureg/nwhrm/project/Joule Centre conf 08/krompholz.pdf.

Atro, A., 2013. ANDRITZ Atro Hydrodynamic screws. Available at: http://grz.g.andritz.com/c/com2011/00/02/13/21383/1/1/0/325941156/oi-atro-hydrodynamic-screws-en.pdf.

Bozhinova, S. et al., 2012. Hydropower converters with head differences below 2.5m. In *Proceedings of the Institution of Civil Engineers*. pp. 1–12. Available at: http://dx.doi.org/10.1680/ener.11.00037.

Brada, K., 1999. Wasserkraftschnecke ermöglicht Stromerzeugung über Kleinkraftwerke [Hydraulic screw generates electricity from micro hydropower stations]. *Maschinenmarkt Würzburg*, 14, pp.52–56.

Brockhaus, F.A., 1903. Brockhaus Konversations-Lexicon. *chapter Wasserraeder*, 16.

Campbell, R.J., 2010. Small Hydro and Low-Head Hydro Power Technologies and Prospects. In *Congressional Research Service*. Available at: http://nepinstitute.org/get/CRS_Reports/CRS_Energy/Renewable_Fuels/Small_hydro_and_Low-head_hydro_power.pdf.

Chanson, H., 2001. *The Hydraulics of Open Channel Flow*, Butterworth Heinemann.

Chongqing Hydropower Equipment Co., L., 2016. S type Kaplan Turbine. Available at: http://www.cchpe.net/ProductInfo.aspx?get=4 [Accessed May 17, 2016].

Coastal Hydropower Corp., 2011. *Very Low Head (VLH) Turbine*, Available at: http://www.owa.ca/assets/files/presentations/FINALCoastalHydropower.pdf.

Dalley, S., 1993. Ancient Mesopotamian Gardens and the Identification of the Hanging Gardens of Babylon Resolved. *Garden History*, 21(1), pp.1–13. Available at: http://www.jstor.org/stable/1587050.

Dalley, S. & Oleson, J.P., 2003. Sennacherib, Archimedes, and the Water Screw: The Context of Invention in the Ancient World. *Technology and Culture*,, 44(1), pp.1–26.

Delabar, G., 1855. Beschreibung des Zuppinger'schenWasserrades.Polytechnisches. *Leipzig*, 185 (LXX), pp.249–253. Available at: http://dingler.culture.hu-berlin.de/article/pj185/ar185070.

Denny, M., 2004. The Effciency of Overshot and Undershot Waterwheels. *European Journal of Physics*, 25, pp.193–202.

Dive turbinen, 2016a. DIVE-Turbine. Available at: http://www.dive-turbine.de/pages/en/product.php?lang=EN [Accessed May 20, 2016].

Dive turbinen, 2016b. Hydro Power Plant Kroatien02. Available at: http://www.dive-turbine.de/pages/en/references/kroatien02.php?lang=DE [Accessed May 20, 2016].

Drachmann, A.G., 1958. The Screw of Archimedes. In *Actes du VIIIe Congrès International d'Histoire des Sciences*. Florence milan.

Eberhard, A. et al., 2011. *Africa's Power Infrastructure Investment, Integration, Efficiency*, Washington DC. Available at: http://www.ppiaf.org/sites/ppiaf.org/files/publication/Africas-Power-Infrastructure-2011.pdf.

Eternoo Machinery, 2016. Tubular trubine. Available at: http://www.eternoohydro.com/turbines/tublar-turbines.html [Accessed May 18, 2016].

European Communities, 2009. Research Priorities For Renewable Energy Technology by 2020 and beyond. In pp. 1–48. Available at: http://www.energy.eu/publications/a06.pdf.

Fairbairn, W., 1849. On Water -Wheels With Ventilated Buckets (Including Plates). In London, p. 18. Available at: http://www.icevirtuallibrary.com/content/article/10.1680/imotp.1849.24133.

Ferial, 2014. Sepuluh Tahun Mendatang, 6.300 MW PLTA Akan Dikembangkan. *Kementerian Energi dan Sumber Daya Mineral Indonesia*. Available at: http://ebtke.esdm.go.id/post/2014/11/27/727/sepuluh.tahun.mendatang.6.300.mw.plta.akan.dikembangkan. [Accessed May 13, 2015].

Fox, R.W., Donald, A.T.M. & Pritchard, P.J., 2003. *Introduction to Fluid Mechanics* 6th ed., John Wiley and Sons Inc.

Fraser, R. et al., 2007. VLH : Development of a new turbine for Very Low Head sites. Available at: http://lamh.gmc.ulaval.ca/fileadmin/docs/Publications_Recentes/VLH_A_New_Turbine_for_Very_Low_Head_Appliucations.pdf.

Gesthidro Recursos Hidroenergeticos, 2013. Hydroelectric Power Plants. Available at: http://www.gesthidro.pt/en/centrais-hidroelectricas-3.html.

Giesecke, J. & Monsonyi, E., 1998. Wasserkraft-Anlagen. In German: Springer.

Gupta, S.C., 2006. *Fluid Mechanics And Hydraulics Machine*, Dorling Kindersley. Available at: http://books.google.co.uk/books?id=9JMsyTymCgwC&pg=PA457&dq=performance+of+francis+turbine&hl=en&sa=X&ei=MvsIU9vSMMqK7AbUuIDoBQ&ved=0CDgQ6AEwAA#v=onepage&q=performance of francis turbine&f=false.

Hakim, L., 2013. Ekonomi Cina tumbuh 7.8% di 2012. Berharap tahun ini bisa lewati 8%. *Finance Roll*. Available at: Ekonomi Cina tumbuh 7.8% di 2012. Berharap tahun ini bisa lewati 8%.

Hydro, V., 2009. Harnessing the power of water with engineered reliability.

Hydropower Generation, 2016. Kaplan Turbine. Available at: http://mbm.net16.net/Model_Turbine_typ_Kaplan.html [Accessed June 7, 2016].

Institute Global Energy Network, 2013. Global Renewable Energy Resources Hydropower. Available

at: http://www.geni.org/globalenergy/library/renewable-energy-resources/hydropowerbig.shtml.

International Energy Agency, 2014. *Key World Energy Statistics*, Available at: http://www.iea.org/publications/freepublications/publication/keyworld2014.pdf.

International Hydropower Association, 2013. World installed hydropower capacity. Available at: http://www.hydropower.org/.

International Renewable Energy Agency (IRENA), 2012. *Renewable Energy Technologies: Cost Analysis Series*, Available at: https://www.irena.org/DocumentDownloads/Publications/RE_Technologies_Cost_Analysis-HYDROPOWER.pdf.

International River, 2008. The World Commission on Dams Framework - A Brief Introduction. Available at: http://www.internationalrivers.org/resources/the-world-commission-on-dams-framework-a-brief-introduction-2654 [Accessed May 25, 2015].

J. Gale, E. Höfler, A.B., 2010. COMPACT VERTICAL AXIAL TURBINE " SAXO ." In *Seminar on Hydropower Plants*. Vienna. Available at: https://www.researchgate.net/publication/280557364_COMPACT_VERTICAL_AXIAL_TURBINE_SAXO.

J. L. Gordon, P.E., 2003. Horizontal axis pit type propeller turbines. In *Turbine selection for small low-head hydro developments*. Canada: NATURAL RESOURCES CANADA. Available at: http://www.small-hydro.com/pdf/workshops/cd/2003/technical/Turbine selection for small low head hydro.pdf.

Kementrian Energi Sumber daya Mineral, 2015. Potensi Energi Baru Terbarukan (EBT) Indonesia. *Kementrian Energi dan Sumber daya Mineral*. Available at: http://esdm.go.id/berita/37-umum/1962-potensi-energi-baru-terbarukan-ebt-indonesia.html [Accessed May 14, 2015].

Kementrian Pekerjaan umum badan penelitian dan pengembangan sosial ekonomi dan lingkungan, 2011. *Penelitian dan Pengembangan Teknologi Berbasis Masyarakat*, Jakarta. Available at: http://sosekling.pu.go.id/attachments/article/349/Penelitian Dan Pengembangan Pengelolaan Teknologi Mikrohidro Berbasis Masyarakat.pdf.

Ketenagalistrikan, D.J., 2014. Kebijakan Tarif dan Subsidi Listrik Tahun 2015. *Ketenagalistrikan, Direktorat Jenderal Kementrian Energyi sumber daya mineral*. Available at: https://www.djk.esdm.go.id/index.php/detail-berita?ide=3836 [Accessed May 13, 2015].

Ketenagalistrikan, D.J., 2013. *Statistik Ketenagalistrikan 2013*, Available at: http://energy-indonesia.com/08data/0140328stats.pdf.

Lars Fjærvold, 2012. *Improvements of a Kaplan type small turbine*. Norwegian University of Science and Technology.

Leclerc, M., 2007. The Very Low Head Turbo Generator A New Turbine For Profitable Harnessing of Very Low Head Applications. Available at: http://vlh-turbine.com/FR/PDF/evenements/MJ2Technologies_TheVeryLowHeadTurbine_WaterPower_Grenade.pdf.

Lepisto, C., 2007. Gravitational Vortex Power Plant is Safe for Fish. *Three hugger*. Available at: http://www.treehugger.com/renewable-energy/gravitational-vortex-power-plant-is-safe-for-fish.html.

Linton, N.P., 2014. *Field Trials and Development of a Hydrostatic Pressure Machine*. University of Southampton.

Lyons, M. & David, W.L., 2013. Archimedes Screws for Microhydro Power Generation. In *Proceedings of the ASME 2013 7th International Conference on Energy Sustainability & 11th Fuel Cell Science, Engineering and Technology Conference ESFuelCell2013*.

Maria, 2011. Mikrohidro, Menunggu Dilirik dan Dimanfaatkan. *Kompasiana*. Available at: http://teknologi.kompasiana.com/terapan/2011/04/10/mikrohidro-menunggu-dilirik-dan-dimanfaatkan-353628.html.

Mavel, 2016. TM MODULAR MICRO TURBINE RANGE. Available at: http://www.mavel.cz/turbines/tm-micro-turbines [Accessed May 20, 2016].

meauxfiles, 2015. Machines hydrauliques dans la région de Meaux. Available at: http://hist.olieu.net/hydro/.

Meerwarth, K.D., 1935. *Experimentelle und theoretische Untersuchungen am oberschlächtigen Wasserrad. (Experimental and theoretical investigation of an overshot water wheel)*. Technical University of Stuttgart/Germany.

Misoury river, 2016. Typical Vertical-Kaplan Turbine/Generator. *Misoury river*. Available at: http://redrockhydroproject.com/project-overview/.

Le Moulin XII, 2015. The Waterwheels of the two mills on the Moulin XII estate are “Sagebien” waterwheels, from the name of the engineer who invented them. Available at: http://www.lemoulin12.fr/home-page.

Müller, G. & Kauppert, K., 2004. Performance characteristics of water wheels. *Journal of Hydraulics Research*, 42(5), p.9.

Müller, G. & Senior, J., 2009. Simplified theory of Archimedean screws Théorie simplifiée. *Journal of Hydraulic Research*, 47(5), pp.666–669.

Müller, G. & Wolter, C., 2004. The breastshot water wheel: design and model tests. In *Engineering sustainability*. p. 9.

Müller, W., 1899. Die Eisernen Wasserräder: Atlas. (The Iron Waterwheels: technical drawings.). In Leipzig: Veit & Comp. Available at: http://www.hylow.eu/knowledge/all-download-documents/Mueller_1899_3_Teil_Atlas.pdf/view.

Nautilus LLC, 2012. Ultra Low Head Hydro Overview. Available at: http://www.waterturbine.com/products/ultra-low-head-turbines/index.php.

Newmills Engineering Ltd, 2013. Newmills Engineering - Our Products - Kaplan Turbines. Available at: http://newmillsengineering.com/products/item/4/kaplan-turbines.

Oleson, J.P., 1984. Greek and Roman Mechanical Water-Lifting Devices: The History of a Technology. In *Greek and Roman mechanical water-lifting devices: the history of a technology*. Toronto.

Orchard, B., 2009. Pumps as turbines in the water industry. *world pumps*. Available at: http://www.worldpumps.com/view/5086/pumps-as-turbines-in-the-water-industry/ [Accessed May 22, 2016].

Ossberger, 2014. Kaplan Turbines. , pp.1–8. Available at: http://hts-inc.com/images/S-160.pdf.

Paish, O., 2002a. Micro-hydropower: status and prospects. In *Proceedings of the Institution of Mechanical Engineers, Part A: Journal of Power and Energy*.

Paish, O., 2002b. Small hydro power: technology and current status. *Elsevier Science*, 6(6), pp.537–556. Available at: http://dx.doi.org/10.1016/S1364-0321(02)00006-0.

Pioneer systems, 2016. Micro Hydro. Available at: http://pioneer-sys.net/microhydro.htm [Accessed May 20, 2016].

Pradhan, E.G.L., 2013. Food, Water & Energy security through Hydropower development. In *SAARC CCI Council on Climate Change, Energy & water Resources*. Available at: http://nea.org.np/neademo/nea.php?obj=gyanendra_paper.

Reynolds, T.S., 2002. Stronger Than a Hundred Men: A History of the Vertical Water Wheel. In JHU Press, p. 480.

Schobert, H.H., 2002. *Energy and Society*, Taylor and Francis.

Senior, J., 2009. *Hydrostatic Pressure Converters for the Exploitation of very low head Hydropower Potential*. University of Southampton.

Senior, J., Wieman, P. & Muller, G., 2008. The Rotary Hydraulic Pressure Machine for Very Low Head Hydropower sites. In *Hidroenergia conference*. Bled Slovenia.

Smeaton, J., 1759. An Experimental Enquiry concerning the Natural Powers of Water and Wind to Turn Mills, and Other Machines, Depending on a Circular Motion. *Phil. Trans. R.*, 51, pp.100–74. Available at: http://rstl.royalsocietypublishing.org/content/51/100.full.pdf.

Smith, N., 1976. *Man and Water, A History of Hydro-Technology*, Peter Davies,.

Staus, A., 1928. Wasserrad versuche.(Test on water wheels). In Die Mühle, p. 47.

TN SHP, 2005. Proposals for a European Strategy of Research, Development and Demonstrat ion for Renewable Energy from Small Hydropower. , pp.1–13.

uk.rs, 2014a. Timing Belt Contitech 800 5M 15. Available at: http://uk.rs-online.com/web/p/products/475-0484/?origin=PSF_428519|QVTNF-LL.

uk.rs, 2014b. Timing Belt Pulley Aluminum 48 5mm Pitch, To Suit Belt Width 15mm 8mm 26mm 38mm 75.25mm. Available at: http://uk.rs-online.com/web/p/products/184-

690/?origin=PSF_428595|QVTN-LL.

Usman Muhammad, 2012. Rural Solar Electrification-Renewable Energy Potential and Distribution for Development in Nigeria. In C. Fellows, ed. *World Renewable Energy Forum (WREF) 2012*. Denver, Colorado, United States: the American Solar Energy Society. Available at: https://ases.conference-services.net/resources/252/2859/pdf/SOLAR2012_0232_full paper.pdf.

voith hydro, 2016. *Bulb/pit/S-turbines and generators*, Available at: file:///C:/Users/hh8g11/Dropbox/new project muller/literature/Voith_Bulb_Pit_turbines.pdf.

Water 21, 2011. Ossberger Crossflow Turbine. Available at: http://www.water21.org.uk/hydropower/ossberger-hydroturbines/the-ossberger-turbine/.

WaterWheels, 98AD. No Title. *Encyclopaedia Britannica*.

Weidner, C.., 1913a. Test of a steel overshot water wheel. , pp.39–40.

Weidner, C.., 1913b. Theory and Test of an overshot water wheel. In Bull Univ Wisconsin, pp. 117–254.

Widhiatmaka, 2010. PENGEMBANGAN PLTMH TURBIN SIPHON : PROSPEK DAN HAMBATANNYA DI INDONESIA. *MIneral dan Energi*, 8(3), pp.82–87. Available at: http://litbang.esdm.go.id/images/stories/pengembangan.pdf.

Wikander, O., 2000. *Handbook of Ancient Water Technology*, Leiden.

World Energy Council, 2013. *World Energy Resources 2013 Survey*, Available at: http://www.worldenergy.org/wp-content/uploads/2013/10/WER_2013_5_Hydro.pdf.

Zotlöterer, F., 2005. Wasserwirbeltechnik. Available at: http://www.watervortex.net/download/DE_Wasserwirbeltechnik.pdf.